LIÈGE université
Sciences Appliquées

Computational fluid dynamics to guide the search for victims of drowning in urban rivers

A thesis submitted in partial fulfillment of the requirements
for the degree of Doctor of Philosophy (Phd) in Engineering Science

by

Clément DELHEZ

Supervisor: Benjamin DEWALS

DOCTORAL COLLEGE IN ARCHITECTURE, ENGINEERING AND GEOLOGY

AUGUST 2025

Abstract

Drowning in freshwater is a major cause of death worldwide. Given climate change and the increasing migration of populations to urban areas, urban drowning is expected to become even more prevalent than it already is. Despite the existence of significant search methods for drowning victims in watercourses, their effectiveness remains limited.

This thesis aims to provide a complementary tool for search teams to help them identify areas with a higher probability of body presence and improve the efficiency of their searches.

Firstly, the fundamentals of modelling are established through an analytical model characterising drowning in an urban environment. The characteristics of the victim and their accessibility are studied, and a set of equations is proposed to convert received data into usable inputs for the analytical model. A numerical model based on this analytical approach is then developed and tested in an idealised flow. Various features of the model are also refined (Monte Carlo simulation, stochastic parameters, Lagrangian model, etc.). A sensitivity analysis is conducted in this idealised flow, highlighting the influence of uncertainties in different model parameters on the results.

Following this analysis, a comparison between marine and river drowning is carried out, revealing characteristic scale differences between the flow and the body in each case. A description of the typical position of a drowning victim is then provided. The corresponding hydrodynamic coefficients are determined through wind tunnel tests at different yaw angles, for two types of clothing and two positions (drowning-like position and lying position). These results are compared with existing literature, and their validity is discussed, along with the torque applied to the body.

Concurrently, a database compiling drowning cases from various sources is created. Statistical tests indicate that the victim's age and water temperature appear to influence the initial buoyancy of the body. A resurfacing threshold and a risk profile are also identified.

Finally, the complete numerical model is described and tested on seven drowning cases in Liège, using a 2D flow model with depth-averaged velocities. This allows for an evaluation of the model's performance in real-life situations and an assessment of its potential. Horizontal and vertical movements are thoroughly examined.

Future work should ideally refine the representation of turbulence effects into the Lagrangian part of the model, additional experimental validations, and enhanced integration with search teams through Bayesian modelling of body position based on explored areas.

Résumé

La noyade en eau douce est une cause majeure de décès à travers le monde. En raison des changements climatiques et de l'urbanisation croissante, il est prévisible que la noyade en milieu urbain devienne encore plus prévalente qu'elle ne l'est actuellement. Bien que les moyens actuels de recherche des victimes dans les cours d'eau soient significatifs, ils demeurent peu efficaces.

Cette thèse vise à fournir un outil complémentaire aux équipes de recherche afin de leur permettre d'identifier les zones à plus forte probabilité de présence de corps et d'améliorer l'efficacité de leurs recherches.

Tout d'abord, les bases de la modélisation sont posées à travers un modèle analytique caractérisant une noyade en milieu urbain. Les caractéristiques de la victime et leur accessibilité sont étudiées, et un ensemble d'équations permettant de convertir les données reçues en données exploitables par le modèle analytique est proposé. Un modèle numérique basé sur l'approche analytique est ensuite développé et testé dans un écoulement idéalisé. Différentes caractéristiques du modèle sont également approfondies (simulation de Monte-Carlo, paramètres stochastiques, modèle lagrangien, etc.). Une analyse de sensibilité est réalisée sur cet écoulement idéalisé, mettant en évidence l'influence des incertitudes sur différents paramètres du modèle et leurs effets sur les résultats obtenus.

Après cette analyse, une comparaison entre les noyades en milieu marin et en rivière est effectuée, permettant d'identifier les différences d'échelle entre l'écoulement et le corps dans chaque cas. Une description de la position typique adoptée par une victime de noyade est ensuite présentée. Les coefficients hydrodynamiques correspondants sont déterminés grâce à des tests en soufflerie pour différents angles de lacet, deux types de vêtements et deux positions (position type noyé et couchée). Ces résultats sont comparés à la littérature et leur validité est discutée, ainsi que le moment de force appliqué sur le corps.

Parallèlement, une base de données compilant des cas de noyade provenant de diverses sources est créée. Des tests statistiques indiquent que l'âge de la victime et la température de l'eau semblent influencer la flottabilité initiale du corps. Un seuil de réapparition et un profil de risque sont également identifiés.

Enfin, le modèle numérique complet est décrit et testé sur sept cas de noyade survenus à Liège dans un écoulement 2D avec des vitesses moyennes sur la hauteur. Cela permet d'évaluer les performances du modèle en situation réelle et d'apprécier son potentiel. Les déplacements horizontaux et verticaux sont minutieusement étudiés.

Les perspectives de ce travail incluent une meilleure prise en compte de la turbulence dans la partie lagrangienne du modèle, des validations expérimentales supplémentaires et une intégration accrue avec les équipes de recherche, notamment via une modélisation bayésienne de la position du corps en fonction des zones explorées.

Remerciements

Cette thèse n'est pas un projet comme les autres, ce n'est pas une thèse comme les autres non plus. Non pas que le travail réalisé diffère mais bien les personnes qui l'ont rendu possible. Cette thèse résulte de la collaboration et du soutien d'énormément de personnes d'horizons différents que je souhaite tous remercier chaleureusement.

Je souhaite tout d'abord remercier Benjamin Dewals, mon promoteur, qui m'a d'abord proposé de travailler sur ce sujet pour mon travail de fin d'étude puis m'a ensuite permis d'étendre ce travail de 6 mois en un travail de 4 ans. Il a rapidement su évaluer ma méthode de travail et m'a laissé avancer en autonomie comme je l'apprécie tant, tout en m'apportant sa supervision dès que je m'égarais dans ma recherche. Un grand merci à lui pour m'avoir accompagné tout au long de ma recherche ainsi que pour son investissement. Je remercie également Sébastien Erpicum qui m'a particulièrement éclairé sur l'aspect expérimental de ma thèse mais également pour m'avoir offert tant d'opportunités de réaliser des projets divers et variés au laboratoire. A l'opposé du travail expérimental, j'ai pu compter sur Pierre Archambeau pour m'aider dans ma manière de coder, d'adapter mon travail à son objectif final et à le rendre bien plus accessible via son intégration dans WOLF. Cette dernière étape qui, anodine en apparence, fait passer mon travail de « thèse de Clément » à « modèle utilisable pour quiconque utilise WOLF » et rend mon travail bien plus utile qu'il ne l'aurait été sans son aide. Je remercie ensuite Michel Pirotton avec qui j'ai eu moins d'opportunités de collaborer d'un point de vue scientifique mais avec qui les échanges que j'ai eu au bureau ne sont pas moins précieux. Merci également à Nicolas Riviere pour tous ses retours sur mon travail ainsi que les moments partagés toujours très agréables lors de mes visites à Lyon. Je tiens aussi à remercier Joost Bierens, Werner Jacobs, Maarten Arnst et Thomas Andrianne pour les échanges que nous avons pu avoir et votre supervision lors de nos réunions.

Comme je l'ai mentionné, cette thèse a nécessité le soutien de personnes d'horizons très différents qui m'ont permis de travailler dans tous les domaines nécessaires à mon étude. C'est l'occasion de remercier Gregory Thonard, Maxime Mathieu et Claude pour leur aide au labo, et bien plus encore ; Alexia Van Goethem pour son aide et sa supervision à l'institut médico-légal d'Anvers ; Violette Dechamps et Philippe Boxho pour les données auxquelles ils m'ont permis d'avoir accès à l'institut médico-légal de Liège ; à Raphael Dubois pour son aide apporté lors de mes tests en soufflerie ; à Jean-Marie Zanot, Célia Maghakian, Diego Lopez et toute l'équipe du projet ARCO pour cette collaboration sur la noyade à une échelle bien plus grande que la mienne ; et à Pierre Hallot sans qui la modélisation de mon mannequin n'aurait pas été possible.

Et puis, ce travail ça a également été lié à de sacrées rencontres, à commencer par mon collègue du +1/544, Vincent. Notre bonne entente immédiate laissait déjà entrevoir la suite : une complicité professionnelle et personnelle que je ne saurai décrire mais qui m'a fait avancer, travailler, « travailler », me questionner etc. En bref, que du positif, comme ce que je te souhaite pour la suite. Viennent ensuite Damien, Max et Loris avec qui tous les prétextes étaient bons pour prendre un café, dire bonjour, papoter, boire un verre et j'en passe.

J'ai également eu la chance de participer au concours Ma thèse en 180 secondes. Et oui, je me suis jeté à l'eau. Merci à Kim, Irene, Carla, Astrid, Florence, Christina et Aimée, ainsi qu'à Virginie, Amaël et Thérèse. On se sera amusé bien plus que 180 secondes.

Remerciements

Je souhaiterai également remercier tous les autres doctorants et collègues qui ont largement contribué à mon épanouissement dans ce cadre de travail : Christophe, Joris, Pratik, Daniela, Utashi, Kawthar, Maria Paula, Stéphane, Arnaud, Kévin, Léonore, Anass, Julien, Tohid, Solène, Adrien, Julien, Romain, Nayan, François, Laurence et Alexandre.

Finalement, je tiens à remercier mes parents, ma famille, Muf Muf (oui Pol, le nom de notre groupe de copains n'est pas très vendeur) et mes proches en général. Plus besoin de m'envoyer des articles de journaux sur des corps retrouvés à la seconde où ils étaient publiés. Plus besoin de vous soucier du fait que j'arrive à encaisser tous ces drames sans que cela ne m'impacte. Plus besoin de subir mes soirées d'énervement parce que je n'arrivais pas à coder ce que je voulais. Promis, vous ne m'entendrez plus parler de « mes morts qui flottent ». Enfin… Plus aussi souvent.

Table of contents

Introduction

Introduction

Drowning has been a persistent challenge throughout human history, a peril we have continually had to face and adapt to. The first public attempt to aid drowning victims dates back to 1767 with the founding of the Society to Rescue People from Drowning in Amsterdam (Heldring, 2014). This group aimed to establish universal techniques for assisting individuals in critical conditions following a drowning incident. Early methods reflected the medical understanding of the time, recommending interventions such as hanging the victim by the feet to drain ingested water or using a pipe to blow tobacco smoke into the rectum (Meursing, 2014). It was not until the mid-20th century that mouth-to-mouth resuscitation was recognised for its effectiveness and widely adopted. Since then, an increasing number of people have been successfully revived following drowning incidents, with ongoing medical advancements further improving survival rates. However, these resuscitation techniques are effective only under one obvious condition: the quick recovery of the victim's body.

As with resuscitation, body recovery techniques have advanced, with methods now depending on factors such as the location of the drowning, the water flow rate, and turbidity. Modern technology has also expanded search capabilities, employing divers, motorboats, sonar, helicopters, and drones to cover wider areas (Blondel, 2014; Gonzalez et al., 2022; Lunetta et al., 2014), as sketched in Figure 1. However, these technologies come with limitations: safety considerations for divers, irregularities of the river bottom, or the fact that aerial devices can only detect a body if it is visible at the surface (Ng, 2014), among others.

Figure 1: Illustrative representation of the methods currently used in the search for drowned victims in urban rivers.

In parallel, digital tools have emerged and become increasingly powerful, to the point where it is now common practice to digitally recreate phenomena or events for better understanding and analysis (Tao et al., 2019). These digital replicas, known as digital twins, are now found across numerous fields, with examples ranging from digital twins of buildings (Opoku et al., 2021) and engines to human body parts (Tang et al., 2024). However, no digital twin currently exists for river drownings, despite the extensive use of various technologies whose effectiveness is often hindered by operational and safety limitations. This raises an important question: why is there no digital twin for drowning events?

To create a digital twin of an event, it is essential to identify the context, processes involved, and characteristics of each element relevant to the problem. For a building, for example, this involves defining each component, its material composition, its connections with other elements, and their respective positions. Only once every detail is specified can a digital twin of the building be created, enabling simulations of its behaviour under various conditions. Similarly, developing a digital twin of a drowning event requires identifying its key defining elements, which can be summarised in four main elements:

1. The drowning is reported, either by an eyewitness or through suspicion.
2. The submerged body is subjected to various forces and moves according to these influences.
3. The environment with the river morphology, the flow field and the water temperature influences the forces and so, the body motion.
4. The physical properties of the body change over time due to decomposition.

For the first stage, a model must be developed that can generate body representations based on basic characteristics provided by a witness, while accounting for the inherent inaccuracies of eyewitness testimony. This model should be able to deduce properties such as body volume from available data like height, weight, sex, or age even in cases where some of this information is missing.

Next, it is essential to identify and quantify the forces acting on the body. Each force must be specifically characterised for the case under study and requires information about the body, such as its volume, surface area, shape, and frictional interaction with the riverbed or fluid. These forces must not only be identified but also accurately characterised to ensure an accurate representation of the situation.

Afterward, the effects of body decomposition underwater must be quantified. As a hydraulic engineer, this aspect falls outside my core expertise. Rather than quantifying decomposition itself, the focus should be solely on its mechanical effects on the body's characteristics specifically, the increase in volume it causes. This volume variation is then naturally incorporated into the second stage of the process, which accounts for how the body behaves in response to applied forces.

Finally, these stages must be integrated into a digital twin model that is fast enough to be employed in real-time drowning situations. This model should incorporate a flow simulation that accurately represents the real conditions, processing this data to provide an effective, targeted tool for narrowing down the search area for drowning victims.

Introduction

This thesis is organised in four main chapters each based on peer-reviewed scientific papers or submitted manuscripts, organised as depicted in Figure 2. In Chapter 1, we establish an analytical model of a drowned body in an idealised stationary flow and perform a global sensitivity analysis. In Chapter 2, we determine the hydrodynamic coefficients of a drowning victim through experiments in a wind tunnel. In Chapter 3, we analysed 50 real-world drowning cases to identify key factors that influence drift and resurfacing in urban rivers, highlighting the need for empirical data in predictive models to improve body search strategies. In Chapter 4, we combine all the work done into one Lagrangian-Eulerian computational model and we test it on real cases of drowning in a realistic flow.

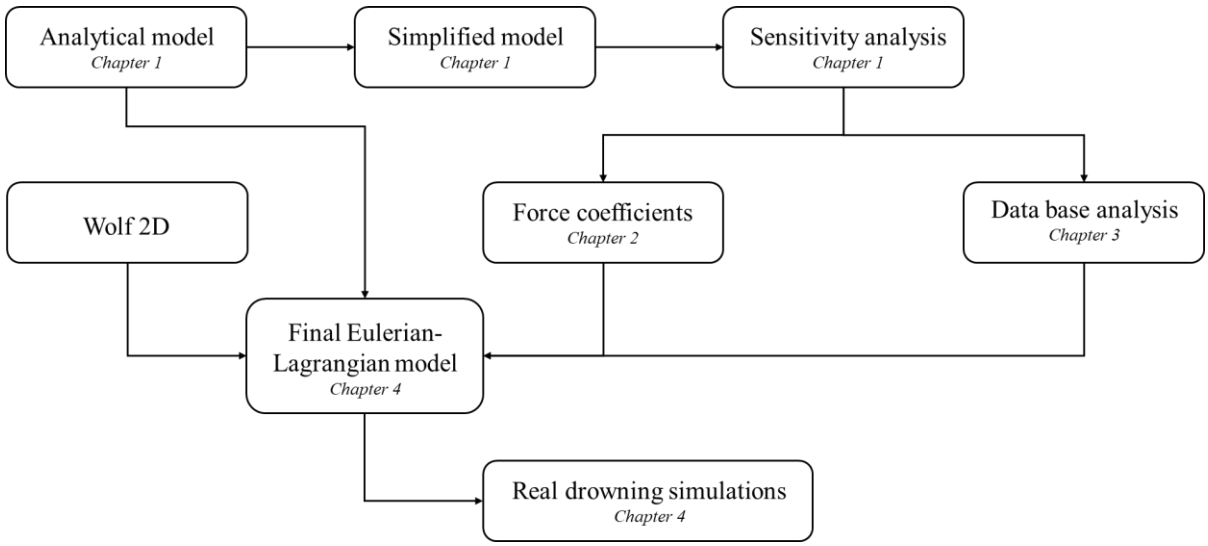

Figure 2: Flow chart of the thesis

This work represents one contribution to the broad and multifaceted subject of drowning victim search. While it intersects two key fields with hydraulic engineering and forensic medicine, it does not address other essential dimensions such as social sciences, geography, fieldwork methodologies, or in-field experimental investigations. Drowning is a complex phenomenon that spans many disciplines, each offering unique insights and tools. Within this wide scope, the present work aims to complement the overall understanding of drowning, focusing on some of the aspects that can be addressed through hydrodynamic modelling and forensic analysis.

The model developed in this thesis is designed to supplement other approaches by offering a quantitative perspective that supports existing practices, particularly in the interpretation of witness testimonies and the analysis of environmental conditions during drowning events.

One of the key motivations behind this work is to enhance field operations. It is crucial that academic research be usable and relevant for practitioners involved in search and recovery efforts. To ensure this, we engaged early in the project with stakeholders like divers or research teams on boats, seeking their input on the practical needs and constraints they face. These discussions guided the development of a flexible and operationally oriented model, capable of simulating various drowning scenarios in known environmental contexts.

Figure 3: Tracking field tests of a dummy carried out as part of a complementary thesis in collaboration with the SDMIS, the fire brigade of the city of Lyon, France.

The model allows for clear, visual representations of results, making it easier to identify potential search areas and support forensic evaluations, as detailed in Chapter 4. However, it must be emphasized that the tool is still in a research phase. It is not yet ready for direct use in the field, but it aims to already demonstrate the potential value of such modelling approaches. The model was designed to be modular and adaptable, facilitating future improvements and integration into more comprehensive, field-ready tools.

Ultimately, this research is part of a long-term, collaborative effort. A direct follow-up is the ongoing ARCO project (French ANR funding) led by academic institutions (including INSA Lyon) and practitioners mostly based in Lyon. By focusing on hydrodynamic modelling within an operational context, this work seeks to bridge the gap between academic research and practical application, contributing to the broader objective of improving the success rate of search for drowned victims in urban rivers.

References

Blondel, P. (2014). Searching for Dead Bodies with Sonar. *Drowning* (2nd ed. 2014 édition., pp. 1161–1165). New York: Springer-Verlag Berlin and Heidelberg GmbH & Co. K. doi:10.1007/978-3-642-04253-9_182

Gonzalez, J. R. P., Escobar-Vargas, J., Vargas-Luna, A., Castiblanco, S., Trujillo, D., Guatame, A. C., Corzo, G., et al. (2022). Hydroinformatics tools and their potential in the search for missing persons in rivers. *Forensic Science International*, 111478. doi:10.1016/j.forsciint.2022.111478

Heldring, B. (2014). Brief History of Maatschappij tot Redding van Drenkelingen (The Society to Rescue People from Drowning). In J. J. L. M. Bierens (Ed.), *Drowning* (pp. 3–6). Berlin, Heidelberg: Springer Berlin Heidelberg. doi:10.1007/978-3-642-04253-9_1

Lunetta, P., Ebbesmeyer, C., & Molenaar, J. (2014). Behaviour of Dead Bodies in Water. *Drowning* (2nd ed. 2014 édition., pp. 1149–1152). New York: Springer-Verlag Berlin and Heidelberg GmbH & Co. K. doi:10.1007/978-3-642-04253-9_179

Meursing, B. J. (2014). The History of Resuscitation. In J. J. L. M. Bierens (Ed.), *Drowning* (pp. 25–36). Berlin, Heidelberg: Springer Berlin Heidelberg. doi:10.1007/978-3-642-04253-9_4

Ng, M. (2014). Helicopter Search and Rescue for Drowning Victims. In J. J. L. M. Bierens (Ed.), *Drowning* (pp. 477–484). Berlin, Heidelberg: Springer Berlin Heidelberg. doi:10.1007/978-3-642-04253-9_72

Opoku, D.-G. J., Perera, S., Osei-Kyei, R., & Rashidi, M. (2021). Digital twin application in the construction industry: A literature review. *Journal of Building Engineering*, *40*, 102726. doi:10.1016/j.jobe.2021.102726

Tang, C., Yi, W., Occhipinti, E., Dai, Y., Gao, S., & Occhipinti, L. G. (2024). A roadmap for the development of human body digital twins. *Nature Reviews Electrical Engineering*, *1*(3), 199–207. doi:10.1038/s44287-024-00025-w

Tao, F., Zhang, H., Liu, A., & Nee, A. Y. C. (2019). Digital Twin in Industry: State-of-the-Art. *IEEE Transactions on Industrial Informatics*, *15*(4), 2405–2415. doi:10.1109/TII.2018.2873186

Chapter 1

Conceptualization and global sensitivity analysis under idealized flow conditions

This chapter corresponds to the journal paper "Drift of a drowning victim in rivers: conceptualization and global sensitivity analysis under idealized flow conditions" by C. Delhez, N. Rivière, S. Erpicum, M. Pirotton, P. Archambeau, M. Arnst, J. Bierens and B. Dewals, published in 2023 in Water Resources Research. The PhD candidate developed the methodology, implemented the numerical models, analysed the results, wrote the manuscript and generated the figures.

Chapter 1: Conceptualization and global sensitivity analysis

Drift of a drowning victim in rivers: conceptualization and global sensitivity analysis under idealized flow conditions

C. Delhez[1], N. Rivière[2], S. Erpicum[1], M. Pirotton[1], P. Archambeau[1], M. Arnst[3], J. Bierens[4] and B. Dewals[1]

[1]Hydraulics in Environmental and Civil Engineering (HECE), Research Unit Urban & Environmental Engineering (UEE), University of Liège, 4000 Liège, Belgium.

[2]Univ Lyon, INSA Lyon, Ecole Centrale de Lyon, Université Claude Bernard Lyon I, CNRS, LMFA, UMR 5509, 20 avenue Albert Einstein, F-69621 Villeurbane, France.

[3]Aerospace and Mechanical Engineering, University of Liège, 4000 Liège, Belgium.

[4]VU University Medical Centre, the Netherlands

Corresponding author: Clément Delhez (clement.delhez@uliege.be)

ABSTRACT

We present a conceptual model of the drift of a drowning victim in a river, accounting for the mechanical effects of body decomposition. The model was tested under idealized flow conditions (uniform flow) and a global sensitivity analysis was performed. Uncertainties in body morphology, flow-body interaction parameters (e.g., drag coefficient) and drowning characteristics were considered. The results emphasize the importance of predicting the body vertical position since it considerably influences the streamwise body drift velocity, due to the significant difference between near-surface and near-bed velocity. The results also highlight the value of testimonies providing information on body mass and height, as decreasing uncertainty on these input data strongly reduces uncertainties on the predicted body streamwise position. Next step of the research will consist in coupling the model with an Eulerian multi-dimensional model of river hydrodynamics.

KEYWORDS: drowning, drift model, human body, sensitivity analysis

1 Introduction

1.1 Context

Worldwide, unintentional drowning is estimated to cause about 400,000 fatalities every year (WHO, 2014). Climate change tends to increase the risk of drowning, due to a rising frequency and magnitude of hydro-meteorological extremes (Musolino et al., 2020). More frequent riverine and flash floods increase the likelihood of persons being drifted by watercourses (Milanesi et al., 2015; Chen et al., 2019; Musolino et al., 2020; Lazzarin et al., 2022). Repeated heatwaves (Simpkins, 2017) lead to a rise in (unauthorized) bathing activities in urban rivers and a corresponding rise in drowning accidents.

Understanding the trajectory of human bodies drifted in streams is of great interest for informing targeted rescue operations and for reducing the resources needed for body search and recovery after drowning. A short reaction time is key for rescue missions. Depending on water temperature, resuscitation may be possible in a time window of up to one and a half hour after drowning (Tipton and Golden, 2011). A quick, target-oriented, and process-informed search can make the difference between finding the victim alive or dead. Even beyond this time frame, a speedy recovery of the human body remains important. It enables search and rescue teams to act quicker, improve resources allocation, and it reduces the risks taken by first-responders such as divers. Body search operations in urban rivers are dangerous and complex due to relatively high flow velocity and momentum combined with a low visibility due to suspended materials and dissolved compounds (Horn, 2014). Search technologies such as sonars typically perform poorly in urban river stretches due the presence of various debris and man-made artefacts on the river bottom (Blondel, 2014). During floods, high flow momentum and transported debris (stones, tree trunks, vehicles …) make it unsafe for search and rescue staff to boat or dive, so that locating a victim of drowning during flood becomes hardly possible (Ray, 2014).

After drowning and loss of consciousness, three stages of vertical body motion may typically be distinguished (Heaton et al., 2010; Mateus et al., 2013; Bierens, 2015). First, the body sinks and reaches the bed as its overall density is generally slightly above that of fresh water. Water inhalation and ingestion also plays a role in this motion since it leads to replacing air in the human body by water and, therefore, it alters the body bulk density. Second, body entrainment takes place on the riverbed. It is influenced by fluid forces, bed friction, bed morphology, gravity, and buoyancy as well as body positioning and deformability. Third, putrefaction gases are generated after a period of time (typically two to five days) which depends on water temperature. The gases increase the buoyancy and, unless the body is entangled at the river bed, it eventually resurfaces and drifts (Lunetta et al., 2014). The exact duration of each of the three stages remains complex to predict as it depends on several factors such as body characteristics, clothing, flow conditions, and water temperature.

1.2 State of the art

So far, studies in forensic medicine focused on aspects such as characterizing the cause of drowning (Stephenson et al., 2020) or estimating of the post-mortem submersion interval (PMSI) for bodies retrieved from water (Heaton et al., 2010; Papadodima et al., 2010; Mateus et al., 2013; Daalen et al., 2017). The PMSI is generally estimated as the time elapsed between the suspected moment of the drowning accident and the moment when an eyewitness noticed the body at the water surface. PMSI may be used as a proxy for the time elapsed until body resurfacing, despite a risk of overestimation of the resurfacing time. The values of PMSI reported in literature vary considerably from one case study to another (e.g., 12-192 days according to Heaton et al. (2010)) . This is due to the influence of temperature on body decomposition (Kaatsch et al., 1994; Megyesi et al., 2005; Hayman and Oxenham, 2016), which is not encompassed in the PMSI.

Therefore, other studies in forensic medicine introduced the concept of accumulated degree day (ADD) as defined by Megyesi et al. (2005). The ADD is evaluated as the integral over time of the temperature of the environment in which the body is situated (e.g., water temperature):

$$ADD = \int_{t_0}^{t} T dt \tag{1}$$

where t_0 stands for the initial time of the drowning, t is the current time and T is the environment temperature. Empirical data suggest that ADD is a reasonable predictor to estimate the degree of decomposition of a dead body (Heaton et al., 2010; Daalen et al., 2017) and, therefore, the resurfacing time (Megyesi et al., 2005). Indeed, the values of ADD corresponding to observed resurfacing time of bodies of victims were found to vary in a narrower range than the corresponding PMSI (Megyesi et al., 2005).

So far, search operations in urban rivers have not been guided by any modelling technique aiming at predicting the trajectory of the victim's body. Existing computational studies of body drift trajectories were developed for marine environments (Carniel et al., 2002; Breivik and Allen, 2008; Mateus et al., 2015; Gunduz, 2017; Ličer et al., 2020; Tu et al., 2021; Hart-Davis and Backeberg, 2023; Wu et al., 2023) and, as such, they focused on the effects of wind, waves, and currents. In most cases, the vertical body motion was neglected (Carniel et al., 2002). This assumption was justified by the relatively higher density of saltwater compared to freshwater, so that the body has a greater chance of floating (Ebbesmeyer and Haglund, 1994; Carniel et al., 2002; Mateus et al., 2015). Life jackets are also more commonly used in marine environments than in the case of drowning accidents in rivers. For inland water bodies, the vertical body motion needs to be considered to enable reliable predictions of body streamwise position (Heaton et al., 2010), hence body decomposition has a considerable influence.

In existing models developed for marine environments, the grid size varies between 1 km and 9 km (Carniel et al., 2002; Breivik and Allen, 2008; Mateus et al., 2015; Gunduz, 2017; Ličer et al., 2020; Hart-Davis and Backeberg, 2023). This is two to three orders of magnitude coarser than the mesh refinement necessary to capture the typical topographic variability of most urban rivers worldwide. The length scale characterizing the body of a victim of drowning remaining unchanged (~ 2 m) irrespective of the drowning context, the two problems appear fundamentally different between river and sea/ocean contexts. Indeed, in marine environments, the body being drifted has a characteristic size way smaller than the length scales characterizing the forcings (flow and wind fields), whereas in rivers they are less separated or even comparable (flow structures such as secondary currents or vertical velocity gradients both developing across the river depth, thus with a O(1-10 m) characteristic length, large vortices downstream bridge piers with a O(1 m) characteristic length, *etc*.). Now, the interaction between body

being drifted and flow is strongly controlled by the ratio of body scale to flow scale (Ghaffarian et al., 2020; Meninno et al., 2020). The time scales are also significantly different. Existing modelling studies in marine environments use time steps between 1 h and 12 h, while a time step suitable for resolving the trajectory of a body in the flow field of an urban river needs to be considerably smaller. Overall, the sea/ocean context enables a separation of scale between the forcings and the drifted body, whereas this does not apply to the context of urban rivers, hence making the coupling between flow and body drift more intricate in the case of rivers since more fine-scale aspects need to be resolved. In one recent computational study (Gonzalez et al., 2022), flow fields in rivers were calculated to identify areas (e.g., vortices) where a body is likely to remain trapped, but the drift of an individual body was not reproduced explicitly.

1.3 Objective

In the present study, we propose a new conceptual and mathematical formulation for describing the drift of the body of a drowning victim in rivers considering the mechanical effects of body decomposition. We first formulate the model in general terms, and then it is analysed for idealized flow conditions (uniform flow). Under this assumption, the body trajectory is computed in two dimensions: along the streamwise direction and over the flow depth. The flow velocity is assumed to vary over the flow depth following a logarithmic profile. The body drift model is Lagrangian. It is based on force balance coupled with a new, original equation for predicting the evolution of the body volume (hence, also, body bulk density) as a function of elapsed time and water temperature (through ADD). This makes the model able to predict the three observed stages of body vertical displacement: sinking, bloating and resurfacing. A global sensitivity analysis is presented to inform on the relative influence of uncertainties in input data and model parameters on model outcomes. Results show a strong correlation between body streamwise motion and vertical positioning of the body over the flow depth.

2 Methodology

This study presents a Lagrangian drift model based on a balance of forces acting on a human body. A general model formulation is first introduced. It is subsequently analysed considering idealized, uniform flow conditions. The modelling strategy involves two components. First, a mechanistic model solves the equations of motion based on a set of input data and model parameters, as well as a new hypothesis on the evolution of body characteristics (volume, bulk density) as a result of body decomposition (Section 2.1). Empirical anthropometric closures are used to infer the necessary geometric and physical characteristics of the body from a limited number of inputs, such as estimated body mass or body mass index (BMI) (Section 2.2). Second, this mechanistic model is embedded within a stochastic modelling framework (Section 2.3), in which a Monte Carlo approach is adopted to account for uncertainties in the input data and model parameters and assess the sensitivity of model outcomes to these uncertainties. The workflow of the modelling is sketched in Figure 1, while more details are given in Figure S1 (Supplementary material A). The new methodology was applied to several scenarios of flow conditions and body characteristics, as defined in Section 2.4.

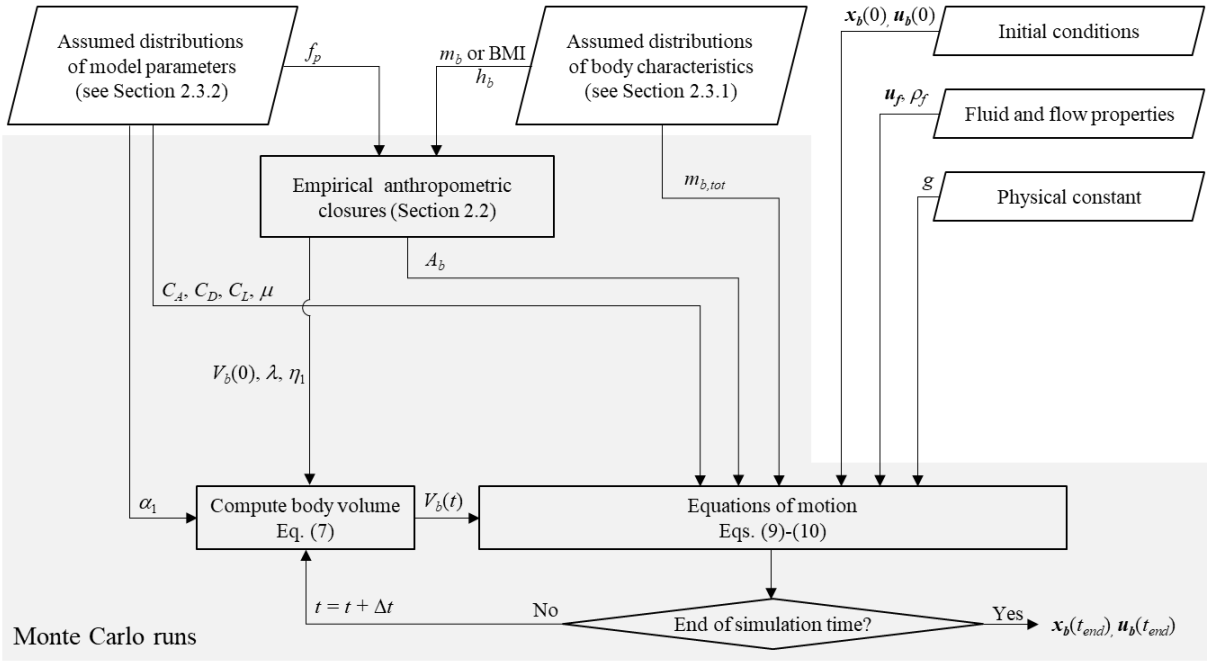

Figure 1: Workflow of the modelling

2.1 Mechanistic model

2.1.1 Governing equations

The body trajectory is described based on the position and velocity of its centre of mass. Neither the body orientation (roll, pitch, and yaw angles) nor possible posture deformations are explicitly predicted by the model. Instead, we consider variations in body orientation and deformation via statistical distributions characterizing the body frontal area, body drag coefficient, or friction coefficient on the riverbed, among others (Section 2.3).

A Cartesian reference frame is used, where the x-axis is aligned with the mean slope of the river bed, as shown in Figure 2. The independent variables are time t and the vector of spatial coordinates $\boldsymbol{x} = [x, y, z]^T$. The angle between the x-axis and the horizontal plane is denoted θ. The flow field is steady and is assumed to be given as input data, i.e., the flow depth $h(\boldsymbol{x}, t)$ and the flow velocity $\boldsymbol{u_f}(\boldsymbol{x}, t) = [u_f, v_f, w_f]^T$ are considered to be known. The bed level $b(x, y)$ is known also.

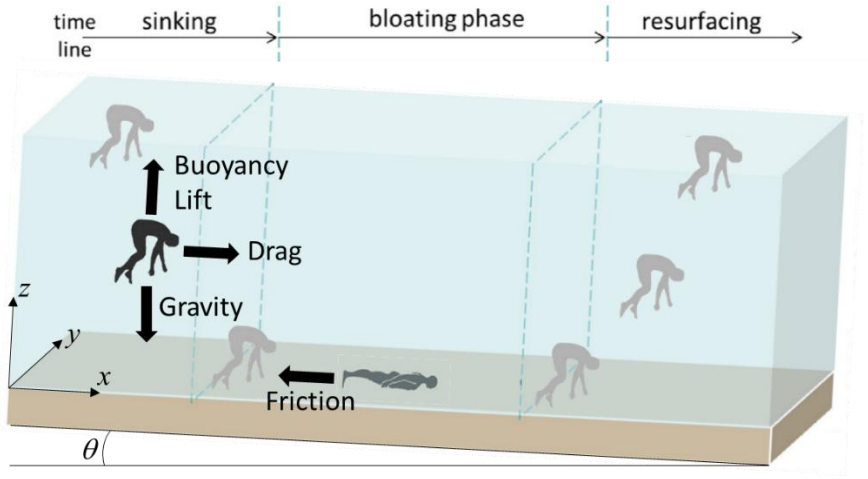

Figure 2: Conceptualization of sinking, bloating, and resurfacing phases (adapted from Matheus et al., 2013)

In the Lagrangian drift model, the state variables are the body position vector $\boldsymbol{x_b} = [x_b, y_b, z_b]^T$ and its associated velocity vector $\boldsymbol{u_b} = [u_b, v_b, w_b]^T$. The model equations write:

$$\dot{\boldsymbol{x}}_b = \boldsymbol{u}_b \tag{2}$$

$$\left(m_{b,tot}\mathbf{I} + \frac{1}{2}\mathbf{C}_\mathbf{A}\rho_f V_{b,sub} \right)\dot{\boldsymbol{u}}_b = \boldsymbol{F}_f + \boldsymbol{F}_g + \boldsymbol{F}_b\,, \tag{3}$$

where a dot over a variable refers to the time derivative, $m_{b,tot}$ is the total body mass, $\mathbf{C_A}$ the second-order tensor of added mass coefficients, ρ_f the fluid density, $V_{b,sub}$ the submerged body volume, $\boldsymbol{F_f}$ the fluid to body forces (drag, side and lift), $\boldsymbol{F_g}$ the resultant of gravity and buoyancy forces, and $\boldsymbol{F_b}$ the friction force on the bottom. The body is assumed unconscious, so that swimming efforts do not need to be considered in the force balance. The "total body mass" differs from the initial body mass by the amount dm of water swallowed and aspirated at the time of drowning: $m_{b,tot} = m_b + dm$. The body volume evolves with time, as detailed in Sub-section 2.1.2.

In general, the variation range of the dependent variables x_b and y_b is constrained by the width of the water course and the presence of rigid obstacles (e.g., bridge piers, abutments). Similarly, the elevation z_b of the body centre of mass varies between a minimum value, equal to $b(x_b, y_b) + \varepsilon_{min}$, and a maximum value, which is close to the free surface elevation. The length ε_{min} is a body characteristic, representing roughly the body "thickness".

The fluid to body force may be expressed as follows, Eq. (4):

$$\boldsymbol{F}_f = -\frac{1}{2}\rho_f \mathbf{C}\left(\boldsymbol{u}_b - \boldsymbol{u}_f\right)\left|\boldsymbol{u}_b - \boldsymbol{u}_f\right|, \tag{4}$$

where $\mathbf{C}$ is a second-order tensor whose elements are products of drag, lift and side coefficients by the respective frontal areas. The balance of gravity and buoyancy forces reads:

$$\boldsymbol{F}_g = \mathbf{g}\left(m_{b,tot} - \rho_f V_{b,sub}\right), \tag{5}$$

where **g** is the gravity acceleration vector $[g\sin\theta, 0, -g\cos\theta]^{T}$.

For the friction force between the body and the bottom, a parametrization based on Coulomb formulation is proposed:

$$\begin{cases} \boldsymbol{F_b} = -\mu\,\gamma(\boldsymbol{x_b})\,g\cos\theta\,\max\left(m_{b,tot}-\rho_f V_{b,sub},0\right)\dfrac{1}{\sqrt{u_b^2+v_b^2}}\begin{bmatrix}u_b\\v_b\\0\end{bmatrix} & \text{if } u_b^2+v_b^2\neq 0 \\ \boldsymbol{F_b}=\boldsymbol{0} & \text{if } u_b^2+v_b^2=0 \end{cases}, \tag{6}$$

where μ is a Coulomb-type friction coefficient and $\gamma(\boldsymbol{x_b})$ is a continuous "shape" function ensuring that $\boldsymbol{F_b}$ becomes non-negligible only when the body is positioned close to the bottom (Figure S2 in Supplementary material B). The exact formulation used for function $\gamma(\boldsymbol{x_b})$ is inspired from the standard Rouse profile for suspended sediments (Rouse, 1950), see Eq. (S1) in Supplementary material B.

2.1.2 Mechanical effects of body decomposition

The submerged body volume $V_{b,sub}$, which intervenes in Eqs. (3), (5) and (6), varies with time due to two effects: the generation of putrefaction gases in the body as body decomposition progresses, and the depth-dependent water pressure acting on the body external surface. We consider that the body volume is composed of two parts: (i) a fixed part which corresponds to the volume occupied by solid material such as bones and flesh, and (ii) a variable part which corresponds to the volume occupied by gas within the body. The former is supposed time-independent while the latter evolves with time. The portion of the total volume occupied by gas, λ, was approximated here as the lungs volume, and estimated by means of empirical closures as detailed in Section 2.2 and in Supplementary material C.

To conceptualize the mechanical effects of body decomposition, we hypothesize that the variable part of the body volume changes under the influence of two competing drivers: the water pressure p_{hydro} acting on the body and the degree of body decomposition η (varying between 0, i.e., no effect of decomposition on body volume, and η_1 a maximum value reached when the body tissues refrain further body expansion or putrefaction ceases). This leads to the following model formulation for the body volume as a function of time:

$$V_b(t) = (1-\lambda)\,V_b(0) + \lambda\,V_b(0)\,(1+\eta)\left(1-\frac{p_{hydro}}{E}\right)^3 \tag{7}$$

with $V_b(0)$ the volume of the body prior to drowning and E the Young modulus of the rib cage. The value of E for the rib cage was estimated at 11.7 MPa (Vezin and Verriest, 2007; Youssef, 2012). The last factor in the right-hand-side of Eq. (7) represents the contraction of the rib cage under the effect of water pressure, while factor $(1+\eta)$ reflects the body expansion due to decomposition.

As highlighted in Section 1, the degree of body decomposition may be predicted based on the ADD, as defined in Eq. (1) and noted α hereafter. Putrefaction is the dominating decomposition process which influences body volume. The kinetics of putrefaction involves a gradual start,

followed by a rapid increase and a stabilization (Bierens, 2015). For these reasons, we propose to link α and the rate η of increase in body volume due to decomposition (Figure S3 in Supplementary material B):

$$\eta\left(\frac{\alpha}{\alpha_1}\right)=\eta_1 \min\left[6\left(\frac{\alpha}{\alpha_1}\right)^5-15\left(\frac{\alpha}{\alpha_1}\right)^4+10\left(\frac{\alpha}{\alpha_1}\right)^3;1\right] \tag{8}$$

with α_1 the value of ADD reached when the body cannot expand further due to tissues resistance or fading of putrefaction processes.

2.1.3 Uniform flow

In the case of uniform (i.e., steady and fully-developed) flow conditions, the flow field is given by $\boldsymbol{u_f} = [\ u_f(z),\ 0,\ 0\ ]^T$, the flow depth h is constant and, in the frame of reference introduced in Figure 2, the bottom elevation b is considered equal to 0 everywhere. Under these conditions, Eqs. (2) and (3) can be written as:

$$\begin{bmatrix}\dot{x}_b\\ \dot{z}_b\end{bmatrix}=\begin{bmatrix}u_b\\ w_b\end{bmatrix} \tag{9}$$

$$\begin{aligned}\left(m_{b,tot}+\frac{1}{2}C_A\rho_f V_b\right)\begin{bmatrix}\dot{u}_b\\ \dot{w}_b\end{bmatrix}&=-\tfrac{1}{2}\rho_f A_b\begin{bmatrix}C_D\\ C_L\end{bmatrix}\left(u_b-u_f\right)\left|u_b-u_f\right|\\ &+g\left(m_{b,tot}-\rho_f V_{b,sub}\right)\begin{bmatrix}\sin\theta\\ -\cos\theta\end{bmatrix}-\operatorname{sign}\left(u_b\right)\mu\,\gamma(z_b)\,g\cos\theta\max\left(m_{b,tot}-\rho_f V_{b,sub},0\right)\begin{bmatrix}1\\ 0\end{bmatrix}\end{aligned} \tag{10}$$

where the effect of added mass was assumed isotropic: $\mathbf{C_A} = C_A\,\mathbf{I}$, with C_A the added mass coefficient. Forces induced by the relative velocity between body and flow along direction z were neglected. This has little influence on the results due to the short duration of the vertical displacements.

For the sake of simplicity, $u_f(z)$ was supposed to follow a logarithmic profile over the flow depth (Figure S4 in Supplementary material B):

$$u_f(z)=\frac{\overline{u}_f}{\frac{z_0}{h}-1+\ln\frac{h}{z_0}}\ln\frac{z}{z_0} \tag{11}$$

with $\overline{u}_f$ the depth-averaged flow velocity, and z_0 the depth at which the flow velocity reaches zero. Parameter z_0 depends on the roughness height k_s and the flow regime (Pope, 2000). To prevent Eq. (11) from predicting negative flow velocities, parameter ε_{min} was set to a value greater than z_0.

The ordinary differential equations Eqs. (9) and (10) were discretised using an explicit Euler scheme. To improve computational efficiency, a variable time step was considered. It varies between 0.01 s in regions where the body experiences substantial acceleration (e.g., during sinking, when approaching the bottom, at the time of resurfacing), and takes values up to 60 s when the body is essentially moving at a constant velocity (e.g., during bloating on the riverbed, or when drifted at the water surface after resurfacing).

2.2 Empirical anthropometric relations

Existing empirical equations were used to provide an estimate of body characteristics required by the model, such as the frontal area A_f, the initial body volume $V_b(0)$, the portion λ of gas in the body volume, and the maximum rate of body expansion η_1. They apply for adult subjects.

2.2.1 Frontal area, A_f

The frontal area of a body depends on the body morphology, posture and orientation with respect to the flow direction. Here, we assumed that the body positioning matches the typical positioning of an unconscious person floating in water, i.e., body facing the bottom with the limbs hanging down (Lunetta et al., 2014) as sketched in Figure 2.

For given values of the body mass and height, the body frontal area was estimated in two steps, as detailed in Supplementary material C.1. First, the body surface area (BSA) was computed using empirical equations proposed by Tikuisis et al. (2001) which is formula among others (Mosteller, 1987; Du Bois and Du Bois, 1989). Second, the frontal area was derived from the body surface area by means of an empirical projection coefficient f_p whose value is estimated to range between 0.16 and 0.36 (Tanabe et al., 2000). The uncertainties arising from the difficulty of setting a clear-cut value for f_p was considered in our sensitivity analysis (Section 2.3).

2.2.2 Initial body volume, $V_b(0)$

The initial body volume $V_b(0)$ was approximated as the body volume at functional residual capacity (FRC) of the lungs. Empirical relations proposed by Liu et al. (2017) and Sendroy and Collison (1965) were used to estimate the body volume at FRC as a function of the body mass, height and BMI. These relations are detailed in Supplementary material C.2.

2.2.3 Functional residual capacity, FRC

As the body volume at lungs FRC was taken as a proxy for the initial body volume $V_b(0)$, the lungs volume at FRC was also estimated to provide a first approximation for parameter λ in Eq. (7). The lungs volume at FRC is known to vary between approximately 1.7 and 3.5L depending on body gender, age, height, and BMI, among other parameters (Stocks and Quanjer, 1995; Miller, 2005; Abston et al., 2017). As detailed in Supplementary material C.3, we combined empirical results of Stocks and Quanjer (1995) and Abston et al. (2017) to determine the FRC from the gender, age, body height and BMI.

2.2.4 Total Lungs Capacity, TLC

The total lungs capacity (TLC) may vary between 3.4 and 9.0 L depending on the gender, body height, BMI, etc (Stocks and Quanjer, 1995; Miller, 2005; Abston et al., 2017). In line with the approximation used for FRC, we combined equations proposed by Stocks and Quanjer (1995) and Abston et al. (2017) to estimate the lungs volume from the gender, body height and BMI, as described in Supplementary material C.4. A first approximate value for η_1 was evaluated by assuming that the maximum increase in the body volume may be appreciated by considering

the difference between the TLC and the FRC. This aspect certainly needs to be refined in further research.

2.3 Stochastic framework

To account for the substantial uncertainties affecting the input data and model parameters (e.g., body height, mass, kinetics of body decomposition, etc.), the model presented in Section 2.1 was run in a stochastic framework using a Monte Carlo approach (Metropolis and Ulam, 1949). The uncertainty affecting each uncertain input data and model parameter was described based on statistical distributions. The considered distributions were either directly derived from observations, or theoretical distributions were adjusted to match observations. Depending on the uncertain variable, a uniform distribution (e.g., Goeury et al., (2022), or a beta distribution was used. Beta distributions involve two parameters (α and β), as detailed in Supplementary material D and described in McDonald and Xu (1995). Table 1 summarizes the main characteristics of the statistical distributions selected for each input data and model parameter, as detailed in Sections 2.3.1 and 2.3.2. Next, total order Sobol' indices were computed to quantify the sensitivity of model outcomes (i.e., body position at time t) to uncertain data and parameters (Section 2.3.3).

2.3.1 Input data

For the body height and mass (or BMI), two scenarios were considered: either it is assumed that no specific information is available on the body characteristics (e.g., absence of eyewitness), or the body characteristics are relatively well known (e.g., description by a relative of the victim).

- In the first case (Scenario "unknown body"), a beta distribution was adjusted to reflect the variety of body heights and BMI over the whole Belgium population, as reported by Van Der Heyden et al. (2018). Distinct distributions were used for female and for male victims (Figure S5 in Supplementary material D). The BMI was considered for the estimation of body mass. This enables accounting for existing correlations between body height and mass. As displayed in Figure S6 in Supplementary material D, a beta distribution was adjusted for BMI to fit data also made available by Van Der Heyden et al. (2018).
- In the second case (Scenario "known body"), the body height was assumed to follow a beta distribution in which the 10^{th} and 90^{th} percentiles correspond to the mode of the distribution ± 2.5 cm (Figure S7 in Supplementary material D). Similarly, the body mass was described by a beta distribution in which the 10^{th} and 90^{th} percentiles correspond to the mode of the distribution ± 2.5 kg (Figure S8 in Supplementary material D). The distribution ranges were selected to reflect the remaining uncertainties in body characteristics even when this information is reported by relatives of the victim or by eye-witnesses of the drowning accident (Meissner et al., 2007).

Modell and Davis (1969) measured the amount of water inside the lungs of 74 victims of drowning in freshwater. The measurements revealed that 14 % of the victims had aspirated more than 22 g of water per kg of body weight. Accordingly, we adjusted here a beta

distribution for the ratio dm / m_b, ensuring that percentile 86 of the distribution corresponds to 22 g/kg.

2.3.2 Model parameters

Delhez et al. (2021) conducted flume experiments to estimate the drag coefficient of a human body. They considered reduced-scale dummies, positioned like the typical posture observed for real-world drowning victims, i.e., face down and limbs hanging down (Section 2.1). The empirical distribution of observed drag coefficients is shown in Figure S9 in Supplementary material D.

To the best of the authors' knowledge, no experimental data exist for the value of the lift coefficient of a human body in a typical drowning position nor in similar postures. Data are mostly available for simple shapes, such as for instance a spherical body, for which C_L is close to 0.5 Legendre and Magnaudet (1998). To be on the safe side, it was assumed that the uncertainty in the value of the lift coefficient may be described by a uniform distribution over the range [0; 1].

The added mass coefficient C_A depends on the shape of the considered object. According to Newman and Grue (2017), C_A equals unity for circular cylinders, as used by Ghaffarian et al. (2020) and Persi et al. (2018), and $C_A = 0.5$ for a sphere. Based on experiments conducted with human subjects, Caspersen et al. (2010) found that C_A for swimmers can be as low as 0.25. We considered this value as a lower bound for our analyses. Given the substantial differences between the typical drowning position and that of swimmers [see photograph below], and the possible effects of clothes or accessories (e.g., backpack), we considered here values of C_A ranging between 0.25 and 1 (i.e., value applicable for a cylinder). The distribution of C_A was assumed uniform in this range. Considering a relatively wide range of possible values for C_A is on the safe side, and the outcomes of the present study enable appreciating whether getting a better knowledge of C_A in the case of drowning would be valuable for the modelling, or whether the model results are hardly sensitive to the value of C_A.

For the projection factor f_p used to estimate the frontal area (Supplementary material C.1), we assumed a uniform distribution over the range [0.16; 0.36], which corresponds to the range of values measured by Tanabe et al. (2000) for seated or standing bodies. Values characterizing standing bodies can be transposed to lying ones as these two positions are equivalent from the perspective of hydrodynamic coefficients provided that the pitch angle is shifted by 90°.

In Eq. (8) describing the kinetics of body decomposition, the value $\alpha_1 / 2$ may be regarded as similar to the threshold value of ADD above which the body resurfaces (Megyesi et al., 2005; Heaton et al., 2010; Mateus et al., 2013). Based on field observations, Mateus et al. (2013) report threshold values for ADD between 95 and 117 °C.days. Therefore, as shown in Figure S10 in Supplementary material D, we considered here a beta distribution for parameter $\alpha_1 / 2$ with parameters $\alpha = \beta = 1.8024$ over the range [95; 117].

For the coefficient μ characterizing the friction between a body and the riverbed, a uniform distribution was assumed over the range [0.3; 1], in line with ranges reported by Keller and Mitsch (1993) and Jonkman and Penning-Rowsell (2008).

	Variable	Symbol	Source	Observations	Distribution	Range	Parameters
Input data	Body height (Scenario "unknown body")	h_b	Van Der Heyden et al. (2018)	p_{25}, p_{50}, p_{75}, and average	Beta	[1.5; 2.05] m (male) [1.4; 1.9] m (female)	α = 5.8697, β = 6.075 (male) α = 3.976, β = 5.965 (female)
	BMI (Scenario "unknown body")	BMI	Van Der Heyden et al. (2018)	p_{25}, p_{50}, p_{75}, and average	Beta	[15; 40] kg/m²	α = 3.0102, β = 4.2628
	Body height ("known body")	h_b	What if scenario	Assumed mode, p_{10} and p_{90}	Beta	[1.5; 2.05] m	α = 116.8, β = 66.65
	Body mass ("known body")	m_b	What if scenario	Assumed mode, p_{10} and p_{90}	Beta	[40; 150] kg	α = 200, β = 467
	Swallowed water	dm / m_b	Modell and Davis (1969)	p_{86}	Beta	[0; 0.026]	α = 1.5 and β = 1.25
Model parameters	Drag coefficient	C_D	Laboratory experiments	Lab data (Figure S9)	Empirical	-	-
	Lift coefficient	C_L	Legendre and Magnaudet (1998)	C_L for a sphere for similar Re	Uniform	[0; 1]	-
	Added mass coefficient	C_A	Newman and Grue (2017)	Values for a cylinder and for a sphere	Uniform	[0.25; 1]	-
	Projection coefficient	f_p	Tanabe et al. (2000)	Range	Uniform	[0.16; 0.36]	-
	ADD Threshold value	α_1 / 2	Mateus et al. (2013)	Range	Beta	[95; 117]	$\alpha = \beta$ = 1.8024
	Friction coefficient	μ	Keller and Mitsch (1993), Jonkman and Penning-Rowsell (2008)	Range	Uniform	[0.3; 1]	-

Table 1: Considered distributions of uncertain inputs and parameters for adult subjects. Notations p_{25}, p_{50} and p_{75} refer to the percentiles 25, 50 and 75.

2.3.3 Variance-based sensitivity analysis

To quantify the sensitivity of the model outcomes to the uncertainties in input data and model parameters, we computed total order Sobol' indices (Sobol, 2001) either for individual uncertain variables (Section 3.2) or for groups of them (Section 3.3). In line with Arnst and Ponthot (2014), we proceeded in three steps:

- first, 20,000 runs of the model introduced in Section 2.1 were performed based on a reference sample generated by randomly assigning values to the uncertain variables listed in Table 1, according to their respective statistical distributions;
- next, to compute the Sobol' index associated to one specific (group of) uncertain variable(s), another series of 20,000 model runs (modified sample) was conducted, in which only the value(s) of the considered (group of) uncertain variable(s) was changed, while all other variables were kept at the same value as in the reference sample;
- the corresponding Sobol' index s_x was calculated as follows:

$$s_x = \frac{\frac{1}{2n}\sum_{i=1}^{n}(x_{b,ref,i} - x_{b,mod,i})^2}{Var(x_b)} \tag{12}$$

with n the size of the sample and x_b the body streamwise position at the considered time. Subscript *ref* refers to the reference sample, and subscript *mod* the modified sample.

The number of 20,000 runs was selected based on a convergence analysis of the model. As shown in Supplementary material E, the necessary number of runs to reach convergence depends on the considered parameter and type of body (e.g., gender). In the case of Sobol' index computation for parameter BMI in the scenario UB-HF (women), almost 10,000 runs are needed to reach convergence (Figure S11 in Supplementary material E). Therefore, we opted for a sample size of 20,000, composed of the same number of men and women.

2.4 Test program

Two flow scenarios and two types of body samples were considered in the analyses presented in Section 3.

A "high flow" (rapid) and a "low flow" (slow) scenario were tested. In the former case, the depth-averaged flow velocity was set to 0.12 m/s, while in the latter case it was taken equal to 3 m/s. Assuming a constant flow depth of 6 m, this corresponds to Froude numbers of 0.016 and 0.39, respectively. These values cover a plausible range for typical Froude numbers in lowland urban rivers. Using the body height as a characteristic length (Ungerechts, 1982), the corresponding Reynolds numbers are respectively of the order of 2×10^5 and 6×10^6 for the high and the low flow scenarios. Note that the assumed value of water depth has limited influence on the modelling results. This is mainly due to the very short duration of vertical motions (sinking or resurfacing) compared to other characteristic times.

As detailed in Section 2.3, the sample of bodies was assumed either completely unknown (e.g., no eyewitness testimony nor indications obtained from relatives), in which case the

distributions of body characteristics extend over a wide range, or the body was considered as relatively well known, with body characteristics spanning over narrower ranges. The body considered in this scenario is a body of 1.85 m and 73 kg irrespective of the gender.

Combining the two flow scenarios and the two types of body samples leads to four scenarios, with an "unknown" body in low flow scenario (UB-LF), "unknown" body in high flow scenario (UB-HF), "known" body in low flow scenario (KB-LF) and "known" body in high flow scenario (KB-HF).

The water density was assumed equal to 1000 kg/m³ and its temperature equal to 24°C. This value is realistic for summer conditions in some large urban rivers. Moreover, the choice of this value of water temperature has little influence on the conducted analyses. Indeed, water temperature is only involved in the estimation of ADD (Eq. (1) in Section 1.2), which is used here to linearly scale the time. Hence, in our study, assuming a smaller water temperature would only linearly shrink the horizontal axes of graphs displaying model results as a function of ADD (such as in Figure 4 hereafter).

Parameter z_0 in Eq. (11) was set equal to 1.3 mm, while parameter ε_{min} was set to 0.2 m. The presented computational results are based on 20,000 Monte Carlo runs, in which men and women are equally represented. This number was enough to ensure convergence of the results analysed here (Supplementary material E).

3 Results and discussion

The results are presented and discussed in two steps. First, an overview of the modelling results is presented through the evolution of the body streamwise position and its standard deviation (Section 3.1). The latter is an indicator of practical relevance as it reflects the extent over which search operations should be targeted. Second, the outcomes of the global sensitivity analyses are introduced, both for individual parameters (Section 3.2) and for groups of parameters (Section 3.3).

3.1 Body streamwise position

3.1.1 Model outcomes

The developed model predicts the evolution of body streamwise position and its relative positioning over the flow depth. In most Monte Carlo runs, the computed body trajectory involves sinking after a relatively short period (2 min ± 1 min), followed by bloating and finally resurfacing. The time elapsed until body resurfacing varies considerably: its median value is 95 hours, with a standard deviation of 16 h. In a limited number of runs (about 2 %), the computed trajectory remains at the water surface (no sinking). This occurs when the randomly selected combination of body characteristics (mass or BMI, heights …) leads to buoyancy exceeding the body submerged weight. Conversely, in few runs (less than 1 %), the model predicts body sinking and bloating but no resurfacing. Again, this results from a randomly selected combination of parameter values (deemed plausible) which led to buoyancy remaining insufficient to trigger resurfacing despite the effects of body decomposition.

Figure 3a displays statistics of body streamwise position as a function of time for scenario UB-HF. Similar figures related to the other scenarios are provided in Supplementary material F. The line corresponding to the median streamwise position shows a change in slope close to $t = 95$ h, which matches the median resurfacing time. The change of slope reflects contrasting body drift velocities depending on whether the body is close to the riverbed (no drift in low flow scenarios, and drift velocity of the order of 2 m/s in high flow scenarios) or near the free surface (drift velocity of the order of 0.1 m/s and 3 m/s in low and high flow scenarios, respectively). This considerable difference in drift velocity explains the observed rise in the dispersion of the body streamwise positions (see the interdecile range) when an increasing number of model runs predicts body resurfacing (Figure 3b). In Figure 3a, the lines representing the minimum and maximum streamwise positions correspond, respectively, to model runs in which the body does not resurface and does not sink.

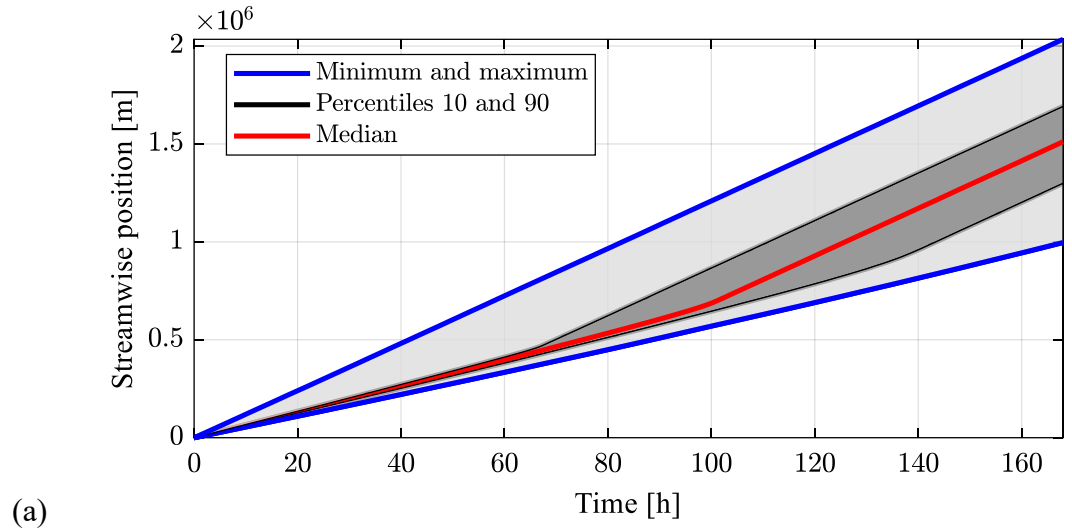

(a)

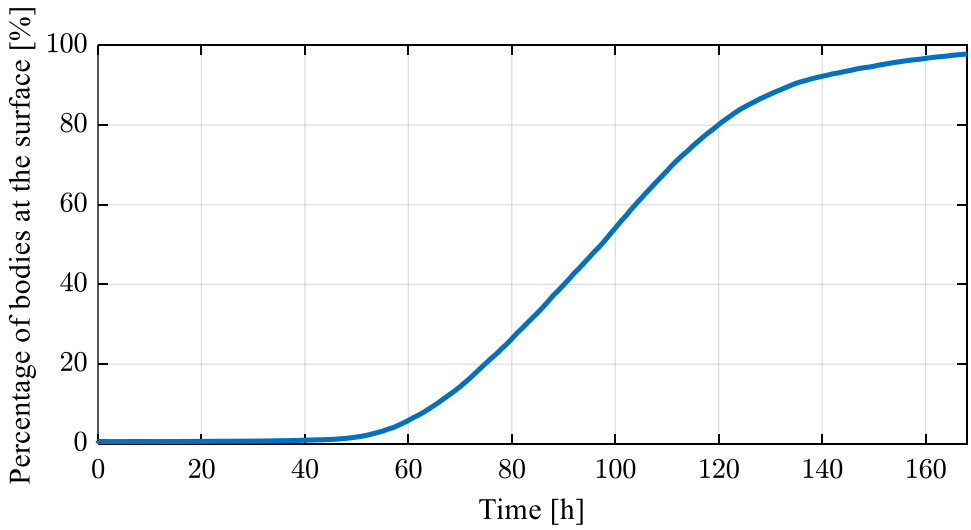

(b)

Figure 3: (a) Streamwise positions of bodies as a function of time in scenario UB-HF; (b) Percentage of bodies at the surface.

Figure 4 shows the evolution of the standard deviation of the body streamwise position as a function of ADD. Irrespective of the considered scenario, the standard deviation of the streamwise position follows the same pattern (Figure 4): a gradual increase (Stage 1), followed by a steeper increase (Stage 2), and eventually a milder increase and stabilisation (Stage 3).

Scenarios UB-LF and UB-HF lead to the highest values of standard deviation over the whole duration of the simulations compared to KB-LF and KB-HF, respectively. Moreover, the standard deviation continues to grow even in Stage 3. In Stage 1, the values of standard deviation obtained for scenarios KB-LF and KB-HF are considerably lower than in the other two scenarios. This difference is reduced in Stage 2. In Stage 3, the computed standard deviations for scenarios KB-LF and KB-HF become independent of time. This contrasts with the results obtained for scenarios UB-LF and UB-HF. The overall behaviour of the computed standard deviations does not change between the low and high flow scenarios, although the values are about 20 % higher in the latter case. Figure 4 highlights that the availability of data on the body characteristics of the victim is instrumental to reduce the level of uncertainty on the body streamwise position. This suggests that collecting testimonies of eyewitnesses giving information on the victim's height and mass (or BMI) is of high value in practice.

Note that the distinctive results obtained here for Scenarios KB-LF and KB-HF, when compared to Scenarios UB, are related to the fact that the chosen body characteristics in these scenarios ensure that there are no bodies which do not sink nor do not resurface. If the particular case of non-sinking or non-resurfacing body was selected in Scenarios KB-LF or KB-HF, three possible outcomes are possible:

- if non-sinking bodies are considered, the standard deviation of the streamwise position becomes quickly a constant as all the bodies tend to travel at the same velocity as the surface flow; the distribution of body streamwise position is unimodal;
- if only non-resurfacing bodies are considered, the distribution of body streamwise position may be either unimodal or bimodal depending on the relative importance of friction and drag forces. The balance of these forces controls whether a body remains at rest or moves on the bottom. The distribution of body streamwise position is bimodal if some of the considered bodies remain at rest while others travel close to the bottom. The distribution is unimodal if, either all considered bodies remain at rest on the bottom, or all of them move close to the bottom.

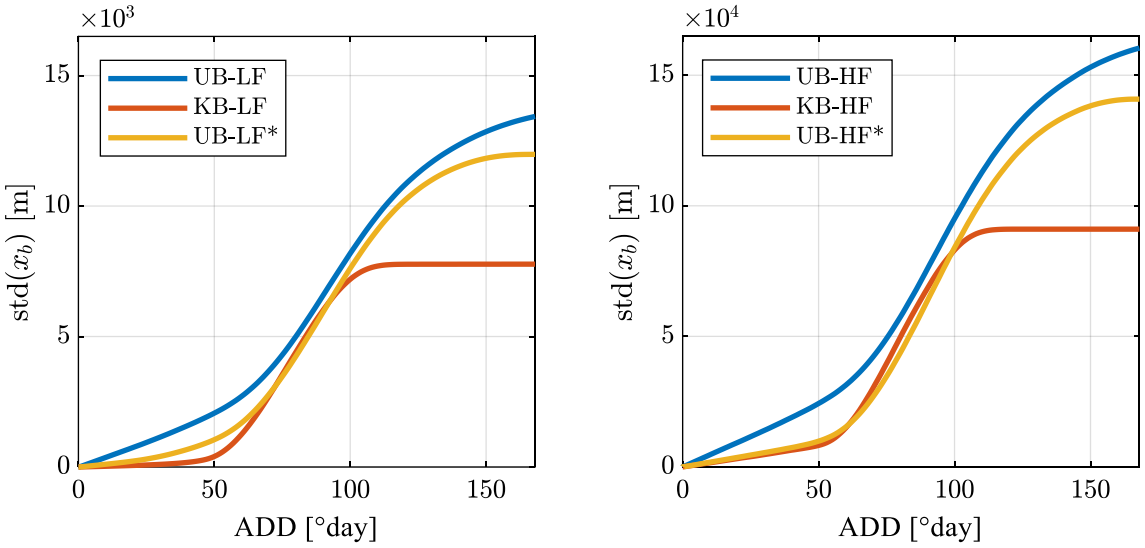

Figure 4: Standard deviation of the streamwise position of the bodies as a function of ADD.

3.1.2 Model runs without uncommon drowning process

As emphasized in Figure 3b, 3% of the sample does not follow the standard sequence of sinking, bloating, and resurfacing. Alternate scenarios labelled UB-LF* and UB-HF* displayed in Figure 4 represents results obtained with the same sample from which this 3% was removed. Note that this share of model runs is comparatively lower than the value of 7 % mentioned by Donoghue and Minnigerode (1977), but it remains plausible. Indeed, unlike in Donoghue and Minnigerode (1977), we focus here on drowned bodies and we consider that water is swallowed and inhaled at the moment of drowning, which tends to reduce the buoyancy.

Relying on the previous analysis of KB scenarios, we hypothesize that the reason why the standard deviation of the streamwise position does not reach a constant value in Stage 3 (scenarios UB-LF and UB-HF in Figure 4) is precisely linked to these specific cases for which no sinking nor resurfacing of the body is computed, with the standard-deviation of UB scenarios keeping increasing due to the non-resurfacing bodies. Figure 5 also hints into this direction, as it reveals a bimodal distribution of the body streamwise position, with a few model runs predicting a significantly larger travel distance due to the absence of body sinking in these runs. For longer time horizons, a third mode in the distribution may also arise due to body trajectories involving sinking but no resurfacing.

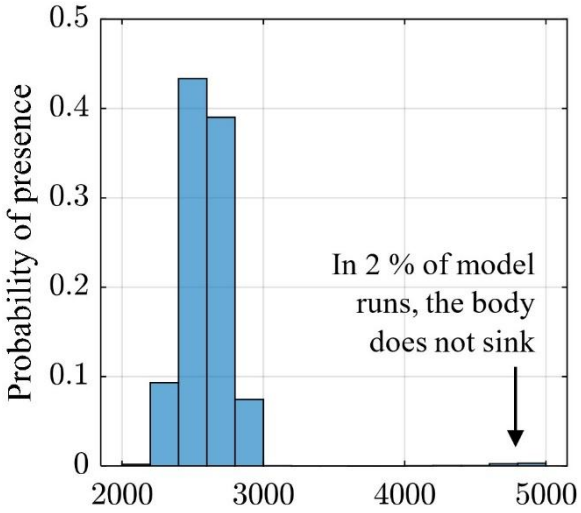

Figure 5: Distribution of body streamwise position computed for scenario UB-HF after 30 min

Therefore, for scenarios UB-LF and UB-HF, the standard deviation of the body streamwise position was recomputed by discarding the cases in which the model did not predict body sinking nor resurfacing.

The results for scenarios UB-LF* and UB-HF* are the following: in Stage 1, the standard deviation remains relatively low; in Stage 2, it is lower than in scenarios UB-LF and UB-HF; and in Stage 3 the standard deviation becomes also independent of time like in scenarios KB-LF and KB-HF (although about 50 °days later). This confirms that the absence of stabilization of the standard deviation in scenarios UB-LF and UB-HF is solely due to a small portion of model runs in which the model does not predict body sinking or resurfacing, combined with the considerable difference in drift velocity between bodies remaining at (or near) the surface, and those situated close to the riverbed. This is further analysed in the next section.

3.1.3 Interpretation

Figure 6 shows the time derivative of the standard deviation of the body streamwise position as a function of the standard deviation of the relative elevation of the bodies in the flow depth. The latter quantity reflects the dispersion in body elevations in the various model runs, i.e., the dispersion between “slowly-drifting” bodies located close to the bed and “fast-drifting” bodies positioned near the surface.

Figure 6 highlights that in every scenario the standard deviation of the streamwise position first rises at an increasing rate, as a rising number of model runs predict body resurfacing while some model runs still predict that the body remains close to the bed. Next, the rate of increase of the standard deviation of the body streamwise position becomes constant or nearly constant, as the dispersion in the vertical body positioning decreases. This is because virtually all model runs predict body resurfacing.

In scenarios KB-LF and KB-HF, as well as UB-LF* and UB-HF*, the rate of change of the standard deviation of the body streamwise position ends up at zero, consistently with Figure 4.

For scenarios UB-LF and UB-HF, neither the standard deviation of the vertical body position nor the rate of change of the standard deviation of the body streamwise position decline to zero, which is also in agreement with Figure 4.

From a practical perspective, this highlights that the uncertainty on the body streamwise position is strongly influenced by the uncertainty in its vertical position, and hence the need for reliably simulating the body decomposition process, which controls the body vertical motion.

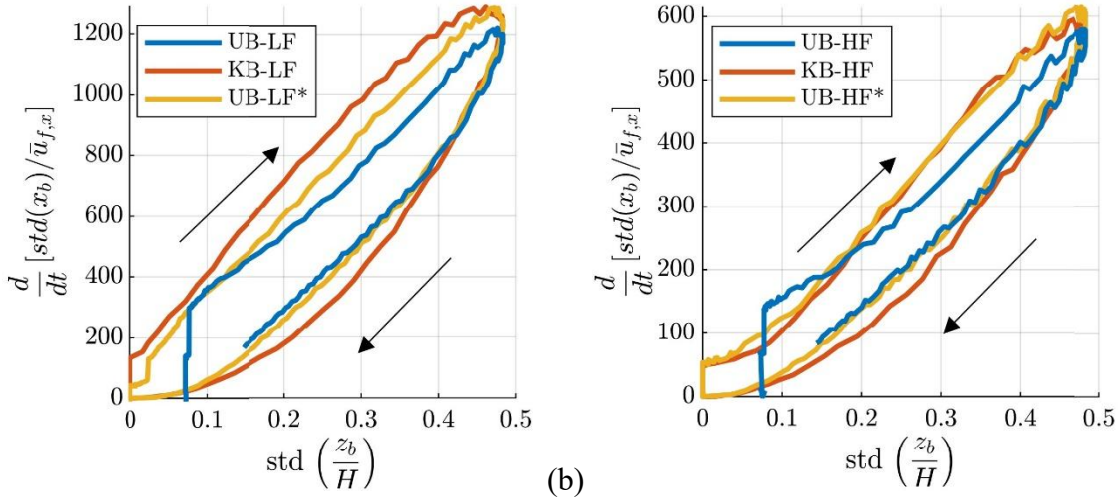

Figure 6: Time derivative of the standard deviation of the streamwise position of the bodies over average flow velocity in the streamwise direction as a function of the standard deviation of the vertical position over the water depth.

3.2 Sobol' indices for individual parameters

Sobol' indices were computed for scenarios UB-LF, UB-HF, KB-LF and KB-HF (Figure 7) considering three different settings:

- over a short time horizon (t = 5 min) and assuming no sinking, i.e., the components along z in Eqs. (9)-(10) are not solved and the body is assumed to remain at the surface,
- over an intermediate time horizon (t = 1 h, i.e., typical duration after which initial search operations are stopped), accounting for sinking but not for body decomposition, i.e., Eq. (7) is not solved and, after sinking, the body is assumed to remain on the river bottom,
- over a longer time horizon (t = 7 days), accounting for sinking and body decomposition.

According to Figure 4, the 7-day time horizon is long enough to ensure that the standard deviation of the body streamwise position becomes independent of time in Scenarios KB-LF and KB-HF. In all cases, Sobol' indices were computed separately for men and women as uncertainty on body height and weight are gender dependent.

3.2.1 Short time horizon

Irrespective of the scenario and of the victim's gender, Figure 7 reveals that, over a short time horizon (t = 5 min), the most influential uncertainties arise from the projection factor, the drag coefficient C_D and the added mass coefficient C_A (Sobol' indices between 0.8 and 1).

Uncertainties in the BMI and/or body mass, and body height, as well as the amount of swallowed water also have a substantial influence (Sobol' indices 0.4 and 0.8). This is consistent with the processes controlling the initial horizontal body acceleration, i.e., the drag force and body inertia. The other potential sources of uncertainties (μ, C_L and α_1) have no influence on the results since the vertical motion was not considered for this short time horizon.

3.2.2 Intermediate time horizon

For the intermediate time horizon (t = 1h), in which body decomposition and resurfacing are not considered, uncertainties in body height, BMI and amount of swallowed water have an overwhelming influence in the case of Scenarios UB-LF and UB-HF, with Sobol' indices close to 0.9 for BMI, of the order of 0.4 for *dm* and ranging between 0.3 and 0.7 for h_b. The value of Sobol' index related to all other model parameters remains below 0.1 (Figure 7a and b). In Scenario UB-LF, the value of the Sobol' indices for these other model parameters are even very close to zero (Figure 7a). This is because, after sinking, the simulated bodies tend to remain at rest on the bottom in the scenario involving low flow conditions (UB-LF), as can be seen in Figure S12 in Supplementary material F, whereas they move on the bottom in the other scenario (UB-HF, Figure 3a).

In Scenarios KB-LF and KB-HF, a very small uncertainty is assigned to the input data (h_b and m_b) corresponding to those which show a dominating influence in Scenarios UB-LF and UB-HF, i.e., h_b and m_b or BMI. This difference in the parameters uncertainty explains the smaller corresponding Sobol' indices obtained in the former cases. In Scenarios KB-LF and KB-HF, uncertainties in several parameters (μ, C_D, f_p, C_A) have a strong influence on the model outcomes, while their effects were overshadowed in Scenarios UB-LF and UB-HF due to the assumed large uncertainties in h_b and BMI. The influence of uncertainty in the amount of swallowed water remains also large.

This can be interpreted as follows. In the KB-LF and KB-HF scenarios, the body height and mass vary little (Figure S13 and Figure S14 in Supplementary material F), so that variations in the body density remain also very limited. Hence, since the body density (close to 1015 kg/m³ in our example) remains similar to the water density, small variations in other vertical forces such as the lift have a high chance to completely change the vertical equilibrium, and hence either induce or prevent sinking of the body. Similarly, due to the small buoyancy effect, slight changes in drag force (influenced by C_D and f_p) may trigger, prevent, or alter body motion on the bottom (even in the KB-LF Scenario). This is the reason why uncertainties in the friction coefficient have also a large influence on the results in this scenario.

3.2.3 Long time horizon

For Scenario UB-LF and UB-HF, over a long time horizon (t = 7 days), the uncertainties significantly influencing the body motion are those related to input data and model parameters ruling body resurfacing: BMI, body height, amount of swallowed water and the threshold value of ADD. In Scenarios KB-LF and KB-HF, the most influencing uncertainties remain the same except for body height and mass which become negligible. The differences in the results for female and male victims stem from the gender-dependent empirical closures used to estimate body volume (Section 2.2).

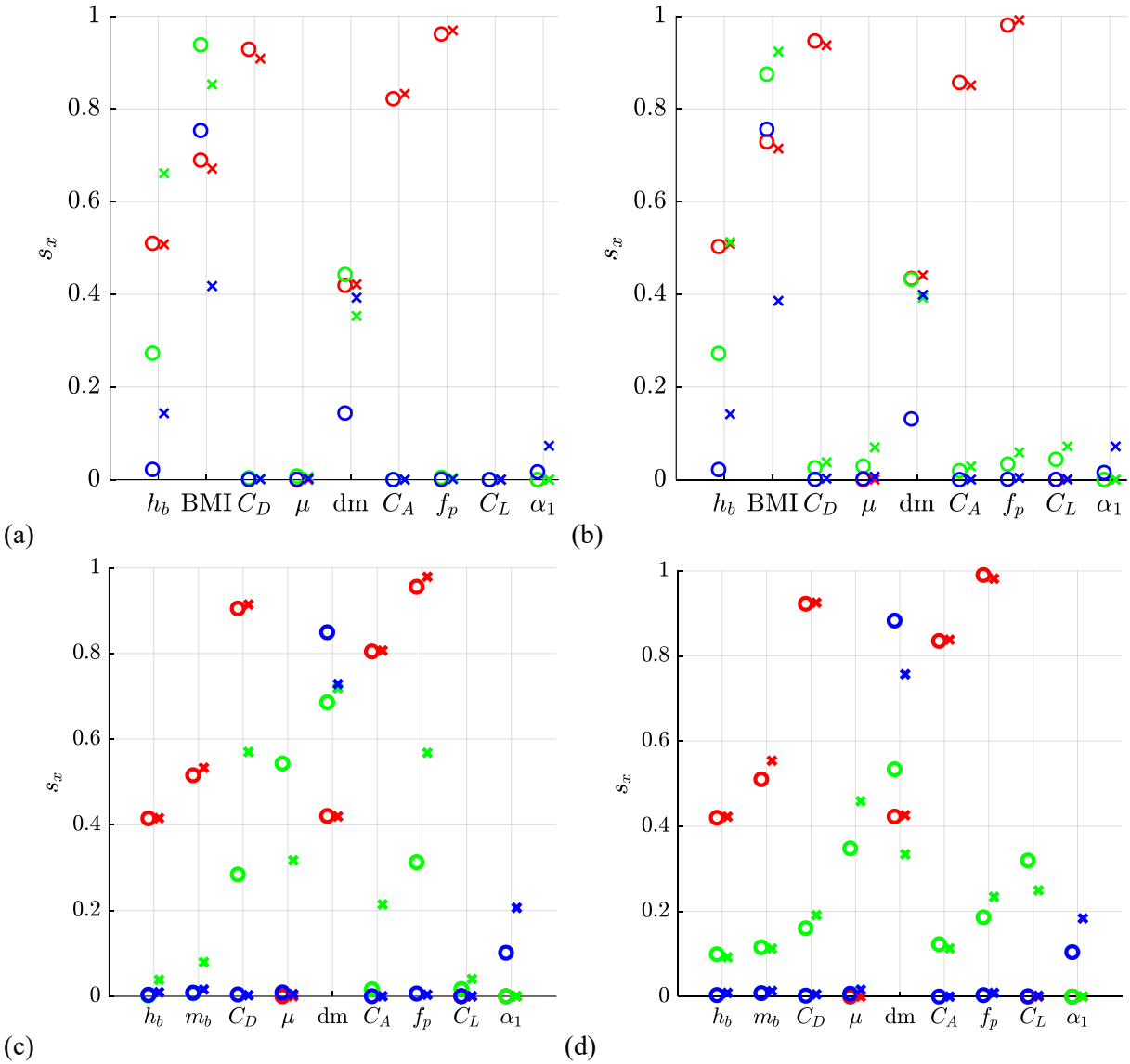

Figure 7: Sobol' indices for Scenarios (a) UB-LF, (b) UB-KF, (c) KB-LF and (d) KB-HF. Red corresponds to the short time horizon (t = 5 min, without sinking), green to the intermediate time horizon (t = 1 h, without resurfacing), and blue to the long time horizon (t = 7 days). Results for male bodies are represented by circles (○) and for female bodies by crosses (×).

3.3 Sobol' indices for groups of parameters

As the interpretation of Sobol' indices evaluated for individual parameters remains intricate due to the number of uncertain parameters, we repeated the procedure for groups of parameters. The following three groups of parameters were considered:

- morphological parameters: h_b, and m_b or *BMI*
- hydrodynamic (flow-body interaction) parameters: C_D, C_A, C_L, and f_p
- internal body parameters: *dm* and α_1.

For the low flow scenario and a short time horizon (t = 5min, without sinking), Figure 8a and Figure 8b show that uncertainties in the hydrodynamic parameters are responsible for most of

the variability in the body horizontal position. The morphological parameters also have an influence through the frontal area and the body inertia, while the internal body parameter *dm* influences the body inertia, hence its initial acceleration. In Scenario KB-LF, uncertainty in morphological parameters is small and it is responsible for limited variations in the body streamwise position. Nonetheless, since the overall variance of body positions over a short time horizon of 5 min is also limited, the Sobol' index still reveals a substantial contribution of these morphological parameters to the overall uncertainty.

Conversely, for the low flow scenario and a long time horizon (t = 7 days – Figure 8c and Figure 8d), the most influential source of uncertainty in Scenario UB-LF is related to the morphological parameters, followed by those on the internal body parameters. The Sobol' indices related to the hydrodynamic parameters are close to zero irrespective of the gender. These results agree with those obtained for the Sobol' indices for individual parameters, and they appear sensible. Indeed, the morphological parameters (body height and BMI) have a direct influence on the body volume, and hence on both the buoyancy (controlling the sinking and resurfacing processes) as well as the Coulomb-type friction force (influenced by buoyancy). Conversely, the acceleration phases, controlled by the hydrodynamic parameters, are of particularly short duration compared to the time horizon considered here, so that the influence of the hydrodynamic parameters becomes negligible.

In contrast, in Scenario KB-LF, the sensitivity to the uncertainty in the morphological parameters is considerably reduced (Figure 8d), and only the internal body parameters show a significant influence since they control the resurfacing process.

Results for the intermediate time horizon (t = 1 h, without resurfacing) as well as for the high flow scenarios can be found in Supplementary material G.

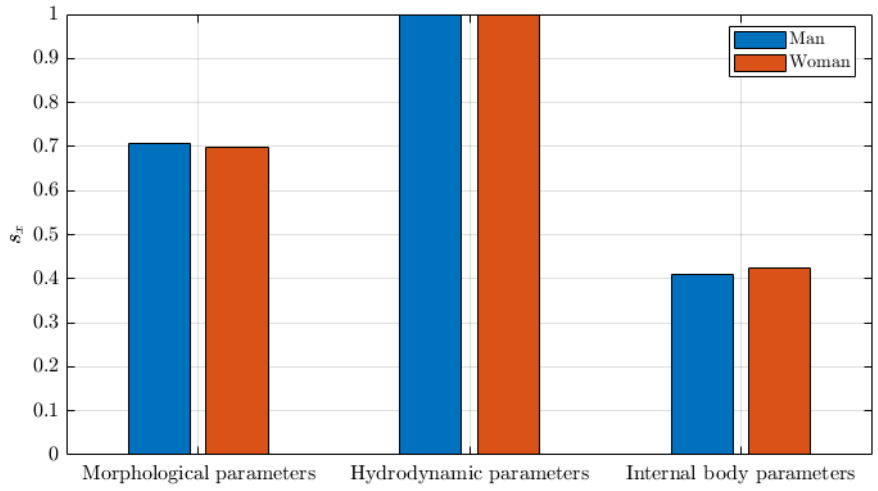

(a) Scenario UB-LF, t = 5 min

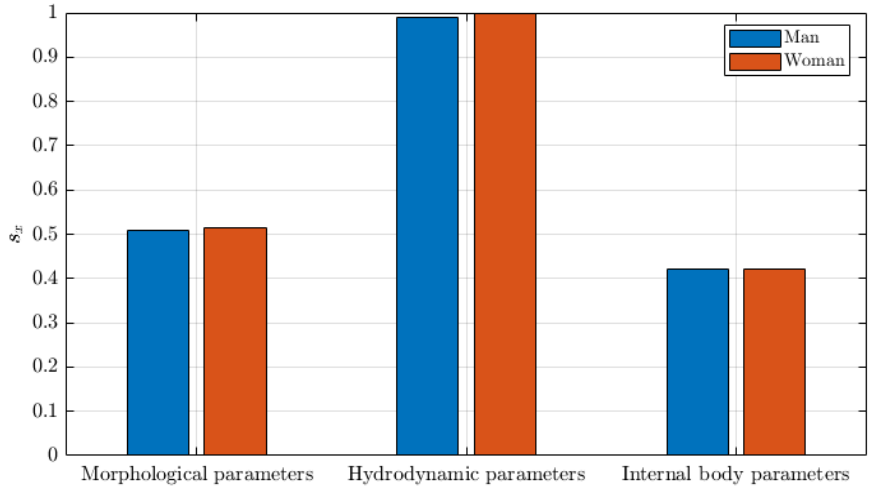

(b) Scenario KB-LF, t = 5 min

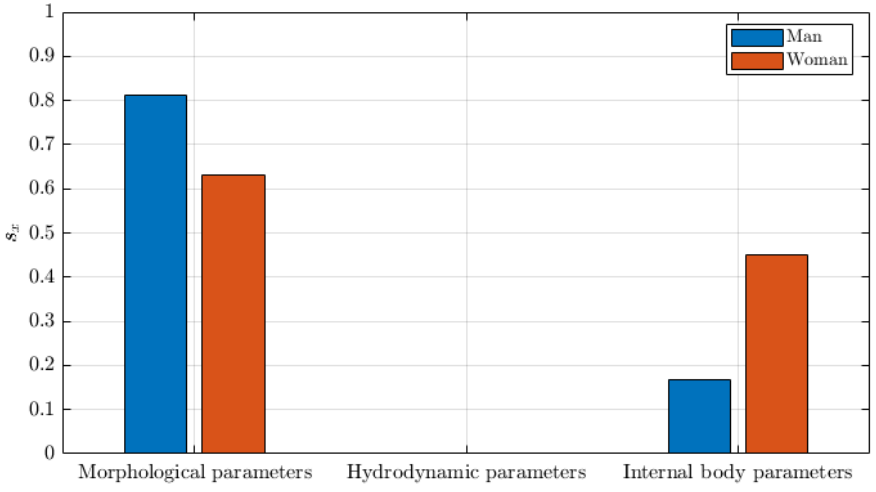

(c) Scenario UB-LF, t = 7 days

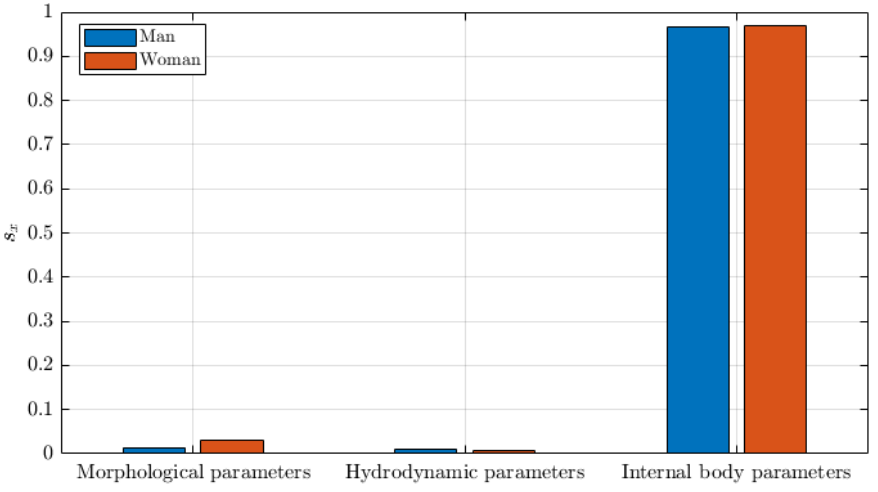

(d) Scenario KB-LF, t = 7 days

Figure 8: Sobol' index for groups of uncertain parameters

4 Conclusion

Existing computational models aiming at predicting the drift of a victim of drowning were mostly developed for marine environments. As such, they do not reproduce the typical pattern followed by a body drowned in a river, i.e., sinking, bloating and resurfacing. Computing the body position over the flow depth is instrumental for predicting the body streamwise position due to the considerable difference in drift velocity between a floating body and a body sliding or rolling on the riverbed. Empirical knowledge in forensic medicine indicates that the body bloating kinetics is controlled by both time and water temperature, and it can be related to the number of accumulated degree days (ADD).

Key findings

We propose here a first formulation of a mathematical model which enables reproducing this pattern. The newly introduced equation describes the evolution of the body volume under the competing influences of body decomposition and external hydrostatic pressure. This new component of the model relies on a limited number of parameters, which all have a physical interpretation: the initial void fraction in the body, a maximal body expansion rate, and a threshold value for ADD.

The model was analysed in detail for idealized flow conditions corresponding to a uniform (i.e., steady and fully-developed) flow. Two flow scenarios were considered (low and high flow). Given the uncertainties affecting the knowledge of body characteristics and model parameters in real-world situations, a stochastic framework was adopted, in which statistical distributions were assumed for the uncertain input data and model parameters. It led to the following findings:

- In the tested cases, the variance of the computed body streamwise positions is reduced by a factor of the order of two if precise information (height, mass) is available on the characteristics of the victim. This highlights the critical importance of testimonies by eyewitnesses of the accidents or by relatives of the victim.
- The computed distribution of body streamwise position is generally multimodal, with one mode corresponding to model runs in which the body does not sink, the main one related to the standard pattern of sinking, bloating and resurfacing, and in rare cases a third mode corresponding to model runs in which the body does not resurface.
- By means of global sensitivity analysis, we highlighted the relative importance of each source of uncertainty. For a short time horizon, i.e., prior to body sinking, the parameters controlling the estimation of drag force and body inertia are the most influential ones since the dominating process during this phase is body acceleration to reach the flow velocity. For longer time horizons, uncertainties in parameters ruling the evolution of body density tend to be very influential since they directly affect the occurrence of sinking and/or resurfacing as well as the Coulomb-type friction force on the riverbed.

- When the body characteristics are assumed highly uncertain, the impact of their uncertainty overwhelm most other sources of uncertainties. This points again at the importance of collecting high-quality information on the victim (e.g., through testimonies).

Remaining challenges

Remaining scientific challenges are numerous. In priority, the model needs to be extended to more general flow settings. The proposed Lagrangian model may be coupled with flow field information irrespective of how the flow field data was generated (e.g., 1D, 2D, or 3D Eulerian modelling). However, specific challenges remain to be addressed, such as modelling the interaction between a drifting body and riverbanks, bridge piers or other obstacles. Whether common river hydrodynamic models provide a sufficient resolution of the flow field at specific locations, such as in the wake of a bridge pier, needs to be investigated. Such questions were partly addressed for the drift of logs in rivers (Ruiz-Villanueva et al., 2014; Persi et al., 2018); but the methods need to be transferred to the case of the drift of a human body. If a 2D Eulerian hydrodynamic model is used, questions arise regarding the parametrization of complex velocity profile over the flow depth in the near-field of structures such as bridge piers, abutments, or weirs …

The influence of turbulence should be considered more explicitly in the model. In the current mathematical formulation, effects of turbulence are only implicitly embedded in the assumed distribution of flow velocity over the depth, as expressed by Eq. (3). However, the randomness arising from turbulence is not yet reflected in the drift model. This may lead to underestimations of the variability in body location. Several options exist to account for the turbulence-induced randomness in body trajectories, such as adding stochastic perturbations to the body position, velocity, or acceleration. These approaches are referred to as "Markov models" of varying order (Berloff and McWilliams, 2002; Reijnders et al., 2022). Previous studies of human body drift in oceans have focused only on random walk approaches (e.g., Carniel et al., 2002). A different approach was used by Ruiz-Villanueva et al. (2014) for simulating the transport of tree logs in turbulent open-channel flow. They added stochastic fluctuations not to the object velocity but to the flow velocity used in the Lagrangian momentum equation. These fluctuations could be calculated from the turbulence model used in the Eulerian flow computation (e.g., k-ε model) and a random number. We recommend transposing this approach to the case of human body drift in rivers. In this way, identical bodies dropped at the same spot would follow various trajectories, which would differ more if the flow turbulence intensity is higher.

There is also room for improvement in the Lagrangian drift model itself. So far, neither the body orientation (roll, pitch, and yaw angles) nor possible posture deformations are explicitly predicted by the model. Also, the model does not account for existing correlations between parameters such as drag or added mass coefficients and the body characteristics (height, mass). The same applies for correlations between the victim's age and body density (Durnin and Womersley, 1974), or the influence of clothing. Tackling these challenges requires more transdisciplinary research involving expertise in forensic medicine, river hydrodynamics, uncertainty quantification as well as experimental techniques for conducting laboratory and

field observations (e.g., using carefully designed dummies able to mimic the behaviour of a human body).

Validation of the presented model against field data will be a cornerstone of further model development and its establishment as a tool to guide rescue and search operations in urban rivers. Gathering the necessary data and developing the framework for model validation also requires interdisciplinary and intersectoral collaborations with forensic medicine, first responders (police, fireplace brigade, civil safety), water authorities and courts.

Although additional practical challenges need to be overcome, related to computational efficiency and data assimilation, among other aspects, this research paves the way for more effective planning of rescue and, above all, search operations for the sake of reducing risks taken by first responders and reducing the time of body retrieval.

Data and software availability statement

Data and software were not used, nor created for this research.

Acknowledgement

The first author gratefully acknowledges a fellowship received through a grant *Fonds Spéciaux pour la Recherche* (FSR) of the School of Engineering of the University of Liege. The authors thank to Dr. Philipp Selzer for his valuable feedback on an early version of the manuscript.

References

Abston, E., Comellas, A., Reed, R.M., Kim, V., Wise, R.A., Brower, R., Fortis, S., Beichel, R., Bhatt, S., Zabner, J., Newell, J., Hoffman, E.A., Eberlein, M., 2017. Higher BMI is associated with higher expiratory airflow normalised for lung volume (FEF25–75/FVC) in COPD. BMJ Open Respiratory Research 4, e000231.

Arnst, M., Ponthot, J.-P., 2014. An overview of nonintrusive characterization, propagation, and sensitivity of uncertainties in computational mechanics 4, 387–421.

Berloff, P.S., McWilliams, J.C., 2002. Material Transport in Oceanic Gyres. Part II: Hierarchy of Stochastic Models. Journal of Physical Oceanography 32, 797–830.

Bierens, J.J.L.M., 2015. Drowning: Prevention, Rescue, Treatment, 2nd ed. 2014 édition. ed. Springer-Verlag Berlin and Heidelberg GmbH & Co. K, New York.

Blondel, P., 2014. Searching for Dead Bodies with Sonar, in: DrowningPrevention,Rescue,Treatment. Springer-Verlag Berlin and Heidelberg GmbH & Co. K, New York, pp. 1161–1165.

Breivik, Ø., Allen, A.A., 2008. An operational search and rescue model for the Norwegian Sea and the North Sea. Journal of Marine Systems 69, 99–113.

Carniel, S., Umgiesser, G., Sclavo, M., Kantha, L.H., Monti, S., 2002. Tracking the drift of a human body in the coastal ocean using numerical prediction models of the oceanic, atmospheric and wave conditions. Science & Justice: Journal of the Forensic Science Society 42, 143–151.

Chen, Q., Xia, J., Falconer, R.A., Guo, P., 2019. Further improvement in a criterion for human stability in floodwaters. Journal of Flood Risk Management 12, e12486.

Daalen, M.A. van, Kat, D.S. de, Oude Grotebevelsborg, B.F.L., Leeuwe, R. de, Warnaar, J., Oostra, R.J., M Duijst-Heesters, W.L.J., 2017. An Aquatic Decomposition Scoring Method to Potentially Predict the Postmortem Submersion Interval of Bodies Recovered from the North Sea. Journal of Forensic Sciences 62, 369–373.

Delhez, C., Erpicum, S., Dewals, B., 2021. Hydrodynamic characterisation of a body-like shape: a contribution to guide the search for victims of drowning in rivers.

Donoghue, E.R., Minnigerode, S.C., 1977. Human body buoyancy: a study of 98 men. Journal of Forensic Sciences 22, 573–579.

Du Bois, D., Du Bois, E.F., 1989. A formula to estimate the approximate surface area if height and weight be known. 1916. Nutrition (Burbank, Los Angeles County, Calif.) 5, 303–311; discussion 312–313.

Durnin, J.V.G.A., Womersley, J., 1974. Body fat assessed from total body density and its estimation from skinfold thickness: measurements on 481 men and women aged from 16 to 72 Years. British Journal of Nutrition 32, 77–97.

Ebbesmeyer, C.C., Haglund, W.D., 1994. Drift trajectories of a floating human body simulated in a hydraulic model of Puget Sound. Journal of Forensic Sciences 39, 231–240.

Ghaffarian, H., Lopez, D., Mignot, E., Piegay, H., Riviere, N., 2020. Dynamics of floating objects at high particulate Reynolds numbers. Physical Review Fluids 5, 054307.

Goeury, C., Bacchi, V., Zaoui, F., Bacchi, S., Pavan, S., Abderrezzak, K. El kadi, 2022. Uncertainty Assessment of Flood Hazard Due to Levee Breaching. Water 14, 3815.

Gonzalez, J.R.P., Escobar-Vargas, J., Vargas-Luna, A., Castiblanco, S., Trujillo, D., Guatame, A.C., Corzo, G., Santos, G., Perez, L.A., 2022. Hydroinformatics tools and their

potential in the search for missing persons in rivers. Forensic Science International 111478.

Gunduz, M., 2017. Possible recovery site of four non-recovered bodies lost in the Marmara Sea by using an ocean circulation model. Australian Journal of Forensic Sciences 49, 154–160.

Hart-Davis, M.G., Backeberg, B.C., 2023. Towards a particle trajectory modelling approach in support of South African search and rescue operations at sea. Journal of Operational Oceanography 16, 131–139.

Hayman, J., Oxenham, M., 2016. Supravital Reactions in the Estimation of the Time Since Death (TSD), in: HumanBodyDecomposition. Elsevier, pp. 1–12.

Heaton, V., Lagden, A., Moffatt, C., Simmons, T., 2010. Predicting the Postmortem Submersion Interval for Human Remains Recovered from U.K. Waterways*. Journal of Forensic Sciences 55, 302–307.

Horn, K., 2014. Underwater Search and Evidence Response Teams, in: Drowning. Springer-Verlag Berlin and Heidelberg GmbH & Co. K, New York, pp. 1175–1177.

Jonkman, S. n., Penning-Rowsell, E., 2008. Human Instability in Flood Flows. JAWRA Journal of the American Water Resources Association 44, 1208–1218.

Kaatsch, H.-J., Schmidtke, E., Nietsch, W., 1994. Photometric measurement of pressure-induced blanching of livor mortis as an aid to estimating time of death: Application of a new system for quantifying pressure-induced blanching in lividity. International Journal of Legal Medicine 106, 209–214.

Keller, R.J., Mitsch, B., 1993. Safety aspects of the design of roadways as floodways, Research report / Urban Water Research Association of Australia. Published for the Urban Water Research Association of Australia, by the Melbourne Water Corporation, Melbourne.

Lazzarin, T., Viero, D.P., Molinari, D., Ballio, F., Defina, A., 2022. A new framework for flood damage assessment considering the within-event time evolution of hazard, exposure, and vulnerability. Journal of Hydrology 615, 128687.

Legendre, D., Magnaudet, J., 1998. The lift force on a spherical bubble in a viscous linear shear flow. Journal of Fluid Mechanics 368, 81–126.

Ličer, M., Estival, S., Reyes-Suarez, C., Deponte, D., Fettich, A., 2020. Lagrangian modelling of a person lost at sea during the Adriatic scirocco storm of 29 October 2018. Natural Hazards and Earth System Sciences 20, 2335–2349.

Liu, X., Niu, J., Ran, L., Liu, T., 2017. Estimation of Human Body Volume (BV) from Anthropometric Measurements Based on Three-Dimensional (3D) Scan Technique. Aesthetic Plastic Surgery 41, 971–978.

Lunetta, P., Ebbesmeyer, C., Molenaar, J., 2014. Behaviour of Dead Bodies in Water, in: Drowning. Springer-Verlag Berlin and Heidelberg GmbH & Co. K, New York, pp. 1149–1152.

Mateus, M., Pablo, H. de, Vaz, N., 2013. An investigation on body displacement after two drowning accidents. Forensic Science International 229, 6–12.

Mateus, M., Pinto, L., Chambel-Leitão, P., 2015. Evaluating the predictive skills of ocean circulation models in tracking the drift of a human body: a case study. Australian Journal of Forensic Sciences 47, 322–331.

McDonald, J.B., Xu, Y.J., 1995. A generalization of the beta distribution with applications. Journal of Econometrics 66, 133–152.

Megyesi, M.S., Nawrocki, S.P., Haskell, N.H., 2005. Using accumulated degree-days to estimate the postmortem interval from decomposed human remains. Journal of forensic sciences 50, 618–626.

Meissner, C., Sporer, S., Schooler, J., 2007. Person description as eyewitness evidence, in: Handbook eyewitness psychology: MemoryPeople. Lawrence Earlbaum & Associates, pp. 3–34.

Meninno, S., Persi, E., Petaccia, G., Sibilla, S., Armanini, A., 2020. An experimental and theoretical analysis of floating wood diffusion coefficients. Environmental Fluid Mechanics 20, 593–617.

Metropolis, N., Ulam, S., 1949. The Monte Carlo Method. Journal of the American Statistical Association 44, 335–341.

Milanesi, L., Pilotti, M., Ranzi, R., 2015. A conceptual model of people's vulnerability to floods. Water Resources Research 51, 182–197.

Miller, M.R., 2005. Standardisation of spirometry. European Respiratory Journal 26, 319–338.

Modell, J.H., Davis, J.H., 1969. Electrolyte changes in human drowning victims. Anesthesiology 30, 414–420.

Mosteller, R.D., 1987. Simplified calculation of body-surface area. The New England Journal of Medicine 317, 1098.

Musolino, G., Ahmadian, R., Xia, J., Falconer, R.A., 2020. Mapping the danger to life in flash flood events adopting a mechanics based methodology and planning evacuation routes. Journal of Flood Risk Management 13.

Newman, J.N., Grue, J., 2017. Marine hydrodynamics, 40th anniversary edition. ed. The MIT Press, Cambridge, Massachusetts.

Papadodima, S.A., Athanaselis, S.A., Skliros, E., Spiliopoulou, C.A., 2010. Forensic investigation of submersion deaths. International Journal of Clinical Practice 64, 75–83.

Persi, E., Petaccia, G., Sibilla, S., 2018. Large wood transport modelling by a coupled Eulerian–Lagrangian approach. Natural Hazards 91, 59–74.

Pope, S.B., 2000. Turbulent Flows, 1st ed. Cambridge University Press.

Ray, S., 2014. Training and Equipping Rescue Personnel for Flood Rescue, in: Bierens, J.J.L.M. (Ed.), DrowningPrevention,Rescue,Treatment. Springer, Berlin, Heidelberg, pp. 491–494.

Reijnders, D., Deleersnijder, E., Van Sebille, E., 2022. Simulating Lagrangian Subgrid-Scale Dispersion on Neutral Surfaces in the Ocean. Journal of Advances in Modeling Earth Systems 14.

Rouse, H., 1950. Engineering Hydraulics, Hoboken. John Wiley & Sons.

Ruiz-Villanueva, V., Bladé, E., Sánchez-Juny, M., Marti-Cardona, B., Díez-Herrero, A., Bodoque, J.M., 2014. Two-dimensional numerical modeling of wood transport. Journal of Hydroinformatics 16, 1077–1096.

Sendroy, J., Collison, H.A., 1965. Determination of human body volume from height and weight. NAVAL MEDICAL RESEARCH INST BETHESDA MD.

Simpkins, G., 2017. Increasing river flood risk. Nature Climate Change 7, 172–172.

Sobol, I.M., 2001. Global sensitivity indices for nonlinear mathematical models and their Monte Carlo estimates. Mathematics and Computers in Simulation, The Second IMACS Seminar on Monte Carlo Methods 55, 271–280.

Stephenson, L., Stockham, P., Heuvel, C. van den, Byard, R.W., 2020. Characteristics of drowning deaths in an inner city river. Legal Medicine 47, 101783.

Stocks, J., Quanjer, P.H., 1995. Reference values for residual volume, functional residual capacity and total lung capacity. ATS Workshop on Lung Volume Measurements. Official Statement of The European Respiratory Society. European Respiratory Journal 8, 492–506.

Tanabe, S., Narita, C., Ozeki, Y., Konishi, M., 2000. Effective radiation area of human body calculated by a numerical simulation. Energy and Buildings 32, 205–215.

Tikuisis, P., Meunier, P., Jubenville, C., 2001. Human body surface area: measurement and prediction using three dimensional body scans. European Journal of Applied Physiology 85, 264–271.

Tipton, M.J., Golden, F.S.C., 2011. A proposed decision-making guide for the search, rescue and resuscitation of submersion (head under) victims based on expert opinion. Resuscitation 82, 819–824.

Tu, H., Wang, X., Mu, L., Xia, K., 2021. Predicting drift characteristics of persons-in-the-water in the South China Sea. Ocean Engineering 242, 110134.

Ungerechts, B., 1982. The Validity of the Reynolds Number for Swimming Bodies Which Change Form Periodically.

Van Der Heyden, J., Nguyen, D., Renard, F., Scohy, A., Demarest, S., Drieskens, S., Gisle, L., 2018. Enquête de santé par examen belge.

Vezin, P., Verriest, J.-P., 2007. Vezin- 1 Development of a Set of Numerical Human Models for Safety.

WHO, 2014. Global report on drowning: preventing a leading killer.

Wu, J., Cheng, L., Chu, S., 2023. Modeling the leeway drift characteristics of persons-in-water at a sea-area scale in the seas of China. Ocean Engineering 270, 113444.

Youssef, M., 2012. Analyse de l'influence des paramètres structuraux et fonctionnels d'une cage thoracique sous chargement dynamique a l'aide d'un modèle simplifié.

A. Complement to the description of the methodology

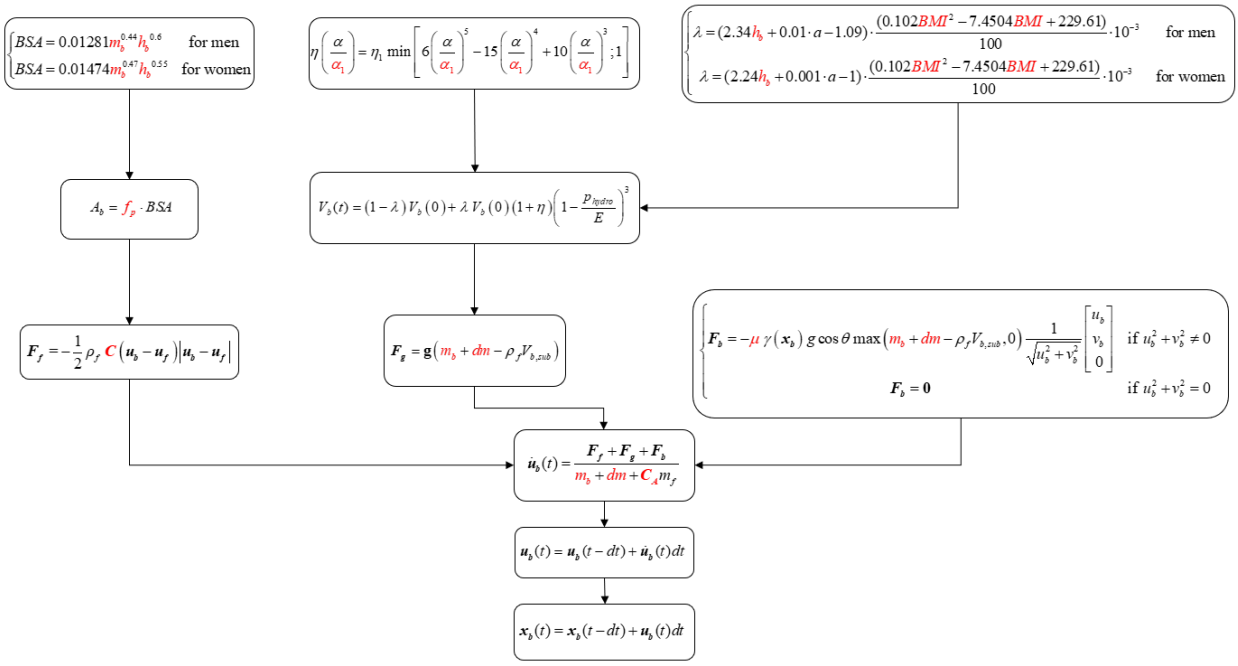

Figure S1: Workflow of equations used in the model.

B. Complements to model formulation

Function $\gamma(\boldsymbol{x_b})$ is parametrized as follows (Figure S2):

$$\gamma(\mathbf{x_b}) = \begin{cases} 1 - \dfrac{z_b - b(x_b, y_b)}{\varepsilon_{max}} \dfrac{\varepsilon_{min}}{\varepsilon_{\max}} \\ \dfrac{z_b - b(x_b, y_b)}{\varepsilon_{max}} \dfrac{\varepsilon_{\max}}{1 - \dfrac{\varepsilon_{min}}{\varepsilon_{\max}}} \end{cases} \quad \text{if } b(x_b, y_b) + \varepsilon_{min} \le z_b \le b(x_b, y_b) + \varepsilon_{max} \qquad \text{(S1)}$$

$$0 \qquad \text{if } \; z_b \ge b(x_b, y_b) + \varepsilon_{max}$$

It is assumed that when the distance between the bottom and the body centre of mass exceeds a threshold ε_{max}, the bottom friction ceases to influence the body motion. The value of ε_{max} differs from that of ε_{min} typically due to limbs hanging down.

The formulation of $\gamma(\boldsymbol{x_b})$ was selected so that the effects of bottom friction on the body motion become significant only when the body is located close to the bottom, i.e., when the elevation z_b of the body centroid is close to the bottom elevation $b(x,y)$. This can be seen in Figure , which displays function γ (horizontal axis) as a function of the distance of the body centroid to the river bottom (vertical axis). The value of γ remains small except in the vicinity of the bottom.

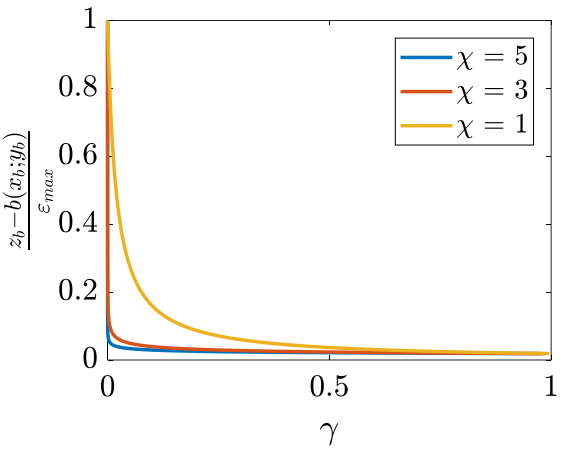

Figure S2: Shape of function $\gamma(\boldsymbol{x_b})$ as a function of the distance between the body centre of mass and the bottom, $z_b - b(x_b, y_b)$, scaled by the length ε_{max}.

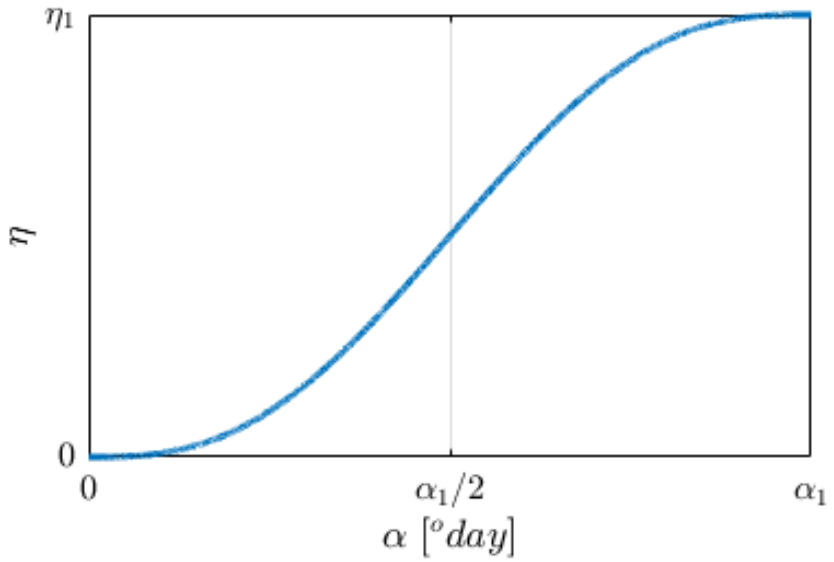

Figure S3: Functional relationship between the ADD, α, and the degree η of influence of body decomposition on body volume.

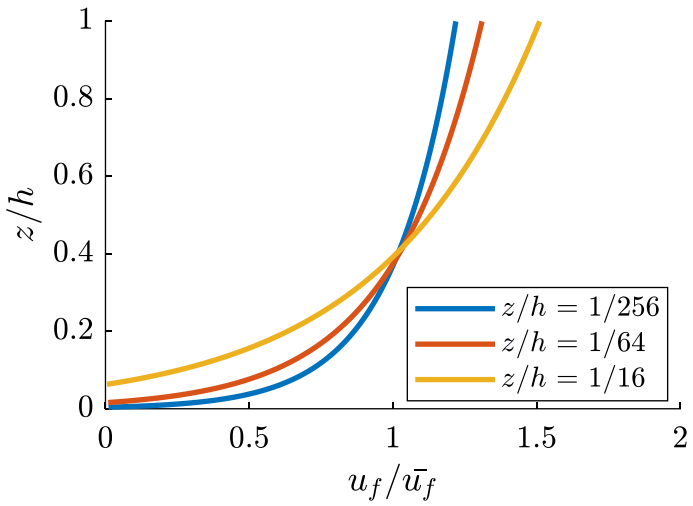

Figure S4: Flow velocity profile over the flow depth.

C. Empirical anthropometric closures

C.1 Estimation of the frontal area

Among the existing empirical relations for determining the body surface area (Mosteller, 1987; Du Bois and Du Bois, 1989; Tanabe et al., 2000; Tikuisis et al., 2001), we opted for the most recent one Tikuisis et al. (2001):

$$BSA = 0.01281 m_b^{0.44} h_b^{0.6} \quad [\text{m}^2] \quad \text{for men} \tag{S2}$$

$$BSA = 0.01474 m_b^{0.47} h_b^{0.55} \quad [\text{m}^2] \quad \text{for women} \tag{S3}$$

with m_b in kg and h_b in cm.

Following Tanabe et al. (2000), the frontal area may be approximated by multiplying the body surface area by a projection factor f_p which depends on the body positioning and orientation (pitch, yaw and roll angles):

$$A_b = f_p \cdot BSA \quad [\text{m}^2] \tag{S4}$$

Based on the work of Tanabe et al. (2000), a plausible range of values of the projection factor is given by [0.16; 0.36].

C.2 Estimation of the body initial volume

Three cases were distinguished for the estimation of the body initial volume, as detailed hereafter.

- If $BMI < 29$ kg/m² and $m_b < 85$ kg:

$$V_b(0) = (0.992 m_b + 0.701) \cdot 10^{-3} \quad [\text{m}^3] \tag{S5}$$

This formula is taken from a study by Liu et al. (2017), which is based on a sample of Chinese people (average mass of 65 kg, with a standard deviation of 7 kg). As such, Eq. (S5) is not adapted to taller people.

- If $BMI < 29$ kg/m² and $m_b \geq 85$ kg:

$$V_b(0) = BSA \cdot (51.44 \frac{m_b}{h_b} + 15.3) \quad [\text{m}^3] \tag{S6}$$

This formula is taken from Sendroy and Collison (1965).

- If $BMI \geq 29$ kg/m²:

$$V_b(0) = BSA \cdot (51.44 \frac{m_b}{h_b} + 15.3) \cdot 1.04 \quad [\text{m}^3] \tag{S7}$$

This equation reflects the tendency of people with a higher BMI to be generally more fat than muscled ($\rho_{\text{fat}} = 900$ kg/m³, while $\rho_{\text{muscle}} = 1100$ kg/m³).

C.3 Estimation of lungs functional residual capacity (FRC)

The lungs volume at FRC (in m³) was estimated here as a function of the gender, age a (in years), body height (in m) and BMI using results by Stocks and Quanjer (1995) and Abston et al. (2017) results:

$$\begin{cases} V_{lung,FRC} = (2.34 h_b + 0.01 \cdot a - 1.09) \cdot \dfrac{(0.102 BMI^2 - 7.4504 BMI + 229.61)}{100} \cdot 10^{-3} & \text{for men} \\ V_{lung,FRC} = (2.24 h_b + 0.001 \cdot a - 1) \cdot \dfrac{(0.102 BMI^2 - 7.4504 BMI + 229.61)}{100} \cdot 10^{-3} & \text{for women} \end{cases} \tag{S8}$$

C.4 Estimation of the total lung capacity (TLC)

The total lung capacity (TLC, in m³) was approximated here using formulae developed by Stocks and Quanjer (1995) and Abston et al. (2017), which involve the body height h_b (in mà) and the BMI:

$$\begin{cases} TLC = (7.99 h_b - 7.08) \cdot \dfrac{(0.0403 BMI^2 - 3.1049 BMI + 149.58)}{100} \cdot 10^{-3} & \text{for men} \\ TLC = (6.6 h_b - 5.79) \cdot \dfrac{(0.0403 BMI^2 - 3.1049 BMI + 149.58)}{100} \cdot 10^{-3} & \text{for women} \end{cases} \tag{S9}$$

A first approximation for the value of parameter η_1 in Eq. (8) was obtained as follows:

$$\eta_1 \approx \frac{TLC - FRC}{FRC} \tag{S10}$$

D. Statistical distributions

The beta distribution is a family of continuous probability distributions defined on the interval [0; 1]. The shape of the distribution is controlled by two parameters α and β, which take positive values and appear as exponents of the random variable in the probability density function (McDonald and Xu, 1995):

$$PDF(x,\alpha,\beta) = \frac{x^{\alpha-1}(1-x)^{\beta-1}}{B(\alpha,\beta)} \tag{S11}$$

with x in the range [0; 1] and $B(\alpha, \beta)$ defined as:

$$B(\alpha,\beta) = \frac{\Gamma(\alpha)\Gamma(\beta)}{\Gamma(\alpha+\beta)} \tag{S12}$$

with Γ the Gamma function.

Here, the distribution of a random variable X varying in an arbitrary range $[X_1; X_2]$ was related to the random variable x as follows:

$$X = \left(X_2 - X_1\right)x + X_1 . \tag{S13}$$

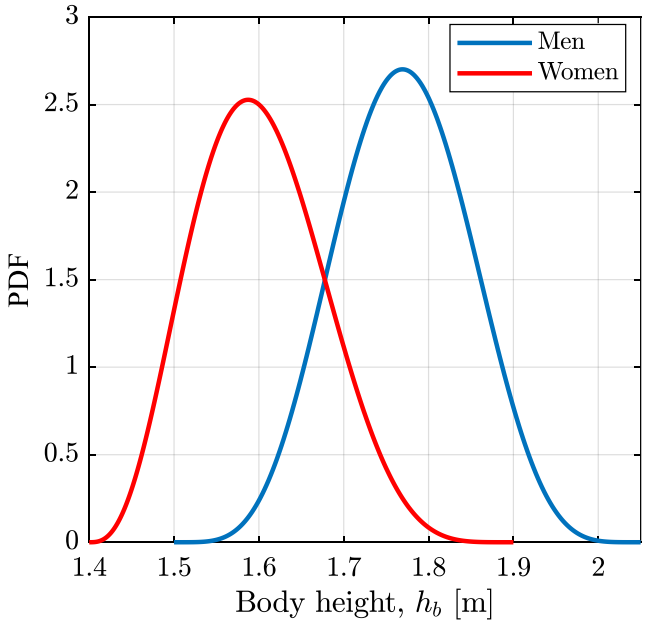

Figure S5: Beta distributions assumed for body height h_b in Scenario "unknown body" for men (α = 5.8697 and β = 6.075, in the range [1.5; 2.05] m) and for women (α = 3.976 and β = 5.965, in the range [1.4; 1.9] m) in Scenarios UB-LF and UB-HF.

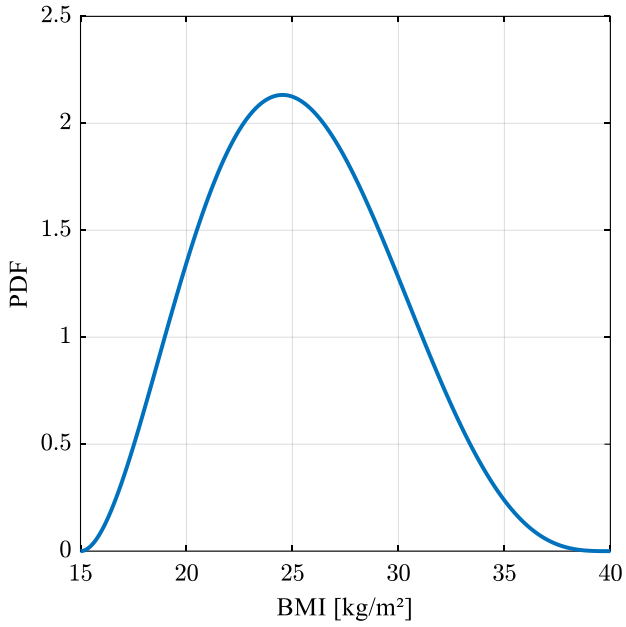

Figure S6: Beta distributions assumed for BMI for both genders (α = 3.0102 and β = 4.2628, in the range [15; 40] kg/m²) in Scenarios UB-LF and UB-HF.

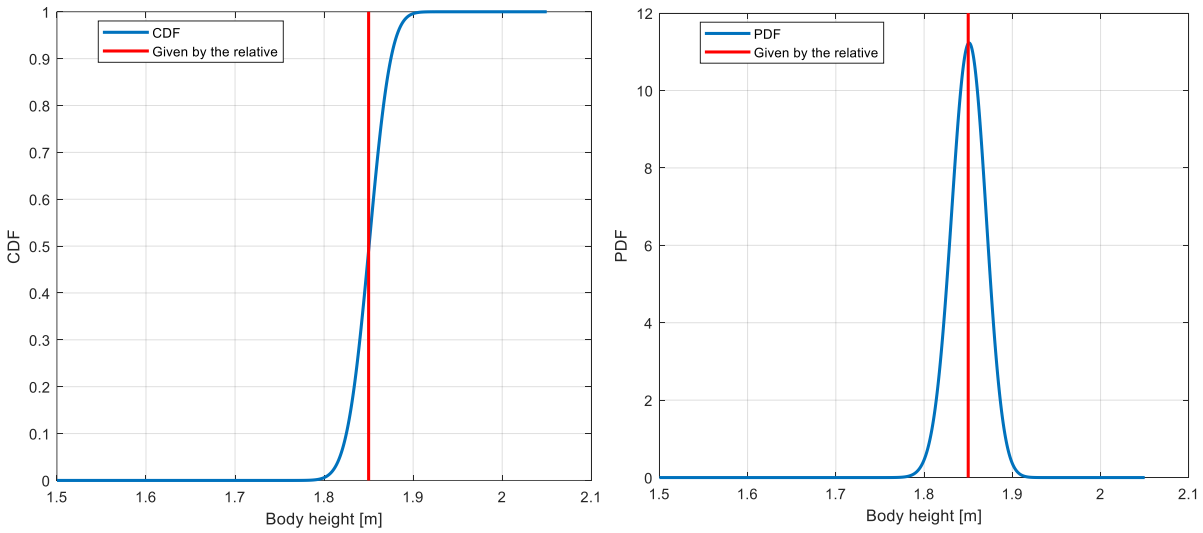

Figure S7: Cumulative distribution function and probability density function of a beta distribution for h_b of a victim with a mode of 1.85 m and a difference between the mode and the percentiles 10 and 90 of 0.025 m (Scenarios KB-LF and KB-HF).

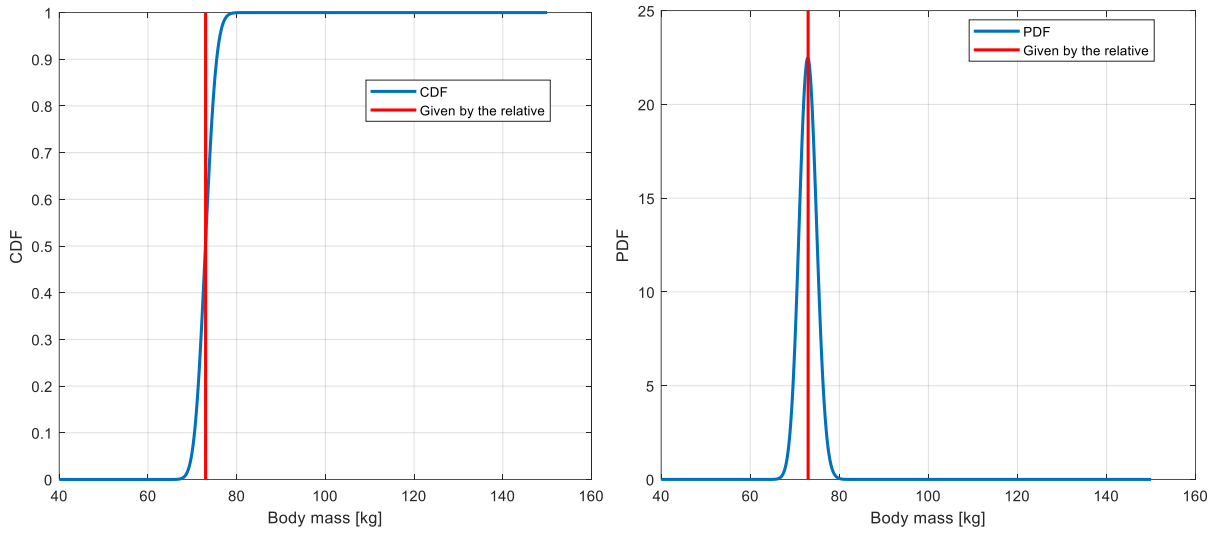

Figure S8: Cumulative distribution function and probability density function of a beta distribution for the mass m_b of a victim with a mode of 73 kg and a difference between the mode and the percentiles 10 and 90 of 2.5 kg (Scenarios KB-LF and KB-HF).

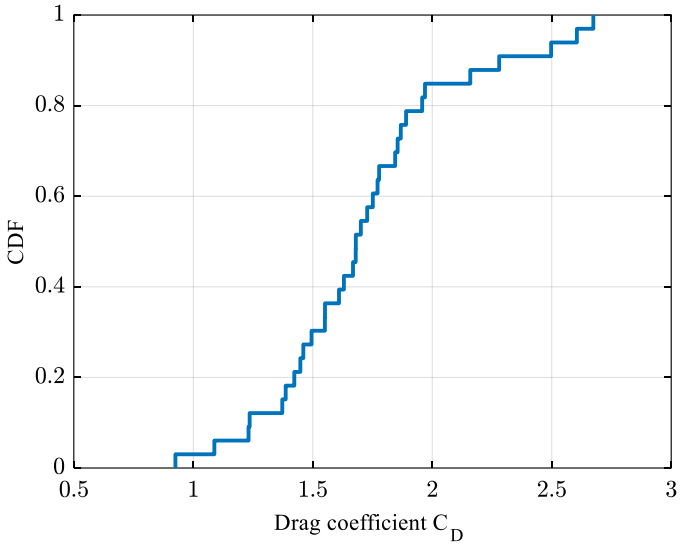

Figure S9: Empirical cumulative density function (CDF) of observed drag coefficient of a human-like body obtained from laboratory experiments (in a hydraulic flume) involving reduced-scale dummies, i.e., dummies which are about six times smaller than a typical human body (Delhez et al., 2021).

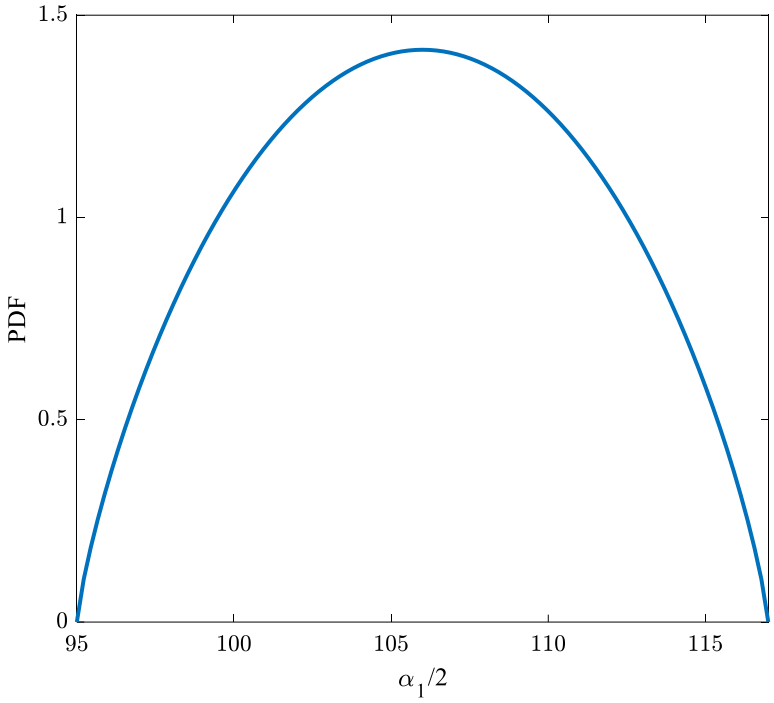

Figure S10: Beta distribution considered for $\alpha_1 / 2$, with parameters $\alpha = \beta = 1.8024$.

E. Convergence analysis in the most critical case

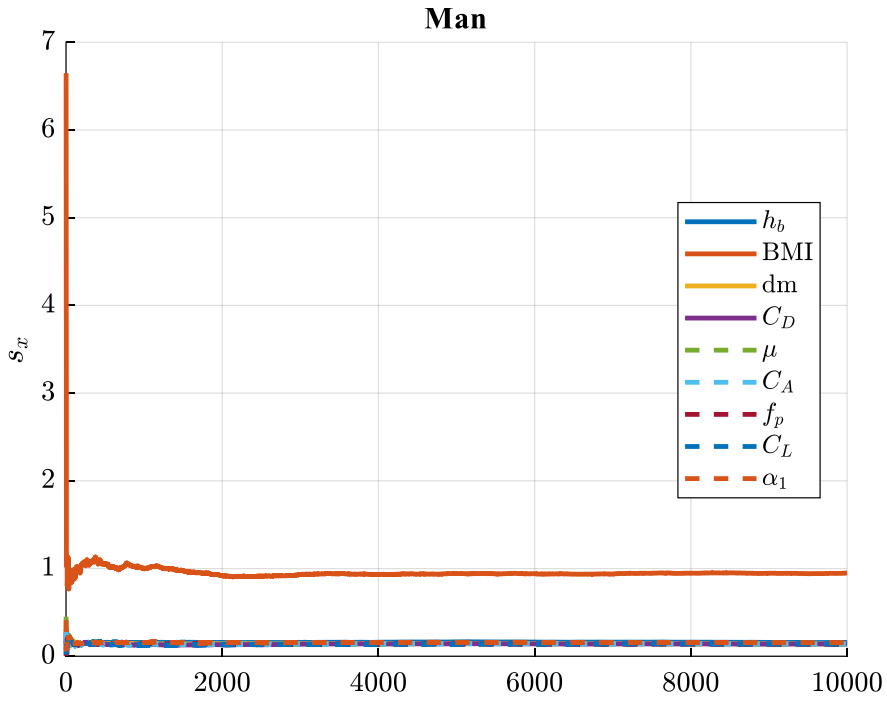

(a)

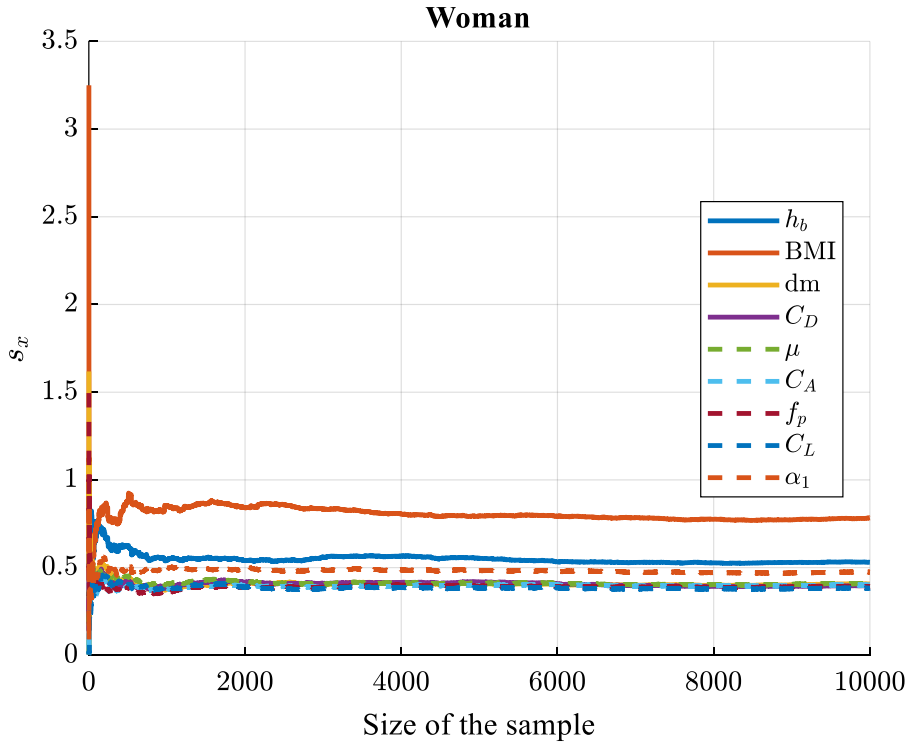

(b)

Figure S11: Sobol' index as a function of the number of runs for the case UB-HF

F. Bodies streamwise positions

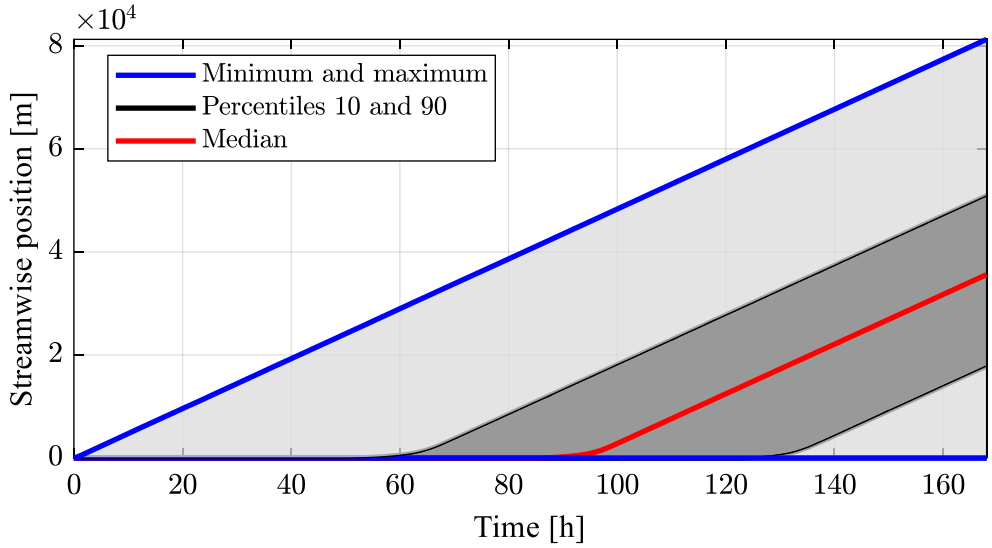

Figure S12: Scenario UB-LF

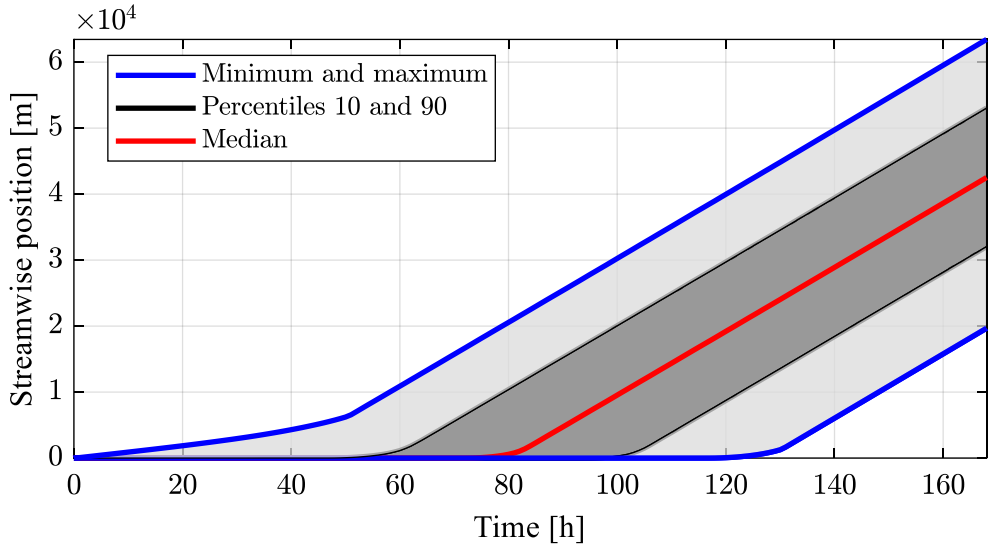

Figure S13: Scenario KB-LF

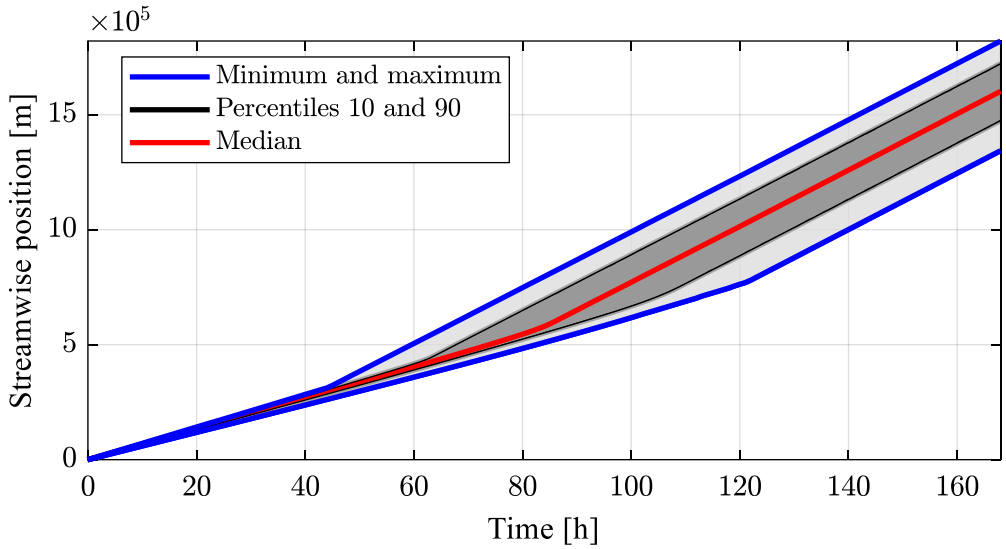

Figure S14: Scenario KB-HF

G. Sobol' index for grouped parameters without decomposition and for HF scenarios

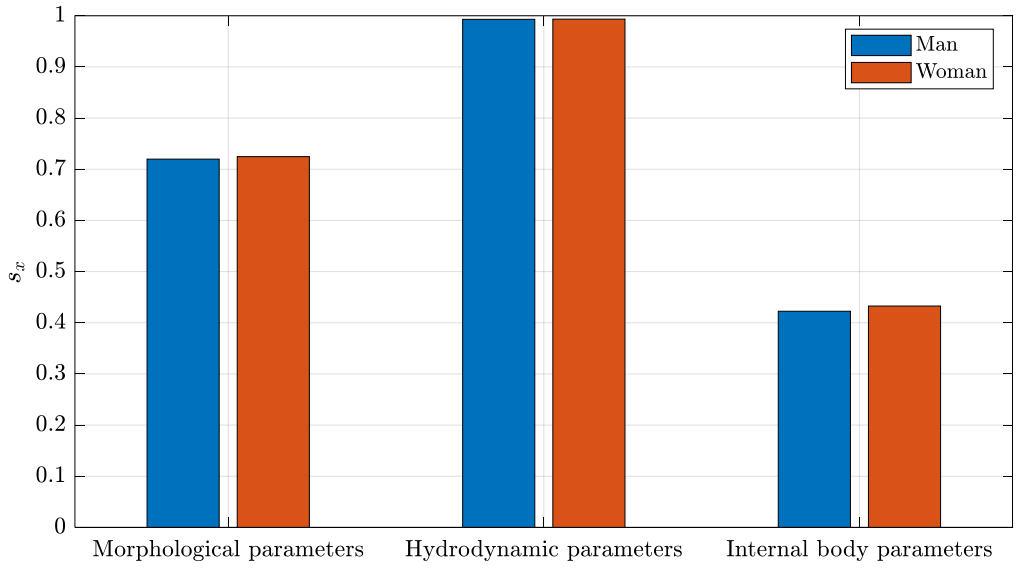

Figure S15: Without vertical motion, Scenario UB-HF

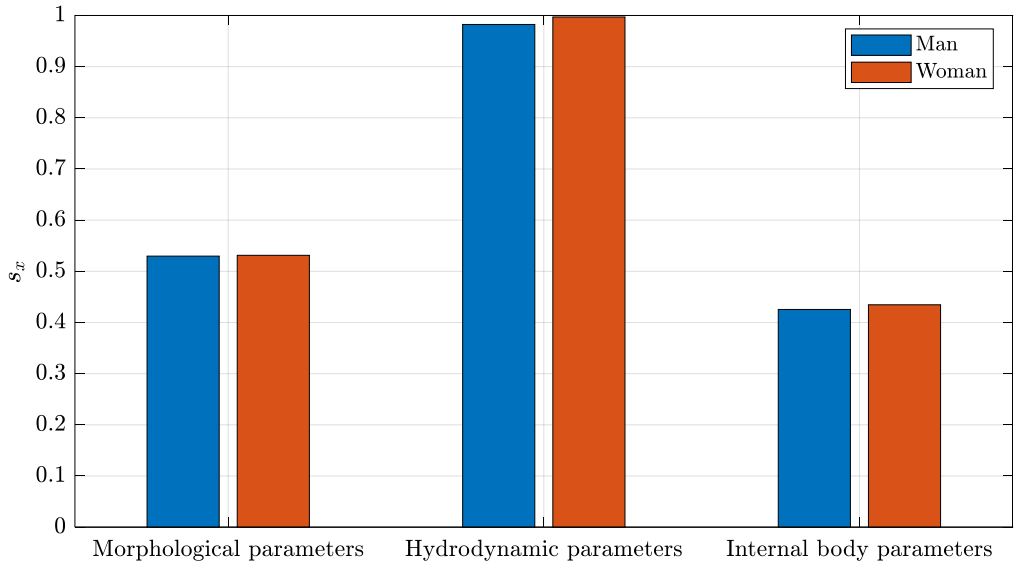

Figure S16: Without vertical motion, Scenario KB-HF

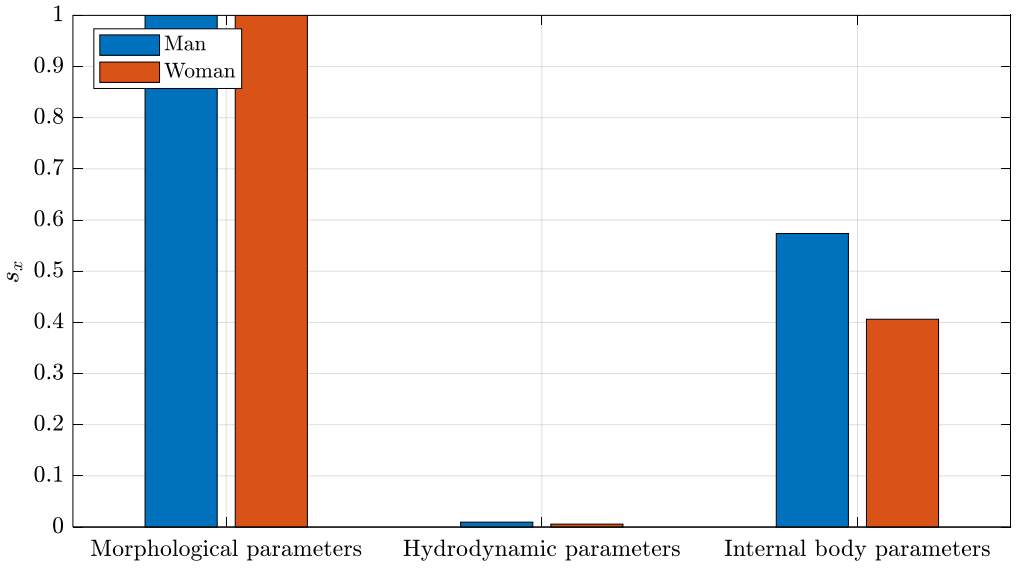

Figure S17: Without decomposition, Scenario UB-LF

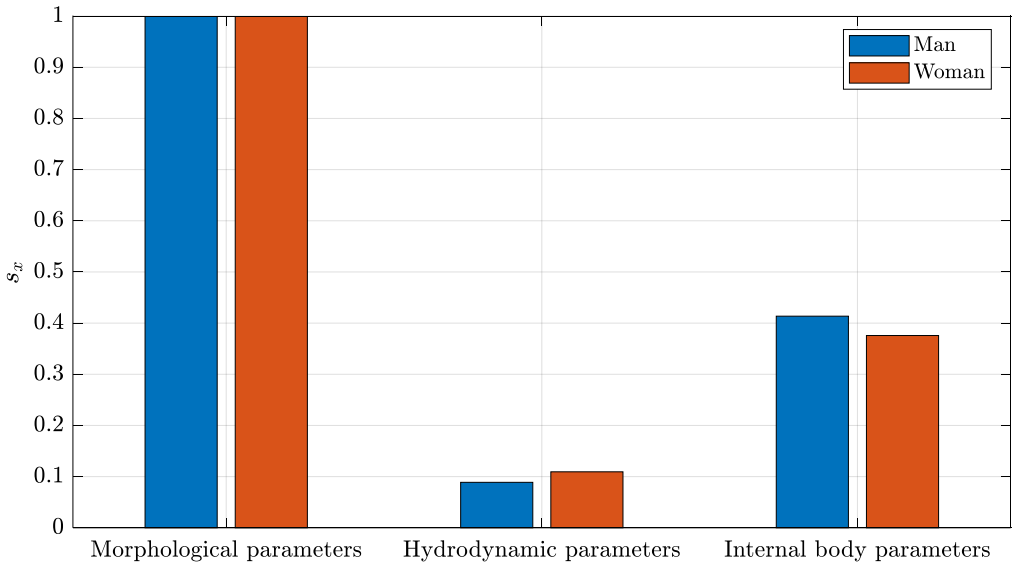

Figure S18: Without decomposition, Scenario UB-HF

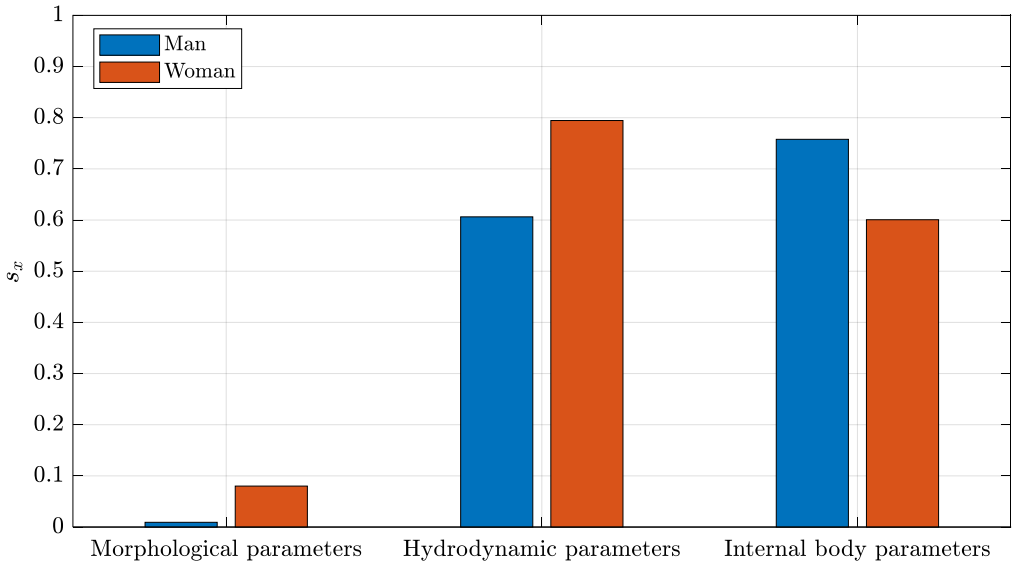

Figure S19: Without decomposition, Scenario KB-LF

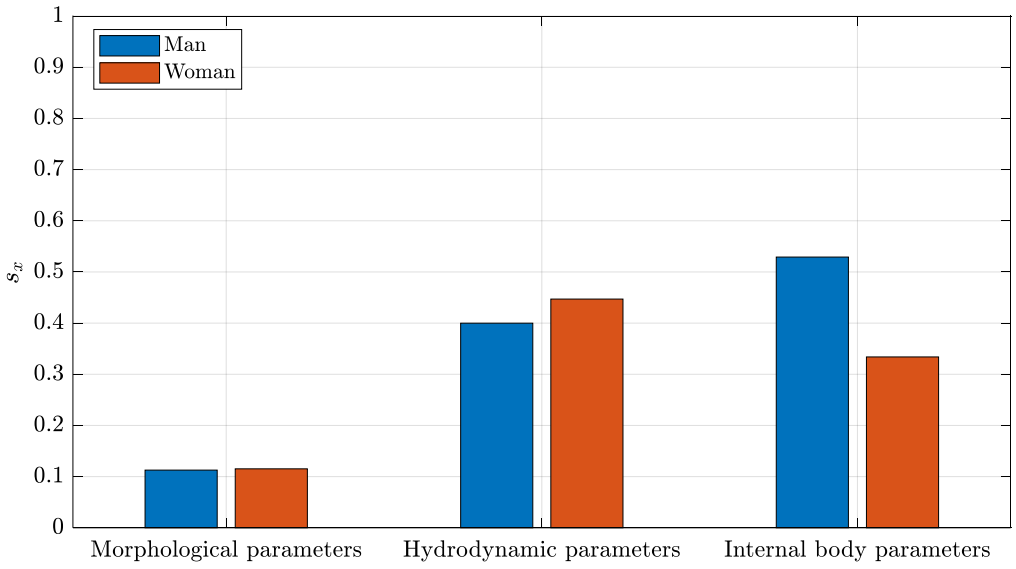

Figure S20: Without decomposition, Scenario KB-HF

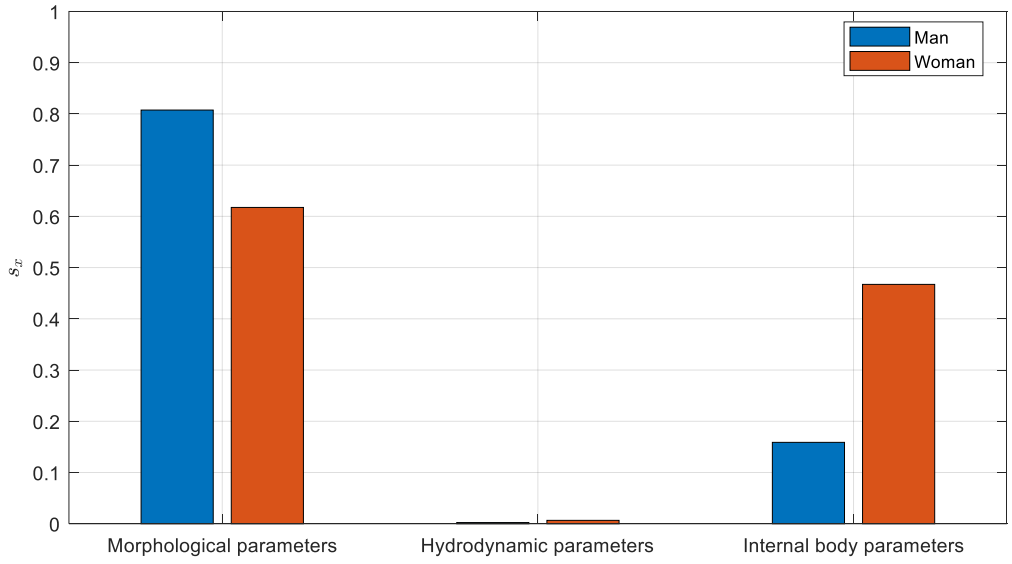

Figure S21: Classic drowning, Scenario UB-HF

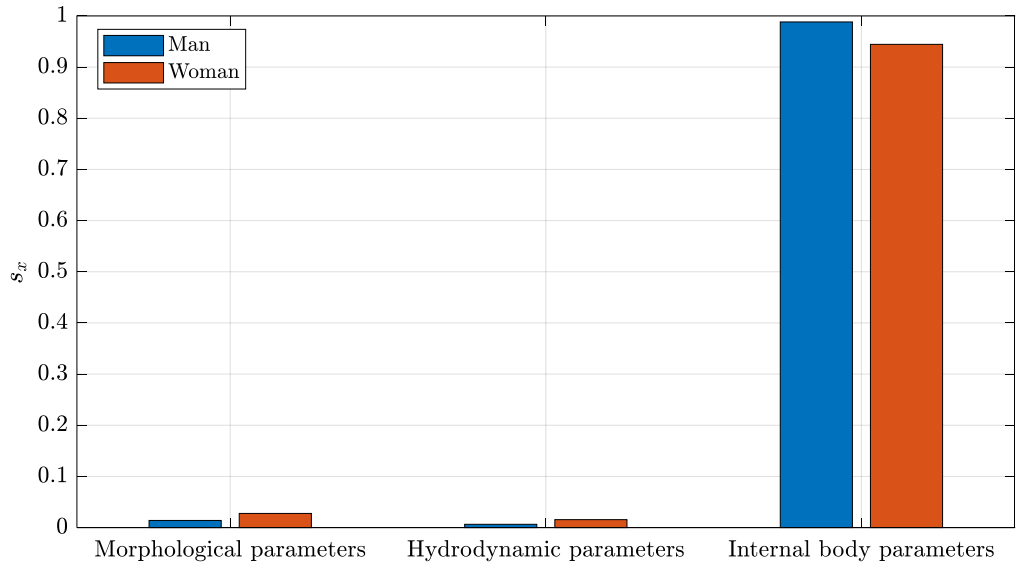

Figure S22: Classic drowning, Scenario KB-HF

References

Abston, E., Comellas, A., Reed, R.M., Kim, V., Wise, R.A., Brower, R., Fortis, S., Beichel, R., Bhatt, S., Zabner, J., Newell, J., Hoffman, E.A., Eberlein, M., 2017. Higher BMI is associated with higher expiratory airflow normalised for lung volume (FEF25–75/FVC) in COPD. BMJ Open Respiratory Research 4, e000231.

Du Bois, D., Du Bois, E.F., 1989. A formula to estimate the approximate surface area if height and weight be known. 1916. Nutrition (Burbank, Los Angeles County, Calif.) 5, 303–311; discussion 312–313.

Liu, X., Niu, J., Ran, L., Liu, T., 2017. Estimation of Human Body Volume (BV) from Anthropometric Measurements Based on Three-Dimensional (3D) Scan Technique. Aesthetic Plastic Surgery 41, 971–978.

McDonald, J.B., Xu, Y.J., 1995. A generalization of the beta distribution with applications. Journal of Econometrics 66, 133–152.

Mosteller, R.D., 1987. Simplified calculation of body-surface area. The New England Journal of Medicine 317, 1098.

Sendroy, J., Collison, H.A., 1965. Determination of human body volume from height and weight. NAVAL MEDICAL RESEARCH INST BETHESDA MD.

Stocks, J., Quanjer, P.H., 1995. Reference values for residual volume, functional residual capacity and total lung capacity. ATS Workshop on Lung Volume Measurements. Official Statement of The European Respiratory Society. European Respiratory Journal 8, 492–506.

Tanabe, S., Narita, C., Ozeki, Y., Konishi, M., 2000. Effective radiation area of human body calculated by a numerical simulation. Energy and Buildings 32, 205–215.

Tikuisis, P., Meunier, P., Jubenville, C., 2001. Human body surface area: measurement and prediction using three dimensional body scans. European Journal of Applied Physiology 85, 264–271.

Chapter 2

Force coefficients for modelling the drift of a victim of river drowning

This chapter corresponds to the journal paper "Force coefficients for modelling the drift of a victim of river drowning" by C. Delhez, T. Andrianne, S. Erpicum, N. Rivière, P. Hallot, M. Pirotton, P. Archambeau and B. Dewals, published in 2024 in Natural Hazards. The PhD candidate developed the methodology, realised the experiments, analysed the results, wrote the manuscript and generated the figures.

Force coefficients for modelling the drift of a victim of river drowning

C. Delhez[1], T. Andrianne[2], S. Erpicum[1], N. Riviere[3], P. Hallot[4], M. Pirotton[1], P. Archambeau[1], B. Dewals[1]

[1]Hydraulics in Environmental and Civil Engineering (HECE), Research Unit Urban & Environmental Engineering (UEE), University of Liège, 4000 Liège, Belgium.

[2] Aerospace and Mechanical Engineering, University of Liège, 4000 Liège, Belgium.

[3] Univ Lyon, INSA Lyon, Ecole Centrale de Lyon, Université Claude Bernard Lyon I, CNRS, LMFA, UMR 5509, 20 avenue Albert Einstein, F-69621 Villeurbanne, France.
[4] DIVA, Art Archaeology Heritage, University of Liege, 4020 Liege, Belgium.

Acknowledgments
The authors thank Dr. Raphael Dubois for his support and expertise in the use of the wind tunnel and its equipment.

ABSTRACT
The global annual death toll due to drowning is of the order of 10^5. Rescue and search operations in urban rivers show a low rate of success. Operational computational drift models have been developed for marine environments but not for the case of river drowning. In the latter case, no scale separation occurs between the body and flow length scales. To model them, three hydrodynamic force coefficients of representative bodies, such as drag, side and lift coefficients, are needed. So far, their value was not characterized for the typical positioning of the body of a drowning victim. In this work, we used full-scale laboratory experiments to identify the range of value of these hydrodynamic coefficients based on 249 tests conducted in a wind tunnel. Observations in the air can be transferred to water environment thanks to flow similarity. For the typical body positioning of a drowning victim, the drag coefficient was found to vary in the range 0.5 to 1.2. Changing the yaw angle of the body, induces variations in the drag coefficient by about 50 %. Considering loose clothes instead of tight clothes leads to an increase in the drag coefficient by about 30 %, whereas adding a backpack has a limited influence (less than 5 %). With the available experimental setup, it has been difficult to detect distinctive patterns and trends for the side and lift coefficients. This study is part of a multidisciplinary effort for developing scientific knowledge and technologies contributing to a reduction of drowning-induced fatalities in rivers.

KEYWORDS: drowning, river, wind tunnel, drag coefficient, lift coefficient, side coefficient

1 Introduction

1.1 Context

Worldwide, unintentional drowning claims a total of nearly 400,000 lives every year (WHO, 2014), and drowning is among the main causes of death of young people (Ung et al., 2019). Climate change increases the risk of drowning, as hydro-meteorological extremes are becoming more frequent (Parks et al., 2020). Both floods and heatwaves cause drowning accidents. In urban rivers, heatwaves trigger a rise in (unauthorized) bathing activities, hence also in accidental drowning. Recent urban planning policies promoting the use of riverbanks for their amenities (cooler atmosphere, scenic views, safe paths for walking and cycling) make it particularly timely to address the issue of drowning in urban rivers. Compared to drowning in swimming pools or at the seaside, the chance of survival after river drowning is two to three times lower (Byard, 2017).

Causes of drowning in urban rivers are numerous, including bathing, traffic accidents, influence of drugs or alcohol, and suicidal or criminal acts (e.g., Kringsholm et al., 2001). Reducing the number of fatalities due to drowning requires a holistic approach combining epidemiological studies, prevention measures (education, rising risk awareness, fences, bathing surveillance or bans), improved resuscitation techniques and medical treatment (Bierens, 2006), as well as a better preparation for rescue and search operations. Compared to the case of lakes or pools, body search operations in urban rivers are particularly complex due to relatively high flow velocity and low visibility, as well as the presence of subsurface vortices created by obstacles (Strom et al., 2017), such as bridge piers and weirs, or by ship motion. Technologies such as sonars perform poorly in urban rivers due to debris lying on the bottom, which make it harder to discern a body shape (Blondel, 2014; Ruffell et al., 2017). So far, search operations in urban rivers have not been guided by existing modelling technologies enabling accurate simulation of the flow field in a river. Though, such models have the potential to inform more targeted rescue and search operations, and to provide valuable information for forensic analyses (Carniel et al., 2002; Ruffell et al., 2017; Mateus et al., 2020). So far, modelling studies on drowning in rivers focused on the incipient motion of human bodies, which may result from toppling or sliding (Jonkman and Penning-Rowsell, 2008). Such studies did not extend to modelling the victim's trajectory in water.

1.2 Background

To the best of the authors' knowledge, only a single modelling study investigated the drift of human bodies in a real river. Gonzalez et al. (2022) combined an Eulerian flow model of La Miel river in Colombia (grid size of the order of 1 m × 1 m) with a Lagrangian drift model. Though they pointed at regions where synthetic floats tend to accumulate, they mostly presented hydrodynamic results and did provide an in-depth analysis of flow-body interactions in rivers. They are primarily interested in the drift of human remains in the context of an armed conflict, and not to accidental drowning. In contrast, a range of computational studies addressed the drift of a victim of drowning at sea or ocean. They are

summarized in Table 1. Delhez et al. (2023) tested a similar model but only in highly idealized flow conditions.

Carniel et al. (2002) used a computational model to confirm the plausibility of the drift of a floating body over 300 km in two weeks in the Mediterranean sea. Ocean currents and waves were simulated by an Eulerian ocean circulation model forced by regional atmospheric models. The grid resolution was 10 km and the time step 12 hours. The outcomes of the ocean circulation model were used to drive a Lagrangian model of the drifting body, accounting for the effects of currents, waves (Stokes drift) and wind. A random walk component was included to reproduce the influence of fluctuations not resolved by the Eulerian model.

Breivik and Allen (2008) combined oceanic and atmospheric models with a drift model for a range of objects, including human bodies. In the drift model, current and wind effects were explicitly considered. The Stokes drift (i.e., effect of waves) was not modelled explicitly because it is considered as already incorporated in leeway empirical coefficients used for parametrizing wind forcing. A Bayesian stochastic framework was adopted to account for uncertainties in the forcing fields (wind and current), body characteristics and initial position. The model outcome is a time-dependent probability density function of the object location.

Mateus et al. (2015) studied the case of a body drifted over only 2 km in 8.6 days in a coastal area of Portugal, as previously reported by Mateus et al. (2013). The flow field was simulated by an ocean circulation model forced by wind, tide, and discharge of a river, whereas the body motion was computed with a Lagrangian drift model forced by currents only. The same modelling approach was used by Gunduz (2017) to investigate an accident in which victims drifted over 100 km in seven days.

Table 1: Existing computational models of the drift of victims of drowning in coastal waters.

	Grid size	Time step	Considered drivers of body drift			
			Current	Waves	Wind	Body inertia
Carniel et al. (2002)	1 km	12 h	✓	✓	✓	No
Breivik and Allen (2008)	4 km	6 h	✓	(✓)[1]	✓	No
Mateus et al. (2015)	6.5 km	1 h	✓			No
Gunduz (2017)	4 km	Not specified	✓			No
Ličer et al. (2020)	1 km	12 min	✓	(✓)[1]	✓	No

Hart-Davis and Backeberg (2023)	9.2 km	1 h	✓	(✓)[1]	✓	No
Tu et al. (2021), Wu et al. (2023)	N/A[2]	10 min	✓		✓	No

[1] The brackets indicate that the effect of waves is not explicitly reproduced in the Lagrangian model because it is considered as already incorporated in the empirical leeway coefficients used for modelling wind effects.

[2] Tu et al. (2021) and Wu et al. (2023) used field measurements of flow and wind velocity (instead of Eulerian models) to force their Lagrangian body drift computations.

More recently, similar modelling frameworks were presented by Ličer et al. (2020) and by Hart-Davis and Backeberg (2023). For the same reasons as Breivik and Allen (2008), both studies explicitly considered the influence of currents and wind in the Lagrangian drift model but not the effect of waves. Tu et al. (2021) and Wu et al. (2023) also applied a Lagrangian model for simulating the drift of a human body at sea, but their model was forced by field observations of current and wind velocity.

All computational studies reported in Table 1 analysed the drift of bodies in sea or ocean environments, which differs from the case of river drowning in two key aspects. First, all these studies considered the body as a passive float. This assumption is reasonable in sea or ocean environments because the body length scale (of the order of 1 to 2 m) is way smaller compared to the flow lengths scales. This is illustrated in Figure 1, which highlights that the grid size (considered as a proxy for the resolved flow lengths scales) in the models listed in Table 1 exceed the body length scale by three to four orders of magnitude. This length scale separation, together with the large considered time scales (vertical axis in Figure 1 and Table 1), supports the idealization of the body as a passive float, for which the duration of body acceleration phases is negligible compared to time resolution of the computations (Breivik and Allen, 2008).

In contrast, in urban rivers, the characteristic length scales of the flow are much smaller due the topographic variability induced by features such as bridge piers, hydraulic structures, riverbanks, meanders. This leads to variations in velocity direction and magnitude over comparatively small distances and durations. In such conditions, assuming that the body velocity remains equal to the flow velocity does not hold true (Breivik and Allen, 2008; Ghaffarian et al., 2020). Indeed, due to body inertia, the velocity changes induce a non-zero relative velocity between the drifted body and the river flow. Hence, the drag and, to a lesser extent, the side forces induced by the relative motion between the body and the flow need to be considered, unlike for large scale modelling in sea or ocean environments (Table 1). This requires the knowledge of the corresponding hydrodynamic coefficients (drag and side coefficients).

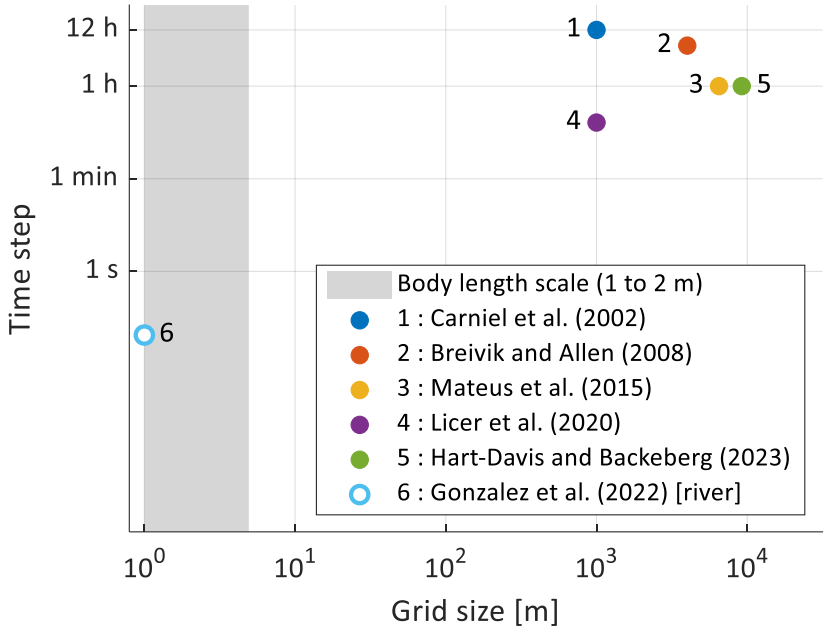

Figure 1: Characteristic time- and length-scales in sea and ocean environments compared to the body size and the corresponding scales in rivers.

Second, all previous models assumed a positively-buoyant body, so that only a 2D horizontal body motion was reproduced. Since freshwater has a lower density than sea water and lifejackets are less often worn in the case of river drowning, the body of a victim of river drowning may be either positively or negatively buoyant (Donoghue and Minnigerode, 1977; Martlin et al., 2023). As the drift velocity differs substantially whether the body is at the surface or close to the bottom, it is of most importance to predict the body vertical motion. This motion over the flow depth is influenced by several parameters relatively intricate to predict (Martlin et al., 2023), such as body morphology (Modell and Davis, 1969; Gallagher et al., 1996; Barwood et al., 2011; Laurent et al., 2013; Van Hoyweghen et al., 2015), presence of air or water in the lungs (Modell and Davis, 1969; Gallagher et al., 1996; Barwood et al., 2011; Laurent et al., 2013; Van Hoyweghen et al., 2015), amount of water swallowed by the victim (Modell and Davis, 1969), type of clothes (Modell and Davis, 1969; Gallagher et al., 1996; Barwood et al., 2011; Laurent et al., 2013; Van Hoyweghen et al., 2015), accessories such as a backpack. Since a human body in water may be close to neutrally buoyant, even a relatively small lift force induced by the flow may change the direction of the net force along the vertical direction. Therefore, estimating the lift coefficient of the body of a drowning victim is of practical importance.

1.3 Objectives

No study so far focused on the determination of hydrodynamic coefficients, such as drag, side and lift coefficients, for a human body in conditions representative of a victim of river drowning. The forces resulting from body-flow interactions depend on the body positioning. Field observations suggest a typical body positioning for victims of drowning, irrespective of

whether the body is close to the surface, in sinking phase, or resurfacing (Figure 2): as long as the body is not in contact with the bottom, unconscious bodies are mainly found face downwards, limbs hanging down (Blanco Pampín and López-Abajo Rodríguez, 2001; Lunetta et al., 2014). This positioning results from the relative value of the limbs and torso densities. Regardless of the precise drowning circumstances, a certain quantity of air remains in the lungs, giving them a lower density than the rest of the body. Besides, after the heart stops, the blood pressure drops, and blood accumulates in the lower parts of the body (i.e., hands and feet in this case), consistently with the *livor mortis* phenomenon (Amendt et al., 2004). In the case of a resurfacing body, putrefaction gases cause inflation of the abdomen (Laurent et al., 2013), leading to a similar positioning as in the sinking phase. The case of a body in contact with the bottom is out of the scope of the present study.

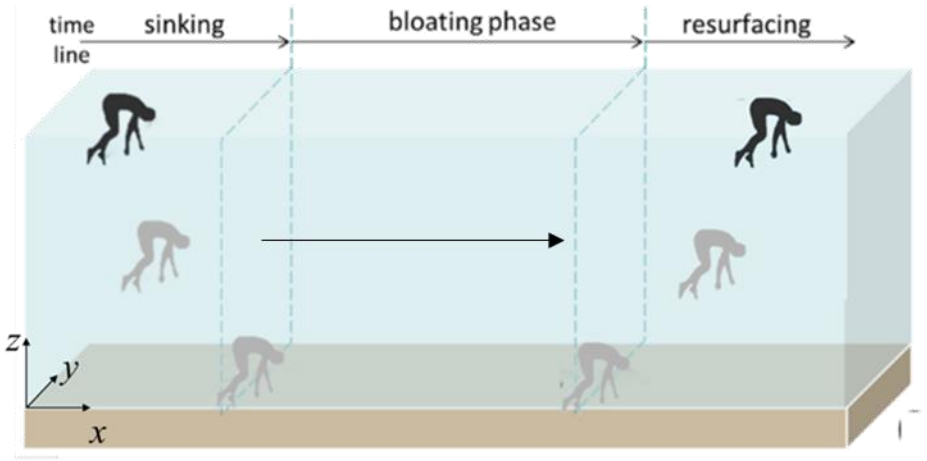

Figure 2: Sketch of typical body positioning of a drowning victim. The body trajectory generally follows three stages: body sinking, body bloating (due to the generation of gases as a results of body decomposition) usually on the bottom, and body resurfacing. Adapted from Mateus et al. (2013).

In previous studies analysing the drag coefficient, and to a lesser extent the side and lift coefficients, of a human body, the body positioning differed from the typical one of a drowning victim, as they focused on the cases of swimming (Bixler et al., 2007; Marinho et al., 2009, 2011, 2012; Zamparo et al., 2009; Mantha et al., 2014), ice skating (Ingen Schenau, 1982), ski jumping (Müller, 2009; Wolfsperger et al., 2021), speed skiing (Barelle et al., 2004), cycling (García-López et al., 2008), and standing, sitting or supine positions (Schmitt, 1954) but not for the case of a drowning position.

In this study, we undertook laboratory experiments with a full-scale dummy to determine the drag, side, and lift coefficients of a human body in a typical position of river drowning (face down, limbs hanging down). The body yaw angle (i.e., the rotation of the body around the vertical axis) was systematically varied (Figure 3). For the sake of assessing the influence of the body position, tests with a lying body were also undertaken. The experiments were conducted in a wind tunnel, which offers more flexibility and an easier access to the body than a towing tank or a hydraulic flume. The results may be transferred to the case of a body

in water using similarity rules. The influence of clothes and of presence of accessories, such as a backpack, were also investigated.

Section 2 presents the experimental setup, the test program, and the measurement techniques. The results are detailed in Section 3, while they are compared to previous studies in Section 4. Concluding remarks are formulated in Section 5.

2 Materials and methods

When a body is immerged in a fluid with a non-zero relative velocity, friction stresses and pressure differences around the body add up so that a resulting force is induced by the flow on the body (Hoerner, 1965; Cook, 2007). As sketched in Figure 3, this force is generally separated into three components, referred to as drag (F_D), side (F_S) and lift (F_L) forces, which are respectively aligned along the direction of the approaching flow, horizontally in the plane normal to the approaching flow, and vertically in the same plane (Cook, 2007). Each of these three force components is generally estimated as a function of the fluid density, the body frontal area and the square of the relative velocity, using corresponding hydrodynamic coefficients called drag (C_D), side (C_S) and lift (C_L) coefficients (Cook, 2007). These coefficients are Reynolds-dependent, and they vary with the body shape, positioning and directionality. Here, the value of these coefficients was experimentally determined for a human body in a typical position of a drowning victim.

In this section, the wind tunnel and the dummy used for the laboratory tests are presented (Sections 2.1 and 2.2). The considered flow scenarios are introduced in Section 2.3. In Section 2.4, the hydrodynamic coefficients are described, as well as the method used to obtain each of them from the experimental measurements. Finally, the test program is detailed in Section 2.5.

2.1 Experimental setup

The experimental tests were conducted in the wind tunnel laboratory of University of Liege (Belgium). For technical reasons, a wind tunnel was preferred over a towing tank or a current flume. The wind tunnel enables rapid data acquisition and easy access to the test area, making it simple to systematically vary the dummy configuration (e.g., covering a high number of different yaw angles, changing dummy positioning and/or clothes). Preliminary tests were performed in a towing tank (100 m in length, 6 m in width, and 4 m in depth); but repeatedly adjusting the dummy position and test configuration proved more challenging due to the underwater location of the dummy and attachment system. Since a wind tunnel was utilized, the influence of a river free surface on the results should be investigated in a subsequent step of the research.

The cross-section of the wind tunnel is 2.5 m wide and 1.8 m high (Figure 3). The wind is blown along the wind tunnel longitudinal direction, referred to as streamwise direction x, positive in the wind direction. The lateral and vertical directions to the flow direction are labelled y and z, respectively (Figure 3). In the present tests, the wind velocity U_x ranges from 3.2 to 6.5 m/s with a turbulence intensity of 0.5%. The facility is equipped with a load balance

(Omega 160 ATI sensor) enabling force and torque measurements in the three directions. The load balance has a sensing range of 1000 N in the streamwise and lateral directions and 2500 N in the vertical direction. All sensing ranges are 120 Nm for the torques. The resolution of the sensors on each force is 0.25 N, of 0.025 Nm for the torques around direction x and y and of 0.0125 Nm for the torque around the vertical axis. Data were acquired at a frequency of 200 Hz. Based on a convergence analysis, the mean and standard deviation of each measured time series were computed, and the sampling time was set to 15 s (Figures S1 to S3 in Supplement). This sampling time is long enough to allow each of the measured component to converge in each configuration except for the force in the vertical direction. However, the average of this force is comparable to the resolution of the sensor in many configurations, so that these measurements were mostly discarded from the analyses.

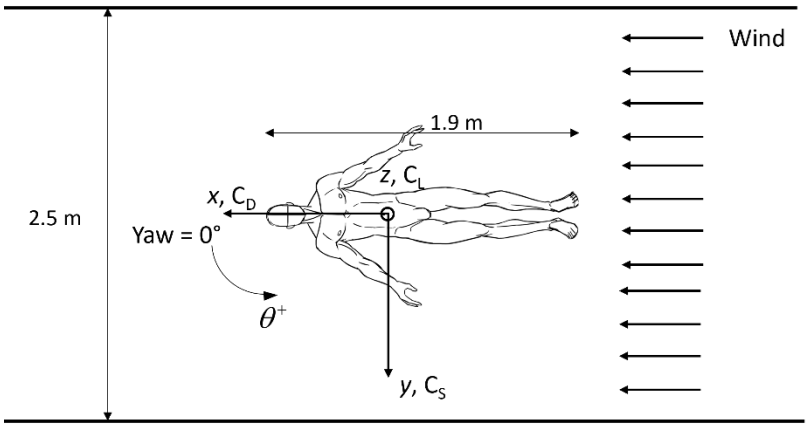

Figure 3: Sketch of the wind tunnel setup, with the dummy in lying position and a yaw angle $q = 0°$.

A full-scale dummy was selected instead of a reduced-scale dummy to avoid issues related to geometric scaling of the test results, and to ensure that the measured forces can be reliably captured by the sensors. Indeed, using a reduced scale dummy would have led to considerably smaller forces, while even in the present tests some of the forces (particularly the lift component) are already relatively small compared to the sensors resolution (Figure S6 in Supplement).

The full-scale dummy used in the tests is an adjusted version of the Rescue Randy 9000 manufactured by 3B Scientific (Figure 4). It is made of rugged polyethylene. The dummy represents a male adult, 1.9 m tall, with a shoulder width of 0.54 m, arms of 0.77 m in length, 0.93 m-long legs and a body surface area of 2.46 m². Without clothes nor accessories, the dummy weights 30 kg. The dummy has joints, equipped with connecting screws, which give access to a wide variety of limbs positioning. Using tailored 3D-printed interlocking parts (Figure S7 in Supplement), the joints have been modified to enable firmly fixing the position of each ball joint to ensure enough rigidity for wind velocity up to 6.5 m/s. In all configurations, limbs and head are at least 15 cm away from walls and their development of boundary layer.

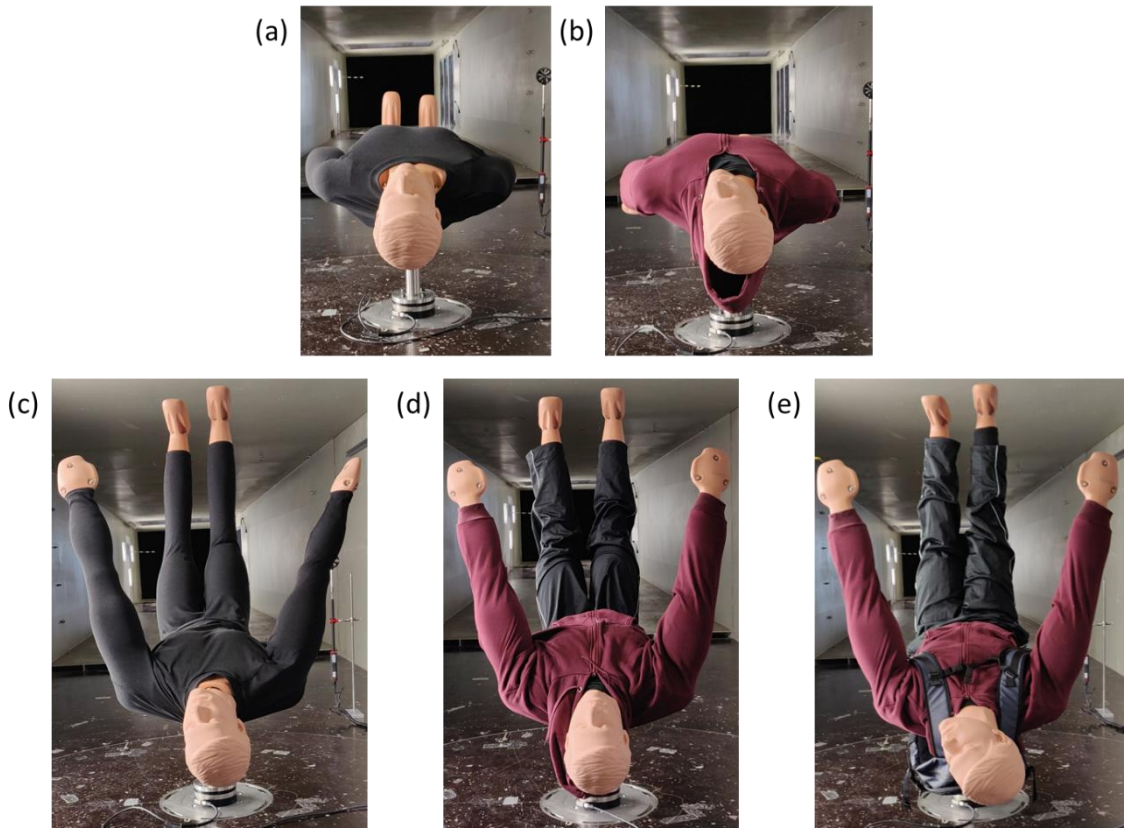

Figure 4: Positions and types of clothes of the dummy (represented with wind coming from the background and a yaw angle of 0°): (a, b) lying position, (c, d, e) drowned position. (a, c) tight clothes, (b, d, e) loose clothes. (e) body wearing a backpack.

2.2 Dummy positioning

In the experiments, two distinct dummy positions were tested. First, for the sake of comparison with existing measurements, the body was set lying with arms alongside the trunk and face up (Figure 4a, b). The second position mimics the typical drowning positioning, as introduced in Section 1.3. This typical position of a drowning victim is mostly described in qualitative terms in literature and limited geometric details are available on the body positioning (Blanco and Lopez-Abajo, 2001; Lunetta et al., 2014). This prompted us to make plausible assumptions on the relative positioning of the torso, limbs, and head. In the conducted experiments, an angle of 75° was considered between the torso and the arms, and between the pelvis and the legs. The limbs were kept straight due to a lack of information on the degree of bending in actual cases. For technical reasons, the torso was placed horizontally in the wind tunnel and the limbs formed an angle of 15° with the vertical (Figure S8 in Supplement). In the wind tunnel, the dummy was positioned upside down (i.e., head facing up) compared to the body position typically observed in the field when a victim of drowning is found (i.e., head facing down). This choice does not affect the results. It was made to reduce the length of the measurement sting and keep parasitic moments in the measurements at a minimum. Nonetheless, for each considered wind velocity, tests were also conducted without the dummy for estimating the forces induced by the flow on the measurement arm, and correct for them (Section 2.4)

For each body positioning, the body yaw angle (noted q) was systematically varied. This angle is defined equal to 0 when the spine is aligned with the main flow direction and the head is located downwind (Figure 3). The yaw angle is positive in the counterclockwise direction. Thirty different values of the body yaw angle were tested, in the range from 0° to 345°.

The dummy was dressed in either tight or loose clothes (Figure 4). The former aim at representing a victim of a river bathing accident (i.e., naked or wearing a swimming suit), while still hiding the screws present at the dummy joints (Figure S9 in Supplement) which would otherwise bias the measurements. The loose clothing was used to represent more standard clothing of a drowning victim. In some tests, an empty backpack was added to appreciate the influence of such accessories (Figure 4e).

2.3 Flow scenarios

In the wind tunnel, experiments could be conducted for wind velocity ranging from $U_x = 3.2$ m/s up to $U_x = 6.5$ m/s. Below 3.2 m/s, the sensitivity of the sensors did not allow retrieving a stable signal due to the low values of forces. Above 6.5 m/s, unacceptable vibrations of the dummy limbs were detected. Tests were conducted for the minimum value $U_x = 3.2$ m/s, the maximum one, $U_x = 6.5$ m/s, and an intermediate one, $U_x = 4.5$ m/s (Table 2).

During the tests, the air temperature was 9.8°C and the atmospheric pressure was 100,100 Pa. This leads to a value of $n = 1.4 \times 10^{-5}$ m²/s for the kinematic viscosity of air. Considering the body height as a characteristic length ($L = 1.9$ m, irrespective of the dummy positioning) like Bixler et al. (2007), Marinho et al. (2009) and Marinho et al. (2011), the Reynolds number $\mathrm{Re} = U_x L / n$ can be evaluated for each considered wind velocity (Table 2). In the tests, the Reynolds number ranges between 4.3×10^5 and 8.8×10^5. From the value of the kinematic viscosity of water ($n = 1.007 \times 10^{-6}$ m²/s), we may infer that the hydrodynamic coefficients determined from the tests conducted in the wind tunnel are comparable to those that would be obtained with the dummy immerged in a water flow with a relative velocity ranging between 0.23 and 0.46 m/s (Table 2). Although narrow, this range of relative velocity between the body and the flow is plausible. Besides, Reynolds numbers of the order of 10^5 correspond to a turbulent regime, in which the hydrodynamic coefficients, particularly the drag coefficient, vary little with the Reynolds number. Indeed, preliminary tests have revealed no drag crisis for Reynolds numbers in the range from 2.5×10^5 to 1.6×10^6.

Table 2: Tested wind velocities, Reynolds numbers
and corresponding water velocities, if the same Reynolds number is assumed.

Wind velocity [m/s]	3.2	4.5	6.5
Reynolds number [-]	4.3×10^5	6.1×10^5	8.8×10^5
Water velocity [m/s]	0.23	0.32	0.46

2.4 Determination of hydrodynamic coefficients

In each experimental test, the three components of the fluid-induced force were measured. They are referred to F_D, F_S and F_L. They are respectively aligned along the x, y and z reference axes (Figure 3). The value of the torques along these three reference directions were also measured in each test. They are referred to T_x, T_y and T_z. These quantities are also referred to as moments (Tropea et al., 2007; Anderson, 2011). Consistently with Section 2.1, each of these quantities was measured over a duration of 15 s and time-averaged. The forces and torques acting on the measurement arm alone were subtracted from the respective quantities to obtain the aerodynamic loading of the body only.

It is customary to relate the three force components to the square of the relative approach velocity U, the fluid density r, the body frontal area A and non-dimensional coefficients, as follows:

$$F_D = \frac{1}{2}\rho C_D A U^2, \qquad F_S = \frac{1}{2}\rho C_S A U^2 \qquad \text{and} \qquad F_L = \frac{1}{2}\rho C_L A U^2, \tag{1}$$

where C_D, C_S and C_L are the drag, side and lift coefficients, respectively. In the experimental conditions, air density was 1.23 kg/m³.

In Section 3, the experimental results are displayed in two different forms. On the one hand, we show the value of the products of the respective hydrodynamic coefficients and the corresponding frontal area:

$$C_D A = \frac{2F_D}{\rho U^2}, \qquad C_S A = \frac{2F_S}{\rho U^2} \qquad \text{and} \qquad C_L A = \frac{2F_L}{\rho U^2}. \tag{2}$$

The obtained quantities, $C_D\,A$, $C_S\,A$ and $C_L\,A$, are referred to as drag, side and lift areas, respectively. They offer the advantage of being independent of the evaluation of a frontal area, which is intricate as this area is strongly influenced by the body positioning, yaw angle, clothes and their interaction with moving air/water (swelling). This approach also avoids the selection of a particular reference area (e.g., kept unchanged when the yaw angle is varied), which would inevitably be somehow arbitrary.

It is common in sport aerodynamics to compare the aerodynamic effects in various positions of a given body (Blocken et al., 2018; Mannion et al., 2019; Wolfsperger et al., 2021). As such, the drag, side, and lift areas measured for one body do not apply for a body of similar geometry but at another scale. It is possible to scale these areas by dividing them by a reference area, independent of the yaw angle, of the body considered in the experiments and multiplying by the corresponding area of the body of interest. The obtained coefficients will experience the same variations as the force areas, but with values that depend on the reference area chosen, which could be the body surface area (Mosteller, 1987; Du Bois and Du Bois, 1989; Tikuisis et al., 2001; Yu et al., 2010).

We also evaluated the standard non-dimensional coefficients C_D, C_S and C_L, defined as follows:

$$C_D = \frac{2F_D}{\rho A U^2}, \qquad C_S = \frac{2F_S}{\rho A U^2} \qquad \text{and} \qquad C_L = \frac{2F_L}{\rho A U^2}. \tag{3}$$

This requires an estimation of the body frontal area, for each body positioning and each considered yaw angle. To achieve this, a 3D digital model of the dummy was created based on a LIDAR scan. The obtained frontal areas for both body positions and tight clothes are depicted in Figure 5. For both positions, a periodicity can be observed in the variation of the frontal areas with the yaw angle. Frontal areas for the drowned position exhibit additionally local minima corresponding to yaw angles for which one limb hides another.

In the case of loose clothes, the frontal area is expected to be slightly larger irrespective of the body position and yaw angle. However, frontal areas with loose clothes could not be reliably measured due to the deformable nature of such clothes. Loose clothes are prone to catching the wind/water flow and can therefore inflate, increasing the frontal area. Such effects cannot be reproduced during a LIDAR scan of the dummy, since such a scan cannot be performed during a wind tunnel test. In the following, frontal areas estimated with tight clothes are used as a proxy for both types of clothes.

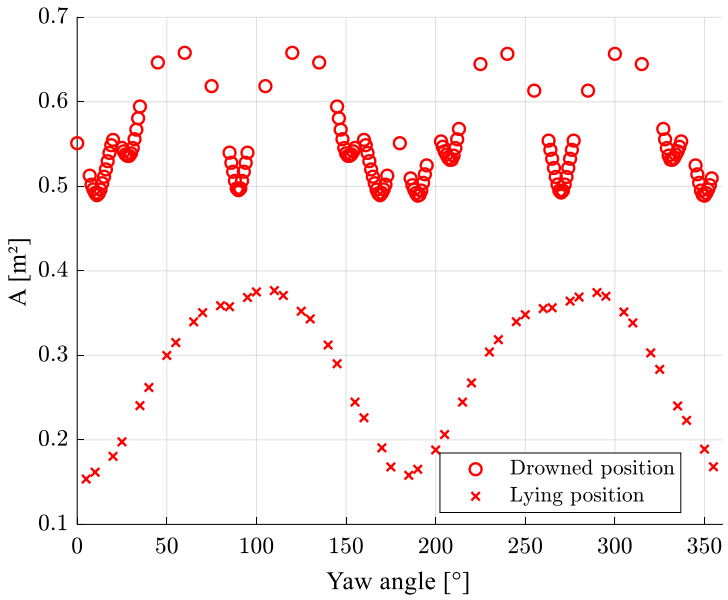

Figure 5: Frontal area of the dummy in lying and drowned positions in tight clothes, as a function of yaw angle.

2.5 Test program

The test program is detailed in Table 3. By varying the yaw angle, the dummy positioning, the type of clothes and the presence of a backpack, 83 configurations were considered. In each of them, measurements were conducted for the three wind velocities given in Table 2, leading to a total of 249 experimental tests.

Table 3: Test program. All tests were performed for the three wind velocities given in Table 2.

Yaw angle	Lying position		Drowned position		
	Tight clothes	Loose clothes	Tight clothes	Loose clothes	Loose clothes and backpack
0°	X	X	X	X	X
15°	X	X	X	X	
25°				X	
30°	X	X	X	X	
35°				X	
45°	X	X	X	X	X
60°	X	X	X	X	
75°	X	X	X	X	
90°	X	X	X	X	X
105°			X	X	
120°			X	X	
135°	X	X	X	X	X
145°				X	
150°			X	X	
155°				X	
165°			X	X	
180°	X	X	X	X	X
195°			X	X	
205°				X	
210°			X	X	
225°	X	X	X	X	
240°			X	X	
255°			X	X	
270°	X	X	X	X	

285°			X	X
300°			X	X
315°	X	X	X	X
330°			X	X
335°				X
345°			X	X

3 Results

The experimental results for the drag area and coefficient are presented in detail in in Section 3.1. Results inferred from the experimental observations for the side and lift areas and coefficients are depicted in Section 3.2. The observed torques around the vertical axis are discussed in Section 3.3. The measured forces are displayed in Figures S4 to S6 in Supplement.

3.1 Drag

The evaluated drag areas and coefficients are discussed in the following paragraphs. A summary of the main findings is provided in Table 4. Note that all measured values of the force component F_D fall well above the resolution of the corresponding sensor, as shown in Figure S4 in Supplement. Moreover, in all configurations but four (out of a total of 249, in 98 % of the cases), the ratio of the standard deviation of the drag force to the time-averaged value remains below 10 % (Figures S29 in Supplement).

3.1.1 Drag area

Figure 6 represents the drag areas evaluated according to Eq. (2), as a function of yaw angle and the configuration (i.e., dummy position, type of clothes, and presence or not of a backpack) for the highest tested Reynolds number. Boxplots in Figure 7 provide a summary of the measured values of drag area for each configuration. For the sake of readability, Figures S10 to S12 in Supplement show the variation of the drag area as a function of the yaw angle for each individual configuration.

Overall, the observed values of drag area vary in a relatively large range, between 0.09 and 0.59 m^2, which corresponds to almost an order of magnitude of variation (Figure 6). These variations are mostly explained by the influence of the yaw angle, dummy position, type of clothes, and presence of a backpack. In contrast, the wind velocity (i.e., Reynolds number) shows a limited influence on the drag area (Figure 8). Regardless of the configuration and the yaw angle, the drag area generally does not vary by more than 15 % when the Reynolds number is varied in the range tested here (Figures S15 to S17 in Supplement).

As shown in Figure 6, varying the yaw angles has a substantially stronger influence in the case of the lying position than in the drowned position. In the former case, the drag area varies by a factor two (tight clothes) to four (loose clothes) when the yaw angle is changed. In the latter case, the drag area does not vary by more than 50 %, irrespective of the type of clothes. This is due to the lower influence of the yaw angle on frontal area in the drowned position than in the lying position.

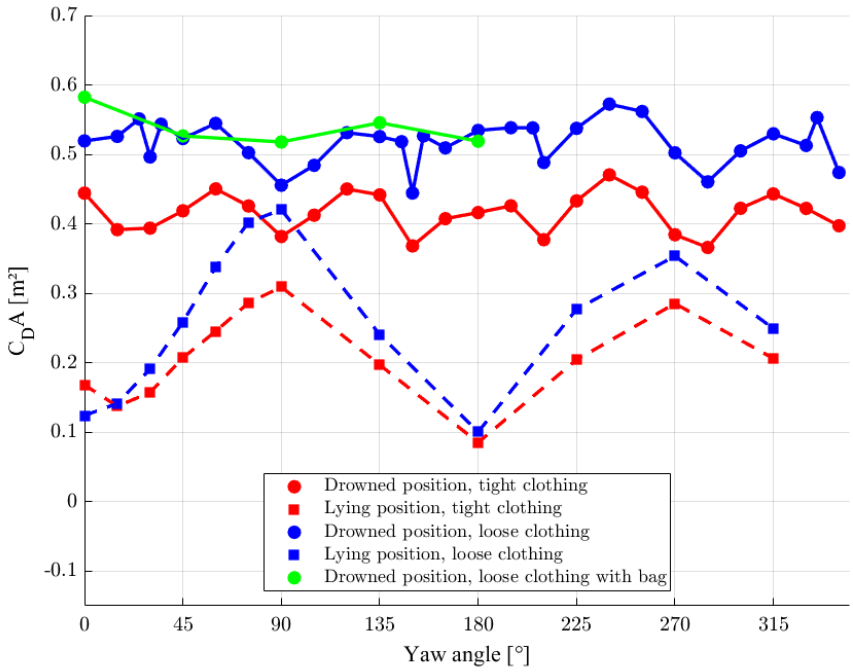

Figure 6: Drag area as a function of yaw angle in the tested configurations for Re = 8.8×10^5.

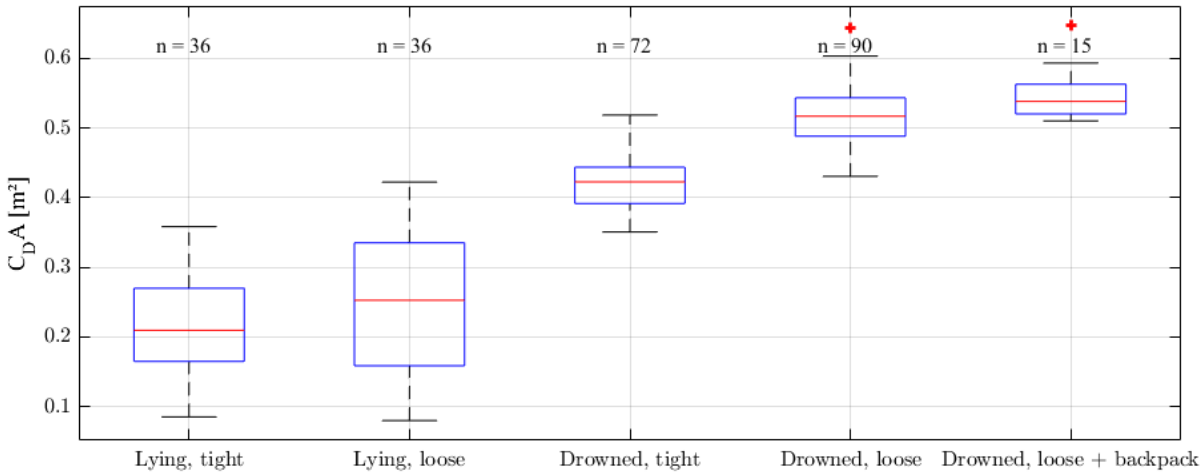

Figure 7: Boxplots of drag areas for all yaw angles and Reynolds numbers in each configuration (dummy position and type of clothes). For each of them, symbol *n* indicates the number of tests, out of a total of 249, and red crosses represent outliers.

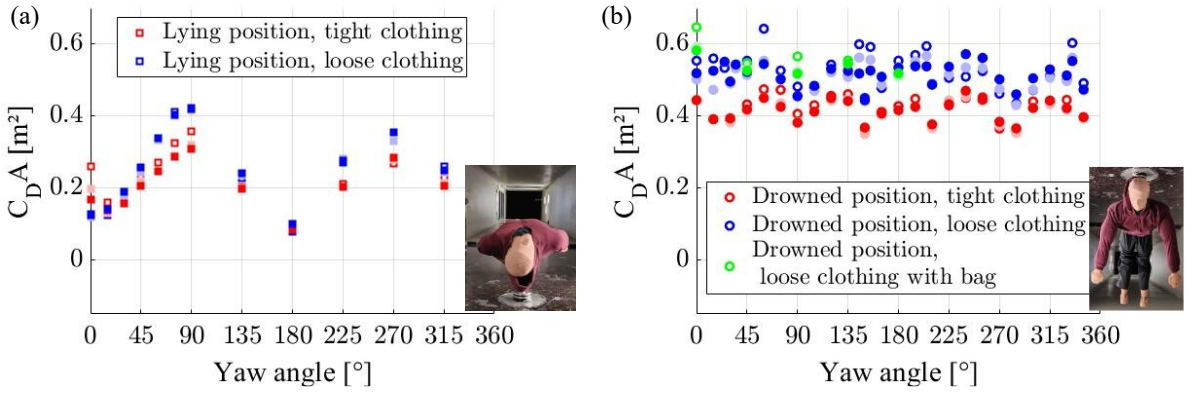

Figure 8: Drag area as a function of yaw angle in the configurations with loose clothes (a) and with tight clothes (b). The markers face colour refers to the Reynolds number considered in each test. Empty markers: $Re = 4.3 \times 10^5$, light plain markers: $Re = 6.1 \times 10^5$, and dark plain markers: $Re = 8.8 \times 10^5$.

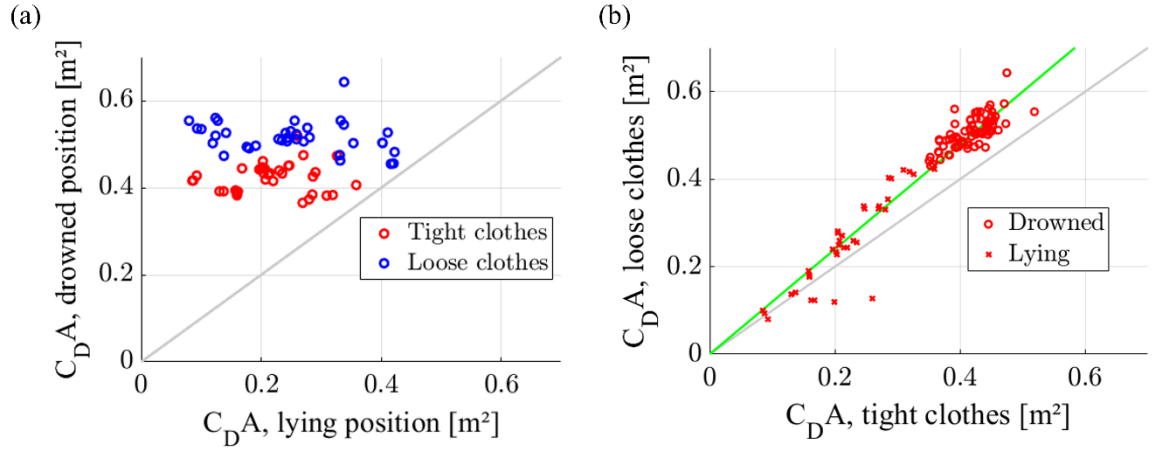

Figure 9: Influence of (a) the dummy position and (b) the type of clothes on the observed drag areas. The 1:1 line is represented in grey, while the green line follows the slope 1:1.15.

In the lying position, the drag area varies between 0.08 and 0.42 m^2 (Figure 7). This range is lower than the range of values observed for the drowned position, which is between 0.35 and 0.52 m^2 with tight clothes, and between 0.43 and 0.64 m^2 with loose clothes (Figure 9a). The median value of the observed drag areas increases by about a factor two when the dummy position is changed from lying to drowned (Figure 7). The difference between the two positions is maximum when the yaw angle is 0° or 180°, and minimum when the yaw angle is 90° or 270°. This may be due to differences in the streamwise body length which is maximum for yaw angles of 0° and 180°, and minimum for 90° and 270°. At 0° yaw angle, the drag area can be 2.5 times (tight clothes) to 4 times larger in the drowned position than in the lying one (Figure S18 in Supplement). At a yaw angle of 180°, these factors grow to 4.5 and 6, respectively.

Unlike the influence of the yaw angle, the effect of loose or tight clothes is slightly stronger in the drowned position than it is in the lying position. In the latter case, the values are increased

by about 15 % when loose clothes are used instead of tight ones (with some cases in which these values are decreased), while in the drowned position, the values are magnified by about 20 % when loose clothes are used instead of tight ones (Figure 9b). Adding a backpack further increases the drag area by up to 18% (Figure 13a).

3.1.2 Drag coefficient

For the highest tested Reynolds number, Figure 10 represents the drag coefficients evaluated according to Eq. (3), as a function of the yaw angle and the configuration. In Figure S19 to S21 in Supplement, the drag coefficients are also represented for each configuration individually and for all tested Reynolds numbers. Boxplots in Figure 11 display the variability of the estimated drag coefficient for each configuration.

Compared to the range of variation of the drag area (Figure 6), the observed values of the drag coefficient vary in a much smaller range (i.e., between 0.5 and 1.2), except for a few outliers (Figure 10 and Figure 11). Like in the case of the drag area, the influence of the Reynolds number remains small in the tested range (generally less than 15 % of variation in the drag coefficient, Figure S19 to S21 in Supplement).

When the yaw angle is systematically varied, the drag coefficient corresponding to the lying position varies between 0.5 and 1.1 (Figure 11). The ratio of the highest value to the lowest is of the order of two, which is considerably lower than the factor four to five obtained for the drag areas. This ratio is slightly higher in the case of loose clothes than with tight clothes, suggesting that the drag coefficient is more sensitive to the yaw angle for loose clothes than for tight ones. For the drowned position, the variations of the drag coefficient with the yaw angle remain lower than 50 %. This is similar to the results obtained for the drag area, as the frontal area shows limited variations with the yaw angle in the case of the drowned position. For the lying position, the variation of the drag coefficient with the yaw angle follows a similar pattern as the corresponding frontal area (Figure 6), with extrema at comparable yaw angles. For the drowned position, an opposite pattern is observed.

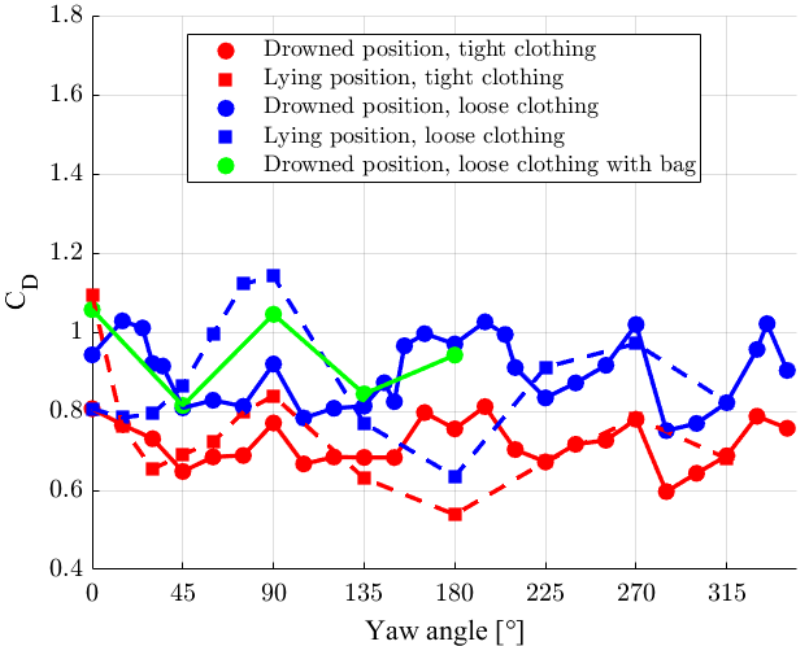

Figure 10: Drag coefficient as a function of yaw angle in the tested configurations for Re = 8.8×10^5.

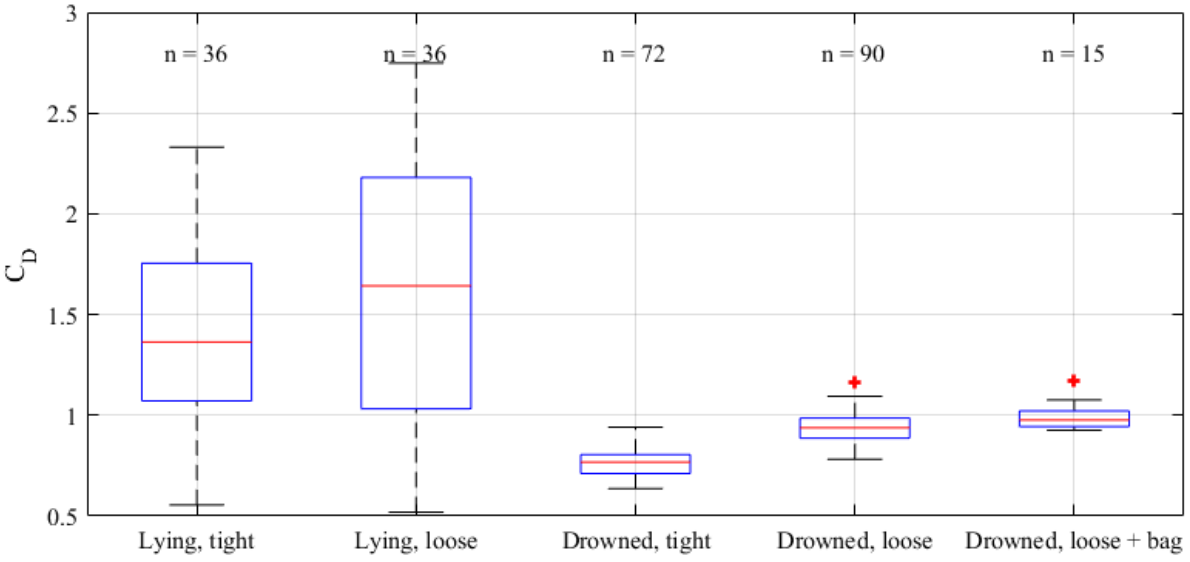

Figure 11: Boxplots of drag coefficients in each configuration (dummy position and type of clothes). For each of them, symbol *n* indicates the number of tests, out of a total of 249, and red crosses represent outliers (all at a yaw angle of 0°).

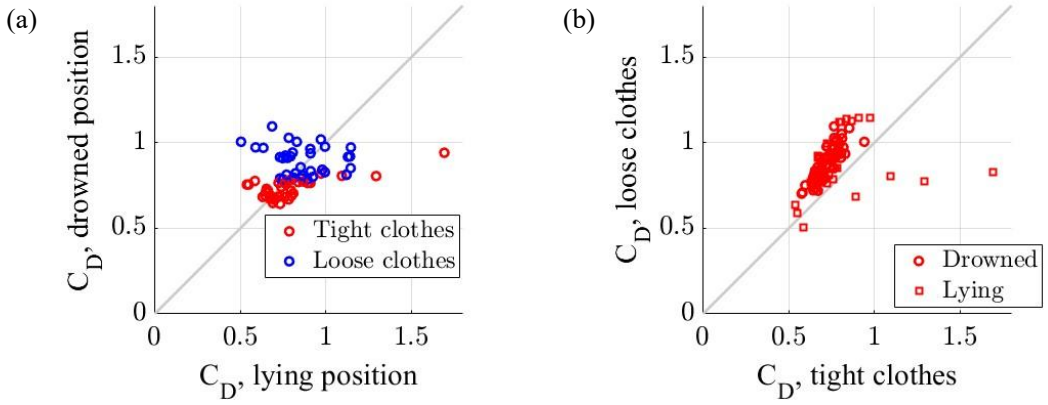

Figure 12: Influence of (a) the dummy position and (b) the type of clothes on the drag coefficient.

In the lying position, the drag coefficient varies between 0.5 and 0.9 for tight clothes and between 0.5 and 1.2 for loose clothes (Figure 11). In the drowned position, the ranges are even thinner for both types of clothes (0.6 to 0.9 for tight clothes, and 0.7 to 1.1 for loose clothes). Unlike in the case of the drag areas (Figure 9a), Figure 12a reveals that no systematic relation appears between the drag coefficients in drowned and in lying positions. This hints at the capacity of a position-dependent frontal area (Figure 5) to encompass to a great extent the influence of the dummy position.

Like for the drag areas, the effect of changing the type of clothes is stronger in the drowned position than in the lying position. The mean value of the drag coefficient increases by a about 15 % when the type of clothes is changed from tight to loose in the lying position, while this increase reaches 30 % for the drowned position (Figure 11 and Figure 12b).

When a backpack is added in the drowned position (with loose clothes), Figure 7 and Figure 11 show that the median value is increased by 4% and 3% for the drag area and coefficient, respectively. Such changes are of little significance compared to other effects, such as the variability induced by changes in the yaw angle. The scatter plots in Figure 13 reveal that, for a given configuration, an increase in the drag coefficient is not systematic when a backpack is added though it can be as high as 18% in some cases. However, these increases may be partly attributed to an increased frontal A due to the presence of the backpack. This change in the frontal area could not be systematically measured (as in Figure 5) but it is estimated at maximum 13 %.

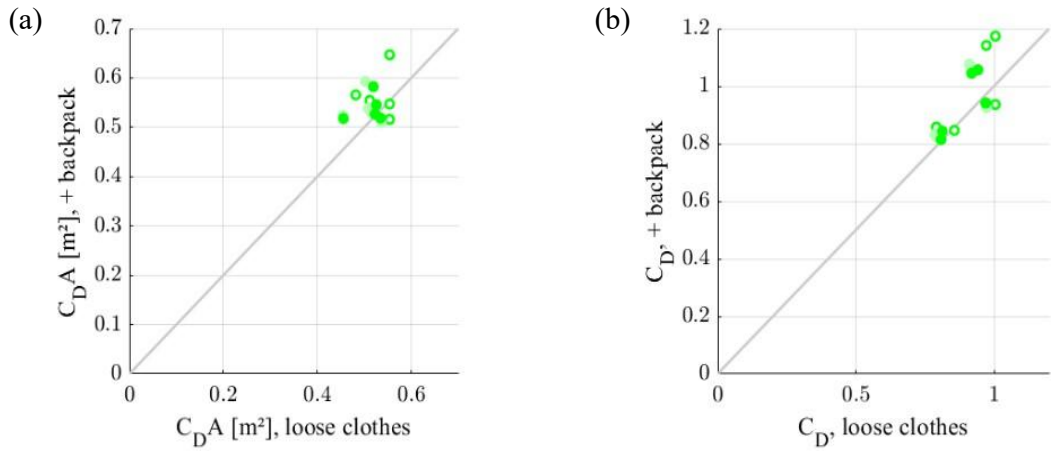

Figure 13: Influence of the backpack on the (a) drag area and (b) drag coefficient.

Table 4: Outcomes of parameter study for the drag area and coefficient of a human-like body.

	Drag area	Drag coefficient
Typical range of variation	0.08 – 0.65 m² (Figure 6 and Figure 7)	0.5 – 1.2 (Figure 10 and Figure 11)
Influence of Reynolds number	Limited: ± 15 % (Figure S15 to S17 in Supplement)	Limited: ± 15 %
Influence of yaw angle	Lying position: factor 4 to 5 Drowned position: change by no more than 50 % (Figure 6 to Figure 8)	Lying position: factor 2 Drowned position: change by no more than 50 % (Figure 10 and Figure 11)
Influence of body position	Median values on all yaw angles change by a factor 2 (Figure 7) At a yaw angle of 0° or 180°, the difference may reach a factor of 2.5 to 6 (Figure 8 and Figure 9a)	No systematic trend (Figure 12a)
Influence of considering loose clothes instead of tight clothes	+ 20 % (Figure 9b)	Lying position: + 15 % Drowned position: + 30 % (Figure 11 and Figure 12)
Influence of adding a backpack	Increase by up to 18 % (Figure 13a)	Increase by up to 18 % (Figure 13b)

3.2 Side and Lift

The side area was computed according to Eq. (2). The results are displayed in Figure 14 for the tested yaw angles, Reynolds numbers and configurations. The yaw angle has a significant influence on the side area, leading to variations ranging mostly from – 0.1 m² to + 0.15 m² (Figure 14). This influence is stronger in the lying position than in the drowned position, as shown in Figure S14 in Supplement. A quasi-periodic pattern can be identified in the results of the lying position, with a period of 180° (Figure 14), whereas visual inspection of Figure 14b does not reveal a distinctive pattern in the case of the drowned position. Similarly, no systematic trend is observed for the influence of the type of clothes (Figure S22 in Supplement), nor for the effect of adding a backpack (Figure S23 in Supplement). The absence of trend in some cases may be attributed to the relatively low values of the measured forces, which in a number of configurations are of comparable magnitude as the resolution of the sensor. Figure S5a in Supplement indicates that about 30 % of the tested configurations lead to a value of the force component F_S lower than the sensor resolution. The ratio of the standard deviation of the side force to the time-averaged drag force remains below 10 % in about 90 % of the tested configurations, and the maximum value of this ratio is 25 % (Figure S30 in Supplement).

Like for the side area, the side coefficient is less affected by changes in the yaw angle in the case of the drowned position than it is for the lying position (Figure 15). In the former case, the side coefficient varies between – 0.11 and 0.15, whereas in the latter case it ranges between – 0.35 and 0.4. No significant effect on the side coefficient could be detected when the type of clothes was varied (Figure S22 in Supplement), nor when a backpack was added (Figure S23 in Supplement).

The evaluated lift areas and coefficients are displayed Figure S24 and Figure S25 in Supplement. The lift areas vary between 0 m² and about 0.2 m² for the lying position (Figure S24a in Supplement) and between 0 m² and 0.3 m² for the drowned position (Figure S24b in Supplement). The lift coefficient varies mostly between 0 and 0.6 irrespective of the considered configuration (Figure S25 in Supplement). In the drowned position, the lift area and coefficients reach a maximum when the yaw angle is close to 180°. Apart from this, the experimental data do not enable detecting any significant pattern, neither when the yaw angle (Figures S24 and S25 in Supplement) or type of clothes (Figure S23 in Supplement) is varied, nor when a backpack is added (Figure S23 in Supplement), which may result from the measured force component F_L being too close to the sensor resolution. Figure S6 in Supplement reveals that, in about 20 % of the tested configurations, the value of F_L is lower than the sensor resolution, while issues with the time convergence of this measurement also arise (Figure S3a in Supplement). Moreover, in a quarter of the tested configurations, the standard deviation of the lift force exceeds 10 % of the time-averaged drag force, reaching up to about 30 % (Figure S3a in Supplement).

The difficulties faced to detect significant trends in the results obtained for the lift area and coefficient, as well as to some extent for the side area and coefficient, may result from limitations in the measurement accuracies. Such difficulties were not encountered in the case of the drag area and coefficient (Section 3.1). This may be explained by the relatively lower

values of side and lift forces, hence also area and coefficients, compared to the drag, as confirmed in Figure S26 in Supplement.

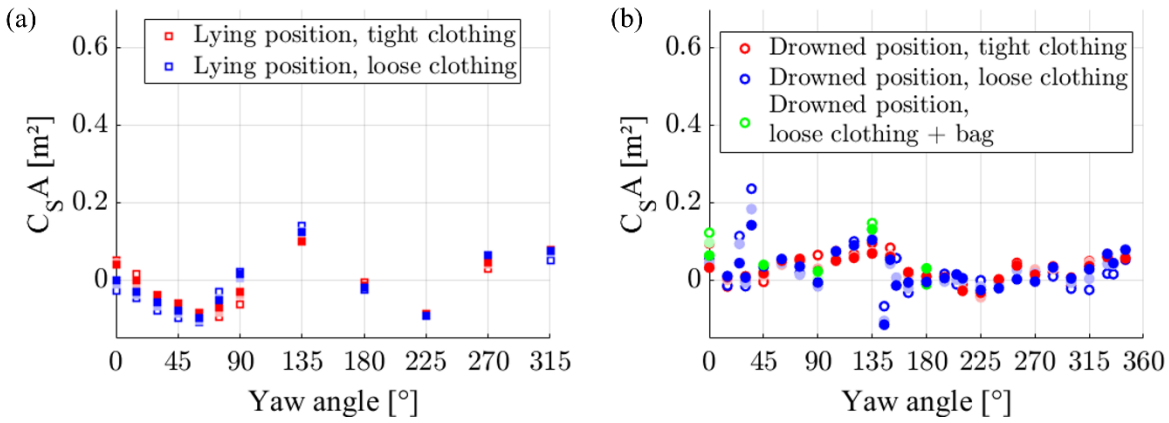

Figure 14: Side area as a function of yaw angle (a) in the lying position and (b) in the drowned position. The markers face colour refers to the Reynolds number considered in each test. Empty markers: Re = 4.3×10^5, light plain markers: Re = 6.1×10^5, and dark plain markers: Re = 8.8×10^5.

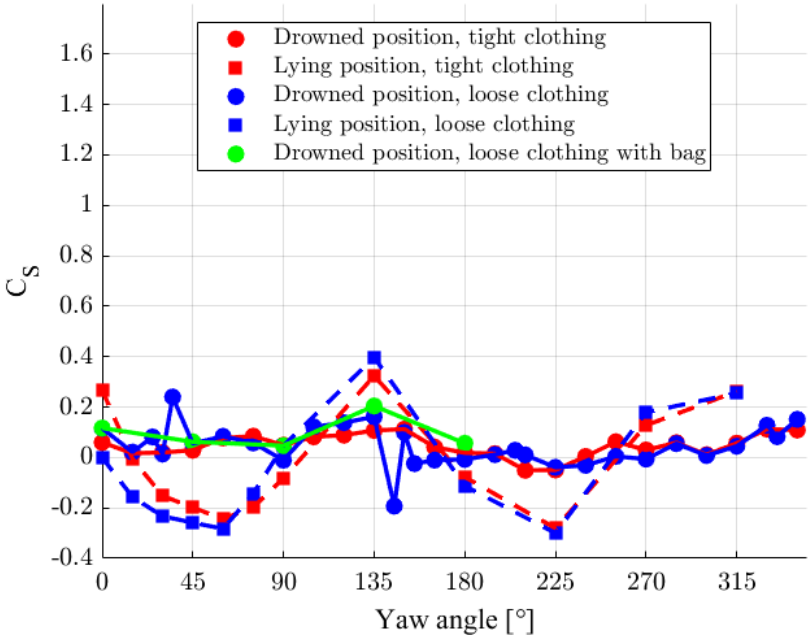

Figure 15: Side coefficient as a function of yaw angle in the tested configurations for Re = 8.8×10^5. Continuous lines are interpolations between the measurements represented by discrete data.

3.3 Torque in the vertical direction

For the three considered Reynolds numbers, Figure 16 represents the vertical torques (T_z, also called yawing moments) as a function of yaw angle. Most values of torque lie between – 1 Nm and + 1 Nm. In magnitude, 95 % of these measurements are larger than the sensor resolution (Figure 6b in Supplement). In a few cases, corresponding all to the lying position (and irrespective of the type of clothes), the observed torque values reach – 2 Nm or extend

up to + 2.8 Nm. In the drowned position, the torque values range between – 0.5 and + 0.5 Nm with tight clothes, and from – 1.2 to 0.9 Nm with loose clothes. These values are strongly dependent on the Reynolds number. Compared to the case of $Re = 4.3 \times 10^5$, the torque values are about twice higher for $Re = 6.1 \times 10^5$, and about four times higher for $Re = 8.8 \times 10^5$, as detailed in Figure S24 in Supplement. Both the body position and the type of clothes also have a substantial influence on the torque values.

The pattern of variation of the torque with the yaw angle differs between the lying and the drowning positions. In the lying position, vertical torques are positive between 0° and 180°, with a maximum value captured around a yaw angle of 75°. The torques become negative for yaw angles 180° and 360°, with a maximum absolute value captured at 270°. In the drowned position, vertical torques are mostly negative between 0° and 180°, though lower in magnitude than in the lying position. They are generally positive for yaw angles between 180° and 360°.

In lying position, the type of clothes has no significant effect on the vertical torque (Figure 16). In contrast, in the drowned position, extreme values are greater in magnitude in the case of loose clothes than with tight clothes and torques are strictly positive for yaw angles over 180° with loose clothes. Adding a backpack does not lead to any significant difference in torques compared to the same configurations without backpack.

The observed torque values suggest that different equilibria exist depending on the body position. In the lying position, equilibrium at $q = 0°$ is unstable. Indeed, if the body deviates slightly, say towards positive values of the yaw angle, a positive moment acts on the body which makes it rotate further and leave its initial equilibrium position. Vice-versa, equilibrium with a yaw angle of $q = 180°$ is stable, as slight variations in the yaw angle around $q = 180°$ induce moments which tend to shift back the body to its equilibrium position at $q = 180°$. For the drowned, the opposite is found: the equilibrium at $q = 0°$ is stable, while the equilibrium at $q = 180°$ is unstable. Consequently, depending on the body position (lying or drowned), the body tends to align with the flow with the head located either upwind (lying position) or downwind (drowning position).

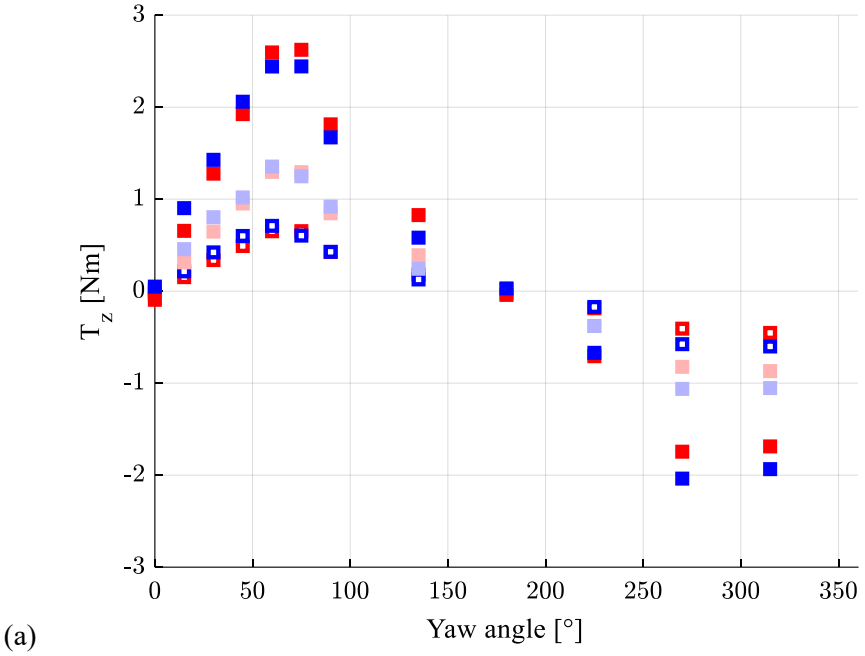

(a)

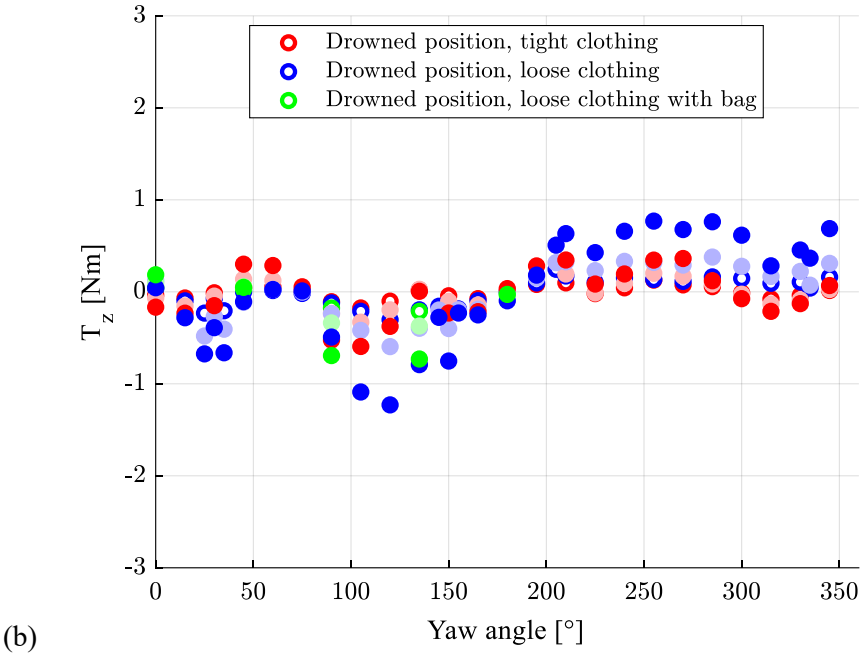

(b)

Figure 16: Vertical torque as a function of yaw angle (a) for the lying position and (b) for the drowned position. The markers face colour refers to the Reynolds number considered in each test. Empty markers: Re = 4.3 ´ 10^5, light plain markers: Re = 6.1 ´ 10^5, and dark plain markers: Re = 8.8 ´ 10^5.

4 Discussion

4.1 Comparison with standard shapes

Drag coefficients are influenced by multiple parameters, including Reynolds number, wall roughness, turbulence intensity, shear in approach flow, proximity of a wall, and interactions between multiple obstacles (Achenbach, 1974; Dubois and Andrianne, 2022). Here, for setting in perspective the drag coefficients obtained for novel configurations (human body in drowning position, with various clothes types and body orientations with respect to the approach flow), they are compared to a few well-known reference configurations, without systematically exploring the effect of all possible influencing parameters on the reference cases.

In Figure 17, the ranges of variation of the drag coefficient derived from our experimental observations are compared to values characterizing two reference shapes: a smooth sphere (Morrison, 2013), and a smooth cylinder of radius 0.2 m and of finite length equal to 1.9 m, with its axis either aligned with or normal to the approach flow (Hölzer and Sommerfeld, 2008). To estimate the drag coefficient of smooth cylinders and spheres, Hölzer and Sommerfeld (2008) and Morrison (2013) used data from experiments conducted both with air and with water. They systematically applied Reynolds similarity to combine data originating from tests carried out with different fluids (Roos and Willmarth, 1971). This relatively standard procedure of using Reynolds similarity for transferring results obtained with one fluid to another one also supports our approach consisting in performing tests with air (wind tunnel) and transfer the outcomes to water (rivers).

For each tested configuration (body position and type of clothes), Figure 17 represents the drag coefficient as a function of the Reynolds number, using boxplots to reflect the variability of the coefficient with the yaw angle.

Compared to the variability of the drag coefficients with the yaw angle, the drag coefficients evaluated here hardly vary with the Reynolds number in the tested range. In the case of a sphere, variations are visible in Figure 17 due to the drag crisis occurring in this range of Reynolds number. For the cylinders the considered range of Reynolds number is below the range corresponding to the drag crisis.

The relative positioning of our experimental results compared to the reference values appears reasonable, both in terms of extent of the influence of the yaw angle and in terms of absolute values.

4.1.1 Influence of yaw angle

The difference between the drag coefficients of cylinders with axis normal (i.e., perpendicular) to the approach flow (i.e., yaw angle of 90° or 270°, $C_D = 1.24$) and aligned with the approach flow (i.e., yaw angle of 0° or 180°, $C_D = 0.21$) is of the order of 1. This is similar to the extent of the variation of the drag coefficients (as represented by the boxplots) when the yaw angle is varied for the dummy in lying position. The cylinder used by Hölzer and Sommerfeld (2008) may be seen as a highly idealized version of the dummy, leading to

comparable changes in the drag coefficient when the yaw angle is varied. Figure 10 shows that the drag coefficient is maximum when the yaw angle is 90° or 270° (similar to the cylinder normal to the approach flow) and minimum when the yaw angle is 0° or 180° (similar to the cylinder aligned with the flow).

When the yaw angle is varied, the changes in the values of the drag coefficient of the dummy in drowned position are considerably lower than the difference between the drag coefficients of the cylinders normal to the approach flow and aligned with the approach flow. This is due to the more compact shape of the drowned positioning compared to a cylinder.

4.1.2 Absolute values

Despite some similarity between the body in lying position and cylinders, the drag coefficients found for the body in lying position are above those of cylinders. The lowest values of the drag coefficients estimated here are around 0.5 (corresponding to yaw angles of 0° or 180°, as shown in Figure 10), which is about 2.5 times greater than the corresponding values for a cylinder with its axis aligned with the approach flow (Figure 17). This is because a cylinder is a more streamlined shape than a human-like body. For the same reason, the highest values of the drag coefficients found for the dummy in lying position (corresponding to yaw angles of 90° or 270°, as shown in Figure 10) are also above the values characterizing a cylinder with axis normal to the flow, i.e. with the same yaw angle.

Drag coefficients obtained for the body in drowned position lie in-between the case of a cylinder with axis aligned with the approach flow and that of a cylinder with axis normal to the approach flow. Irrespective of the body positioning, the drag coefficients obtained for a human-like body are at least four times larger than the value characterizing a sphere ($C_D \sim 0.1$) in the same range of Reynolds number.

4.1.3 Reynolds dependency

In the considered range of Re, the drag coefficient of a sphere varies between 0.4 and 0.15 due to the drag crisis while this coefficient is equal to 0.21 for a cylinder aligned with the flow and 1.24 for a finite cylinder perpendicular to the flow. Figure 18 shows no drag crisis in the case of a human body and no clear influence of the Reynolds number on the values of drag coefficient in the tested range of Reynolds number. These observations are not affected by the choice of a particular characteristic length in the definition of the Reynolds number (e.g., body height vs. trunk height for the drowning position).

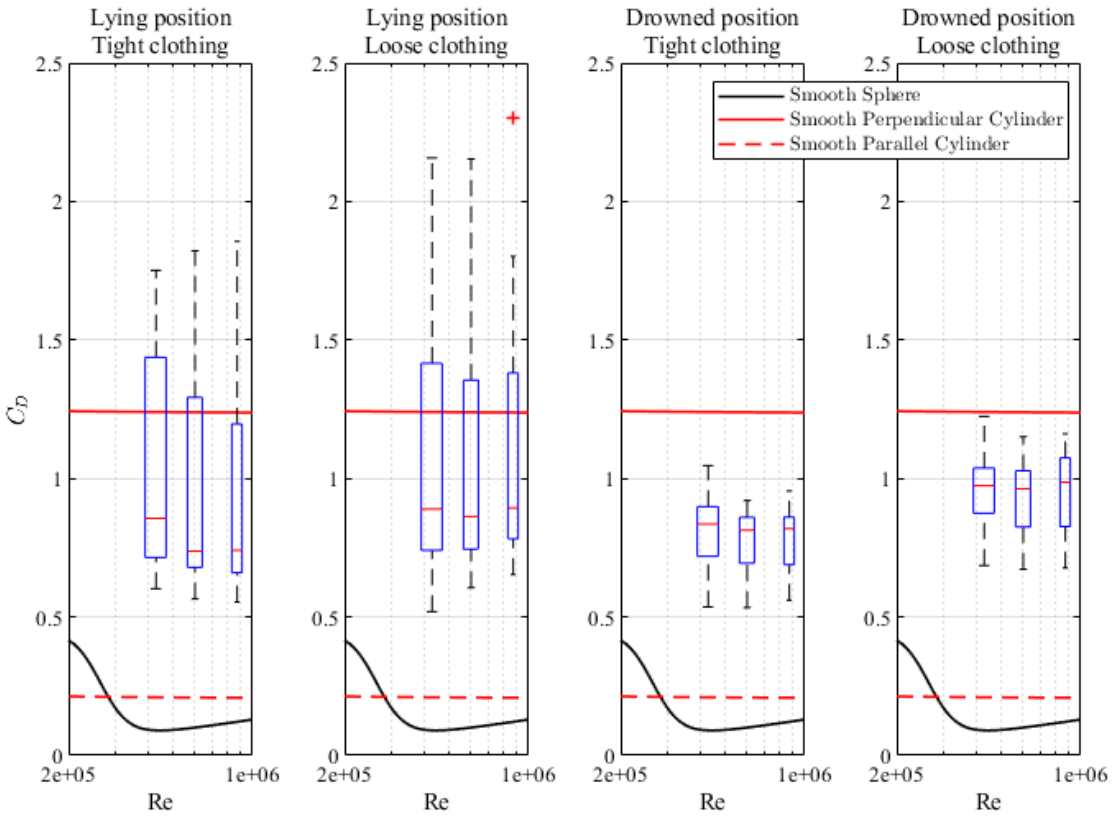

Figure 17: Estimated drag coefficient as a function of the Reynolds number, for each configuration (body position and type of clothes), with boxplots reflecting the variability of the drag coefficient with the yaw angle. Comparison with reference values for a smooth sphere (Morrison, 2013) and smooth cylinders, either aligned with (i.e., parallel to) or normal (i.e., perpendicular) to the approach flow (Hölzer and Sommerfeld, 2008).

4.2 Comparison with studies on swimming

The drag coefficient characterizing a human body has been studied for a variety of settings, including positions corresponding to swimming (Bixler et al., 2007; Marinho et al., 2009, 2011, 2012; Zamparo et al., 2009; Mantha et al., 2014), ice skating (Ingen Schenau, 1982), ski jumping (Müller, 2009; Wolfsperger et al., 2021), speed skiing (Barelle et al., 2004), cycling (García-López et al., 2008), standing, sitting or supine positions (Schmitt, 1954). Although most of these positions differ substantially from the drowned and lying positions of interest here, the swimming position shows some similarities with the lying position considered here when the head is oriented towards upwind. In Figure 18, we compare our results in lying position with a yaw angle of 180° and tight clothes and a yaw angle of 0° and 180° for loose clothes against values of drag coefficient reported in literature for swimmers (Bixler et al., 2007; Marinho et al., 2009). Measurements in lying position with a yaw angle of 0° and tight clothes are considered as inconsistent. Indeed, these values fail to agree with the pattern observed in C_D as a function of the yaw angle in all other considered configurations (see Figure 28 in Supplement). The range of Reynolds number tested here is about five times lower than the ranges considered by Bixler et al. (2007) and Marinho et al. (2009), and it is consistent with what could be observed in a river.

Bixler et al. (2007) performed flume tests with a dummy and with a real swimmer, as well as simulations using a 3D computational fluid dynamics (CFD) model. A body positioning typical of swimming was considered, with the limbs aligned with the trunk and arms in front of the head. In each case, the body was positioned at a distance of 0.75 m from the free surface, so that the surface had no significant effect when bodies are at such a depth (Vennell et al., 2006). They found a remarkable agreement between their experimental observations with a dummy and their computations, leading to a drag coefficient of about 0.3. A slightly higher value was obtained in the tests conducted with a real swimmer ($C_D \approx 0.36$).

The results of Marinho et al. (2009) are solely based on computations. Though the 3D simulations of Marinho et al. (2009) consider the same body positioning as Bixler et al. (2007) but at a depth of 2 m, they lead to a drag coefficient about 50 % higher than in the experimental data of Bixler et al. (2007). They found that the drag coefficient in lying position is about 75 % higher than in gliding position. The experimental data of Bixler et al. (2007) are 80 % lower than the values of our tests with the dummy in lying position at a yaw angle of 180° and tight clothes. This is consistent with the less streamlined nature of the lying position compared to the swimming one with arms in front of the head. Marinho et al. (2009) estimate this effect at about 75% higher, which matches fairly well the value of 80 % obtained by comparing the present tests to those of Bixler et al. (2007).

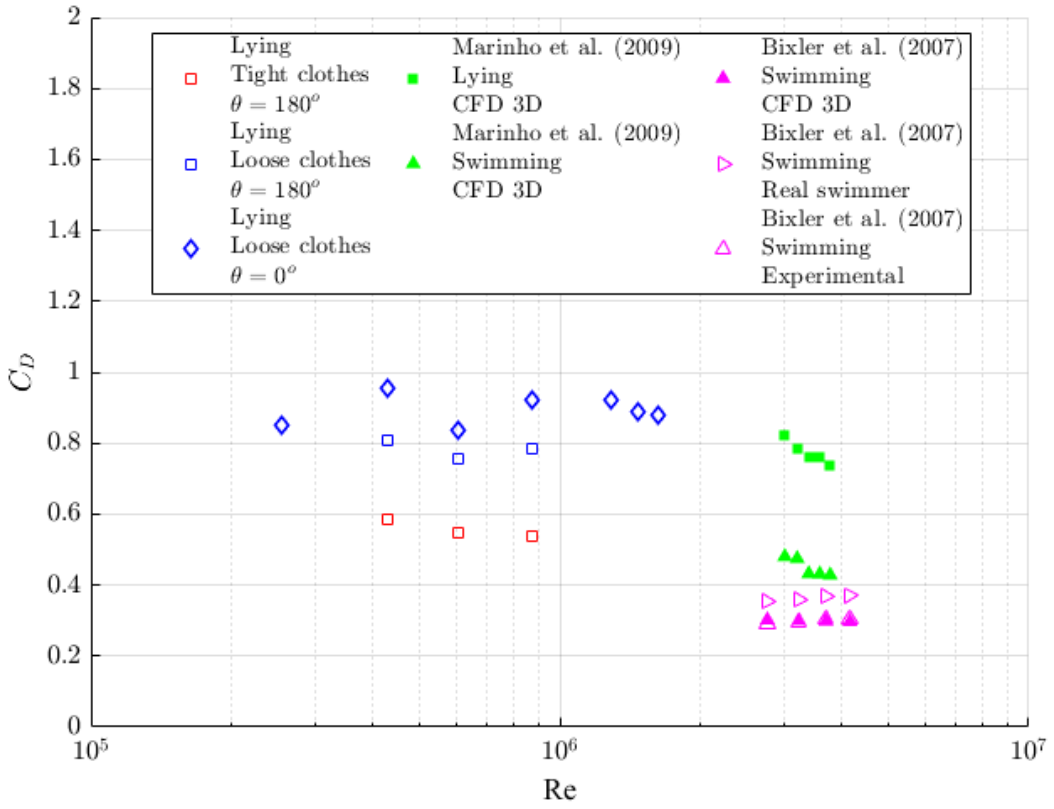

Figure 18: Comparison between this study and previous studies focused on body in swimming position, based either on experiments with a real swimmer or a dummy, or on computational fluid dynamics (CFD). Square and diamond markers refer to the lying position described in Section 2.2, while triangle markers correspond to swimming position (lying position with arms aligned in the front of the head).

5 Conclusion

Full scale experimental tests have been conducted with a dummy in a wind tunnel to evaluate hydrodynamic coefficients of interest for reproducing the effect of drag, side and lift forces in a computational model of the drift of a victim of drowning. The experimental results are presented (i) in terms of drag, side and lift areas, which are independent of a particular estimation of the frontal area but are not transferrable across scales, and (ii) in terms of drag, lift, and side coefficients. In the conducted laboratory tests, the wind velocity ($Re = 4.3 \times 10^5$ to 8.8×10^5), the yaw angle, the type of clothes (tight vs. loose), and the body position (lying vs. typical position of a victim of drowning) were systematically varied. The following observations could be made:

- Both the drag coefficient and the drag area change by maximum 15 % when the Reynolds number is varied in the tested range.
- Changing the yaw angle has a considerably stronger influence on the drag area for a body in lying position than when it is in the typical position of a drowning victim, which is more compact. In the former case, the maximum and minimum drag areas differ by a factor two (with tight clothes) to four (with loose clothes) when the yaw angle is varied, while in the latter case the drag area does not change by more than 50 %.
- For a body in lying position, the drag coefficient tends to be less influenced by the yaw angle than the drag area, as the minimum ($C_D \approx 0.5$) and maximum ($C_D \approx 1$) values of the drag coefficient differ by a factor two. In the drowned position, changing the yaw angle induces variations in the drag coefficient ($C_D \approx 0.6$ to 1) of approximately 50 %, like for the drag area.
- While the drag area differs substantially between a body lying position and in drowned position, no distinctive effect of the body position could be detected for the drag coefficient.
- Compared to the case of a body equipped with tight clothes, the drag area for a body with loose clothes is about 20 % higher, while the drag coefficient is increased by 15 % (lying position) and 30 % (drowned position).
- Adding a backpack does not systematically alter the drag area and coefficient; but in several configurations it induces an increase by up to 20 %.

The measured side and lift forces are generally lower than the corresponding drag force for the same configuration and wind velocity. Since the measured side and lift forces are in many cases comparable to the sensitivity of the sensors, it was difficult to detect distinctive trends in the side and lift coefficients when the yaw angle, type of clothes or body position were varied. It could nonetheless be observed that the side coefficient is less affected by changes in the yaw angle in the case of the drowned position (variations between – 0.11 and 0.24) than it is for the lying position, (variations between – 0.35 and 0.5).

The present study has a number of limitations, as detailed hereafter.

- While the available experimental setup enabled a systematic exploration of the influence of body orientation and position, only a relatively narrow range of Reynolds

numbers could be tested. Hence, future research should aim at further analysing the influence of the Reynolds number on the hydrodynamic coefficients of a human-like body in drowned position.

- Similarly, the effect of turbulence intensity in the approach flow and the influence of the distance to the wall need further investigations since these parameters remained fixed in the present series of tests.
- It is also necessary to study the force coefficients in configurations in which the flow velocity varies over the height of the body, as typically observed in shear flow in rivers, since the velocity profile has an influence on the hydrodynamic forces.
- Since our data were obtained solely based on a dummy reproducing a male adult individual, future research should assess the validity of our results when transferred to the case of a female adult or a child.
- The influence of the free surface on the force coefficients could not be captured in the present series of tests, while they are not negligible when the distance from the body to the surface is relatively low (e.g., below 0.75 m according to Vennell et al. (2006) for the case of swimmers). This specific aspect should be analysed in future experiments based on a towing or a current flume.

Finally, the scope of the research should be extended towards more reliable assessment of the side and lift coefficient (e.g., using more sensitive sensors along the corresponding direction than for monitoring the drag force), and towards the evaluation of other parameters critical for drift modelling such as the added mass coefficient.

References

Achenbach, E., 1974. The effects of surface roughness and tunnel blockage on the flow past spheres. Journal of Fluid Mechanics 65, 113–125.

Amendt, J., Krettek, R., Zehner, R., 2004. Forensic entomology. Naturwissenschaften 91, 51–65.

Anderson, J., 2011. Fundamentals of aerodynamics, 5th ed. McGraw-Hill.

Barelle, C., Ruby, A., Tavernier, M., 2004. Experimental Model of the Aerodynamic Drag Coefficient in Alpine Skiing. Journal of Applied Biomechanics 20, 167–176.

Barwood, M.J., Bates, V., Long, G., Tipton, M.J., 2011. Float First:“ Trapped Air Between Clothing Layers Significantly Improves Buoyancy on Water After Immersion. International Journal of Aquatic Research and Education 5.

Bierens, J.J.L.M. (Ed.), 2006. Handbook on drowning: prevention, rescue, treatment. Springer.

Bixler, B., Pease, D., Fairhurst, F., 2007. The accuracy of computational fluid dynamics analysis of the passive drag of a male swimmer. Sports Biomechanics 6, 81–98.

Blanco Pampín, J., López-Abajo Rodríguez, B.A., 2001. Surprising drifting of bodies along the coast of Portugal and Spain. Legal Medicine 3, 177–182.

Blocken, B., Druenen, T. van, Toparlar, Y., Andrianne, T., 2018. Aerodynamic analysis of different cyclist hill descent positions. Journal of Wind Engineering and Industrial Aerodynamics 181, 27–45.

Blondel, P., 2014. Searching for Dead Bodies with Sonar, in: DrowningPrevention,Rescue,Treatment. Springer-Verlag Berlin and Heidelberg GmbH & Co. K, New York, pp. 1161–1165.

Breivik, Ø., Allen, A.A., 2008. An operational search and rescue model for the Norwegian Sea and the North Sea. Journal of Marine Systems 69, 99–113.

Byard, R.W., 2017. Drowning deaths in rivers. Forensic Science, Medicine and Pathology 13, 388–389.

Carniel, S., Umgiesser, G., Sclavo, M., Kantha, L.H., Monti, S., 2002. Tracking the drift of a human body in the coastal ocean using numerical prediction models of the oceanic, atmospheric and wave conditions. Science & Justice: Journal of the Forensic Science Society 42, 143–151.

Cook, M.V., 2007. Flight dynamics principles: a linear systems approach to aircraft stability and control, 2nd ed. ed, Elsevier aerospace engineering series. Butterworth-Heinemann/Elsevier, Oxford [UK] ; Burlington, MA.

Delhez, C., Rivière, N., Erpicum, S., Pirotton, M., Archambeau, P., Arnst, M., Bierens, J., Dewals, B., 2023. Drift of a Drowning Victim in Rivers: Conceptualization and Global Sensitivity Analysis Under Idealized Flow Conditions. Water Resources Research 59, e2022WR034358.

Donoghue, E.R., Minnigerode, S.C., 1977. Human body buoyancy: a study of 98 men. Journal of Forensic Sciences 22, 573–579.

Du Bois, D., Du Bois, E.F., 1989. A formula to estimate the approximate surface area if height and weight be known. 1916. Nutrition (Burbank, Los Angeles County, Calif.) 5, 303–311; discussion 312–313.

Dubois, R., Andrianne, T., 2022. Flow around tandem rough cylinders: Effects of spacing and flow regimes. Journal of Fluids and Structures 109, 103465.

Gallagher, D., Visser, M., Sepulveda, D., Pierson, R.N., Harris, T., Heymsfield, S.B., 1996. How Useful Is Body Mass Index for Comparison of Body Fatness across Age, Sex, and Ethnic Groups? American Journal of Epidemiology 143, 228–239.

García-López, J., Rodríguez-Marroyo, J.A., Juneau, C.-E., Peleteiro, J., Martínez, A.C., Villa, J.G., 2008. Reference values and improvement of aerodynamic drag in professional cyclists. Journal of Sports Sciences 26, 277–286.

Ghaffarian, H., Lopez, D., Mignot, E., Piegay, H., Riviere, N., 2020. Dynamics of floating objects at high particulate Reynolds numbers. Physical Review Fluids 5, 054307.

Gonzalez, J.R.P., Escobar-Vargas, J., Vargas-Luna, A., Castiblanco, S., Trujillo, D., Guatame, A.C., Corzo, G., Santos, G., Perez, L.A., 2022. Hydroinformatics tools and their potential in the search for missing persons in rivers. Forensic Science International 111478.

Gunduz, M., 2017. Possible recovery site of four non-recovered bodies lost in the Marmara Sea by using an ocean circulation model. Australian Journal of Forensic Sciences 49, 154–160.

Hart-Davis, M.G., Backeberg, B.C., 2023. Towards a particle trajectory modelling approach in support of South African search and rescue operations at sea. Journal of Operational Oceanography 16, 131–139.

Hoerner, S., 1965. Fluid-Dynamic Drag: Practical Information on Aerodynamic Drag and Hydrodynamic Resistance, 2nd ed. Cambridge University Press, Brick Town, New Jersey.

Hölzer, A., Sommerfeld, M., 2008. New simple correlation formula for the drag coefficient of non-spherical particles. Powder Technology 184, 361–365.

Ingen Schenau, G.J. van, 1982. The influence of air friction in speed skating. Journal of Biomechanics 15, 449–458.

Jonkman, S. n., Penning-Rowsell, E., 2008. Human Instability in Flood Flows. JAWRA Journal of the American Water Resources Association 44, 1208–1218.

Kringsholm, B., Jakobsen, J., Sejrsen, B., Gregersen, M., 2001. Unidentified bodies/skulls found in Danish waters in the period 1992–1996. Forensic Science International 123, 150–158.

Laurent, P.-E., Coulange, M., Bartoli, C., Boussuges, A., Rostain, J.-C., Luciano, M., Cohen, F., Rolland, P.-H., Mancini, J., Piercecchi, M.-D., Vidal, V., Gorincour, G., 2013. Appearance of gas collections after scuba diving death: a computed tomography study in a porcine model. International Journal of Legal Medicine 127, 177–184.

Ličer, M., Estival, S., Reyes-Suarez, C., Deponte, D., Fettich, A., 2020. Lagrangian modelling of a person lost at sea during the Adriatic scirocco storm of 29 October 2018. Natural Hazards and Earth System Sciences 20, 2335–2349.

Lunetta, P., Ebbesmeyer, C., Molenaar, J., 2014. Behaviour of Dead Bodies in Water, in: Drowning. Springer-Verlag Berlin and Heidelberg GmbH & Co. K, New York, pp. 1149–1152.

Mannion, P., Toparlar, Y., Clifford, E., Hajdukiewicz, M., Andrianne, T., Blocken, B., 2019. The impact of arm-crank position on the drag of a paralympic hand-cyclist. Computer Methods in Biomechanics and Biomedical Engineering 22, 386–395.

Mantha, V.R., Marinho, D.A., Silva, A.J., Rouboa, A.I., 2014. The 3D CFD study of gliding swimmer on passive hydrodynamics drag. Brazilian Archives of Biology and Technology 57, 302–308.

Marinho, D., Barbosa, T., Rouboa, A., Silva, A., 2011. The Hydrodynamic Study of the Swimming Gliding: a Two-Dimensional Computational Fluid Dynamics (CFD) Analysis. Journal of Human Kinetics 29, 49–57.

Marinho, D.A., Mantha, V.R., Vilas-Boas, J.P., Ramos, R.J., Machado, L., Rouboa, A.I., Silva, A.J., 2012. Effect of wearing a swimsuit on hydrodynamic drag of swimmer. Brazilian Archives of Biology and Technology 55, 851–856.

Marinho, D.A., Reis, V.M., Alves, F.B., Vilas-Boas, J.P., Machado, L., Silva, A.J., Rouboa, A.I., 2009. Hydrodynamic Drag during Gliding in Swimming. Journal of Applied Biomechanics 25, 253–257.

Martlin, B.A., Anderson, G.S., Bell, L.S., 2023. A review of human decomposition in marine environments. Canadian Society of Forensic Science Journal 56, 92–121.

Mateus, M., Canelas, R., Pinto, L., Vaz, N., 2020. When Tragedy Strikes: Potential Contributions From Ocean Observation to Search and Rescue Operations After Drowning Accidents. Frontiers in Marine Science 7, 55.

Mateus, M., Pablo, H. de, Vaz, N., 2013. An investigation on body displacement after two drowning accidents. Forensic Science International 229, 6–12.

Mateus, M., Pinto, L., Chambel-Leitão, P., 2015. Evaluating the predictive skills of ocean circulation models in tracking the drift of a human body: a case study. Australian Journal of Forensic Sciences 47, 322–331.

Modell, J.H., Davis, J.H., 1969. Electrolyte changes in human drowning victims. Anesthesiology 30, 414–420.

Morrison, F.A., 2013. An introduction to fluid mechanics. Cambridge University Press, Cambridge ; New York.

Mosteller, R.D., 1987. Simplified calculation of body-surface area. The New England Journal of Medicine 317, 1098.

Müller, W., 2009. Determinants of Ski-Jump Performance and Implications for Health, Safety and Fairness: Sports Medicine 39, 85–106.

Parks, R.M., Bennett, J.E., Tamura-Wicks, H., Kontis, V., Toumi, R., Danaei, G., Ezzati, M., 2020. Anomalously warm temperatures are associated with increased injury deaths. Nature Medicine 26, 65–70.

Roos, F.W., Willmarth, W.W., 1971. Some experimental results on sphere and disk drag. AIAA Journal 9, 285–291.

Ruffell, A., Pringle, J.K., Cassella, J.P., Morgan, R.M., Ferguson, M., Heaton, V.G., Hope, C., McKinley, J.M., 2017. The use of geoscience methods for aquatic forensic searches. Earth-Science Reviews 171, 323–337.

Schmitt, T.J., 1954. Wind-tunnel Investigation of Air Loads on Human Beings. U.S. Navy, David W. Taylor Model Basin, Aerodynamics Laboratory.

Strom, M.A., Pasternack, G.B., Burman, S.G., Dahlke, H.E., Sandoval-Solis, S., 2017. Hydraulic hazard exposure of humans swept away in a whitewater river. Natural Hazards 88, 473–502.

Tikuisis, P., Meunier, P., Jubenville, C., 2001. Human body surface area: measurement and prediction using three dimensional body scans. European Journal of Applied Physiology 85, 264–271.

Tropea, C., Yarin, A.L., Foss, J.F. (Eds.), 2007. Springer Handbook of Experimental Fluid Mechanics. Springer Berlin Heidelberg, Berlin, Heidelberg.

Tu, H., Wang, X., Mu, L., Xia, K., 2021. Predicting drift characteristics of persons-in-the-water in the South China Sea. Ocean Engineering 242, 110134.

Ung, A., Gautier, A., Chatignoux, É., Beltze, N., 2019. Main results of the NOYADES survey carried out during summer 2018 in France. Bulletin épidémiologique hebdomadaire 286–94.

Van Hoyweghen, A.J.L., Jacobs, W., Beeck, B. Op de, Parizel, P.M., 2015. Can post-mortem CT reliably distinguish between drowning and non-drowning asphyxiation? International Journal of Legal Medicine 129, 159–164.

Vennell, R., Pease, D., Wilson, B., 2006. Wave drag on human swimmers. Journal of Biomechanics 39, 664–671.

WHO, 2014. Global report on drowning: preventing a leading killer.

Wolfsperger, F., Meyer, F., Gilgien, M., 2021. Towards more valid simulations of slopestyle and big air jumps: Aerodynamics during in-run and flight phase. Journal of Science and Medicine in Sport 24, 1082–1087.

Wu, J., Cheng, L., Chu, S., 2023. Modeling the leeway drift characteristics of persons-in-water at a sea-area scale in the seas of China. Ocean Engineering 270, 113444.

Yu, C.-Y., Lin, C.-H., Yang, Y.-H., 2010. Human body surface area database and estimation formula. Burns 36, 616–629.

Zamparo, P., Gatta, G., Pendergast, D., Capelli, C., 2009. Active and passive drag: the role of trunk incline. European Journal of Applied Physiology 106, 195–205.

Statement and Declarations

Funding

The authors declare that no funds, grants, or other support were received during the preparation of this manuscript.

Competing interests

The authors have no relevant financial or non-financial interests to disclose.

Author Contributions

All authors contributed to the study conception and design. Material preparation, data collection and analysis were performed by Clément Delhez, Benjamin Dewals and Thomas Andrianne. The first draft of the manuscript was written by Clément Delhez and all authors commented on previous versions of the manuscript. All authors read and approved the final manuscript.

1 Forces and torques – convergence and data

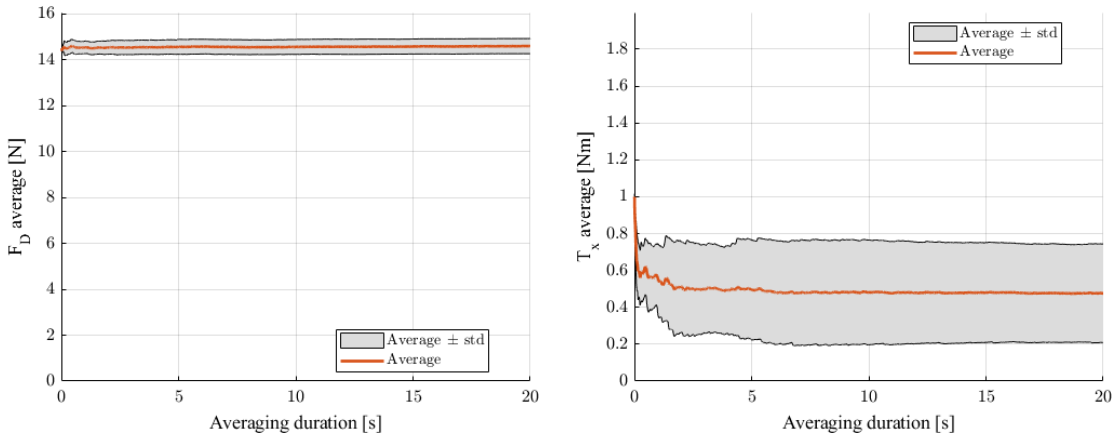

Figure 1: Time average and standard deviation of force and torque in the x-direction for the configuration in drowned position with loose clothes and yaw angle of 0°.

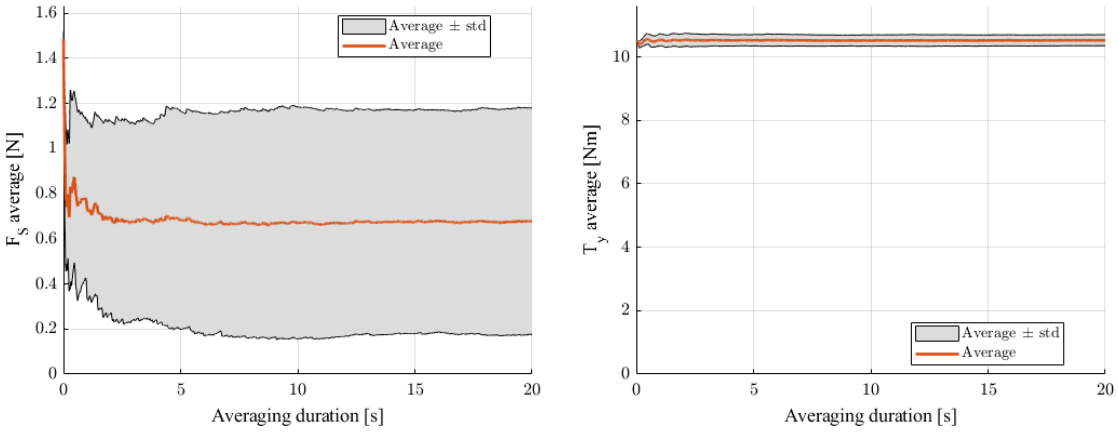

Figure 2: Time average and standard deviation of force and torque in the y-direction for the configuration in drowned position with loose clothes and yaw angle of 0°.

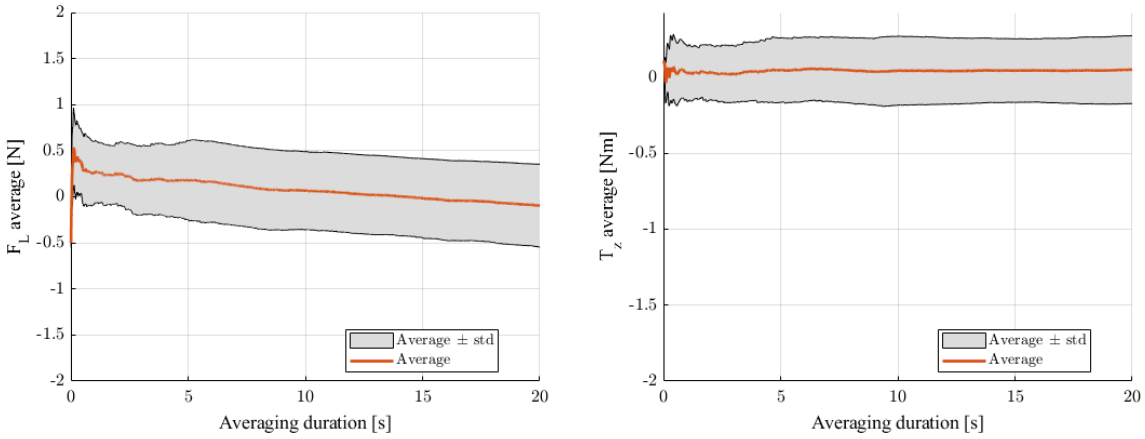

Figure 3: Time average and standard deviation of force and torque in the z-direction for the configuration in drowned position with loose clothes and yaw angle of 0°.

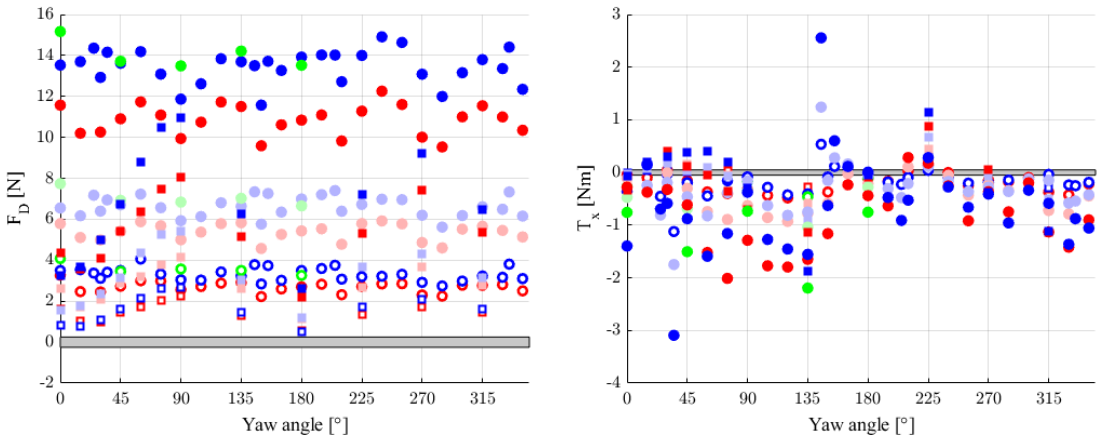

Figure 4: Forces and torques in the x-direction. The grey shaded area represents the resolution of the sensors.

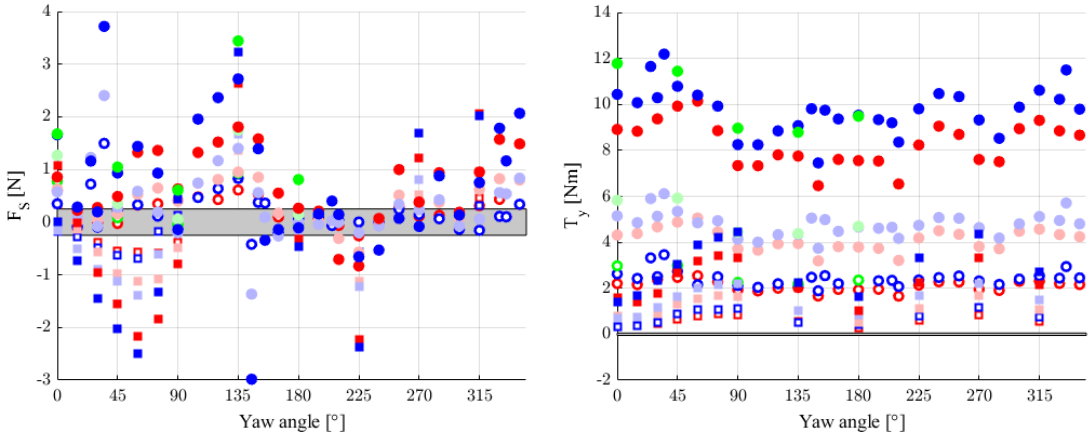

Figure 5: Forces and torques in the y-direction. The grey shaded area represents the resolution of the sensors.

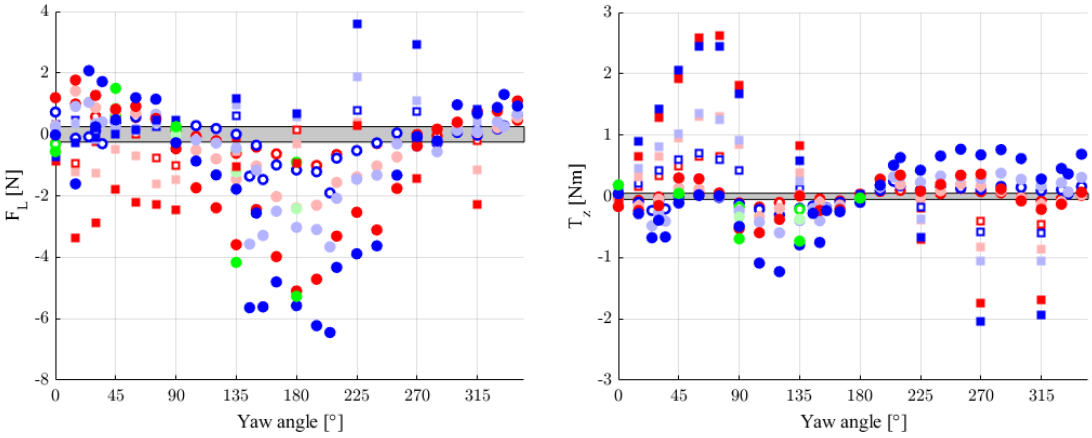

Figure 6: Forces and torques in the z-direction. The grey shaded area represents the resolution of the sensors.

2 Mannequin and modifications

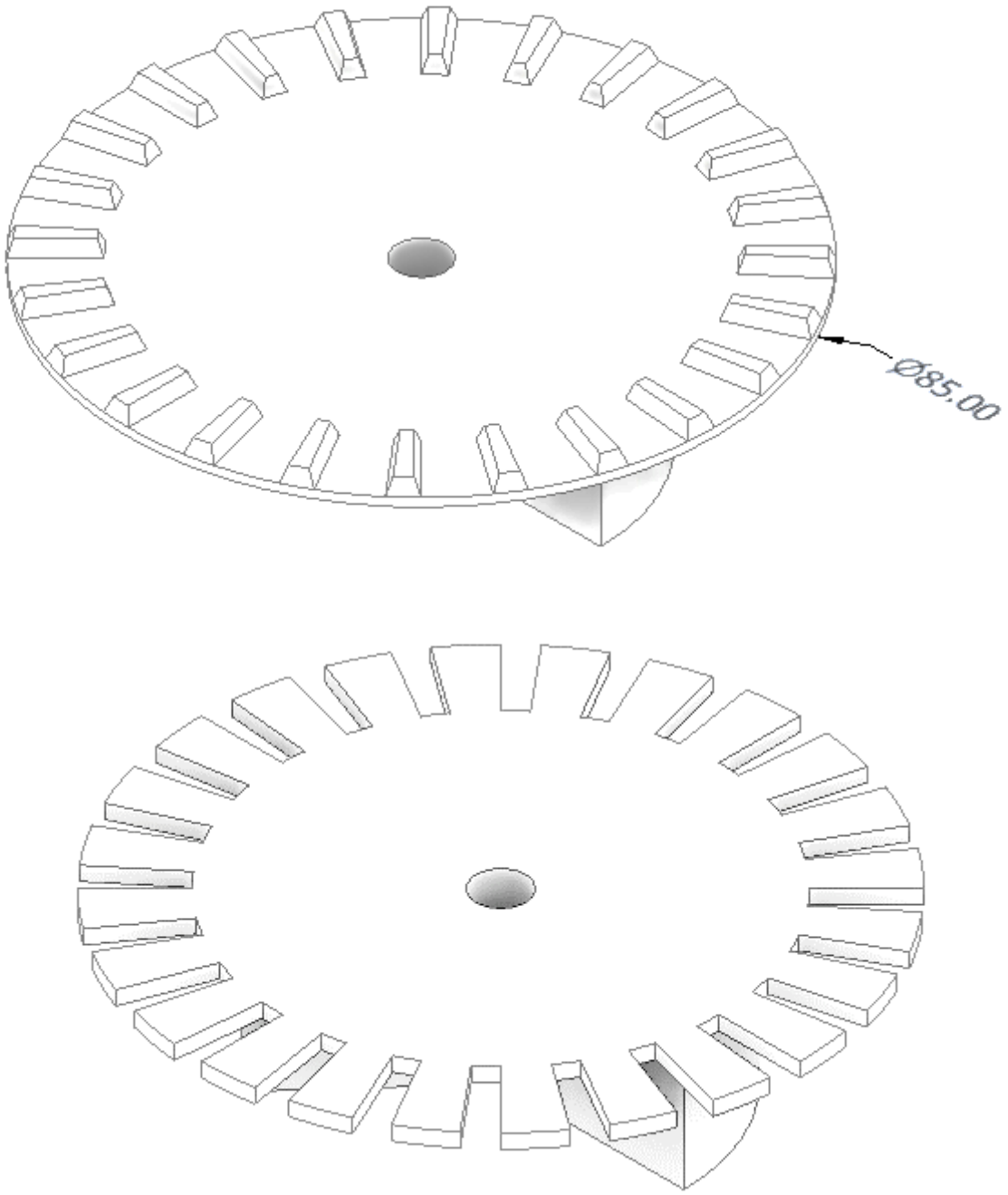

Figure 7: Male and female interlocking 3D-printed parts inside the articulations.

Figure 8: Mannequin in drowned position, tight clothing and yaw angle of 90°. Articulations blocked to have limbs with an angle of 75° with the horizontal.

Figure 9: Mannequin naked in lying position.

3 Drag, side and lift areas and coefficients

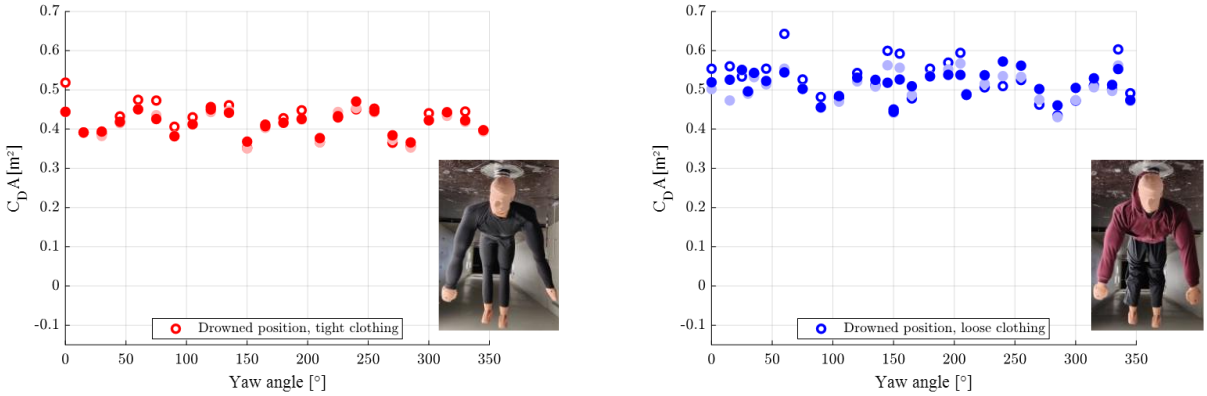

Figure 10: Drag area as a function of yaw angle, drowned position.

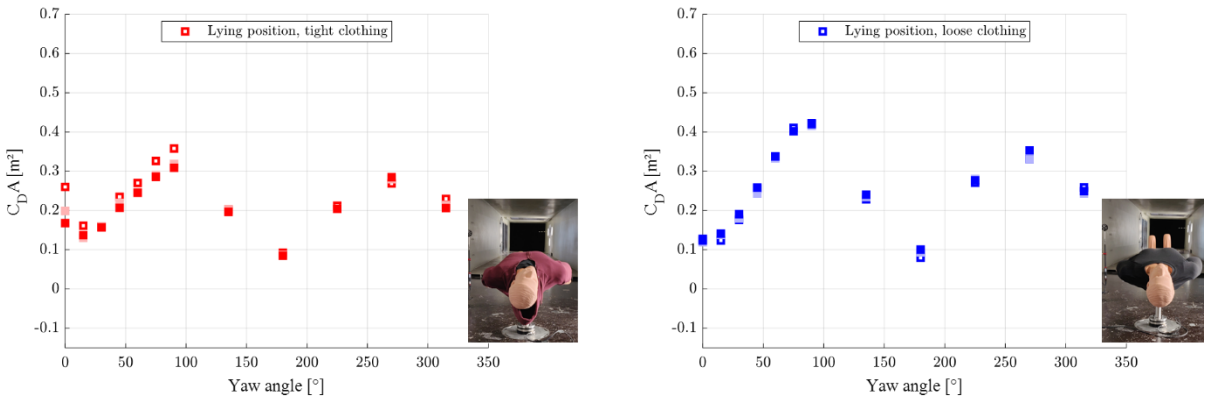

Figure 11: Drag area as a function of yaw angle, lying position.

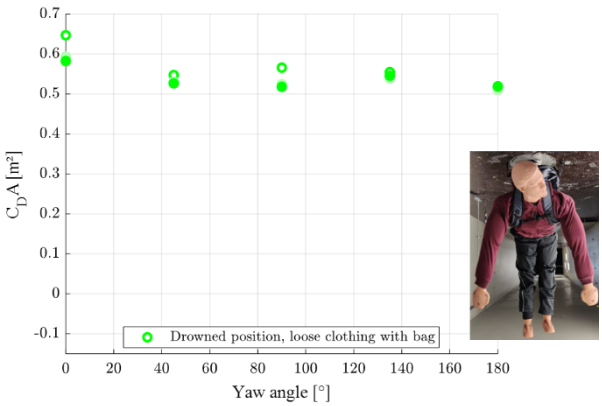

Figure 12: Drag area as a function of yaw angle, drowned position, loose clothes with a backpack.

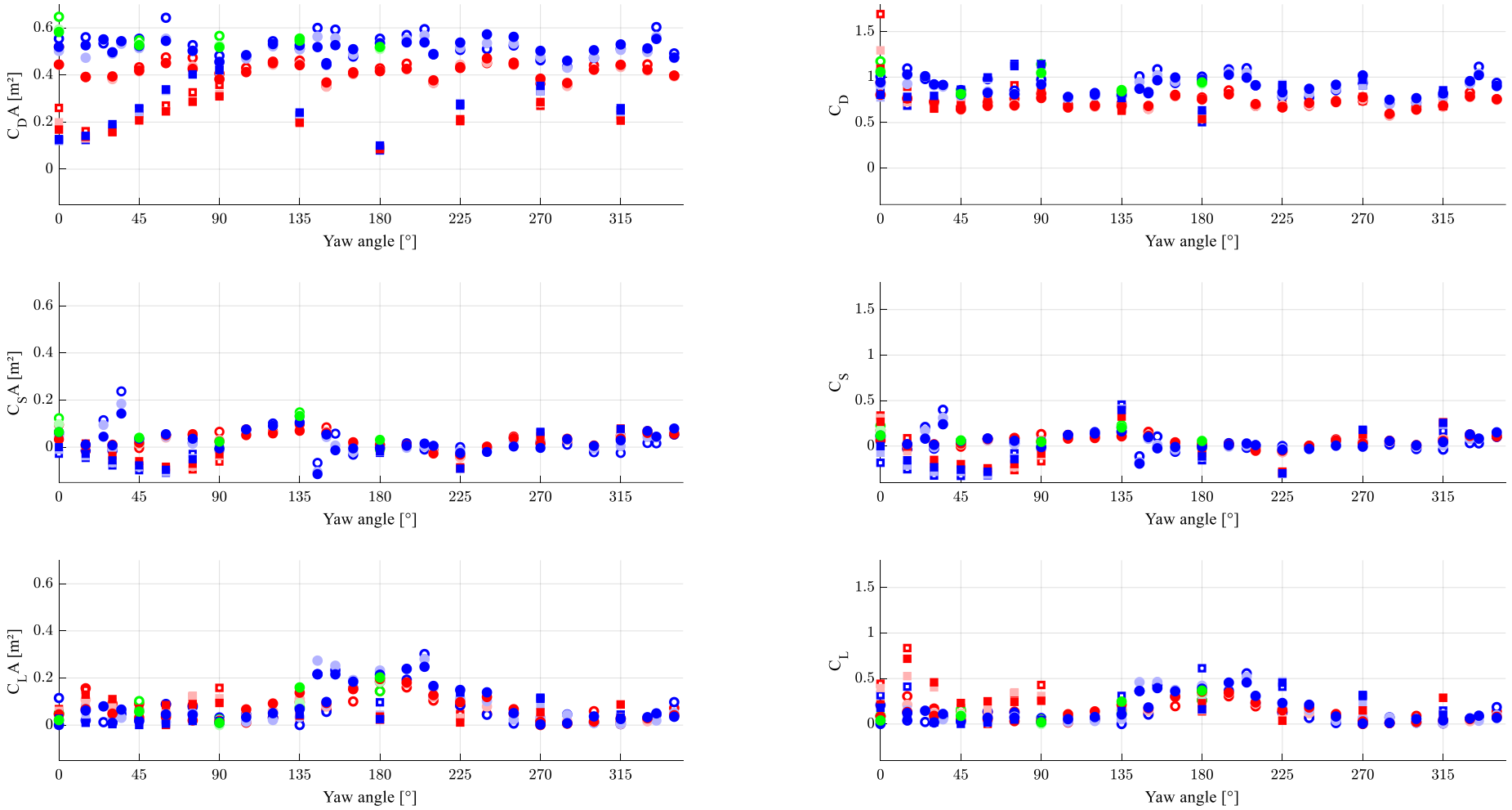

Figure 13: Drag, side and lift areas and coefficients for each configuration.

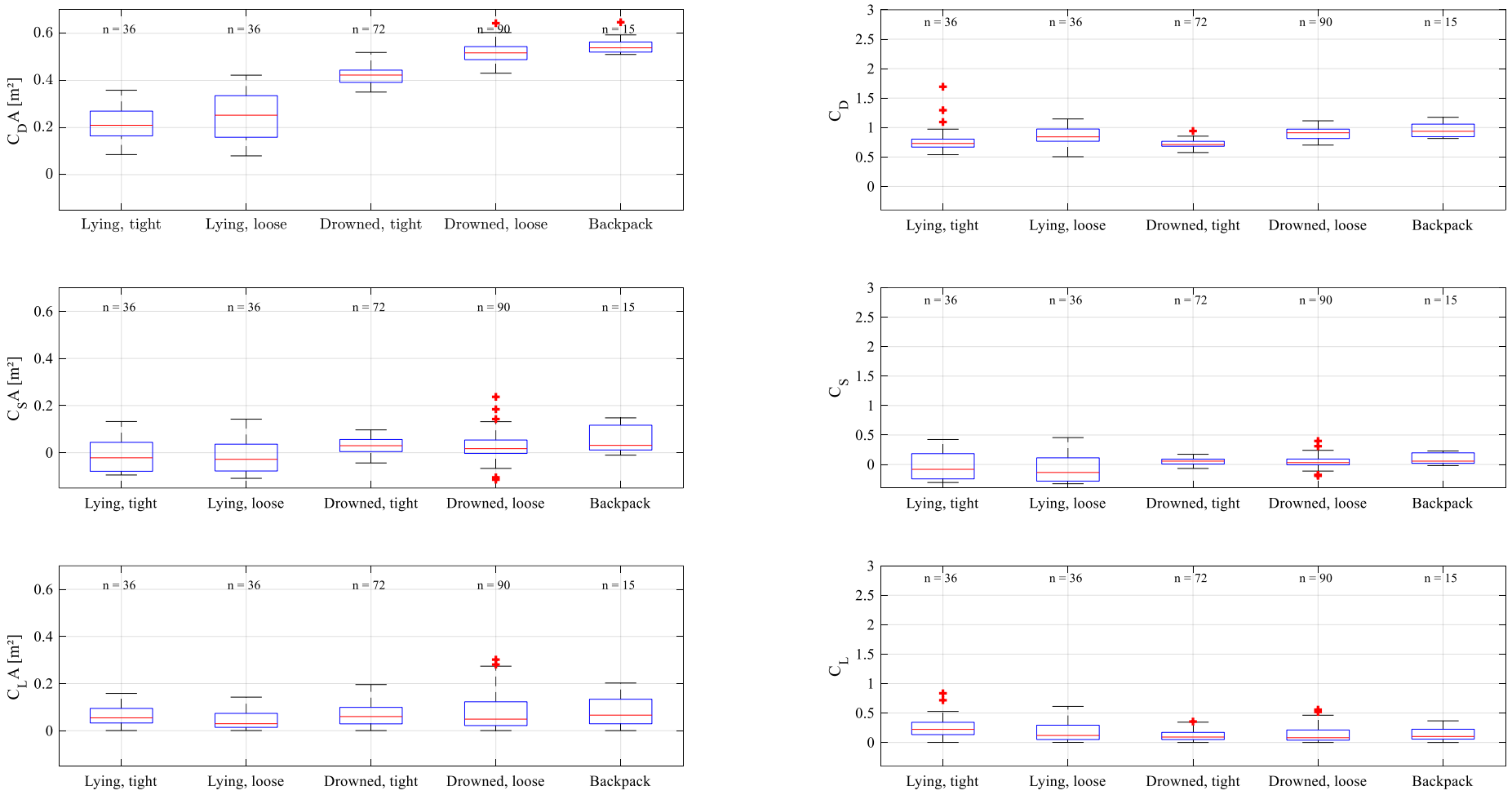

Figure 14: Boxplots of drag, side and lift areas and coefficients for each configuration.

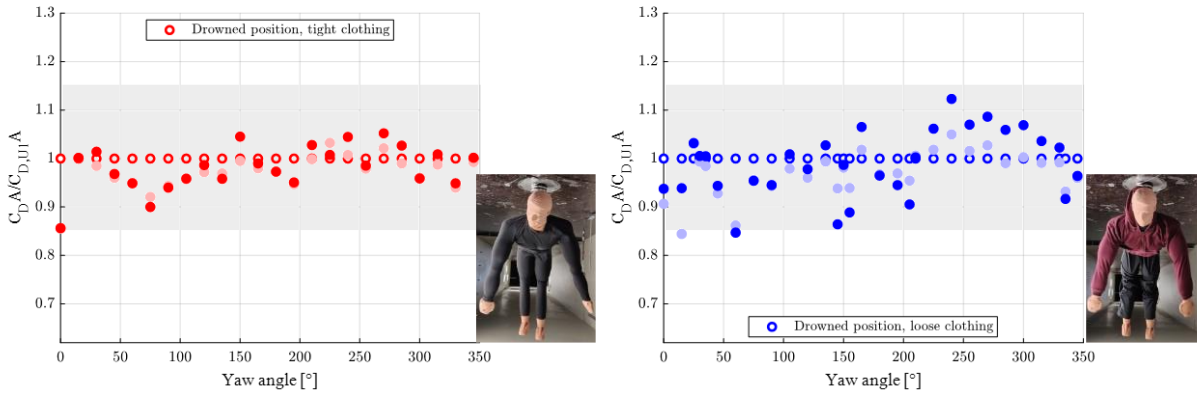

Figure 15: Drag area over the drag area at minimum speed as a function of yaw angle in drowned position.

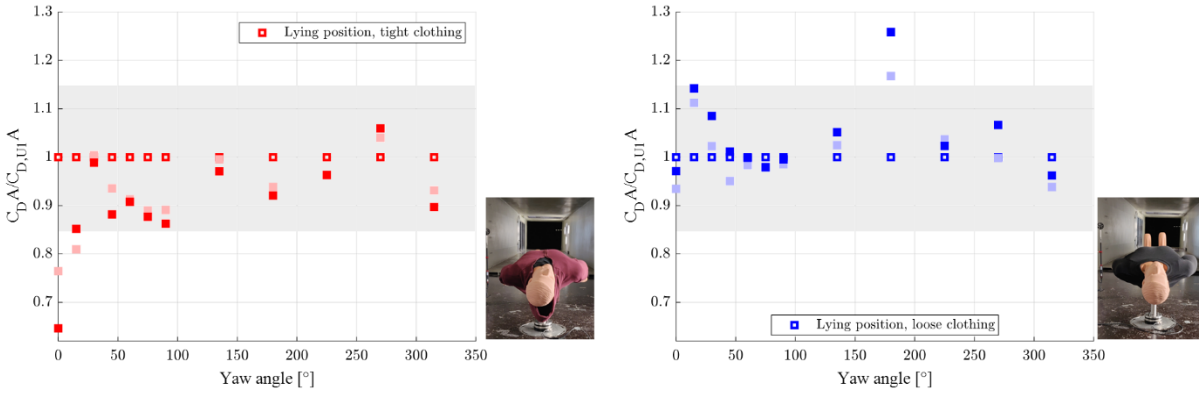

Figure 16: Drag area over the drag area at minimum wind velocity as a function of yaw angle in lying position.

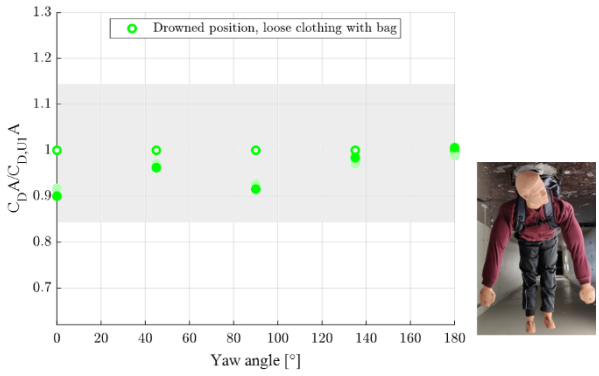

Figure 17: Drag area over the drag area at minimum wind velocity as a function of yaw angle in drowned position with a backpack.

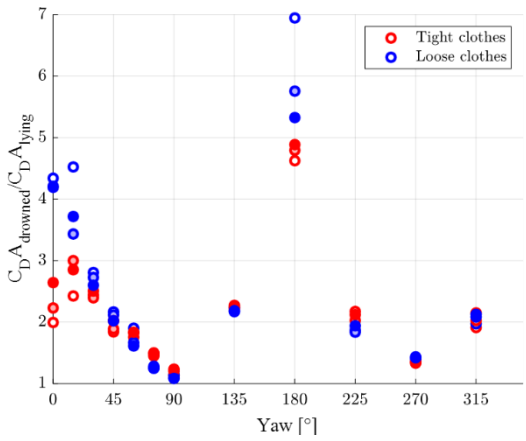

Figure 18: Drag area in drowned position over drag area in lying position as a function of yaw angle.

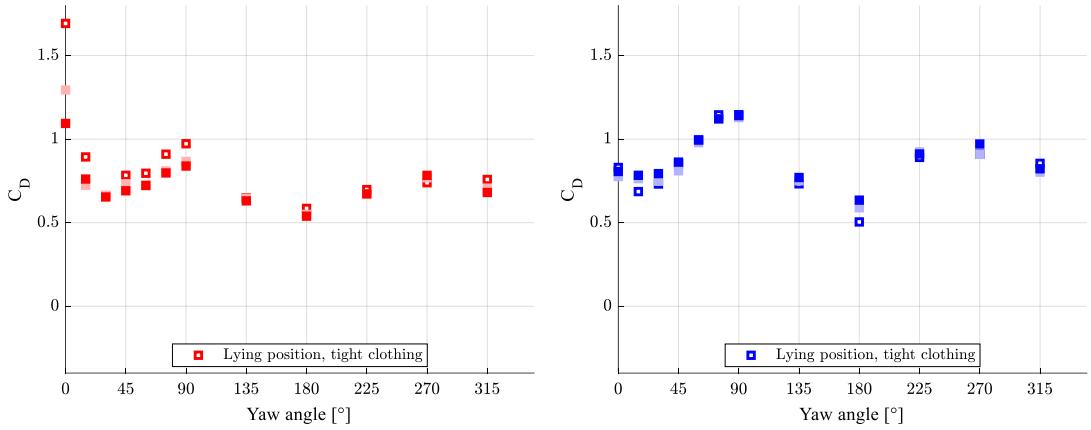

Figure 19: Drag coefficient as a function of yaw angle, lying position.

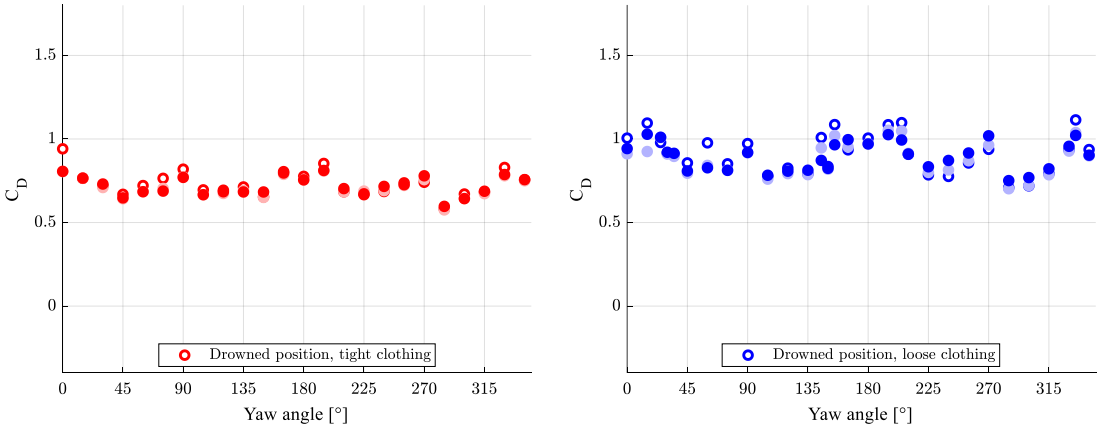

Figure 20: Drag coefficient as a function of yaw angle, drowned position.

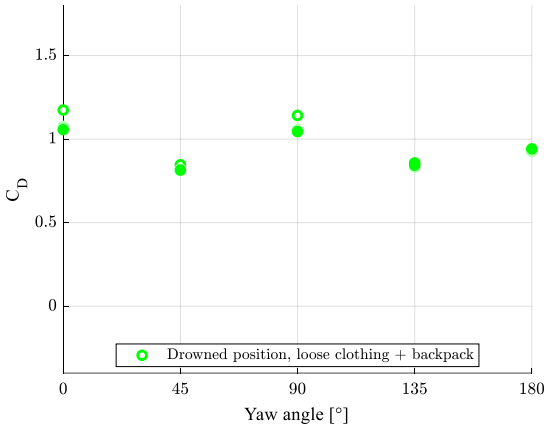

Figure 21: Drag coefficient as a function of yaw angle, drowned position with a backpack.

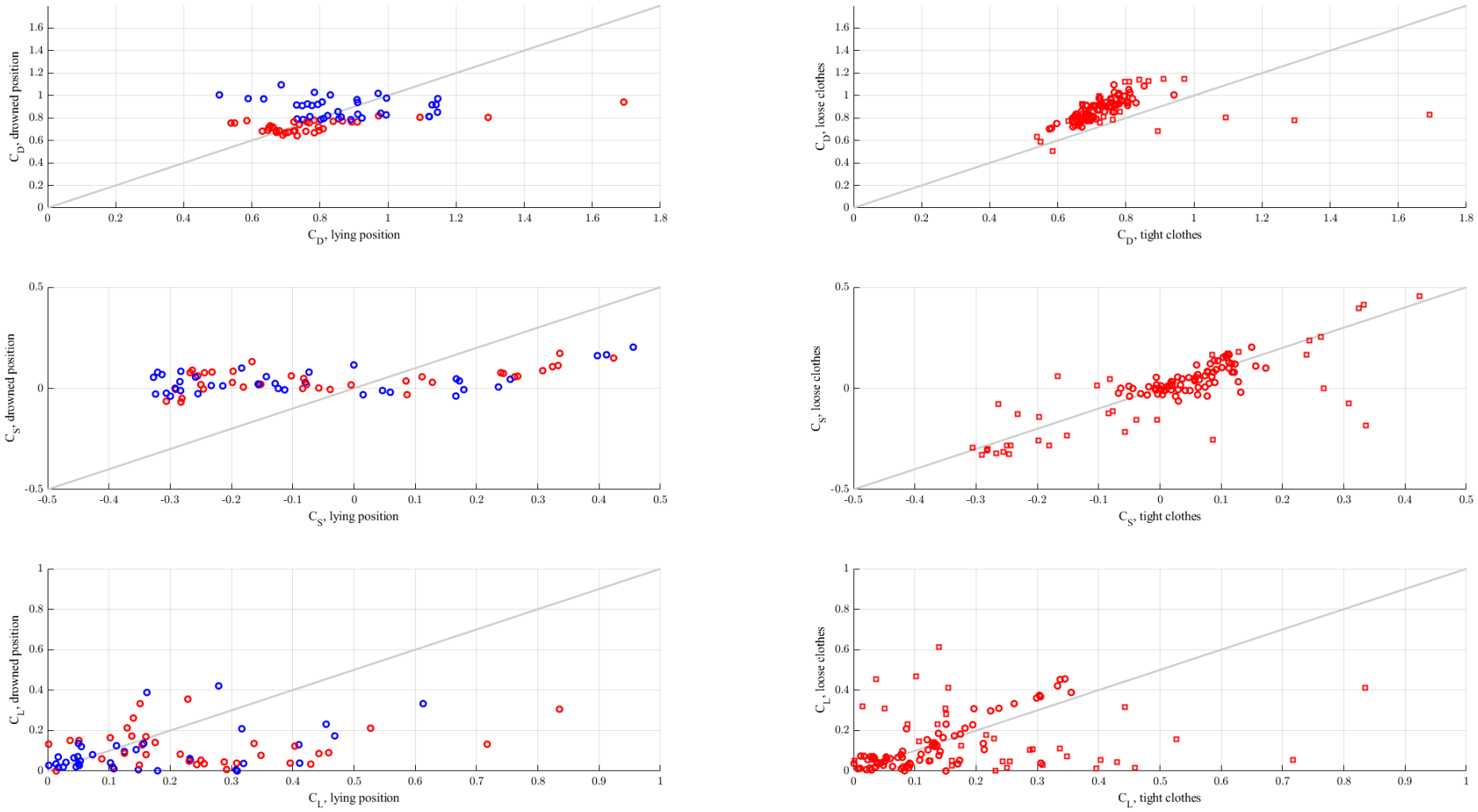

Figure 22: Influence of clothes and position for all type of areas and coefficients.

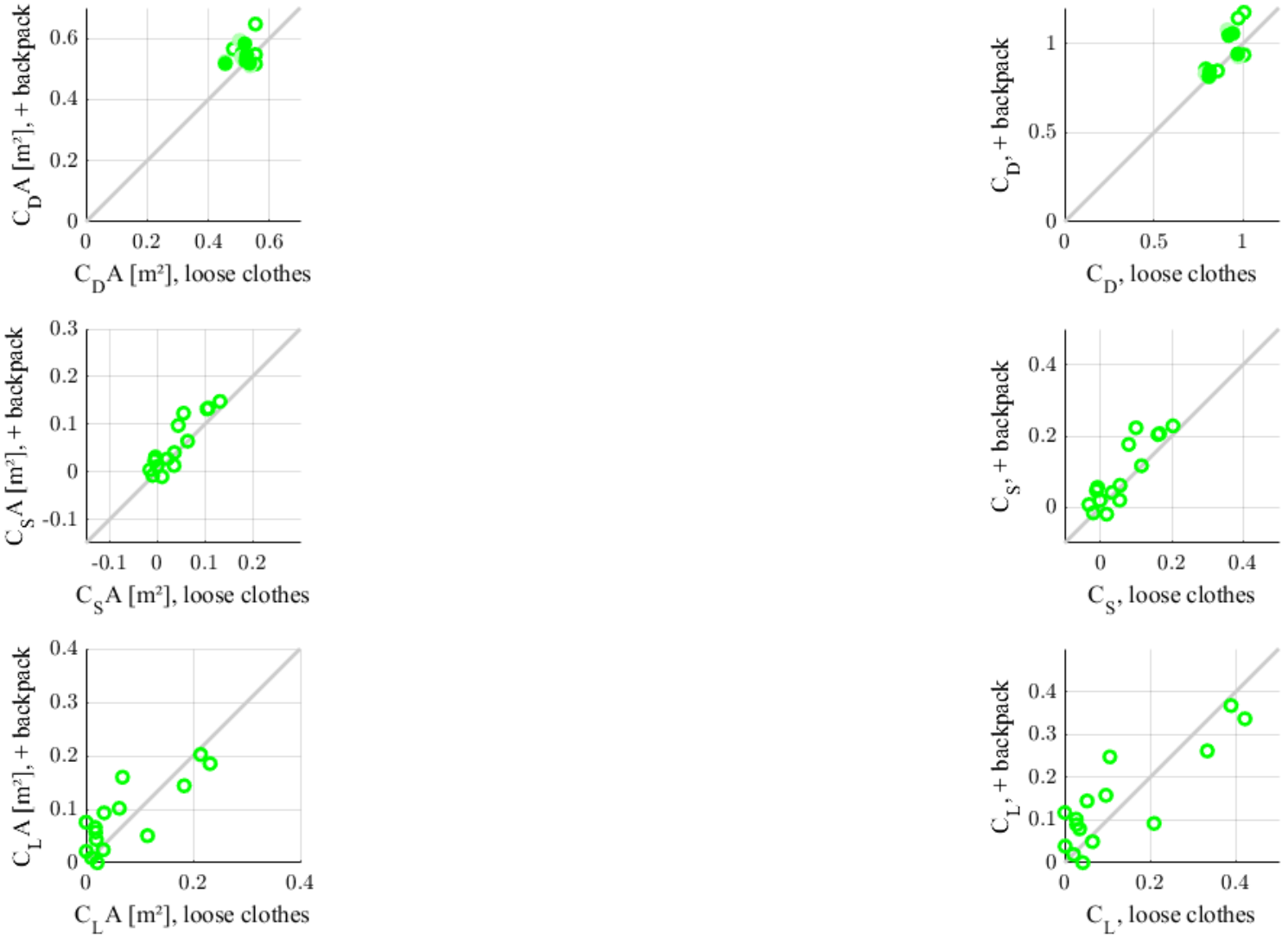

Figure 23: Influence of a backpack.

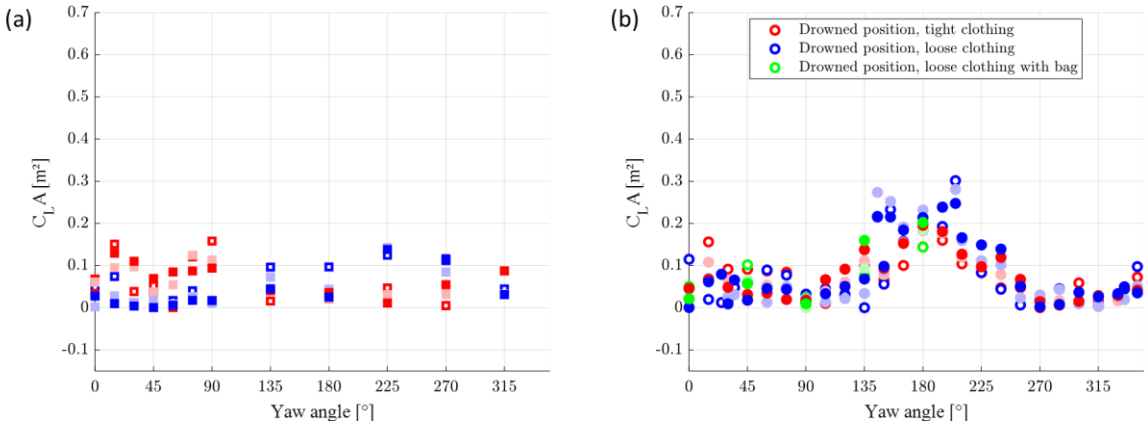

Figure 24: Lift area as a function of yaw angle (a) in the lying position and (b) in the drowned position. The markers face colour refers to the Reynolds number considered in each test. Empty markers: Re = 4.3×10^5, light plain markers: Re = 6.1×10^5, and dark plain markers: Re = 8.8×10^5.

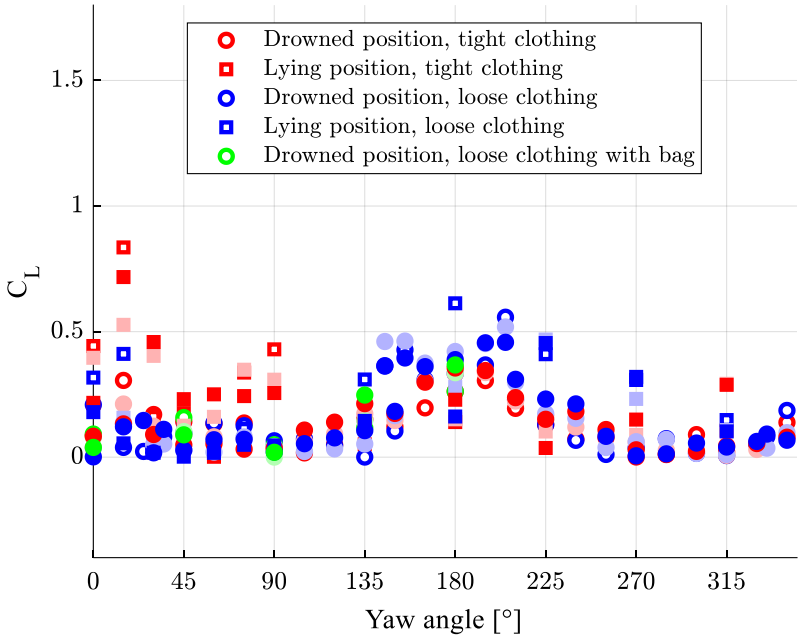

Figure 25: Lift coefficient as a function of yaw angle in the tested configurations. The markers face colour refers to the Reynolds number considered in each test. Empty markers: Re = 4.3×10^5, light plain markers: Re = 6.1×10^5, and dark plain markers: Re = 8.8×10^5.

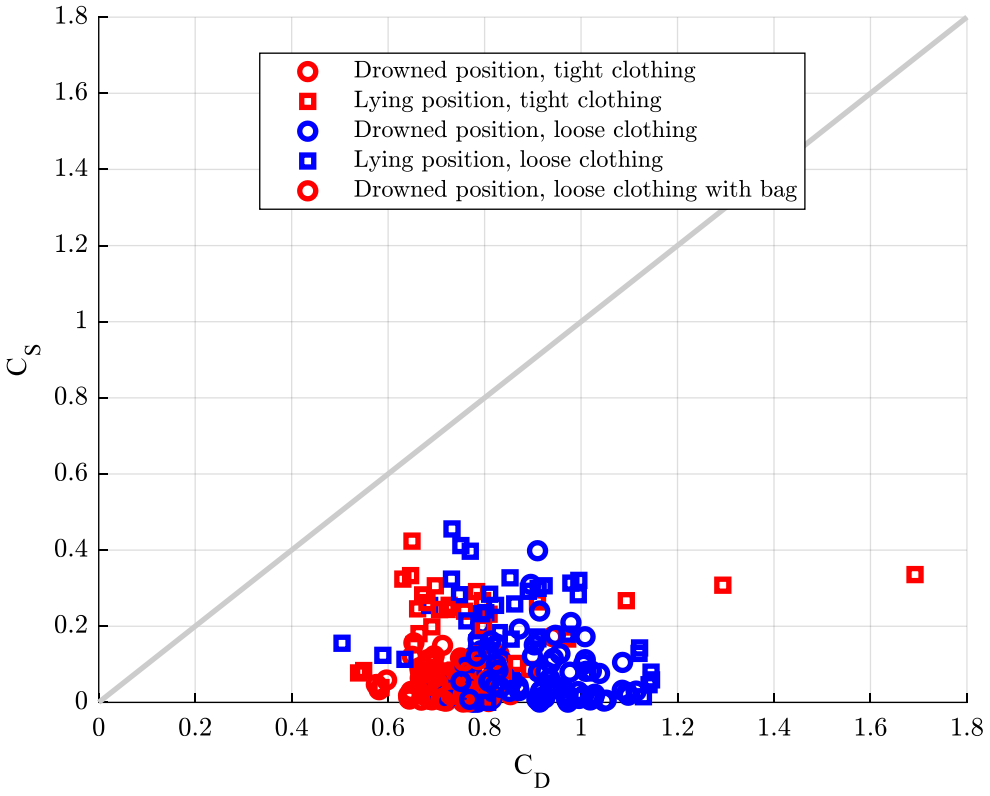

(a)

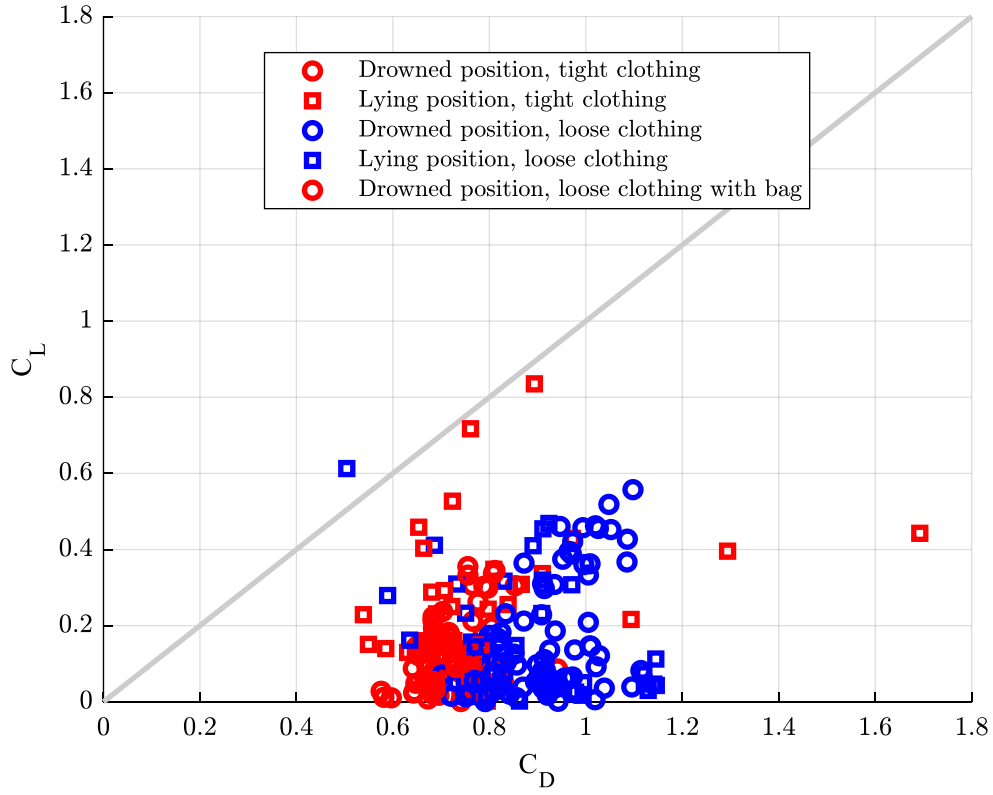

(b)

Figure 26: (a) Side and (b) lift coefficient as a function of the drag coefficient for the same configuration and Reynolds number.

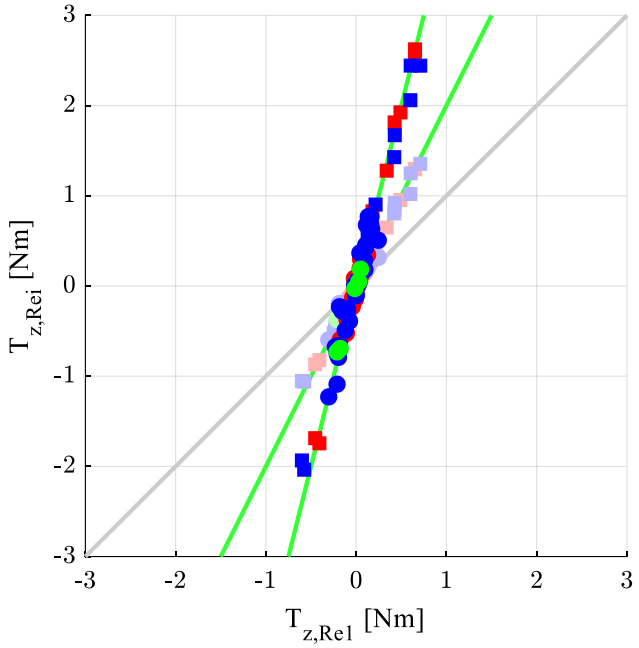

Figure 27: Torque in the vertical direction as a function of torque at the slowest wind velocity. Square markers represent the lying position while circular ones correspond to the drowned position (as described in Section 2.3). The marker face colour refers to the Reynolds number: shaded colours for $Re = 6.1 \times 10^5$ and plain colours for $Re = 8.8 \times 10^5$.

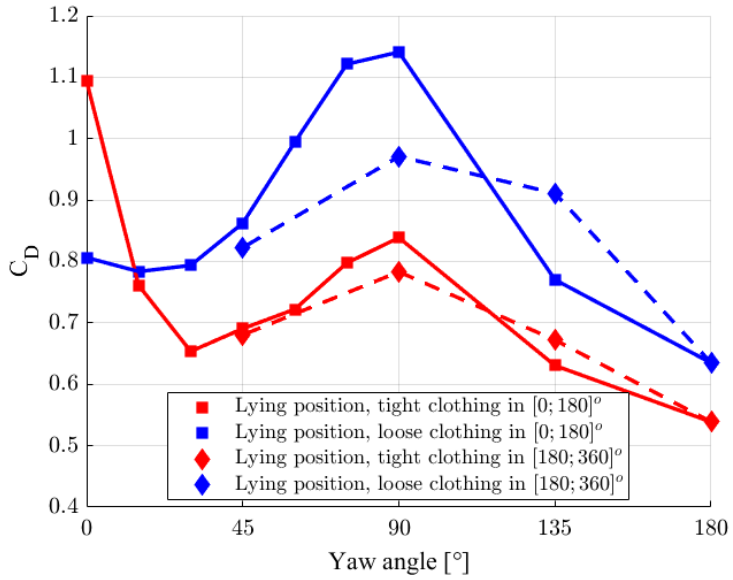

Figure 28: Drag coefficient as a function of yaw angle in lying position. Squares and plane lines correspond to the body between 0° and 180° while diamonds and dashed correspond to the mentioned angle taken symmetrically compared to the axis 0-180°. With for example diamond at 135° refers without considering the symmetry of the body.

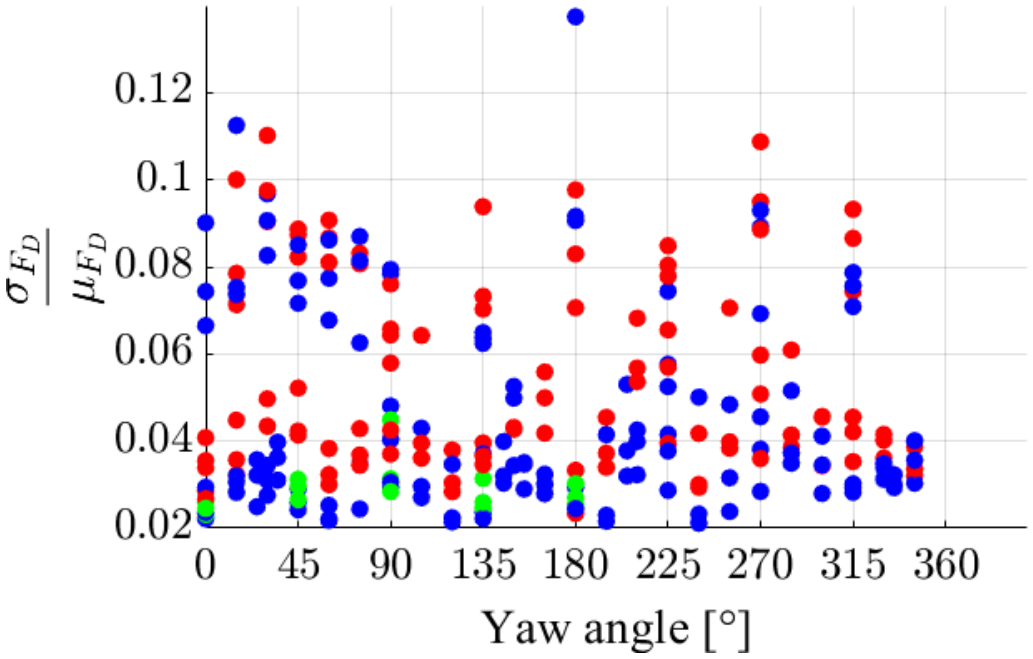

Figure 29: Standard deviation of F_x divided by the corresponding average of F_x.

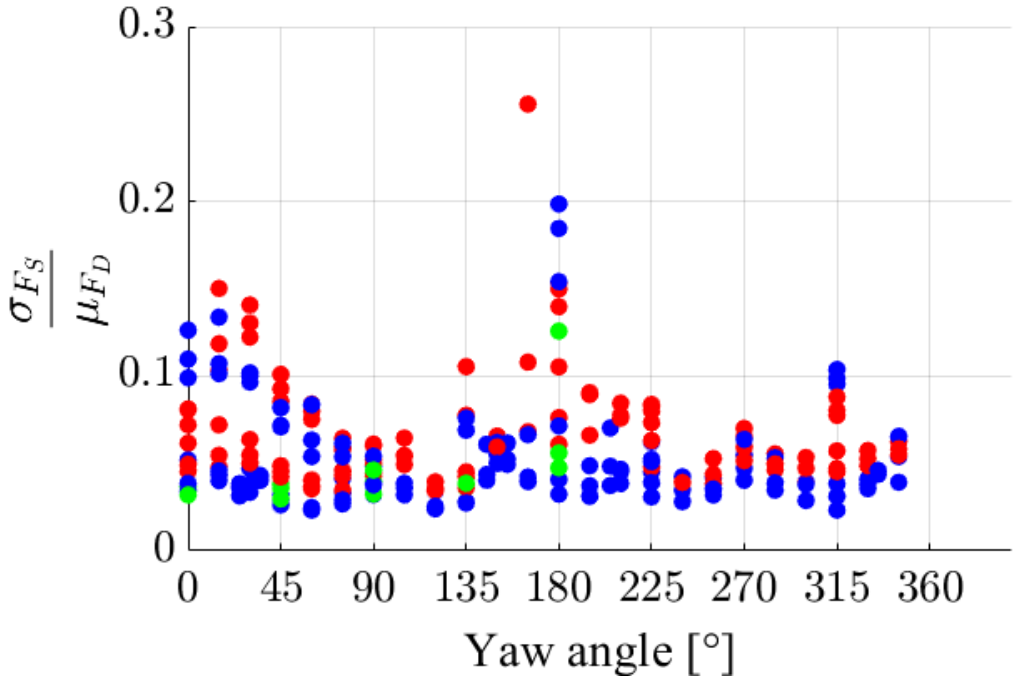

Figure 30: Standard deviation of F_y divided by the corresponding average of F_x.

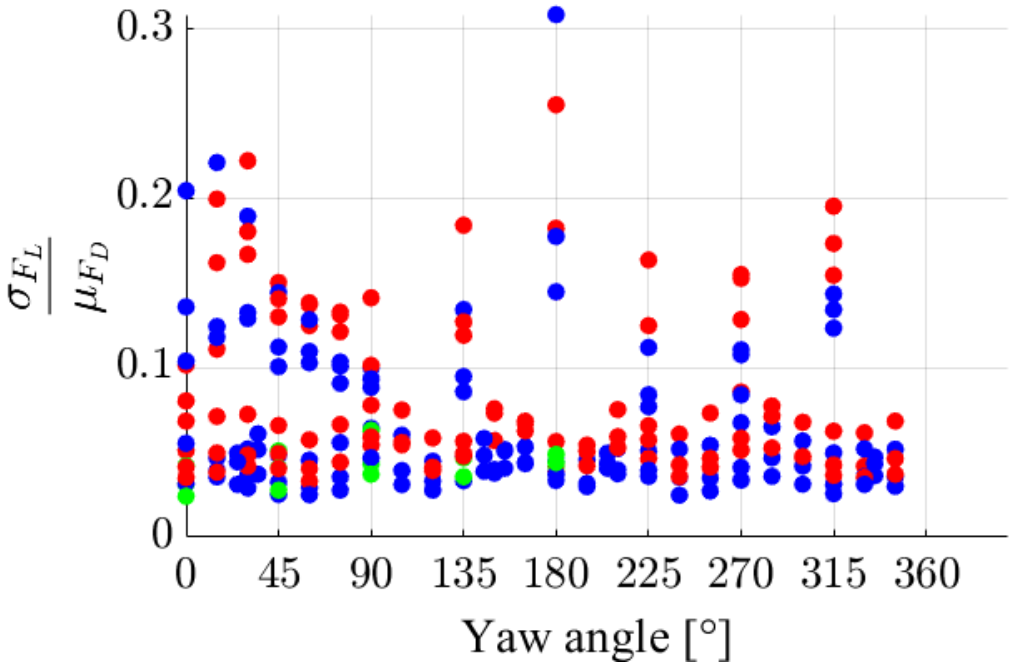

Figure 31: Standard deviation of F_z divided by the corresponding average of F_x.

Chapter 3

To float or not to float? Insights from a database of fatal drownings in urban rivers

This chapter corresponds to the journal paper "To float or not to float? Insights from a database of fatal drownings in urban rivers" by C. Delhez, Ph. Boxho, W. Jacobs, S. Erpicum, M. Pirotton, P. Archambeau and B. Dewals, submitted in a journal in 2025. The PhD candidate developed the methodology, built the database, made the statistics, analysed the results, wrote the manuscript and generated the figures.

To float or not to float?
Insights from a database of fatal drownings in urban rivers

C. Delhez[1], Ph. Boxho[2], W. Jacobs[3], S. Erpicum[1], M. Pirotton[1], P. Archambeau[1], B. Dewals[1]

[1]Hydraulics in Environmental and Civil Engineering (HECE), Research Unit Urban & Environmental Engineering (UEE), University of Liège, 4000 Liège, Belgium.

[2]Faculty of Medicine, University of Liège, 4000 Liège, Belgium.

[3]Department of Forensic Medicine and Pathology, University Hospital Antwerp, Edegem, Belgium.

Corresponding author: Clément Delhez (clement.delhez@uliege.be)

KEYWORDS: river drowning, sinking, ADD, PMSI, human body density, buoyancy

HIGHLIGHTS

- Drowning in urban rivers is a growing risk, worsened by climate change.
- Search operations to recover drowning victims can be assisted by means of hydrodynamic simulations and body drift modelling.
- This study identifies initial body buoyancy and body submersion interval, which are key parameters to improve body drift modelling.
- Older age of the victim and a higher body mass index increase initial body buoyancy, while lower water temperature delays body resurfacing.
- A distinct suicide risk profile (older, female, high BMI) was identified and should be considered in prevention policies.

Chapter 3: Insights from a database of fatal drownings

ABSTRACT

Drowning is a major global health concern, and urban rivers pose a significant risk. Climate change is leading to increasingly frequent extreme floods and heatwaves, which drive people to bathe in urban water bodies. The rapid recovery of victims is critical for their survival, as well as for investigations, and responder safety. Recent research highlights the potential of combining hydrodynamic computer simulations with drift modelling to predict the trajectory of drowning victims' bodies. The present study uses a unique dataset of 50 real-world fatal drowning cases to identify two key parameters needed to improve computer simulations of body drift in urban rivers: the initial body buoyancy and the body submersion interval. The results reveal that older age and a higher body mass index are significantly correlated with increased initial buoyancy, due to physiological factors such as lower bone density and higher body fat content. Bodies of victims over the age of 65 are almost four times more likely to remain afloat. A temperature threshold of around 7 °C appears to limit body floatability, and lower water temperatures are associated with longer body submersion intervals due to slower decomposition. A resurfacing value of 97 °C days was estimated for the 'accumulated degree days' (ADD), a criterion which has been recommended for predicting the body resurfacing time but has barely been quantified in prior studies. Additionally, older female individuals with a higher BMI were found to be significantly more likely to be victims of suicidal drowning, indicating a distinct risk profile that is important developing prevention strategies. These findings emphasise the importance of incorporating empirical data into drift models and building larger, transnational databases to improve predictive accuracy and save lives.

Chapter 3: Insights from a database of fatal drownings

1 Introduction

1.1 Context

Unintentional drowning is a major public health issue worldwide, resulting in around 400,000 fatalities each year (WHO, 2014). In many regions in the world, rivers are a common location for drowning (Peden et al., 2016a, 2016b; Maghakian et al., 2024). Climate change exacerbates this risk by intensifying hydro-meteorological extremes (Musolino et al., 2020), such as riverine and flash floods, which can sweep individuals away (Milanesi et al., 2015; Chen et al., 2019; Musolino et al., 2020; Lazzarin et al., 2022). The increasing frequency of heatwaves, which are associated with the urban heat island effect (Heaviside et al., 2017), leads to more people bathing in unsupervised urban rivers to cool off, thereby further increasing the risk of drowning (Fralick et al., 2013; Sindall et al., 2022).

A rapid response is crucial after drowning, as victims can be resuscitated for up to about one and a half hours after the accident, depending on the water temperature (Tipton and Golden, 2011). Therefore, the time taken to recover the victim has a critical influence on their chances of survival. Speeding up body recovery is also essential for other reasons: it reduces the burden on first responders, the risks taken by staff involved in aquatic and subaquatic search operations, and the time families and loved ones have to wait for news about the missing person. It also facilitates subsequent police and court investigations, as a less decomposed body tends to provide more evidence on the circumstances of drowning.

Search operations in urban rivers are challenging due to the potentially high velocity and momentum of the flow (Byard, 2017), as well as the poor visibility caused by suspended materials and dissolved compounds (Horn, 2014). Traditional search technologies, such as sonar, tend to be ineffective in urban rivers due to debris and artefacts present on the riverbed (Blondel, 2014). Floods exacerbate these challenges, rendering boating or diving unsafe, hence hindering the localisation of drowning victims (Ray, 2014). Despite considerable resources mobilized for aquatic and subaquatic search operations, victims of drowning are mostly found after several days, when their body resurfaces (Dennison-Wilkins et al., 2023). Improving our understanding and prediction capacity of the drift of a drowning victim is essential to guide more targeted search and rescue operations and to inform more tactical allocation of resources after a drowning accident. So far, very little academic research has been conducted into predicting the movement of a body in a river environment. This contrasts with the abundant existing research on predicting the behaviour of missing persons on land based on insights from the social sciences (Dennison-Wilkins et al., 2023).

The combination of computational simulations of river hydrodynamics and Lagrangian drift modelling has recently been explored as a promising method for predicting the trajectory of a drowning victim's body in a river (Gonzalez et al., 2022; Delhez et al., 2023). A pioneering modelling study by Delhez et al. (2023) has shown that determining whether the victim's body floats or lies on the riverbed is instrumental to enable reliable predictions of the body location over time. This is due to the considerable difference in drift velocity between a body floating at the surface and a body moving on the riverbed, where hydrodynamic driving forces (e.g., drag) are lower and resistance forces (e.g., solid-solid friction between the body and the

riverbed) are higher. Hence, predicting whether the body of a particular drowning victim is likely to initially sink or remain at the surface, as well as estimating how long a sunk body would remain on the riverbed before resurfacing, is of critical importance to inform detailed modelling of the drift of drowning victims in urban rivers. Distinguishing between initial body buoyancy (i.e. before the effects of decomposition) and body buoyancy at subsequent time intervals was also adopted in previous research (Dennison-Wilkins et al., 2023).

1.2 Initial body buoyancy

In the case of drowning in sea or coastal environments, the victim's body usually floats due to the widespread use of lifejackets in the marine context and the higher density of seawater compared to freshwater (Byard, 2017). In the case of river drowning, the body may be either positively or negatively buoyant (Donoghue and Minnigerode, 1977; Martlin et al., 2023) depending on factors such as the body morphology (Modell and Davis, 1969; Gallagher et al., 1996; Barwood et al., 2011; Laurent et al., 2013; Van Hoyweghen et al., 2015), the presence of air or water in the lungs (Modell and Davis, 1969; Gallagher et al., 1996; Barwood et al., 2011; Laurent et al., 2013; Van Hoyweghen et al., 2015), the amount of water swallowed by the victim (Modell and Davis, 1969), the type of clothes (Modell and Davis, 1969; Gallagher et al., 1996; Barwood et al., 2011; Laurent et al., 2013; Van Hoyweghen et al., 2015), or the presence of accessories such as a backpack.

Although experimental studies have been conducted to assess the buoyancy of living humans, they are barely representative of typical drowning conditions. For instance, Donoghue and Minnigerode (1977) analysed the buoyancy of U.S. Navy officers (aged between 20 and 40 years) based on experiments conducted by Behnke et al. (1942). At functional residual capacity (FRC) of the lungs, which is similar to the lungs volume of a recently deceased person, they found that only 7% of the subjects would float in freshwater. This rate is expected to be significantly higher in a sample that is more representative of the general population than a group of Navy officers. To date, no study has attempted to predict whether a drowning victim's body would float or sink based on their physical characteristics (such as sex, age, and build) and environmental parameters (such as water temperature and the time of year).

1.3 Body submersion interval

When a body sinks to the bottom of a river and remains there for a period of time, the decomposition processes release putrefaction gases within the body. These gases cause the body to swell and decrease in density (Heaton et al., 2010; Mateus et al., 2013; Lunetta, Ebbesmeyer, et al., 2014; Daalen et al., 2017). Consequently, the body usually refloats after a time interval that depends on various factors controlling the kinetics of body decomposition, primarily the water temperature. In a specific drowning case, significant uncertainty remains in the prediction of the body submersion interval (BSI), i.e. the time elapsed between body sinking and resurfacing.

To establish a relationship between the degree of body decomposition and time and temperature, Megyesi et al. (2005) employed the concept of accumulated degree days (ADD). ADD is defined as the integral of the external temperature (in this case, the water temperature) over time since body sinking:

$$ADD(t) = \int_{t_0}^{t} T_w(\tau)\, d\tau \tag{1}$$

with t_0 the time of the drowning, t the considered time and T_w the water temperature (in °C). This definition of ADD has also been adopted in many subsequent studies (Heaton et al., 2010; Mateus et al., 2013; Lunetta, Zaferes, et al., 2014; Daalen et al., 2017; Delhez et al., 2023).

Heaton et al. (2010) and Daalen et al. (2017) have matched different degrees of body decomposition in water with ADD values at the time of body recovery. Assuming the water temperature is known, these results can be used to estimate the time elapsed since body submersion based on observations made on the recovered body. However, this approach cannot predict the body submersion interval, as it relies on observations made on the recovered body.

Mateus et al. (2013) proposed a threshold of 95–117 °C days for ADD to predict body resurfacing, but these values were derived from only two cases of drowning in a marine environment. It is unclear whether this threshold can be applied to drowning in freshwater environments, such as in urban rivers. Currently, there is no predictive approach for estimating the submersion interval of a drowning victim's body in urban rivers. This would be highly valuable for optimally allocating resources between surface and subaquatic search operations, and for modelling the drift of a drowning victim's body.

1.4 Specific objectives of the present study

The objective of the present research is to investigate whether analysing a database of past drowning cases could provide valuable insights into the initial body buoyancy of river drowning victims and, in cases where the body sank, the submersion interval (i.e., the time elapsed between drowning and body resurfacing). Table 1 provides an overview of recent drowning studies based on an analysis of a drowning database. The database reported in literature cover drowning occurrences in a limited number of countries (Australia, New Zealand, Canada, United Kingdom and France), some of which include large samples (up to over 8,000 entries). These databases are mostly restricted to fatal drowning cases, as the source of information comes often primarily from coronial and police reports (Peden et al., 2016b, 2019, 2023; Dennison-Wilkins et al., 2023). Only those populated by data from first responders (e.g., the fire brigade or rescuers) include non-fatal drowning cases (Ung, 2014; Maghakian et al., 2024), but these non-fatal cases are not always analysed (Hills et al., 2021). Only two of the reported databases focus solely on river drowning (Peden et al., 2016b; Maghakian et al., 2024), but neither report information on initial body buoyancy nor the body submersion interval.

Five of the reviewed studies primarily aim to inform drowning prevention strategies (Ung, 2014; Peden et al., 2016b, 2023; Hills et al., 2021; Maghakian et al., 2024). As such, these studies focus on various aspects of drowning epidemiology, such as identifying the profile of drowning victims and predicting circumstances that lead to drowning (Peden et al., 2016b). Another study aims solely to assess the comparability of existing databases in three countries: Australia, Canada and New Zealand. Similarly, Hills et al. (2021) audited the quality of an official database in the United Kingdom.

Of the seven studies reported in Table 1, the study by Dennison-Wilkins et al. (2023) stands out as the only one that is directly relevant to the present research. They focus on river drowning as we do here, and they aim to guide search operations and to increase the chances of prompt body recovery. This contrasts with most other studies, which address means for preventing drowning. Dennison-Wilkins et al. (2023) were the first researchers to utilize a database of real-world inland and near-shore drowning cases to analyse factors affecting the body motion in water, particularly initial body buoyancy and submersion interval. Here, we aim to extend the work initiated by Dennison-Wilkins et al. (2023) by complementing their analysis using data from a different context, mostly two cities in continental Europe, whereas the analyses of Dennison-Wilkins et al. (2023) rely solely on data collected in the United Kingdom.

In the present study, we have gathered and analysed a database of 50 real-world river drowning cases, primarily from two Belgian cities (Liège and Antwerp). This data was used to predict two key pieces of information to enable reliable calibration and validation of drift modelling of drowning victims in urban rivers: the initial body buoyancy of the body and the body submersion interval. These predictions are based on environmental variables (water temperature and drowning circumstances, i.e., accident or suicide) and five pre-mortem body characteristics (such as body mass index, victim's age, height and sex, and type of clothing).

Section 2 introduces the data used in this paper and how they were obtained, while Section 3 presents the methods used for data analysis. The results are depicted in Section 4 and discussed in Section 5. Conclusions are drawn in Section 6.

Reference	Region covered	Types of water bodies	Analysed period	Number of unique cases	Fatal and/or non-fatal cases	Main source(s) of information	Main objective of the study	Initial body buoyancy	Body submersion interval (BSI)
Maghakian et al. (2024)	Lyon (France)	Rivers	2015-2021	386	Fatal and non-fatal	Fire brigade (rescuers) reports	Predict the occurrence of drowning (epidemiology)	Not reported	Not reported
Peden et al. (2023)	Australia	Diverse, incl. rivers, ocean, swimming pools …	2002-2022	5,692	Fatal	Mostly coronial records, supplemented by other reports (media, police)	Mostly inform drowning prevention strategies, and research	Not reported	Date of incident and date of death
Ung et al. (2022)	France	Diverse, incl. rivers and lakes (~ 23%)	Summer 2021	1,753 (incl. 1,480 accidental ones)	Fatal (31%) and non-fatal	Survey of first respondents (fire brigade, police, emergency care units …)	Inform drowning prevention strategies	Not reported	Not reported

Reference	Region covered	Types of water bodies	Analysed period	Number of unique cases	Fatal and/or non-fatal cases	Main source(s) of information	Main objective of the study	Initial body buoyancy	Body submersion interval (BSI)
Hills et al. (2021)	United Kingdom	Not explicitly reported, but includes coastal and river environments	2012*-2019	5,051 (fatal cases)	Fatal*	Multiple sources, including safety, rescue and public organisations	Audit an existing official database, inform drowning prevention strategies	Not reported	Date and time of incident and/or of body recovery
Peden et al. (2019)	Australia, Canada and New Zealand	Diverse, incl. ocean, harbour, ponds, lakes and bathtubs	2005-2014	8,176	Fatal	Mostly coronial records, supplemented by other reports (media, police)	Assessing the comparability of database from different countries	Not reported	Not reported
Peden et al. (2016a)	Australia	Rivers	2002-2012	2,892	Fatal	Coronial data	Identify the profile of drowning victims (epidemiology)	Not reported	Not reported

Reference	Region covered	Types of water bodies	Analysed period	Number of unique cases	Fatal and/or non-fatal cases	Main source(s) of information	Main objective of the study	Initial body buoyancy	Body submersion interval (BSI)
(Dennison-Wilkins et al., 2023)Dennison-Wilkins et al. (2023)	United Kingdom	Inland waters (or near-shore)	2008 onwards	280 (quantitative analyses based on n = 74 to 77)	Fatal	Police reports	Inform search operations by predicting body movement in water	Reported and analysed (see Figure 1 in Dennison-Wilkins et al., 2023)	Reported and analysed (see Table 3 in Dennison-Wilkins et al., 2023)
Present study	Mostly Liège and Antwerp (Belgium)	Mostly urban rivers (two cases of other urban water bodies)	2019-2022	50	Fatal	Forensic medicine reports, missing notices, media	Examine key inputs for modelling of the drift of the body	Yes	Yes

[*] Non-fatal drowning cases are also included in the corresponding database, but the analyses by Hills et al. (2021) focus on the fatal cases. Similarly, drowning cases from 2009 onward are reported in the database but the study focuses on the period 2012-2019.

Table 1: Overview of recent studies based on the analysis of drowning database.

2 Data

The dataset considered here contains information on 50 cases of drowning in urban water bodies between 2019 and 2022. Most of them occurred in or nearby the Belgian cities of Liège (36 cases) and Antwerp (11 cases). Only three cases occurred elsewhere (in Ghent, Namur and Strasbourg). The dataset includes two variables describing the behaviour of the victim's body after drowning (i.e., whether it sank or remained at the surface and, if it sank, its submersion interval), as well as seven potential explanatory variables characterizing the victim (sex, age, height, body mass index, and clothing type) and the context of the drowning (water temperature and circumstances).

Table 2 provides an overview of the data types, their distribution and the sources of information used to retrieve them. Comprehensive forensic reports, including photographs, were available for all 11 cases in the Antwerp region. This made it possible to retrieve all the necessary data for these cases. For the 36 cases in the Liège region, forensic reports were also available, but they were less complete. Therefore, information from wanted notices and/or media reports was used to supplement the Liège reports. Previous studies based on drowning databases recommended employing such mixed data collection approach to supplement the weaknesses of some data sources (Peden et al., 2023). For the remaining three cases (in Ghent, Namur and Strasbourg), only wanted notices and media reports were available. Further insights into the collected data are provided below, while descriptive statistics for each variable can be found in Supplements S1 and S2.

2.1 Body behaviour after drowning

A first variable in the dataset indicates whether the victim's body sank or remained at the surface after drowning. A case was registered in the latter category where the body was found at the surface and showed no signs of decomposition. Otherwise, it was assumed that the body had sunk and resurfaced. The degree of decomposition was systematically recorded in the forensic medicine reports for the cases in Liège and Antwerp, and this information was often corroborated by the media reports. In most cases of drowning where the body did not sink, forensic medicine reports indicate that witnesses have kept the body in view from the moment it entered the water until it was recovered. This provides strong evidence that the body did not sink in these cases. For the three cases outside of Liège and Antwerp, information from media reports was used. Overall, the victim's body sank in approximately 70% of the considered cases, with no significant difference in this rate between the cases recorded in the Liège and Antwerp regions (Figure S1 in Supplement).

For the cases involving sinking and resurfacing of the victim's body, the submersion interval was estimated as the time elapsed between the victim's reported disappearance and the body recovery. In all cases in Antwerp and in most cases in Liège, the date and time of drowning and of body recovery were recorded in the forensic medicine reports. In some cases in Liège region, drowning date and time were derived from media or wanted notices information. For the three cases outside of Liège and Antwerp, media reports and wanted notices were used.

The median submersion interval for bodies which sank is 5.5 days (Table 2). The 25th and 75th percentiles correspond respectively to 2.9 and 22 days. One outlier case shows a submersion interval of 111 days, while in all other cases the submersion interval does not exceed 41 days (Figure S2 in Supplement). Differences remain limited between the samples from Liège and Antwerp regions. For instance, the mean submersion interval is found to be 16.0, 14.7 and 15.2 days for the Liège region, the Antwerp region and the entire dataset, respectively.

2.2 Victims' characteristics

In the Liege region cases, the age and sex of the victims were obtained from the forensic medicine reports and confirmed by media reports and/or wanted notices. For the Antwerp region cases, only the forensic reports were used. For the cases in other regions, only media reports were consulted. The dataset contains 16 cases involving a female victim and 34 cases involving a male victim. In all cases, the victim was an adult, and female victims in our sample tend to be older than male victims (Table 2).

Information on body height is rarely included in forensic reports. Conversely, it is often given in wanted notices (Figure S5 in Supplement). When the body height could not be found in either of these two sources, it was considered unknown (23 out of the 50 cases). In one case, the height was estimated using a photograph of the body on an autopsy table of known dimensions. The median reported heights are 1.61 m for female victims and 1.79 m for male victims (Table 2).

Body mass index (BMI) was estimated using pictures (e.g., from wanted notices) and information from other sources (Figure S6 in Supplement). Specifically, all forensic reports, as well as in wanted notices and media reports, contained a qualitative description of the victim's body (e.g., 'of slim build'). The estimated BMI was then combined with the height value (generally inferred from wanted notices) to provide an estimate of body mass. In only four cases (Case IDs L23, L15, L11 and L37), the victim's height and mass were reported in the wanted notices. This enabled the BMI to be calculated from the height and mass values in these four cases.

A typology inspired by Barwood et al. (2011) was used to categorise the type of clothing worn by the victims. Four categories of clothing were distinguished: underwear or no clothing; summer clothing (shorts and a T-shirt); spring/autumn clothing (trousers, a T-shirt, a pullover, and possibly a waterproof or windproof jacket); and winter clothing (a T-shirt, a pullover, and a heavy, warm jacket, or additional layers of clothing). In cases where a forensic report was available, the type of clothing was determined based on the descriptions given in the report, which were generally confirmed by wanted notices and photographs. Otherwise, descriptions in wanted notices and media reports were used. As shown in Figure S7 in Supplement, spring/autumn clothing is the most frequently reported type of clothing in the dataset (60%), followed by summer clothing (18%), winter clothing (12%) and underwear or no clothing (10%). No accessories of significance, such as a backpack, were reported in the considered cases.

2.3 Drowning context

The water temperature is recorded in the database (Figure S8 in Supplement). In nine cases (eight of which from the Antwerp region), the recorded water temperature corresponds to that measured on site by the forensic doctor. In all other cases, this information was not included in the forensic medicine report. Therefore, the average water temperature recorded at the nearest measurement station (retrieved mainly from waterinfo.be, rijkwaterstaat.nl or https://eautemp.com/current/france/water-temp-in-strasbourg-in-rhine) during the body submersion period was entered into the database. The median reported values of water temperature is 12.2 °C, with the 25^{th} and 75^{th} percentiles corresponding respectively to 7.0 and 19.58 °C.

Finally, the dataset indicates whether the drowning was accidental or resulted from a suicidal act. This information is only available for 29 cases out of a total of 50. This information was inferred from the context of the drowning, as reported by eyewitnesses, or from forensic reports mentioning a suicide note or relatives mentioning suicidal intentions (as reported in the media or in official reports). In our dataset, suicidal acts (66% of the reported cases) are more frequent than accidental circumstances (33% of the reported cases), as shown in Figure S9 in Supplement.

Feature	Data type	Distribution of values. Counts for data of types B and C; median and quartile for data of types I and R.	Forensic medicine report	Photographs	Wanted notices and/or media reports
Body buoyancy (1 = 'sank'; 0 = 'remained at the surface')	B	Floated (14), Sunk (36)	A and L		L and O
Body submersion interval (BSI, days), for sinking cases	R	5.5 (2.9 – 22)	A and L		L and O
Victim's sex	C	Female (16), Male (34)	A and L		L and O
Victim's age (years)	I	Female: 56.5 (46 - 64.5) Male: 46.5 (27 - 62)	A and L		L and O
Body height h_b (m)	R	Missing values (23) Female: 1.61 (1.60 - 1.67) Male: 1.79 (1.70 - 1.88)	A (seven cases)	A (one case: ID A-42)	L and O
Victim's BMI (kg/m²)	R	Female: 25 (23.5 - 26.5) Male: 24.2 (22.5 - 26)	A and L	A	L and O

Clothing type	C	Underwear/none (5), Summer (9), Spring/fall (30), Winter (6)	A and L	A	L and O
Water temperature (T_w)	R	12.3 (7.0 – 19.8)	A and L		
Circumstances (0 = accident, 1 suicide)	B	Accident (10), Suicide (19), Unknown (21)	A and L		L and O

Table 2: Overview of data types, distribution of data and sources of information. The data types are classified as categorical (C), binary (B), integer (I), or real values (R). For numerical variables, data ranges are described by the median and, in brackets, the quartiles of the data distributions. The source for each variable is provided as a function of the location of the cases, either in the regions of Liège (L) or Antwerp (A), or in another region (O).

3 Methods

The existence of correlations between the considered response variables (initial body buoyancy and body submersion interval) and each explanatory variable was evaluated using different methods depending on the type of involved variables (Table 3).

As the initial body buoyancy is a binary variable and our dataset includes both categorical and numerical explanatory variables, we used two different approaches to analyse the potential relationships between these variables. For the numerical explanatory variables (age, body height, BMI and water temperature), we computed a point-biserial correlation coefficient and its corresponding significance. The point-biserial correlation coefficient measures the extent to which the variation in a continuous variable is associated with the difference between the two groups defined by the binary response variable.

For binary (sex) and categorical (clothing type and drowning circumstances) explanatory variables, we applied a Pearson's chi-squared test to contingency tables, based on dichotomized data in the case of categorical variables (Pearson, 1896; Mickey et al., 2004). This test enables us to assess whether the two variables are independent or not by using a significance threshold (*p*-value).

For the second response variable (body submersion interval), we computed Pearson correlation coefficients for the numerical explanatory variables (age, body height, BMI and water temperature), and point biserial correlations for the binary (sex) and dichotomized categorical (clothing type and drowning circumstances) explanatory variables, together with their significance levels (Table 3).

Explanatory variables	Response variables	
	Initial body buoyancy (binary)	Body submersion interval (BSI, numerical)
Age, body height, BMI, water temperature (numerical)	Point biserial correlation	Pearson correlation coefficient
Sex (categorical, binary)	Pearson's chi-square test applied to contingency table	Point biserial correlation
Clothing, drowning circumstances (categorical, nominal)	Pearson's chi-square test applied to contingency table	Point biserial correlation

Table 3: Correlation coefficients utilized as a function of the types of the tested variables.

4 Results

The main results are briefly summarized in this section and further discussed in Section 5. Table 4 shows the correlation coefficients and their significance (p-value) for pairs of explanatory and response variables, provided that at least one of them is numerical. For binary and categorical explanatory variables combined with the binary response variable 'Initial body buoyancy', Table 4 shows the p-value obtained from a Pearson's chi-squared test applied to the relevant contingency tables. The considered sample size (n) is specified for each case. The full dataset ($n = 50$) was used to analyse the response variable 'Initial body buoyancy', whereas a subsample involving only cases where the body sank ($n = 36$) were used for the response variable 'Body submersion interval'. Due to missing values in the explanatory variable 'Body height', the samples had to be further reduced for analysing the influence of this variable ($n = 26$-27).

4.1 Initial body buoyancy

The results presented in Table 4 show that only two numerical explanatory variables are significantly correlated with the initial body buoyancy: the BMI (p-value = 0.03) and the victim's age (p-value = 0.003). The latter correlation is even highly significant, as the corresponding p-value is way below 0.01. For the BMI, the Pearson correlation coefficient is negative (– 0.31), suggesting that, in the case of victims with a higher pre-mortem BMI, there is a lower chance that the body sinks shortly after entering the water. For the victim's age, the highly significant Pearson correlation coefficient is – 0.41, which is even stronger than the correlation with BMI.

4.2 Body submersion interval

When a standard threshold of 5 % ($p \leq 0.05$) is considered to assess the significance of correlations, no numerical explanatory variable shows a statistically significant correlation with the body submersion interval (Table 4). At a slightly higher threshold ($p \approx 0.1$), the water temperature appears significantly correlated with the body submersion interval. The Pearson correlation coefficient is negative, indicating that body submersion intervals tend to be longer when the water is colder.

	Initial body buoyancy (binary variable: 0 = float; 1 = sink)			Body submersion interval (BSI, days)		
	Correlation coefficients	*p*-values	*n*	Correlation coefficients	*p*-values	*n*
Sex		0.73	50	– 0.015	0.93	36
Age	**– 0.41**	**0.003**	50	0.03	0.87	36
Body height	0.03	0.88	27	– 0.08	0.69	26
BMI	**– 0.31**	**0.03**	50	– 0.015	0.93	36
Clothing type						
- Under-wear/none		0.14	50	– 0.11	0.53	36
- Summer		0.69	50	– 0.096	0.58	36
- Spring/fall		0.70	50	0.15	0.38	36
- Winter		0.76	50	– 0.003	0.99	36
Water temperature (T_w)	– 0.19	0.18	50	– 0.27	0.11	36
Suicide		0.51	29	– 0.18	0.44	21

Table 4: Correlation coefficients and corresponding significance (*p*-value) for pairs of variables involving at least one numerical variable. Significance of chi-square test on contingency table for pairs of variables involving Booleans or dichotomized categorical variables. The sample size (*n*) differs depending on the considered response variable and due to missing values for body height.

5 Discussion

5.1 Initial buoyancy estimation

Statistical analysis reveals that age is a key parameter to evaluate the initial body buoyancy and that elderlies have a higher probability to float. This outcome is statistically highly significant (p-value = 0.003).

This result can also be emphasized through contingency tables, as shown in Figure 3. Contingency tables are based on a dichotomized version of the variable age. We systematically tested multiple thresholds to dichotomize age and examined the p-value obtained from a Pearson Chi-square test applied to the corresponding contingency tables (Figure S16 in Supplement). The lowest p-value (i.e., highest significance) was obtained for an age threshold of 65 years (p-value lower than 0.001). According to on our data, drowning victims aged 65 years or above have 70 % chance of initially floating, whereas below this age, the chance of floating drops below 20 % (Figure 1a). If an age threshold of 45 years is considered, the chance that the victim's body initially floats is as low as 5 % (Figure 1a, p-value = 0.002).

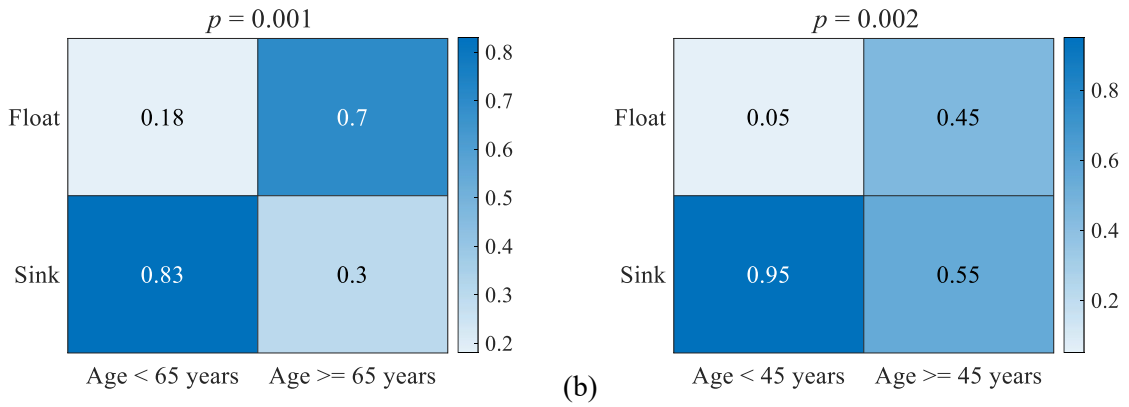

Figure 1: Contingency tables representing the relationship between initial body buoyancy and the victim's age. The age was dichotomized considering (a) 65 years and (b) 45 years as thresholds. The entries in the tables are expressed as a percentage of the sum of the counts in the respective columns.

The overwhelming influence of age on the initial buoyancy of a drowned victim was also highlighted in a recent study by Dennison-Wilkins et al. (2023). These authors did not find a link between more advanced age and body mass. Therefore, they attributed the influence of advanced age on the initial body floatability to body characteristics typical of older persons, such as reduced bone density and reduced muscle mass. They also hypothesized an influence of other features such as clothing type and footwear typically worn by older people. Conversely, in our dataset, we find a highly significant positive correlation between age and BMI (p-value below 0.005), as can be seen in Figure 2 as well as in Figures S10 and S11 in Supplement. This is also consistent with the statistically significant direct correlation found between body buoyancy and BMI (Table 4). From a physical perspective, these relationships between higher age, higher BMI and more positive body buoyancy relate to the known tendency of people of more advanced age to generally have more body fat, so that they have a more buoyant body given the lower density of fat compared to that of water (Siri, 1956a, 1956b; Visser et al., 1997; Wang et al., 1998; Ward and Lieber, 2005; Moon et al., 2013; Nickerson et al., 2018).

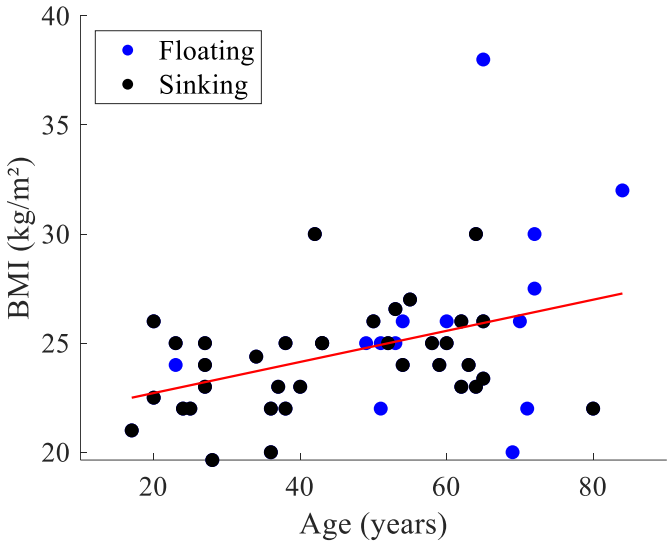

Figure 2: Relationship between age and BMI (Pearson correlation coefficient = 0.39; p-value = 0.005).

Dennison-Wilkins et al. (2023) proposed a mathematical model to estimate the probability of a drowning victim to remain floating at the surface as a function of the victim's age and the drowning circumstances: accident vs. suicide (Figure 3). This model relies on 74 observations and the authors do not report how the model was set up nor its statistical significance. Based on our data, we calibrated a similar model by using a binomial logistic regression to predict the probability that the body floats based on the age of the victim. As shown in Figure 3, a remarkable agreement is found between the model calibrated on our dataset (p-value = 0.008 for the variable age) and the model independently developed by Dennison-Wilkins et al. (2023) for the case of accidents. Our data did not allow us to calibrate statistically significant separate models for the subsets of data corresponding respectively to accidents and to suicides, due to a too low sample size (e.g., n = 10 for accidents). Nonetheless, even if we do not capture the influence of the drowning circumstances (accident vs. suicide), the consistency between our results and those of Dennison-Wilkins et al. (2023) appear promising in light of the relatively small ample sizes on both sides and the exploratory nature of such studies. Building consistent transnational database of drowning, containing relevant information to inform modelling (such as the body initial buoyancy), would certainly enable reaching more robust outcomes.

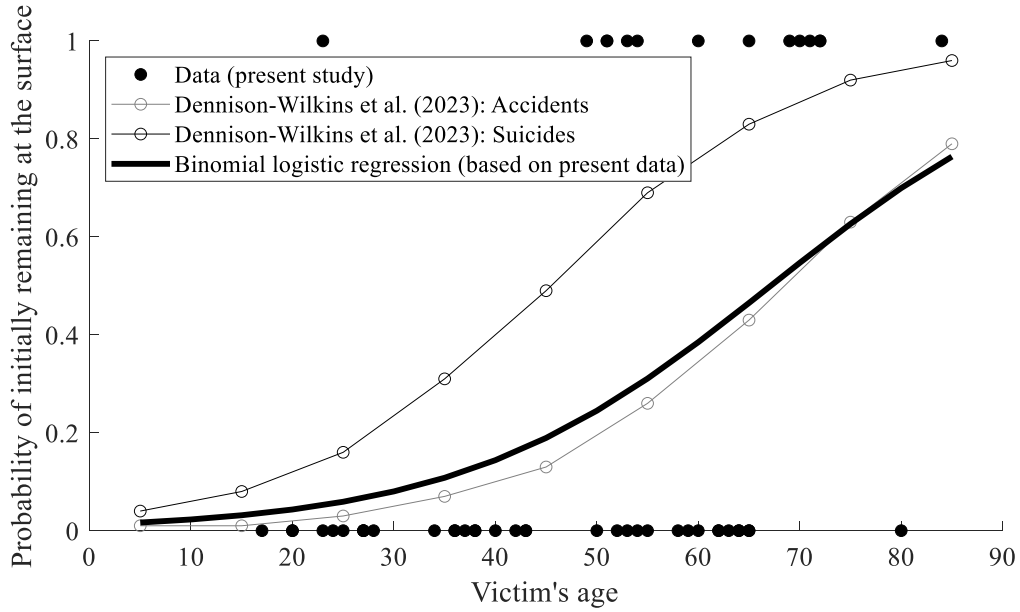

Figure 3: Probability for the drowned body to remain floating at the surface (i.e., not to sink) as a function of the victim's age.

Although our data appear insufficient to unveil a statistically significant association between the circumstances of drowning (accidental vs. suicidal) and initial body buoyancy, Figures S10 and S11 in Supplement reveal highly significant correlations between suicidal drowning and the victim's age and sex. A statistically significant correlation was also found with the victim's BMI. Overall, these results highlight that older female victims with a higher BMI are significantly more likely to drown as a result of a suicidal act than an accident. This constitutes a well-defined profile of victims of suicidal acts leading to drowning and should be considered particularly relevant when targeting prevention policies.

Another variable for which a moderate *p*-value is obtained in the correlation analysis is the water temperature (*p*-value = 0.18, see Figure S11 in Supplement). In a strict sense, this does not reveal a statistically significant correlation between the numerical variable 'water temperature' and the initial body buoyancy, but nonetheless it hints at a possible relationship between the two. To investigate this further, we dichotomized the variable 'water temperature' and resorted to contingency tables. Similarly to the procedure applied for the victim's age (see Figure S16 in Supplement), we systematically tested different thresholds for dichotomizing the variable 'water temperature' and found that a threshold of 7 °C leads to the most significant classification (*p*-value = 0.009) between cases where the body sank or remained at the surface (Figure 4).

This result suggests that in colder water, victim's bodies appear to have less chance of remaining floating at the surface. This trend was not reported in literature earlier, and the interpretation does not seem straightforward. Numerous studies have examined the body's metabolic response to a cold-shock (Hayward et al., 1984; Tipton et al., 1991; Golden et al., 1997; Shattock and Tipton, 2012; Farstad and Dunn, 2019). This mechanism, as well as the hypothermia (Cooper and Ross, 1960; Tipton and Golden, 1998), could have an influence on the quantity of water swallowed or inhaled (Modell et al., 1976; Conn et al., 1995), and hence on the body buoyancy. This aspect deserves further analyses in future studies.

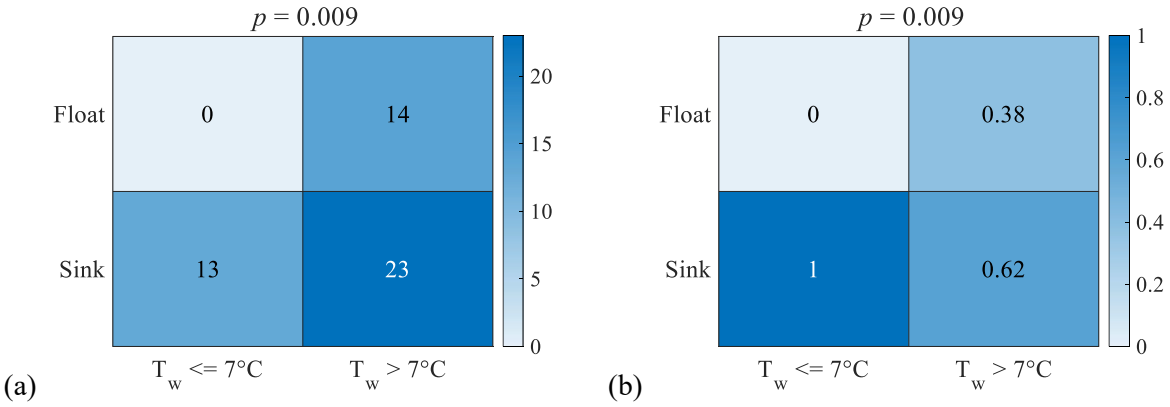

Figure 4: Contingency tables representing the relationship between initial body buoyancy and the water temperature (T_w). The entries in the tables are expressed either as counts (a), or as a percentage of the sum of the counts in the respective columns (b).

5.2 Body submersion interval

A negative correlation was found between the water temperature and the body submersion interval. The direction of the correlation is physically sound: the lower the water temperature, the longer it takes for the body to bloat and resurface (Heaton et al., 2010; Madea and Doberentz, 2010; Mateus and Vieira, 2014; Reijnen et al., 2018; Dalal et al., 2023). Putrefaction processes are indeed slowed down at lower water temperatures, leading to a greater body submersion interval. This observation closely aligns with previous studies using the concept of ADD to predict the time elapsed until body resurfacing (Megyesi et al., 2005; Heaton et al., 2010; Mateus et al., 2013; Daalen et al., 2017; Delhez et al., 2023).

Figure 5 shows the reported body submersion interval as a function of the water temperature, which is the only explanatory variable showing a significant correlation with the body submersion interval. The markers are coloured according to the corresponding ADD value at the time of body resurfacing. Figure S18 in Supplement shows that three entries correspond to outliers in terms of ADD (above 500 °C days, whereas the 75th percentile of the ADD distribution is 22.3 °C days), with one of these also being an outlier in terms of submersion interval (111 °C days). Figure 5 highlights that longer body submersion intervals are associated with lower water temperature and higher ADD values.

Past studies have related specific values of ADD to different stages of body decomposition, which in turn influence body resurfacing and, consequently, the body submersion interval (e.g., Dalal et al., 2023; Heaton et al., 2010; Mateus and Vieira, 2014 and Reijnen et al., 2018). Therefore, here, we fitted a regression corresponding to a constant value of ADD (i.e., a constant value of the product of the body submersion interval *BSI* by the water temperature T_w):

$$T_w \, BSI = \alpha \, , \tag{2}$$

with α representing the ADD value at body resurfacing (Figure 5). The regression yields a value of 97 °C days for α, with a 95% confidence interval of [46, 147] °C days. Despite a relatively large confidence interval due to scatter in the observational data, the regression is found statistically significant (p-value = 0.0004). While this regression provides a first estimate of the value of ADD when the body resurfaces, it fails to capture all the variability of the body submersion interval. Some of the variability in the body submersion interval cannot be explained by water temperature alone. Due to the complexity of the processes underlying human body decomposition in environments such as urban rivers, other parameters influence the BSI, but our dataset does not enable identifying them, partly due to the limited size of our data sample. Random factors, such as trapped air bubbles in clothing or the body becoming temporarily entangled at the bottom of the river, also play a part, but these aspects will certainly remain impossible to predict in a deterministic way.

The resurfacing ADD value found here generally aligns with the 95-117°C days range reported by Mateus et al. (2013), based on only two drowning cases. Similarly, the distribution of body submersion intervals in our dataset is relatively close to that obtained by Dennison-Wilkins et al. (2023), as shown in Figure 6. Given that these two studies were conducted independently, the similarity in the reported distributions lends credibility to the respective datasets. It also highlights the need to assemble larger, transnational datasets to support more robust findings. This entails overcoming challenges related to the sharing of sensitive datasets.

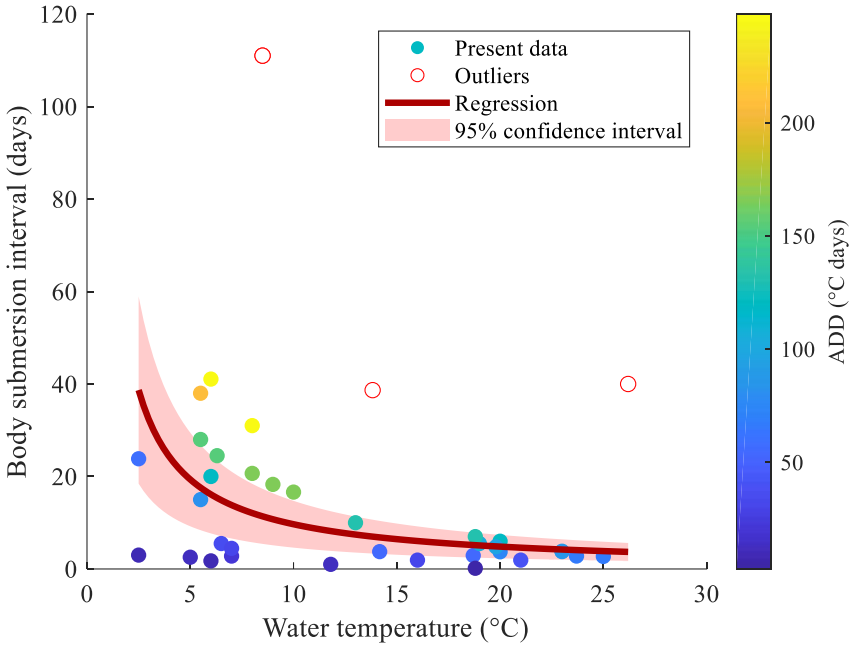

Figure 5: Body submersion interval (*BSI*) as a function of water temperature (T_w). The data markers are coloured as a function of the accumulated degree days (*ADD*) when the body resurfaced.

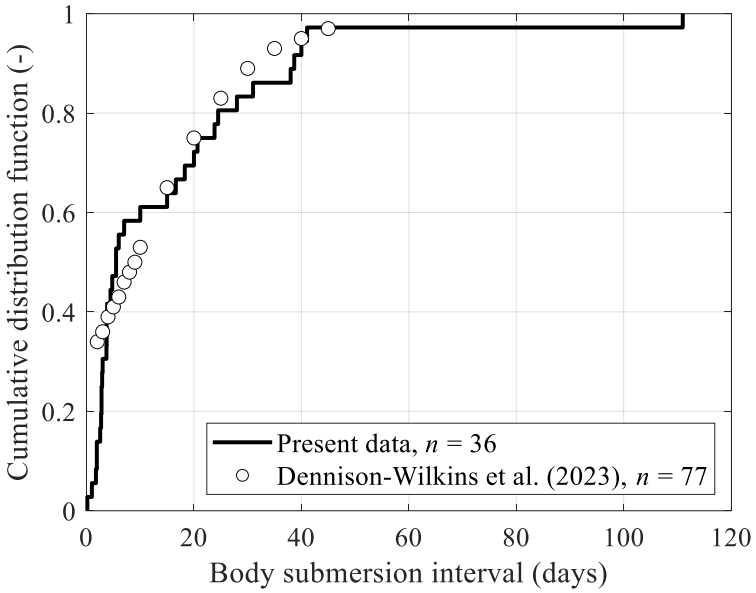

Figure 6: Cumulative distribution function of the body submersion interval in the present dataset compared to the distribution reported by Dennison-Wilkins et al. (2023).

5.3 Limitations

Our dataset, which was compiled specifically for this study, reflects the inherent challenges of retrospective forensic analysis. While certain variables, such as season, age, and, in most cases, sex, are recorded relatively reliably, many others are subject to imprecise estimation. For instance, victim height is usually only documented if an autopsy has been performed or if data are provided by close relatives. In the absence of either of these, this information remains

unknown. Similarly, body mass cannot be accurately measured post-mortem due to the physical changes that occur during immersion and decomposition. Consequently, it must be estimated visually from photographic evidence. In cases where no photographs or witness reports were available, this variable was excluded. To limit inter-observer variability, all BMI estimations were performed by the same researcher.

Classifying clothing also presents complexities. Due to the wide variety of clothing types, materials, cuts, and accessories, creating a fully detailed classification system would be impractical. For the purposes of this study, clothing types were categorised into four broad groups; however, this simplification could mask meaningful differences. For example, a woollen jumper and a leather jacket may have markedly different buoyant properties, yet they are both classified in the same category.

In some cases, a less stringent threshold than 0.05 was used when examining the results of the correlation analysis (e.g., for the correlation between water temperature and body submersion interval). This is deemed acceptable in exploratory studies with relatively small sample sizes like here ($n = 50$), as it helps to avoid overlooking potentially interesting relationships that warrant further investigation. We hope that larger datasets will reveal more significant correlations in the future.

It is anticipated that expanding the dataset in terms of both size and the reliability of recorded variables will enhance the robustness and predictive capacity of the statistical analyses (e.g., Hills et al., 2021). Increased diversity among registered cases would further improve the generalisability of the findings and enable more rigorous testing of correlations. So far, existing large international databases seem to focus primarily on medical aspects and prevention policies (see Table 1), rather than reporting on the variables of interest for guiding computer simulations of drowning victims' body drift.

6 Conclusion

Computer simulations of the drift of a drowning victim's body appear to be a promising technology to improve the success rate of search operations in rivers. This study is one of the few to use a database of real-world fatal drowning cases ($n = 50$) to predict two important variables for simulating the drift of a drowning victim in urban rivers, namely the initial body buoyancy and the body submersion interval.

The results show a highly significant correlation between the victim's age and the initial body buoyancy ($p < 0.003$), meaning that the body of an older victim is more likely to remain at the surface than that of a younger victim. For victims aged over 65 years, the probability of their body remaining afloat is almost four times higher than for younger victims ($p = 0.001$). This may be attributed to body characteristics typically found in older people, such as lower bone density and higher body fat content. The latter aligns with the statistically significant correlation found between the victim's pre-mortem body mass index (BMI) and the body buoyancy ($p \sim 0.03$), given that fat is less dense than water. In addition to the importance of

age and BMI in estimating body buoyancy, there appears to be a temperature threshold (~ 7 °C) below which no instances of body floating have been documented, suggesting that temperature could be a limiting environmental factor in body floatability.

Statistical analyses also suggest a strong association between a prolonged body submersion interval and lower water temperatures, due to putrefaction processes slowing down at lower temperatures. The regression analysis estimates a resurfacing ADD value of 97 °C days ($p < 0.001$), which largely aligns with the findings of a previous study. While this value does not fully account for the variability of body submersion intervals due to the complex and partly unpredictable nature of decomposition processes and urban river environments, it is highly valuable for improving simulations of body drift. These findings highlight the need for larger, transnational datasets to enhance the robustness and generalizability of such estimates.

Finally, significant correlations were found between suicidal drowning and certain characteristics of the victim, such as being older and female, and having a higher BMI. These findings suggest a distinct victim profile of victims of suicidal drowning. This should be considered in prevention efforts.

References

Barwood, M.J., Bates, V., Long, G., Tipton, M.J., 2011. Float First:“ Trapped Air Between Clothing Layers Significantly Improves Buoyancy on Water After Immersion. International Journal of Aquatic Research and Education 5.

Behnke, A.R., Feen, B.G., Welham, W.C., 1942. The specific gravity of healthy men: body weight / volume as an index of obesity. Journal of the American Medical Association 118, 495.

Blondel, P., 2014. Searching for Dead Bodies with Sonar, in: DrowningPrevention,Rescue,Treatment. Springer-Verlag Berlin and Heidelberg GmbH & Co. K, New York, pp. 1161–1165.

Byard, R.W., 2017. Drowning deaths in rivers. Forensic Science, Medicine and Pathology 13, 388–389.

Chen, Q., Xia, J., Falconer, R.A., Guo, P., 2019. Further improvement in a criterion for human stability in floodwaters. Journal of Flood Risk Management 12, e12486.

Conn, A.W., Miyasaka, K., Katayama, M., Fujita, M., Orima, H., Barker, G., Bohn, D., 1995. A canine study of cold water drowning in fresh versus salt water: Critical Care Medicine 23, 2029–2037.

Cooper, K.E., Ross, D.N., 1960. Hypothermia in surgical practice. British Journal of Surgery 48, 350–350.

Daalen, M.A. van, Kat, D.S. de, Oude Grotebevelsborg, B.F.L., Leeuwe, R. de, Warnaar, J., Oostra, R.J., M Duijst-Heesters, W.L.J., 2017. An Aquatic Decomposition Scoring Method to Potentially Predict the Postmortem Submersion Interval of Bodies Recovered from the North Sea. Journal of Forensic Sciences 62, 369–373.

Dalal, J., Sharma, S., Bhardwaj, T., Dhattarwal, S.K., 2023. Assessment of post-mortem submersion interval using total aquatic decomposition scores of drowned human cadavers. Journal of Forensic Sciences 68, 549–557.

Delhez, C., Rivière, N., Erpicum, S., Pirotton, M., Archambeau, P., Arnst, M., Bierens, J., Dewals, B., 2023. Drift of a Drowning Victim in Rivers: Conceptualization and Global Sensitivity Analysis Under Idealized Flow Conditions. Water Resources Research 59, e2022WR034358.

Dennison-Wilkins, L., Hackman, L., Hayatdavoodi, M., 2023. The Body Recovery From Water Study: The application of science to missing person search. Policing: A Journal of Policy and Practice 17, paad037.

Donoghue, E.R., Minnigerode, S.C., 1977. Human body buoyancy: a study of 98 men. Journal of Forensic Sciences 22, 573–579.

Durnin, J.V.G.A., Womersley, J., 1974. Body fat assessed from total body density and its estimation from skinfold thickness: measurements on 481 men and women aged from 16 to 72 Years. British Journal of Nutrition 32, 77–97.

Farstad, D.J., Dunn, J.A., 2019. Cold Water Immersion Syndrome and Whitewater Recreation Fatalities. Wilderness & Environmental Medicine 30, 321–327.

Forslund, A., Johansson, A., Sjödin, A., Bryding, G., Ljunghall, S., Hambraeus, L., 1996. Evaluation of modified multicompartment models to calculate body composition in healthy males. The American Journal of Clinical Nutrition 63, 856–862.

Fralick, M., Denny, C.J., Redelmeier, D.A., 2013. Drowning and the Influence of Hot Weather. PLoS ONE 8, e71689.

Gallagher, D., Visser, M., Sepulveda, D., Pierson, R.N., Harris, T., Heymsfield, S.B., 1996. How Useful Is Body Mass Index for Comparison of Body Fatness across Age, Sex, and Ethnic Groups? American Journal of Epidemiology 143, 228–239.

Golden, F.S., Tipton, M.J., Scott, R.C., 1997. Immersion, near-drowning and drowning. British Journal of Anaesthesia 79, 214–225.

Gonzalez, J.R.P., Escobar-Vargas, J., Vargas-Luna, A., Castiblanco, S., Trujillo, D., Guatame, A.C., Corzo, G., Santos, G., Perez, L.A., 2022. Hydroinformatics tools and their potential in the search for missing persons in rivers. Forensic Science International 111478.

Hanley, J.A., McNeil, B.J., 1982. The meaning and use of the area under a receiver operating characteristic (ROC) curve. Radiology 143, 29–36.

Hayward, J.S., Hay, C., Matthews, B.R., Overweel, C.H., Radford, D.D., 1984. Temperature effect on the human dive response in relation to cold water near-drowning. Journal of Applied Physiology 56, 202–206.

Heaton, V., Lagden, A., Moffatt, C., Simmons, T., 2010. Predicting the Postmortem Submersion Interval for Human Remains Recovered from U.K. Waterways*. Journal of Forensic Sciences 55, 302–307.

Heaviside, C., Macintyre, H., Vardoulakis, S., 2017. The Urban Heat Island: Implications for Health in a Changing Environment. Current Environmental Health Reports 4, 296–305.

Hills, S.P., Hobbs, M., Tipton, M.J., Barwood, M.J., 2021. The water incident database (WAID) 2012 to 2019: a systematic evaluation of the documenting of UK drownings. BMC Public Health 21, 1760.

Horn, K., 2014. Underwater Search and Evidence Response Teams, in: Drowning. Springer-Verlag Berlin and Heidelberg GmbH & Co. K, New York, pp. 1175–1177.

Laurent, P.-E., Coulange, M., Bartoli, C., Boussuges, A., Rostain, J.-C., Luciano, M., Cohen, F., Rolland, P.-H., Mancini, J., Piercecchi, M.-D., Vidal, V., Gorincour, G., 2013. Appearance of gas collections after scuba diving death: a computed tomography study in a porcine model. International Journal of Legal Medicine 127, 177–184.

Lazzarin, T., Viero, D.P., Molinari, D., Ballio, F., Defina, A., 2022. A new framework for flood damage assessment considering the within-event time evolution of hazard, exposure, and vulnerability. Journal of Hydrology 615, 128687.

Lunetta, P., Ebbesmeyer, C., Molenaar, J., 2014. Behaviour of Dead Bodies in Water, in: Drowning. Springer-Verlag Berlin and Heidelberg GmbH & Co. K, New York, pp. 1149–1152.

Lunetta, P., Zaferes, A., Modell, J., 2014. Establishing the Cause and Manner of Death for Bodies Found in Water, in: Bierens, J.J.L.M. (Ed.), Drowning. Springer Berlin Heidelberg, Berlin, Heidelberg, pp. 1179–1189.

Madea, B., Doberentz, E., 2010. Commentary on: Heaton V, Lagden A, Moffatt C, Simmons T. Predicting the Postmortem Submersion Interval for Human Remains Recovered from U.K. Waterways. J Forensic Sci 2010;55(2):302–7. Journal of Forensic Sciences 55, 1666–1667.

Maghakian, C., Navratil, O., Zanot, J.-M., Rivière, N., Honegger, A., 2024. Drowning incidents in urban rivers: An underestimated issue with future challenges in need of an interdisciplinary database to characterise its epidemiology. Environmental Challenges 14, 100822.

Martlin, B.A., Anderson, G.S., Bell, L.S., 2023. A review of human decomposition in marine environments. Canadian Society of Forensic Science Journal 56, 92–121.

Mateus, M., Pablo, H. de, Vaz, N., 2013. An investigation on body displacement after two drowning accidents. Forensic Science International 229, 6–12.

Mateus, M., Vieira, V., 2014. Study on the postmortem submersion interval and accumulated degree days for a multiple drowning accident. Forensic Science International 238, e15–e19.

Megyesi, M.S., Nawrocki, S.P., Haskell, N.H., 2005. Using accumulated degree-days to estimate the postmortem interval from decomposed human remains. Journal of forensic sciences 50, 618–626.

Mickey, R.M., Dunn, O.J., Clark, V., 2004. Applied statistics: analysis of variance and regression, 3. ed. ed, Wiley series in probability and statistics. Wiley, Hoboken, NJ.

Milanesi, L., Pilotti, M., Ranzi, R., 2015. A conceptual model of people's vulnerability to floods. Water Resources Research 51, 182–197.

Modell, J.H., Davis, J.H., 1969. Electrolyte changes in human drowning victims. Anesthesiology 30, 414–420.

Modell, J.H., Graves, S.A., Ketover, A., 1976. Clinical Course of 91 Consecutive Near-Drowning Victims. Chest 70, 231–238.

Moon, J.R., Stout, J.R., Smith-Ryan, A.E., Kendall, K.L., Fukuda, D.H., Cramer, J.T., Moon, S.E., 2013. Tracking fat-free mass changes in elderly men and women using single-frequency bioimpedance and dual-energy X-ray absorptiometry: a four-compartment model comparison. European Journal of Clinical Nutrition 67, S40–S46.

Musolino, G., Ahmadian, R., Xia, J., Falconer, R.A., 2020. Mapping the danger to life in flash flood events adopting a mechanics based methodology and planning evacuation routes. Journal of Flood Risk Management 13.

Nickerson, B.S., Esco, M.R., Bishop, P.A., Fedewa, M.V., Snarr, R.L., Kliszczewicz, B.M., Park, K.-S., 2018. Validity of BMI-Based Body Fat Equations in Men and Women: A 4-Compartment Model Comparison. Journal of Strength and Conditioning Research 32, 121–129.

Nyman, T.J., Antfolk, J., Lampinen, J.M., Korkman, J., Santtila, P., 2021. The effects of distance and age on the accuracy of estimating perpetrator gender, age, height, and weight by eyewitnesses. Psychology, Crime & Law 27, 231–252.

Pearson, K., 1896. VII. Mathematical contributions to the theory of evolution.—III. Regression, heredity, and panmixia. Philosophical Transactions of the Royal Society of London. Series A, Containing Papers of a Mathematical or Physical Character 187, 253–318.

Peden, A.E., Franklin, R.C., Clemens, T., 2019. Exploring the burden of fatal drowning and data characteristics in three high income countries: Australia, Canada and New Zealand. BMC Public Health 19, 794.

Peden, A.E., Franklin, R.C., Leggat, P.A., 2016a. The Hidden Tragedy of Rivers: A Decade of Unintentional Fatal Drowning in Australia. PLOS ONE 11, e0160709.

Peden, A.E., Franklin, R.C., Leggat, P.A., 2016b. Fatal river drowning: the identification of research gaps through a systematic literature review. Injury Prevention 22, 202–209.

Peden, A.E., Willcox-Pidgeon, S., Scarr, J.-P., Franklin, R.C., 2023. Lessons learned through the 20-year development of a national fatal drowning database in Australia. BMC Public Health 23, 1499.

Ray, S., 2014. Training and Equipping Rescue Personnel for Flood Rescue, in: Bierens, J.J.L.M. (Ed.), DrowningPrevention,Rescue,Treatment. Springer, Berlin, Heidelberg, pp. 491–494.

Reijnen, G., Gelderman, H.T., Oude Grotebevelsborg, B.F.L., Reijnders, U.J.L., Duijst, W.L.J.M., 2018. The correlation between the Aquatic Decomposition Score (ADS) and the post-mortem submersion interval measured in Accumulated Degree Days (ADD) in bodies recovered from fresh water. Forensic Science, Medicine and Pathology 14, 301–306.

Shattock, M.J., Tipton, M.J., 2012. Autonomic conflict‘: a different way to die during cold water immersion? The Journal of Physiology 590, 3219–3230.

Sindall, R., Mecrow, T., Queiroga, A.C., Boyer, C., Koon, W., Peden, A.E., 2022. Drowning risk and climate change: a state-of-the-art review. Injury Prevention 28, 185–191.

Siri, W.E., 1956a. The Gross Composition of the Body, in: Advances BiologicalMedicalPhysics. Elsevier, pp. 239–280.

Siri, W.E., 1956b. Body composition from fluid spaces and density: analysis of methods.

Tipton, M., Golden, F., 1998. Immersion in cold water: effects on performance and safety, in: Harries, M., Williams, C., Stanish, W., Micheli, L. (Eds.), Oxfordtextbook sports medicine, OxfordmedicalPublications. Oxford University Press, Oxford, pp. 241–254.

Tipton, M.J., Golden, F.S.C., 2011. A proposed decision-making guide for the search, rescue and resuscitation of submersion (head under) victims based on expert opinion. Resuscitation 82, 819–824.

Tipton, M.J., Stubbs, D.A., Elliott, D.H., 1991. Human initial responses to immersion in cold water at three temperatures and after hyperventilation. Journal of Applied Physiology 70, 317–322.

Twedt, E., Crawford, L.E., Proffitt, D.R., 2015. Judgments of others’ heights are biased toward the height of the perceiver. Psychonomic Bulletin & Review 22, 566–571.

Ung, A., 2014. Main results of the NOYADES survey carried out during summer 2018 in France 9.

Ung, A., Gautier, A., Chatignoux, E., Beltzer, N., 2022. Surveillance épidémiologique des noyades. Résultats de l’enquête NOYADES 2021 50.

Van Der Heyden, J., Nguyen, D., Renard, F., Scohy, A., Demarest, S., Drieskens, S., Gisle, L., 2018. Enquête de santé par examen belge.

Van Hoyweghen, A.J.L., Jacobs, W., Beeck, B. Op de, Parizel, P.M., 2015. Can post-mortem CT reliably distinguish between drowning and non-drowning asphyxiation? International Journal of Legal Medicine 129, 159–164.

Visser, M., Gallagher, D., Deurenberg, P., Wang, J., Pierson, R.N., Heymsfield, S.B., 1997. Density of fat-free body mass: relationship with race, age, and level of body fatness. American Journal of Physiology-Endocrinology and Metabolism 272, E781–E787.

Wang, Z., Deurenberg, P., Guo, S., Pietrobelli, A., Wang, J., Jr, R.P., Heymsfield, S., 1998. Six-compartment body composition model: Inter-method comparisons of total body fat measurement. International Journal of Obesity 22, 329–337.

Ward, S.R., Lieber, R.L., 2005. Density and hydration of fresh and fixed human skeletal muscle. Journal of Biomechanics 38, 2317–2320.

WHO, 2014. Global report on drowning: preventing a leading killer.

Competing interests

The authors have no relevant financial or non-financial interests to disclose.

Acknowledgments

The authors gratefully acknowledge Dr Alexia Van Goethem and Dr Violette Dechamps for their support and expertise in the collection and analysis of forensic data.

Author contributions

CD: Conceptualization, Methodology, Investigation, Data curation, Software, Formal analysis, Visualization, Writing - original draft, **PhB, WJ**: Conceptualization, Investigation, Resources, **SE**: Funding acquisition, Writing – review and editing, **MP**: Funding acquisition, **PA**: Data curation, Software, Funding acquisition, **BD**: Conceptualization, Methodology, Software, Formal analysis, Visualization, Writing - original draft, Writing - review and editing, Supervision, Funding acquisition, Project administration.

S1 Descriptive statistics of response variables

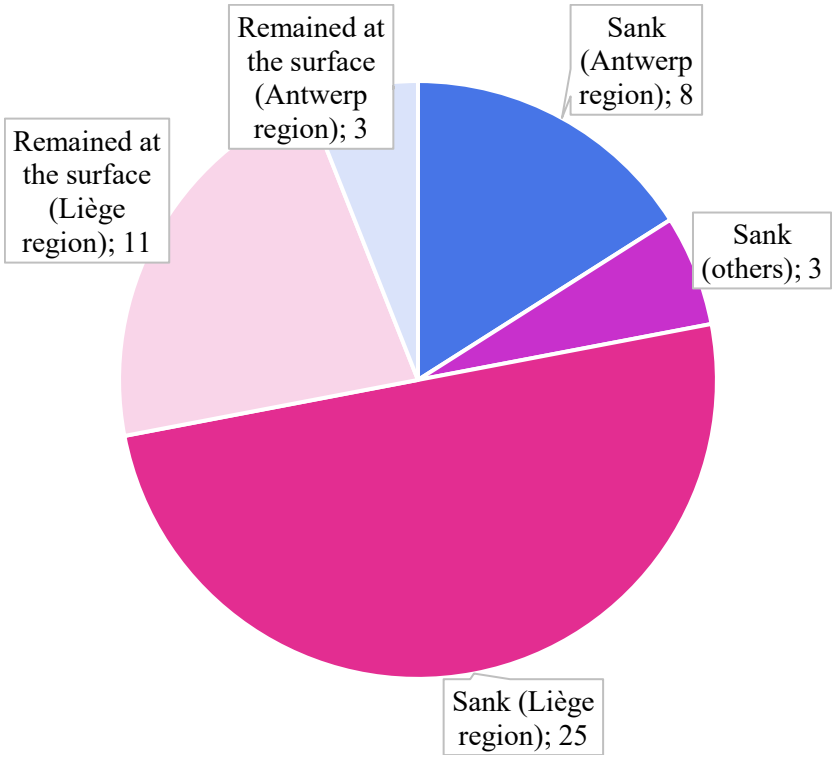

Figure S1: Proportion of cases where the body sank vs. remained at the surface.

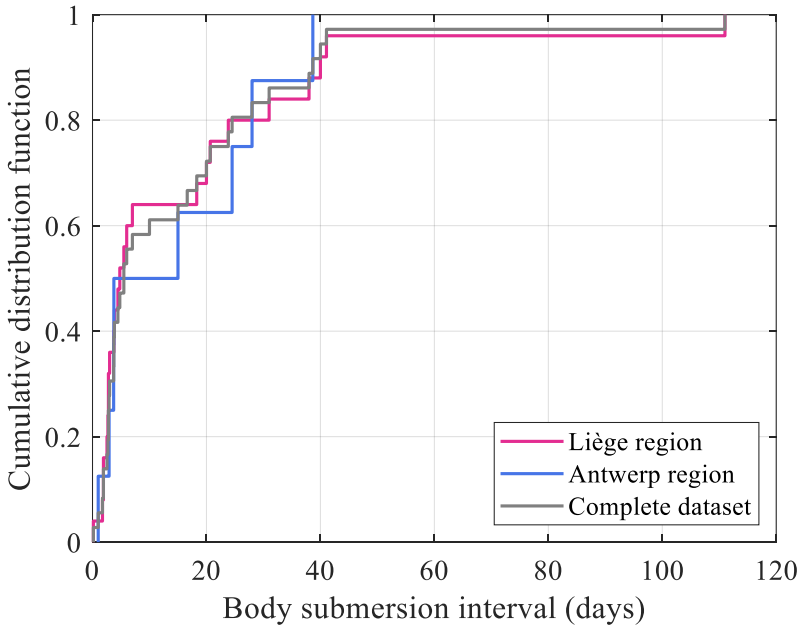

Figure S2: Cumulative distribution of body submersion interval (days) for cases involving sinking .

S2 Descriptive statistics of explanatory variables

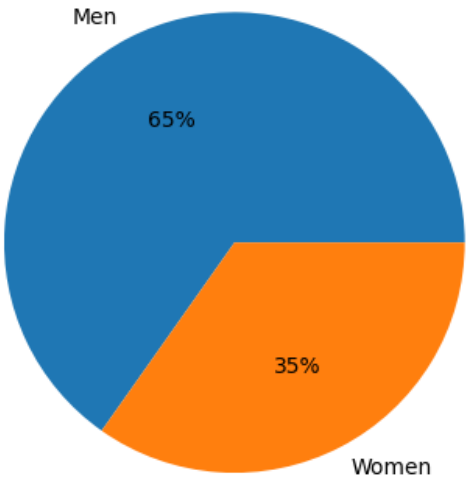

Figure S3: Distribution of victim's sex.

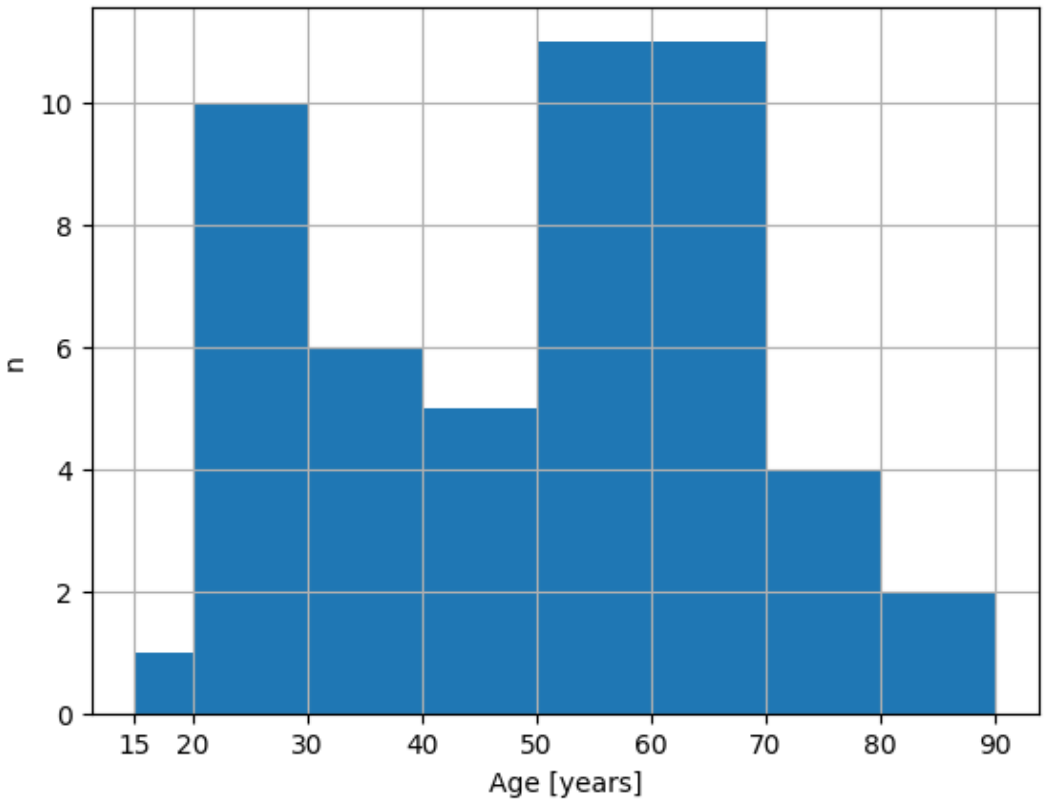

Figure S4: Distribution of victim's age.

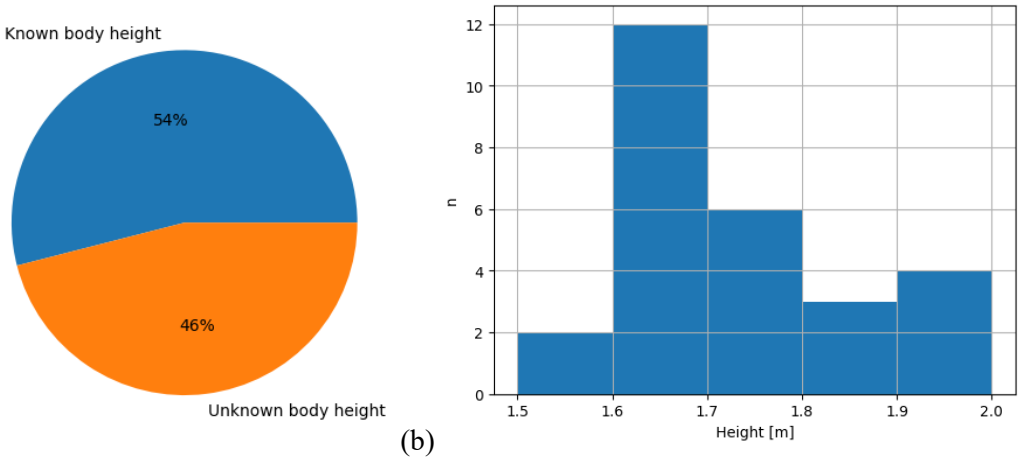

(a) (b)

Figure S5: (a) Proportion of cases with known vs. unknown body height.
(b) Distribution of body height (for the cases where this information is available).

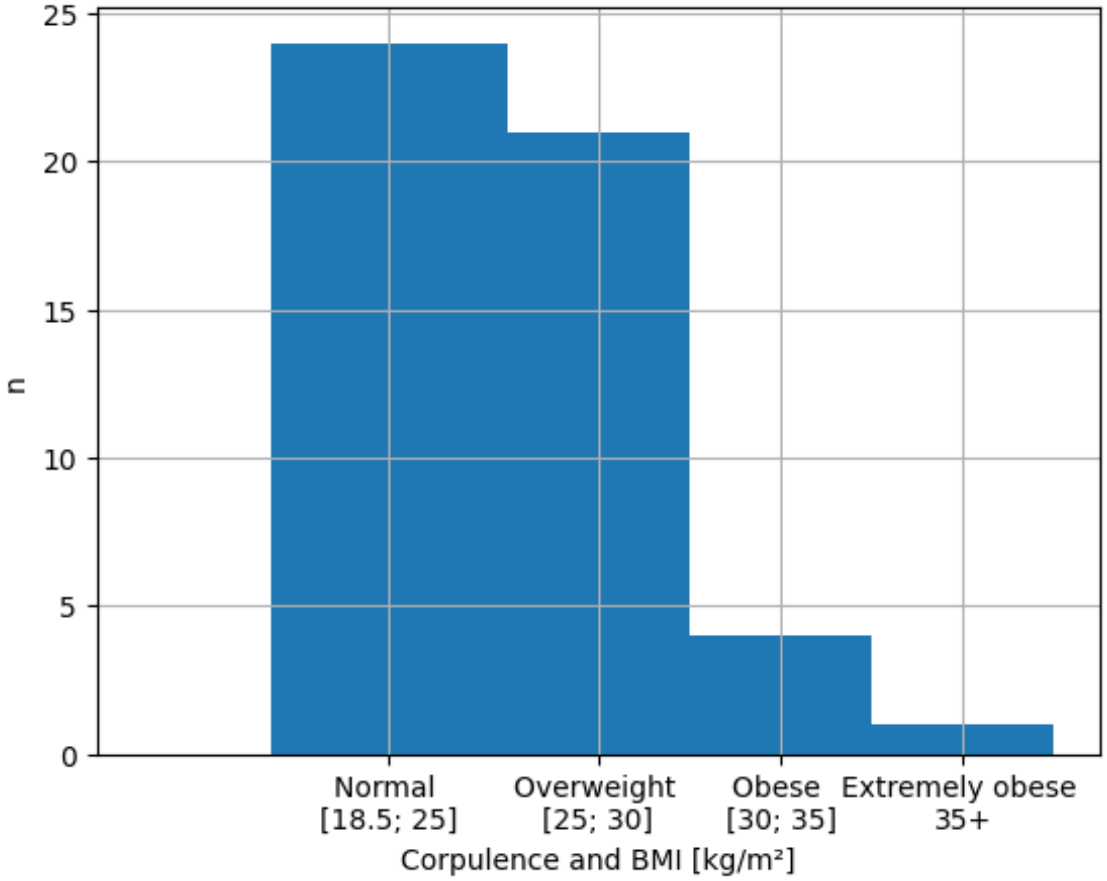

Figure S6: Distribution of body mass index (BMI).

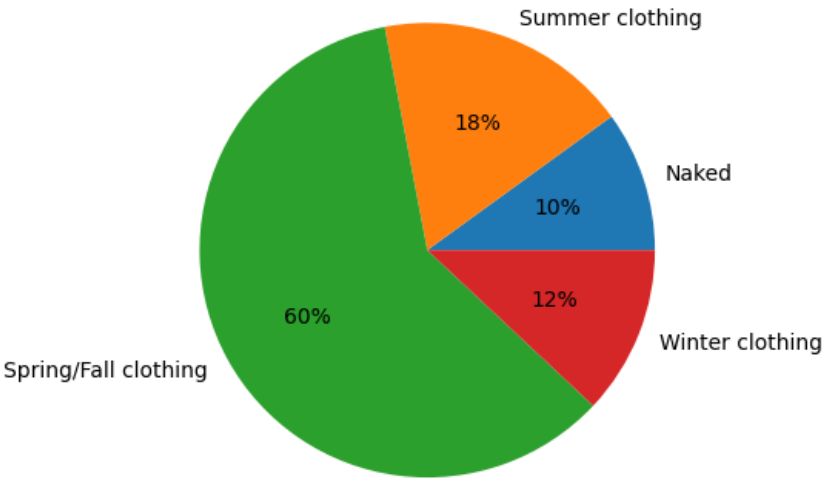

Figure S7: Distribution of clothing type.

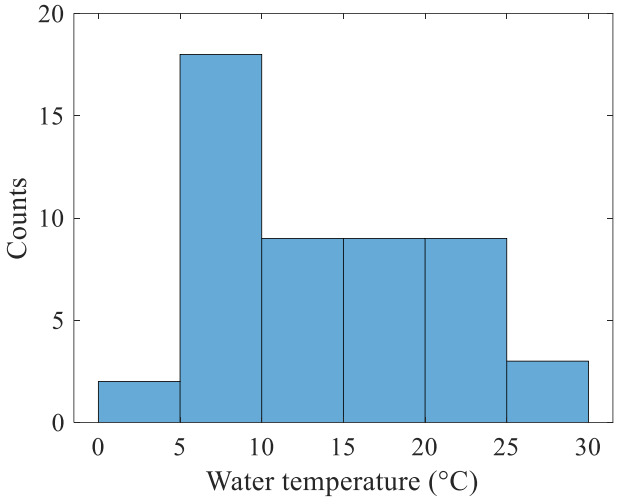

Figure S8: Distribution of water temperature (°C).

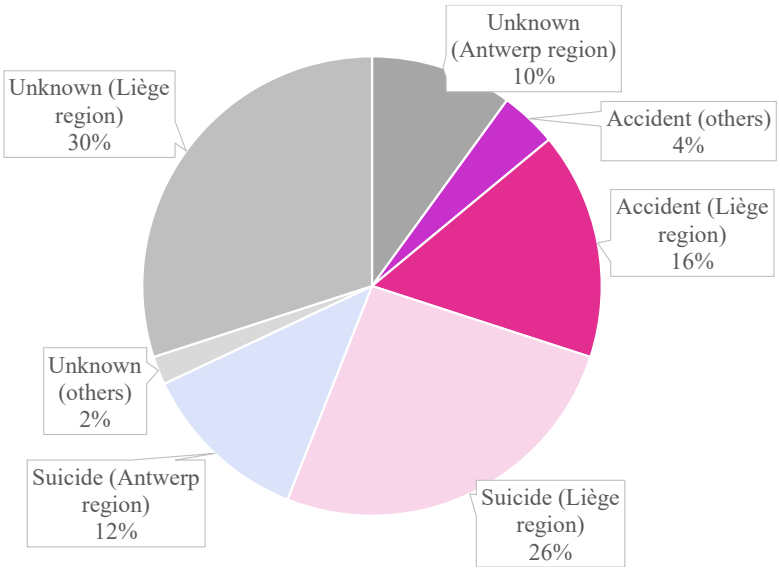

Figure S9: Distribution of drowning circumstances.

S3 Correlation matrix

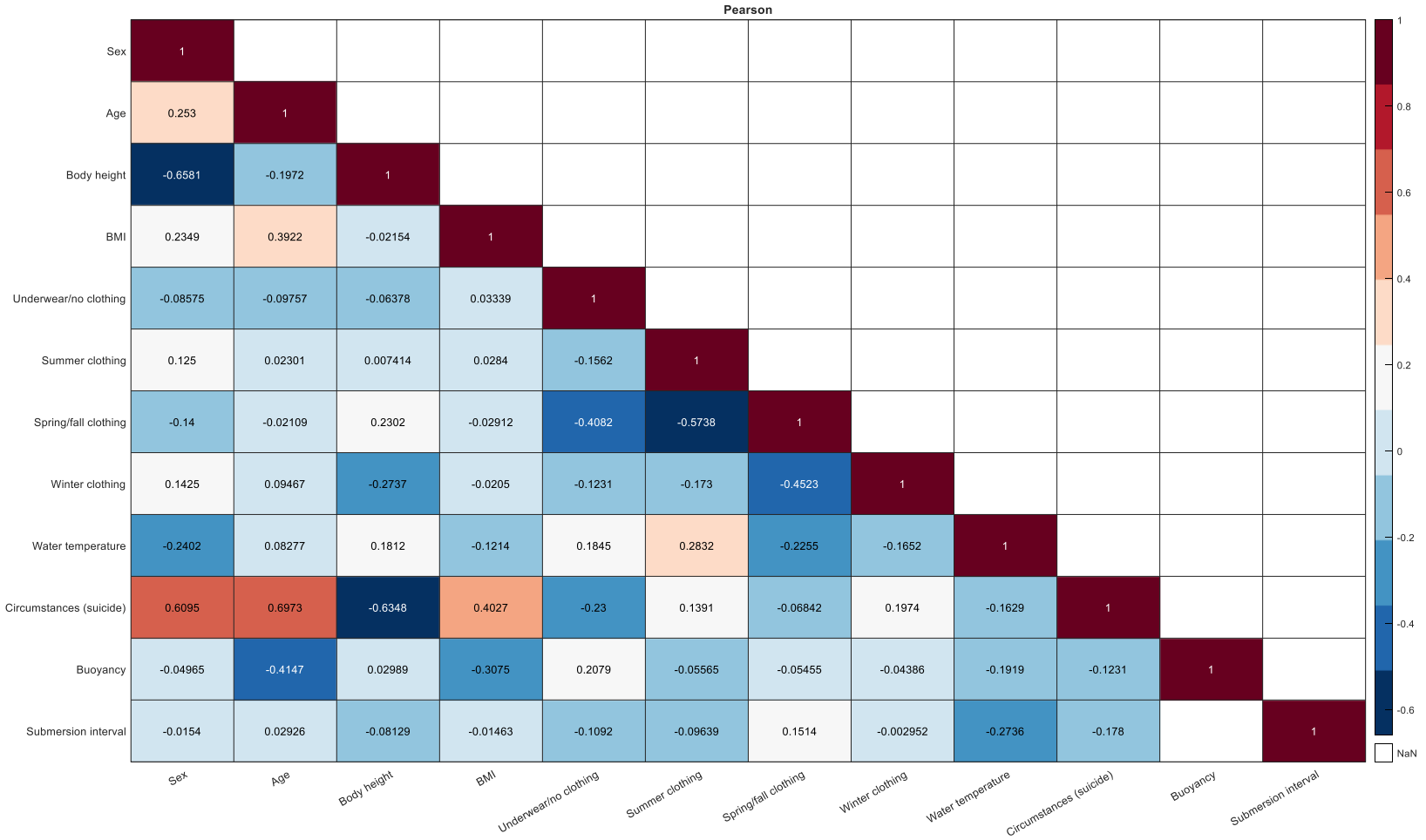

Figure S10: Correlation coefficients computed for all variables.

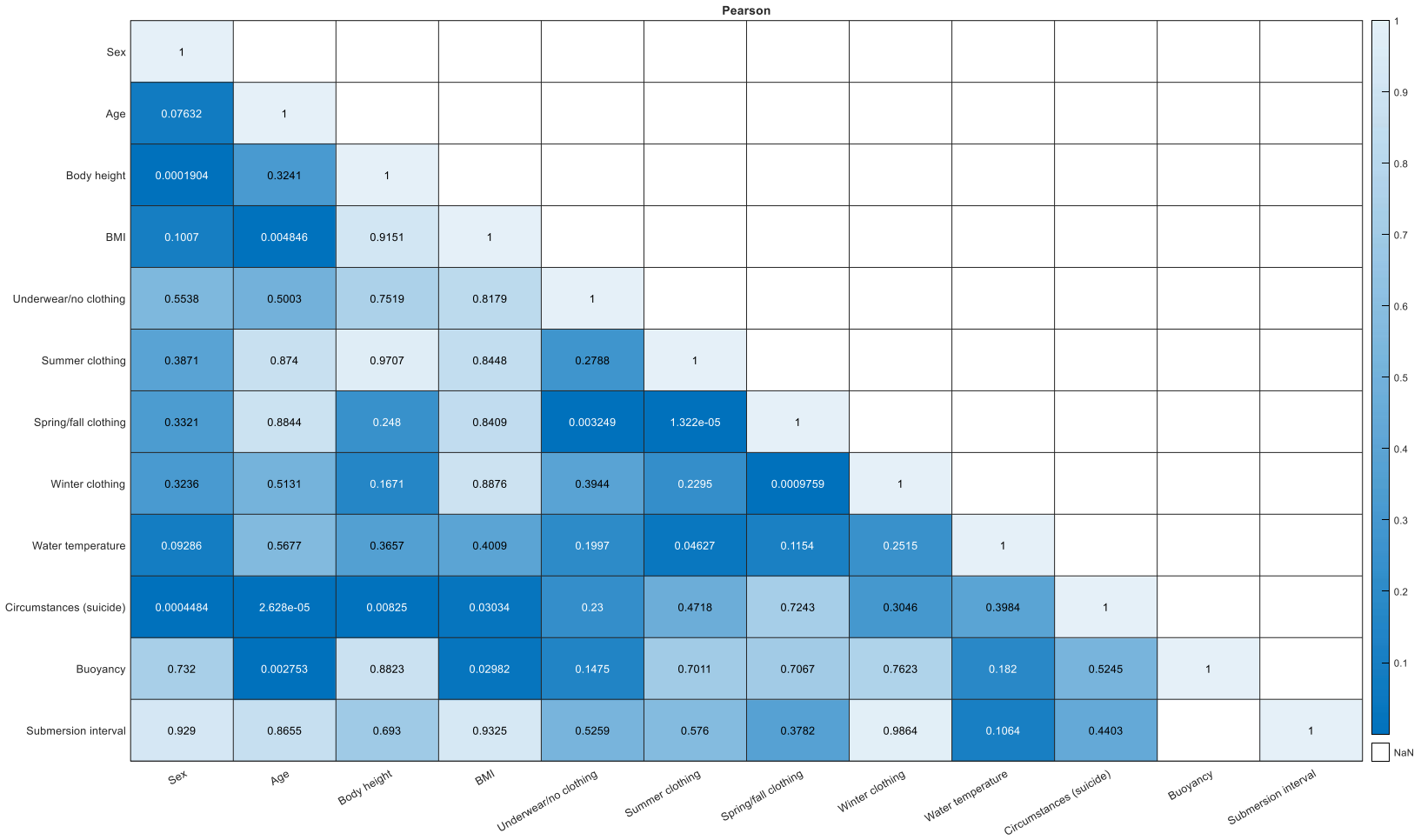

Figure S11: Significance of correlations (*p*-values) for all variables.

S4 Contingency tables

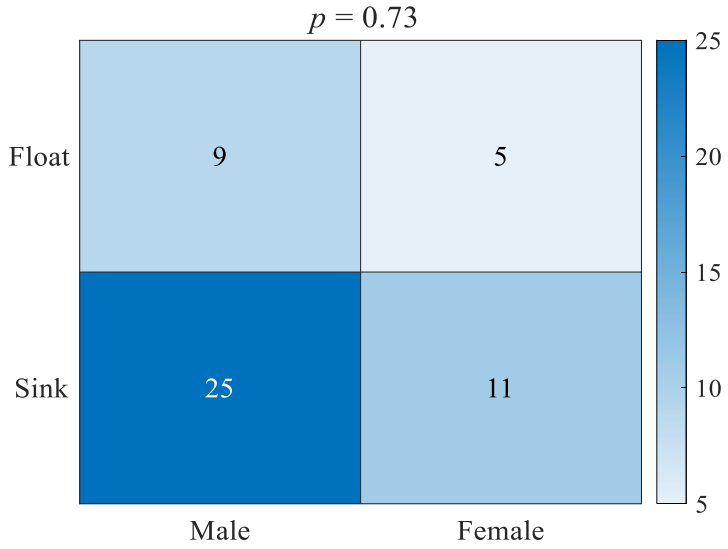

Figure S12: Contingency table to test the dependence of initial body buoyancy to the victim's sex.

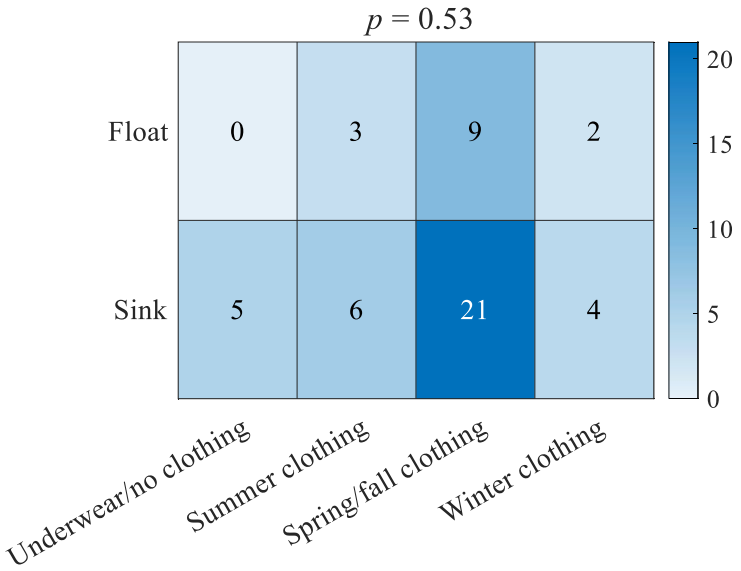

Figure S13: Contingency table to test the dependence of initial body buoyancy to the clothing type.

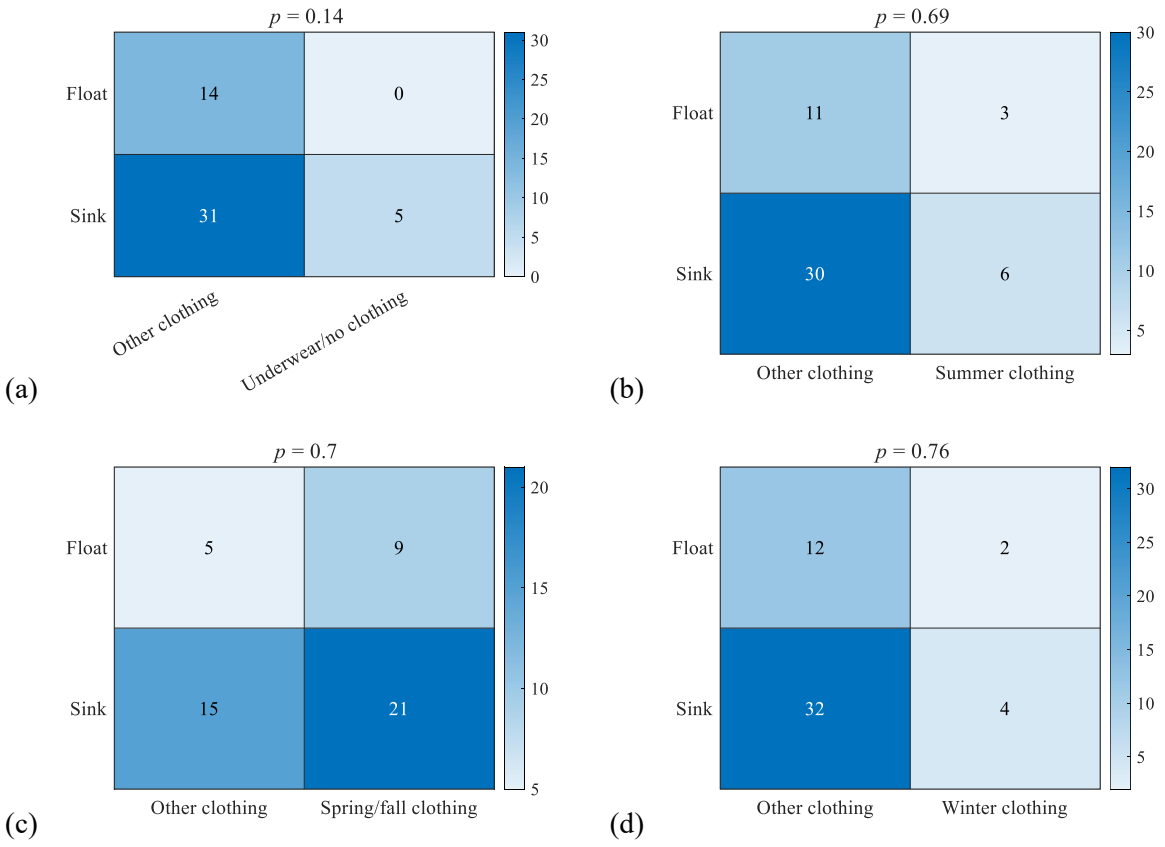

Figure S14: Contingency tables to test the dependence of initial body buoyancy to each individual clothing type (dichotomized categorical variable).

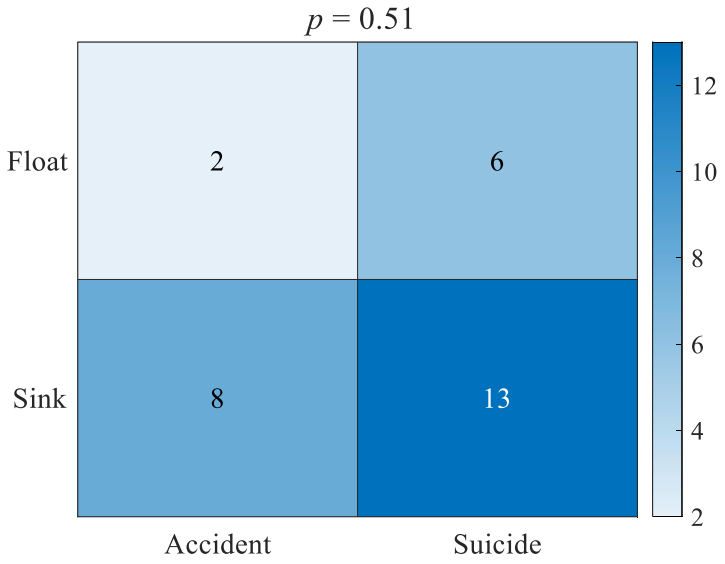

Figure S15: Contingency tables to test the dependence of initial body buoyancy to the drowning circumstances (accident vs. suicide).

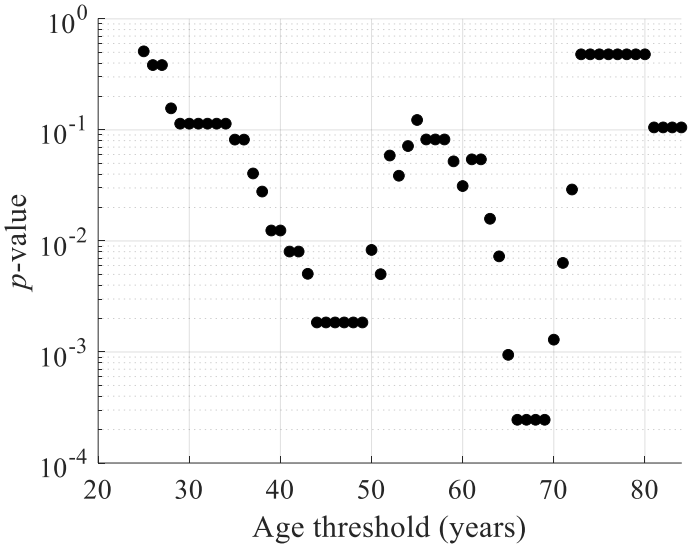

Figure S16: *p*-values characterizing the contingency tables representing the dependence of initial body buoyancy to the victim's age as a function of the age threshold used for dichotomizing the age.

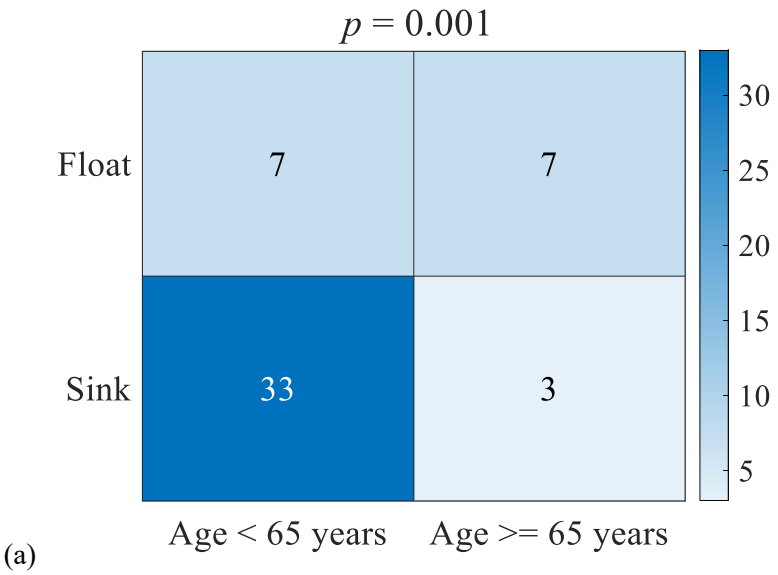

(a)

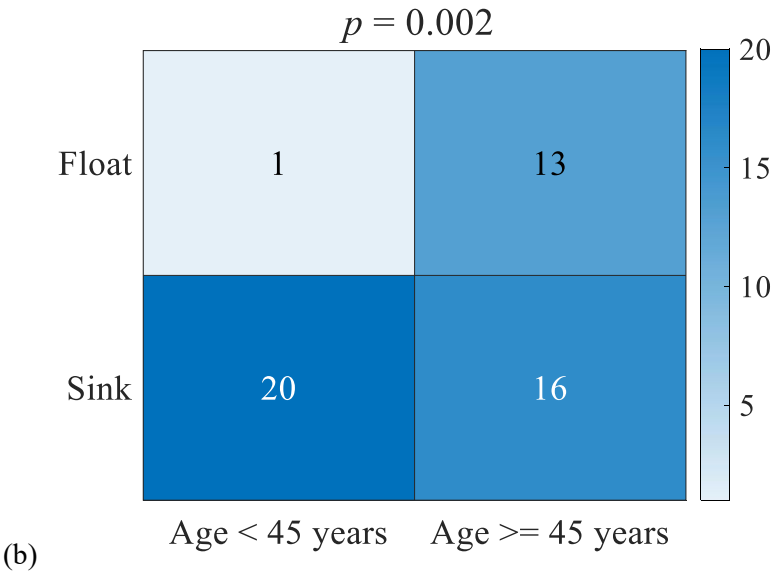

(b)

Figure S17: Contingency tables representing the relationship between initial body buoyancy and the victim's age. The age was dichotomized considering (a) 65 years and (b) 45 years as thresholds.

S5 Body submersion interval

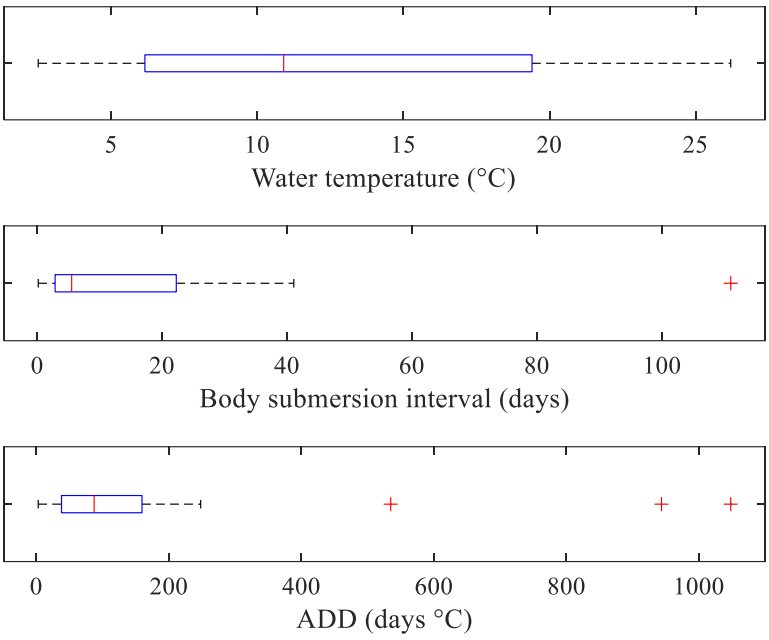

Figure S18: Distributions of water temperature, body submersion interval and accumulated degree days (ADD), with identification of outliers (+).

Chapter 4

Lagrangian modelling of the drift of river drowning victims

This chapter corresponds to the journal paper "Lagrangian modelling of the drift of river drowning victims" by C. Delhez, P. Archambeau, S. Erpicum, Ph. Boxho, D. Lopez, M. Pirotton, N. Riviere and B. Dewals, submitted in 2025 in a scientific journal. The PhD candidate developed the methodology, built the model, realized the simulations, analysed the results, wrote the manuscript and generated the figures.

Lagrangian modelling of the drift of river drowning victims

C. Delhez[1], P. Archambeau[1], S. Erpicum[1], Ph. Boxho[2], D. Lopez[3], M. Pirotton[1], N. Riviere[3], and B. Dewals[1]

[1] Hydraulics in Environmental and Civil Engineering (HECE), Research Unit Urban & Environmental Engineering (UEE), University of Liège, 4000 Liège, Belgium.

[2] Department of Forensic Medicine, Medico-legal Institute of the University of Liège, 4020 Liège, Belgium.

[3] INSA Lyon, Ecole Centrale de Lyon, CNRS, LMFA, UMR 5509, Université Claude Bernard Lyon I, 69621 Villeurbanne, France.

Corresponding author: Clément Delhez (clement.delhez@uliege.be)

ABSTRACT

Climate change increases the frequency of drowning accidents in urban rivers, both during floods or as a consequence of river bathing during heatwaves. The potential of hydrodynamic simulations for guiding search and rescue operations was not explored in previous studies. Here, an Eulerian flow model has been coupled to a Lagrangian drift model to simulate the trajectory of the body of a victim of drowning in a real-world urban river. The model considers the influence of body decomposition on the body buoyancy. Monte Carlo simulations were used to account for uncertainties in input data and model parameters. The model predictions were assessed against seven real cases of drowning. The model predictions appear in better agreement with the field observations for high river discharges than for lower ones, though the results remain largely controlled by particular features in the flow fields such as the influence of hydraulic structures. The accurate prediction of the body buoyancy and resurfacing time appear critical for improving the model performance. The model predictions can be communicated in the form of maps of probability of body presence, which are with valuable information for informing tactical search and rescue operations.

KEYWORDS: drift model, drowning, flood impact, flow modelling, Lagrangian model

1 Introduction

1.1 Context

Unintentional drowning is a global public health issue, resulting in nearly 400,000 deaths annually (WHO, 2014). The risk is exacerbated by climate change, which increases the frequency and intensity of hydro-meteorological extremes, such as riverine floods and heatwaves (Musolino et al., 2020; Parks et al., 2020). Floods increase the likelihood of individuals being swept away by strong currents (Milanesi et al., 2015), while heatwaves encourage unauthorised bathing in urban rivers, leading to more drowning accidents (Simpkins, 2017). This issue is particularly timely as urban planning initiatives tend to promote riverbank areas for recreational activities (cooler environment, scenic views), thereby increasing public exposure to drowning hazard (Ung, 2014). Compared to drownings in swimming pools or at the seaside, survival rates in river drowning are significantly lower, due to more intricate conditions for search operations (Strom et al., 2017; Byard, 2018).

Understanding body motion in rivers is crucial for improving rescue operations and optimising post-drowning resource allocation. The chances of successful resuscitation decline rapidly with time. They drop to almost zero an hour or two after drowning, depending on water temperature (Tipton and Golden, 2011). The search for drowning victims in rivers is particularly challenging due to high momentum flows and low visibility caused by suspended materials (Horn, 2014). Additionally, debris and artefacts on the riverbed impair the performance of sonar technologies (Blondel, 2014), while flood conditions make search and rescue operations unsafe (Ray, 2014). Depending on water temperature, flow conditions, and body characteristics, the body of a drowning victim may either drift at the surface or sink (Lunetta et al., 2014). Currently, in many cases of river drowning, the body is not found until it resurfaces after having sought.

To reduce the death toll of river drowning, a multidisciplinary approach is needed. This includes not only epidemiological research and prevention measures, such as increasing public awareness and enforcing bathing regulations, but also advancements in search technologies. Modelling techniques that simulate river flow have the potential to enhance the effectiveness of rescue efforts and provide critical insights for forensic analysis (Carniel et al., 2002; Ruffell et al., 2017; Delhez et al., 2023). Moreover, a better understanding of body submersion, drift, and resurfacing dynamics, influenced by factors like buoyancy and decomposition processes (Heaton et al., 2010), could further inform both real-time rescue operations and post-drowning investigations.

1.2 State of the art

Most studies on drowning victims have focused on estimating the Postmortem Submersion Interval (PMSI), i.e. the time during which the body remained underwater (Heaton et al., 2010; Mateus et al., 2013; Daalen et al., 2017). These studies estimate the PMSI using the concept of accumulated degree-days (ADD), which is a combination of time and water temperature, and is known to be better at predicting the degree of decomposition of a body than time alone (Megyesi et al., 2005). In these studies, ranges of ADD for which the body should resurface were determined. These ranges of ADD were not related to the victim body characteristics nor to the flow conditions, but only to the state of body decomposition (Heaton et al., 2010; Daalen et al., 2017) or solely based on empirical observations (Mateus et al., 2013). In these studies, no difference was made between drowning in seawater or in freshwater.

So far, Lagrangian modelling of the motion of a victim of drowning was mostly limited to cases of drowning in seawater, under the assumption that the body follows the surface currents

(Carniel et al., 2002; Breivik and Allen, 2008; Mateus et al., 2015; Gunduz, 2017; Ličer et al., 2020; Hart-Davis and Backeberg, 2023), or a combination of the surface currents and wind (Tu et al., 2021; Wu et al., 2023). To the authors' knowledge, only two studies focused on modelling the motion of human bodies or body parts in rivers. In the context of the aftermath of the armed conflict in Colombia, Gonzalez et al. (2022) simulated flow fields in a specific study area to identify locations where human remains have a higher chance of being recovered. Their study relied solely on examining the flow characteristics, and they did not set up a Lagrangian approach taking into account the characteristics of the searched bodies. Delhez et al. (2023) presented a Lagrangian model but it was only applied to idealised flow conditions to highlight which parameters have the greatest influence on the drift of a body. A similar Lagrangian model as presented by Delhez et al. (2023) is the starting point of the present study.

1.3 Objective

The primary objective of this study is to develop and assess a Lagrangian drift model designed to enhance the effectiveness of search and rescue operations for drowning victims in real-world urban rivers. Current search techniques and available data are insufficient in accurately delineating target search areas, whether at the surface or underwater, in urban rivers. This limitation significantly hampers the success rate of search and rescue operations, despite the considerable resources generally allocated to such missions (divers, boats, pedestrians on the riverbanks, etc.). The methodology showcased in our modelling contributes to address this gap by combining an Eulerian flow model with a physically-based Lagrangian model specifically tailored for this application.

2 Data

As summarized in Table 1, we have retrieved data about seven real-world drowning cases which occurred in the city of Liège, Belgium (Figure 1). Two of them are accidental drownings (Cases 14 and 15), Case 8 is a suicide, and there is uncertainty about the circumstances of the other four cases. In none of the cases could the victim be resuscitated.

2.1 Circumstances of drowning and victims' characteristics

In four cases (Cases 8, 14, 15 and 30), the date and time of drowning and recovery of the body, as well as the corresponding locations, could be found in forensic medicine reports. In three other cases (Cases 28, 47 and 50), the same information could only be found in media articles. However, for the cases where forensic medicine reports were available, we compared the information available in these reports with that in media articles and there was a remarkable agreement between the two sources of information. This suggests that a similar level of confidence can be placed in the data used here, irrespective of whether it comes from a forensic medicine report or media articles.

The location and time of the discovery of the body was assumed to be an acceptable proxy for the location and time of the resurfacing of the body. This is a standard assumption in the field (Heaton et al., 2010; Mateus et al., 2013; Daalen et al., 2017), and it is even more relevant in an urban environment, along frequently used footpaths, as in all the cases considered here. It leads to the plausible body trajectories displayed in Figure 1. Except for a single case where the body was found almost at the location of drowning, the distance travelled by the body ranges

from 0.25 km up to 4 km (Table 1). This range is relatively low compared to values reported in literature (Carniel et al., 2002; Mateus et al., 2013); but it can be explained by the urban nature of the river in the centre of Liège, characterized by the presence of obstacles (e.g., bridge piers) and hydraulic structures (e.g., Monsin weir, see Figure 1) where the body can remain trapped. In one case (Case 14), the recovery location of the body is situated 0.25 km upstream of the drowning point. Although this remains challenging to interpret, we did not want to remove this case from the dataset.

In all cases, the date and time of drowning and discovery of the body were known to an hour or less. Their difference was considered a good proxy for the time the body was submerged, as shown in Table 1. This submersion interval of the body ranges from about 6 hours up to almost 40 days.

As shown in Figure 2, there is no direct relationship between the time the body was submerged and the corresponding distance travelled. In particular, the body in Case 28 travelled a considerable distance (2 km), while its submersion interval was the shortest of all cases. This may correspond to a body which did not sink. Figure 2 suggests that the mean discharge in the river (see Section 2.3.3) can be used to classify the cases in terms of submersion interval and distance travelled. The three cases corresponding to the highest mean value of river discharge (Cases 30, 47 and 50) also show the longest submersion intervals and travelled distances. Conversely, all other cases, corresponding to a lower river discharge, also show lower submersion intervals and travelled distances.

Only for Case 8 did the forensic medicine report contain information on water temperature. In the other cases, we considered the water temperature measured at the nearest monitoring station along the river (Eijsden in Figure 3, link). It was averaged over the period of body submersion period, as shown in the time series provided in Supporting Information S1.

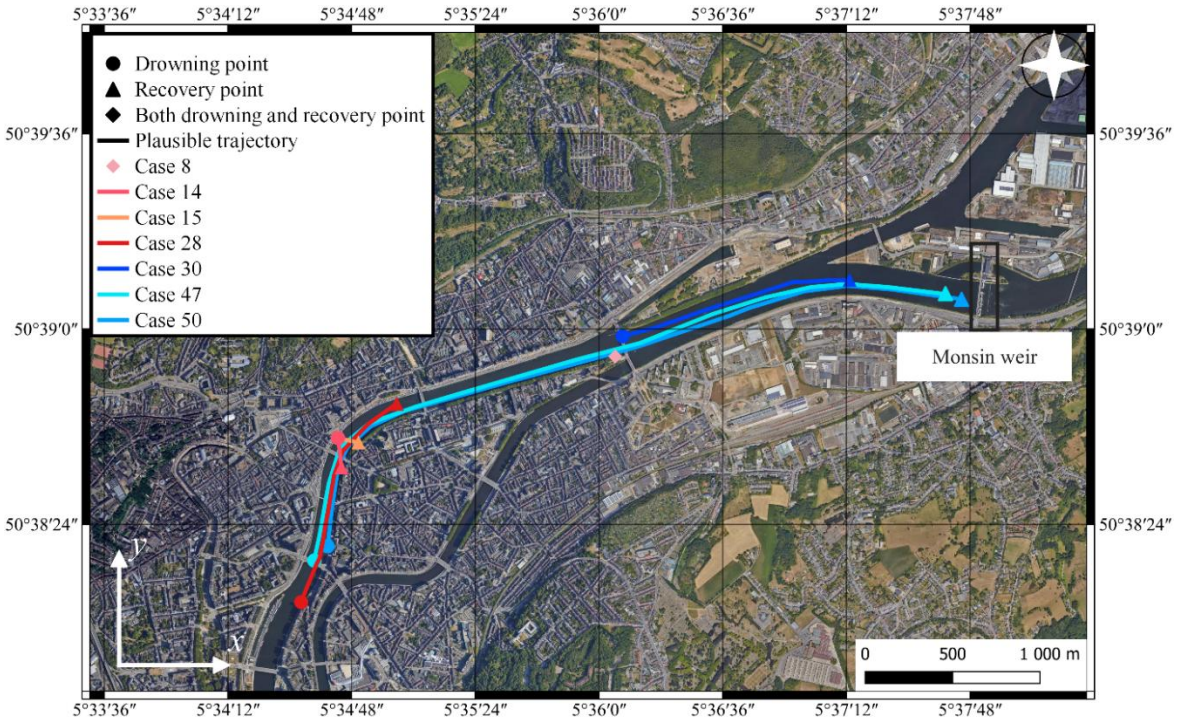

Figure 1: Map of the study area, with the estimated body trajectory of the considered drowning cases.

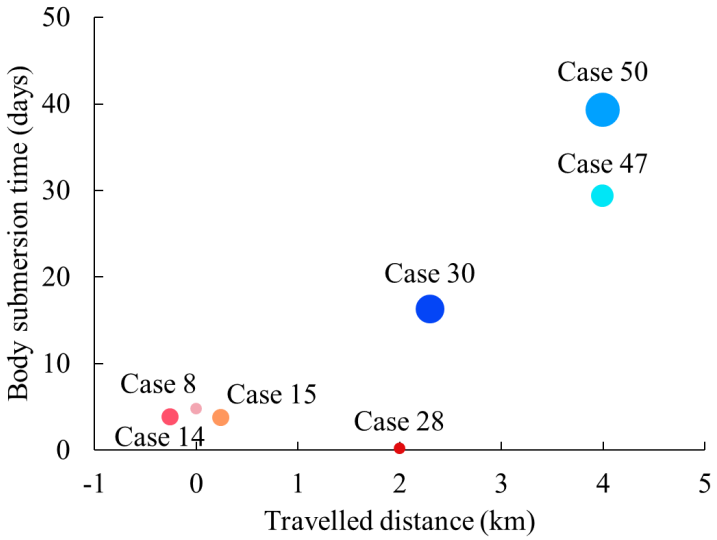

Figure 2: Submersion interval of each body vs. the corresponding travelled distance. The size of each marker is related to the mean river discharge over the period between drowning and body recovery (see Supporting Information S1).

2.2 Victims' characteristics

The age and sex of the victims were recorded in the forensic medicine reports and were also readily available from media reports and/or wanted notices. Body height was rarely recorded in the forensic medicine reports that we could access (only for Case 8). In contrast, this information was often available from wanted notices (Cases 15, 30 and 47). If not available from these sources, body height was considered unknown (Cases 14, 28 and 50).

In Cases 15, 30, 47, the body weight (as well as height) was available from wanted notices, so we were able to calculate the victim's body mass index (BMI). In Cases 8 and 14, we estimated the BMI from qualitative descriptions of the body shape available in forensic medicine reports, combined with pictures of the victim (from wanted notices). For Case 8, the weight could then be computed from the estimated BMI and the known body height. In the other two cases (28 and 50), there was no information available to estimate the body weight or BMI.

We have adopted here the classification of clothing types described by Barwood et al. (2011). Only two of the four clothing categories mentioned by Barwood et al. (2011) are represented in the sample considered here: summer clothing (victim wearing shorts and a t-shirt) or spring/autumn clothing (victim wearing trousers, a t-shirt, a sweater, and possibly a water/windproof jacket). In none of the cases were specific objects or accessories (e.g., a backpack …) reported to have influenced the drowning, except in Case 8 where the victim wore a backpack containing 10 kg weights.

Case ID	Forensic medicine report	Circum-stances	Travelled distance [km]	Body submersion interval [day]	Mean river discharge [m³/s]	Water tempera-ture T_w [°C]	Sex (M/F)	Age [years]	Height [m]	BMI [kg/m²]	Body mass [kg]	Clothing type
Case 8	Yes	Suicide	~ 0	4.8	30	19.5 (19.8)	F	20	1.6	26	Calculated from height and BMI	Summer
Case 14	Yes	Accident	0.25	3.8	300	23	M	24	Unknown	22	Unknown	Spring/Autumn
Case 15	Yes	Accident	0.25	3.75	300	23	M	28	1.84	19.6	67	Spring/Autumn
Case 28	No	Unknown	~ 2	0.2	30	21.5	M	53	Unknown	Unknown	Unknown	Summer
Case 30	Yes	Unknown (alcohol)	2.3	16.3	1100	9.2	M	20	1.9	22	80	Spring/Autumn
Case 47	No	Unknown	~ 4	29.3	750	7.8	M	22	1.69	19.5	56	Spring/Autumn
Case 50	No	Unknown	~ 4	39.25	600	6.5	M	24	Unknown	Unknown	Unknown	Spring/Autumn

Table 1: Summary of the data retrieved for each drowning case. In the column “Water temperature”, all values are those obtained from a monitoring station (Eijsden, see Figure 3), except the value in brackets (Case 8) which comes from a forensic medicine report. ~ X means an approximative value.

2.3 Data for flow modelling

2.3.1 Study area

Although the documented cases of river drowning are located within the city of Liege (Section 2.1), the computational domain of the hydrodynamic simulations is substantially larger to enable the setting of proper boundary conditions.

The study area covers a segment of river Meuse in Belgium, as well as a connected navigation channel (Albert canal). As sketched in Figure 3, it extends over 65 km, from the location of a gauging station (Amay) to a downstream system of locks (Genk). A weir situated in Monsin (Figure 3) regulates the water level in the Meuse and in the navigation channel. The lower segments of two tributaries are also represented: river Ourthe (up to the gauging station Sauheid) and river Vesdre (up to the gauging station Chaudfontaine). In the centre of the study area is the city of Liège, where all the drowning cases considered here took place (Figure 1).

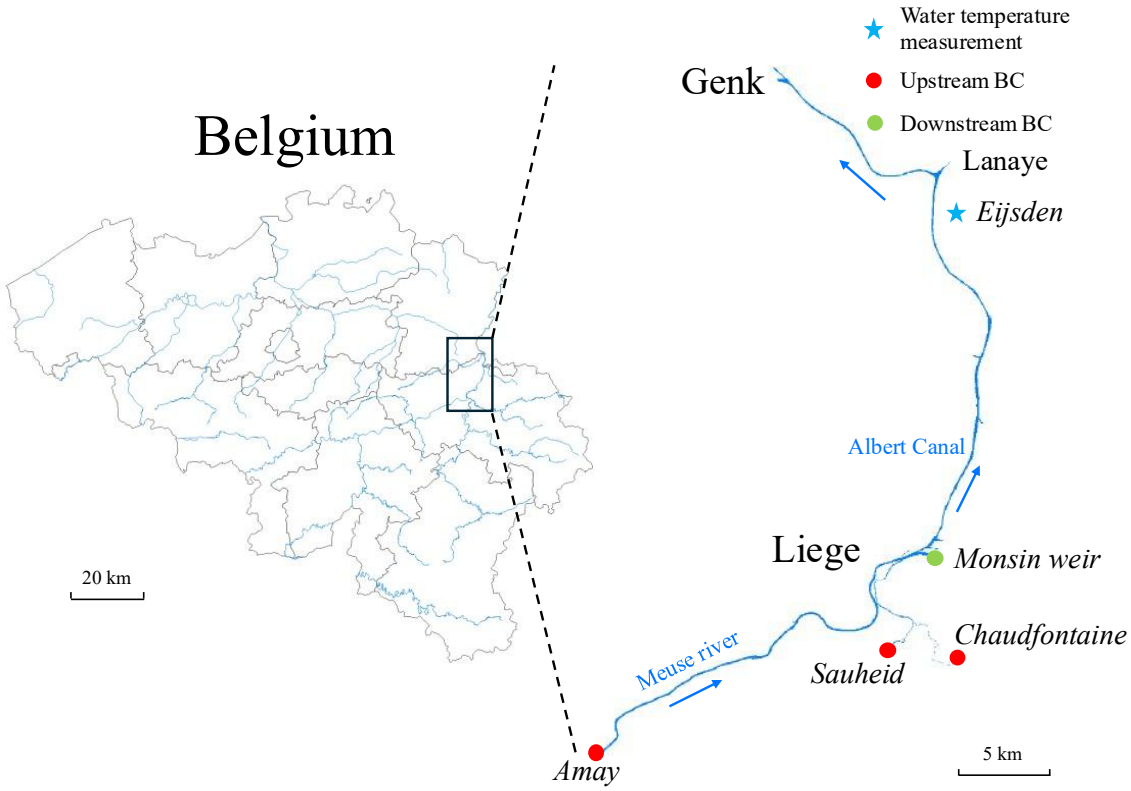

Figure 3: Extent of the computational domain considered for the Eulerian flow model, with upstream (●) and downstream (●) boundary condition and water temperature measurement (★).

2.3.2 Bathymetric data

For the parts of the Meuse river and the Albert canal located in the Walloon region (i.e., upstream of Lanaye), high resolution bathymetric data are available from sonar surveys (0.5 m × 0.5 m, link). This data was resampled to a grid of 5 m by 5 m, consistently with the grid used for the Eulerian flow computations. A "mean" operator was used for resampling, except along the riverbanks where a "maximum" operator was preferred to ensure that the resampled dataset captures the crest level of the flood defences. The spatial extent of the part of the Albert canal situated in the Flemish region (i.e., downstream of Lanaye) was available

(link); but we could not access corresponding bathymetric data. Therefore, a constant bottom elevation was set (54.8 m DNG), consistently with the values in the bathymetric data available in the vicinity of Lanaye. For the two tributaries (Ourthe and Vesdre), available green LIDAR data were used as a proxy for the bathymetry.

2.3.3 Hydrological data

Inflow boundary conditions were prescribed at the three inlets of the computational domain, corresponding to the gauging stations Amay, Sauheid and Chaudfontaine (Figure 3). The boundary conditions were set as time series of hourly flow rates. This data was retrieved from a portal of the river management organization (link). At the gauging station Amay, river Meuse has a mean flow rate of 209 m³/s, while the flow rate in the tributary Ourthe is about 20% of the value in the Meuse (mean flow rate of 45 m³/s at the gauging station Sauheid) and the tributary Vesdre contributes by about 5% of the flow in the Meuse (mean flow rate of 11 m³/s at the gauging station Chaudfontaine). This leads to a mean flow rate between 250 m^3/s and 300 m^3/s in the area of interest.

The time series corresponding to the period of interest for each considered case of drowning are provided in Supporting Information S1. Two cases of drowning (Case 14 and Case 15) occurred when the flow rate in the Meuse was between 200 and 250 m³/s, i.e. slightly above the mean flow rate of the river. Two other cases (Case 8 and Case 28) took place during low flow periods, characterized by a flow rate in the Meuse below the 5th percentile (i.e., 54 m³/s at the gauging station Sauheid). Three other cases of drowning correspond to relatively frequent flood conditions (with a peak flow rate between 700 m³/s and almost 1400 m^3/s), which do not induce any overbank flow given the protection standards in this area.

2.3.4 Operation of hydraulic structures

The Monsin weir is managed so that it ensures a constant water level at the division between river Meuse and the Albert canal (i.e., about 600 m upstream of the Monsin weir). The target water level is 60.1 m DNG. This is reflected in the downstream boundary condition prescribed in the computations (Figure 3). Given that there is virtually no flow in the Albert canal, which is an artificial waterway constructed for the sole purpose of navigation, no-flow boundary conditions were set at the lock systems of Lanaye and of Genk.

3 Eulerian flow model

The academic model WOLF solves the two-dimensional (2D) shallow-water equations, which are a depth-averaged form of the Reynolds-averaged Navier-Stokes equations (Kitsikoudis et al., 2020; Renardy et al., 2021; Dewals et al., 2023; Li et al., 2024). Based on bathymetric data, initial conditions, boundary conditions and a friction coefficient, the model computes the water depth and the two components of the unit discharge on a Cartesian grid.

3.1 Mathematical model

A Cartesian frame of reference was used, with the x and y axis located in the horizontal plane, and the z axis oriented vertically upwards (Figure 1). The conservative form of the shallow-water equations writes:

$$\frac{\partial \boldsymbol{s}}{\partial t} + \frac{\partial \boldsymbol{f}}{\partial x} + \frac{\partial \boldsymbol{g}}{\partial y} = \boldsymbol{S}_0 - \boldsymbol{S}_f \tag{1}$$

with $\boldsymbol{s} = [H, HU, HV]^T$ the vector of the conservative unknowns, H the water depth, U and V the components along x and y of the depth-averaged and Reynolds-averaged flow velocity. Vectors $\boldsymbol{f}$ and $\boldsymbol{g}$ denote the advective and pressure fluxes along directions x and y, respectively. The source and sink terms $\boldsymbol{S_0}$ and $\boldsymbol{S_f}$ represent the effects of the bottom slope and of flow resistance due to friction. The latter is modelled by means of Manning equation. The Manning coefficient has been calibrated based on observed values of water depth and discharge, available at Ampsin and Amay, respectively, for the period from January 1st to December 1st, 2024 (link). The identified optimal value is 0.027 s/m$^{1/3}$.

3.2 Numerical discretization

A cell-centred finite volume scheme was used for the spatial discretization of the shallow-water equations on a Cartesian grid. In the considered case, the grid size was set to $\Delta x = \Delta y = 5$ m, leading to a total number of active wet cells of about 440,000.

The time integration was performed with an explicit two-step Runge-Kutta scheme, which ensures second order accuracy in time. The value of the adaptive time step was determined by utilizing the Courant-Friedrich-Levy number (CFL) which was set in our case to 0.1. This ensures stability of the computation, with a typical time step of the order of 0.04 s. The computed flow fields were stored at an hourly sampling frequency for memory reasons.

3.3 Boundary and initial conditions

A boundary condition was set on the water height at Monsin weir with $Z_s = 60.1$ m where Z_s denotes the free surface elevation above the sea level. No flow leaves the domain at the downstream end of the branches of the Albert canal (Genk and Lanaye, see Figure 3). Three injection zones were set at the upstream limits of the computational domain. The initial conditions for each simulation were generated by running the code in steady mode with inflows corresponding to that of the initial value of the corresponding time series (Supporting Information S1).

4 Lagrangian drift model

4.1 Conceptual model

The Lagrangian model uses a pre-computed flow field ($\mathbf{u_b}$) to calculate the drift of a drowning victim. The trajectory of the body is described by the position of its centre of mass over time. The body acceleration is calculated from the resultant of the forces acting on the body, i.e., the hydrodynamic forces (drag, side and lift forces), the gravity, the buoyancy, the added mass force, and the friction force acting on the body when it is in contact with the river bottom. In the model, the values of body volume and buoyancy are varied with the water temperature, the body submersion depth and the time elapsed since drowning. The model does not predict the orientation of the body (e.g., roll, pitch, and yaw angles).

4.2 Governing equations

The model state variables are the vectors of body position $\mathbf{x_b}$ and body velocity $\mathbf{u_b}$. The governing equations write:

$$\dot{\mathbf{x}}_\mathbf{b} = \mathbf{u}_\mathbf{b} \tag{2}$$

$$\left(m_T + C_A \rho_f V_b\right)\dot{\mathbf{u}}_\mathbf{b} = \mathbf{F}_\mathbf{f} + \mathbf{F}_\mathbf{g} + \mathbf{F}_\mathbf{b} + \mathbf{F}_\mathbf{A} \tag{3}$$

where a dot over a variable denotes the time derivative, m_T is the total body mass, C_A the added mass coefficient, ρ_f the fluid density, and V_b, the body volume (as defined in Section 4.2.2 hereafter). The total body mass m_T is the sum of the body mass m_b, the mass of accessories (e.g., backpack) and the mass of swallowed water dm, that can vary between 0 and 10% of the body mass (Conn et al., 1995). The complete governing equations can be found in Supporting Information S3a.

4.2.1 Considered forces

The following forces were considered:

- the hydrodynamic forces $\mathbf{F_f}$ (drag, side and lift) induced by the relative velocity between the body and water in the horizontal plane and the drag induced by the vertical body velocity, expressed as:

$$\mathbf{F}_\mathbf{f} = -\frac{1}{2}\rho_f \mathbf{C}\left(\mathbf{u}_\mathbf{b} - \mathbf{u}_\mathbf{f}\right)\left\|\mathbf{u}_\mathbf{b} - \mathbf{u}_\mathbf{f}\right\| + \frac{1}{2}\rho_f C_L A\left\|\mathbf{u}_\mathbf{b} - \mathbf{u}_\mathbf{f}\right\|^2 \mathbf{e}_z - \frac{1}{2}\rho_f C_D A_z\left(\mathbf{u}_{\mathbf{b},z}\right)\left\|\mathbf{u}_{\mathbf{b},z}\right\|\mathbf{e}_z \tag{4}$$

where $\boldsymbol{u_f} = [\, u_{f,x},\, u_{f,y},\, 0\,]^{\mathrm{T}}$ denotes a vector containing the components of the fluid velocity, assumed horizontal, $\mathbf{e}_z$ a unit vector along the vertical direction, $C_D A_z$ is the drag area in the horizontal plane, considered here as twice the one in the xy plane to be conservative as we don't know its value and $\mathbf{C}$ is a second-order tensor evaluated as follows:

$$\begin{aligned}\mathbf{C} &= \begin{pmatrix}\cos\theta & -\sin\theta & 0\\ \sin\theta & \cos\theta & 0\\ 0 & 0 & 1\end{pmatrix}\begin{pmatrix}C_D A & C_S A & 0\\ C_S A & C_D A & 0\\ 0 & 0 & 0\end{pmatrix}\begin{pmatrix}\cos\theta & \sin\theta & 0\\ -\sin\theta & \cos\theta & 0\\ 0 & 0 & 1\end{pmatrix}\\ &= \begin{pmatrix}C_D A - C_S A\sin(2\theta) & C_S A\cos(2\theta) & 0\\ C_S A\cos(2\theta) & C_D A + C_S A\sin(2\theta) & 0\\ 0 & 0 & 0\end{pmatrix}\end{aligned} \tag{5}$$

with θ the angle between the direction of the body-fluid relative velocity and the x axis, $C_D A$ the drag area, $C_S A$ the side area and $C_L A$ the lift area. The side coefficient was randomly set to a positive or negative sign at each time, and the magnitude of the corresponding force remains very small (Delhez et al., 2024).
The drag, side and lift areas ($C_D A$, $C_S A$ and $C_L A$) were used here instead of the corresponding coefficients (C_D, C_S and C_L) because the former were directly measured in laboratory experiments conducted by Delhez et al. (2024) using a human-like dummy in a typical drowning position. This approach avoids the need to estimate a frontal area for each considered body. To estimate the values of $C_D A$, $C_S A$ and $C_L A$ for a given real body from the known values for the dummy, the ratio of the total body surface areas (BSA) was used as a scaling factor. The BSA of the dummy (2.46 m²) was known from Delhez et al. (2024), while the BSA of a particular body can be estimated from body height, mass and sex using various empirical equations (Mosteller, 1987; Du Bois and Du Bois, 1989; Tanabe et al., 2000; Tikuisis et al., 2001). Here, we estimated the BSA

with Tikuisis et al. (2001) formula and then calculated the drag, side and lift areas from the corresponding values ($[\ldots]_{\text{dummy}}$) measured for the dummy (Delhez et al., 2024):

$$C_D A = \frac{BSA}{2.46}\left[C_D A\right]_{\text{dummy}},\ C_S A = \frac{BSA}{2.46}\left[C_S A\right]_{\text{dummy}} \text{ and } C_L A = \frac{BSA}{2.46}\left[C_L A\right]_{\text{dummy}}. \quad (6)$$

- the resultant $\mathbf{F_g}$ of gravity and buoyancy forces,

$$\mathbf{F_g} = \mathbf{g}\left(m_t - \rho_f V_b\right) = \left[0,\quad 0,\quad -g\left(m_t - \rho_f V_b\right)\right]^T, \quad (7)$$

where $\mathbf{g}$ is the gravity acceleration vector $[\ 0,\ 0,\ -g\ ]^T$;

- the added mass force linked to flow non-uniformity and unsteadiness, $\mathbf{F_A}$,

$$\mathbf{F_A} = \left(1 + C_A\right)\rho_f V_b \frac{D\mathbf{u_f}}{Dt} \quad (8)$$

which involves the material derivative of the flow velocity, $D\mathbf{u_f}/Dt = \partial\mathbf{u_f}/\partial t + \mathbf{u_f} \bullet \nabla\ \mathbf{u_f}$;

- and the friction force $\mathbf{F_b}$ induced by the river bottom.

The components of the friction force $\mathbf{F_b}$ between the body and the river bottom were estimated by means of a Coulomb formulation:

$$\begin{pmatrix} F_{b,x} \\ F_{b,y} \\ F_{b,z} \end{pmatrix} = -\mu \max(N;0)\,\gamma\left(z_b - Z_b\left(x_b, y_b\right)\right)\frac{1}{\sqrt{u_{b,x}^2 + u_{b,y}^2}}\begin{pmatrix} u_{b,x} \\ u_{b,y} \\ 0 \end{pmatrix} \quad (9)$$

Where μ is the friction coefficient (value given in Table S5 in Supporting Information), Z_b denotes the bottom elevation and N is the vertical component of the forces acting on the body, i.e., the reaction force of the resultant of the gravity, buoyancy, and lift force induced by the horizontal flow. In line with Delhez et al. (2023), function $\gamma(z_b - Z_b)$ is a "shape function" ensuring that F_b becomes non-negligible only when the body is positioned close to the bottom. The exact formulation used for function $\gamma(z_b - Z_b)$ is given in Supporting Information S2. The force $\mathbf{F_b}$ is aligned with the body velocity and acts in the opposite direction. When the body is at rest, the force $\mathbf{F_b}$ acts in the direction opposite to the resultant of the other forces. Our implementation ensures that the friction force does not induce body motion but resists the forces driving the body.

4.2.2 Mechanical effects of body decomposition

The body volume V_b is composed of three components: a fixed solid volume V_s, representing bones and flesh, a variable gaseous volume V_g, and a volume V_c accounting for air or water trapped beneath or within the clothing. The incompressible volume V_s and the volume of clothing V_c are assumed time-independent. The gaseous volume evolves with body decomposition, water temperature and hydrostatic pressure acting on the body. The evaluation of each of these volume components and their evolution in time is detailed in Supporting Information S4 and summarized hereafter as well as in the flowchart in Figure 7 (in Supporting Information S4).

Initial value of body volume

First, the initial body volume $V_b(0)$ is estimated by means of empirical equations developed by Meeuwsen et al. (2010) and Siri (1956a, 1956b). These equations use as inputs the victim sex, age and BMI. An intermediate quantity for the estimation of the body volume $V_b(0)$ is the percentage of fat. To reflect the variability in human body (Nickerson et al., 2018, 2020), we added a stochastic contribution ε_{fat} to the value of the percentage of fat estimated from empirical equations (see Section a in Supporting Information S4). The modelling of ε_{fat} depends on the age and sex of the victim, as detailed in Section 6.

Clothing volume and total initial volume

The clothing volume V_c is estimated based on observations by Barwood et al. (2011) who measured the buoyancy force of persons either remaining still or moving in water (see Section b in Supporting Information S4). Here, we assume that in the case of cold water ($T_w < 15$°C), the victim has not moved after being immerged (cold shock), and vice-versa for water temperatures greater or equal to 15°C (Farstad and Dunn, 2019). The corresponding clothing volumes, V_{c1} and V_{c2}, and their associated uncertainties are modelled as detailed in Section 6.

Initial gaseous volume

The initial gaseous volume $V_g(0)$ is assumed equal to the functional residual capacity (FRC) of the lungs. In line with Delhez et al. (2023), FRC is calculated by combining an empirical equation proposed by Stocks and Quanjer (1995) and an analysis by Abston et al. (2017), which consider as inputs the victim height, BMI and age (see Section c in Supporting Information S4). The incompressible volume V_s is taken equal to the difference $V_b(0) - V_g(0)$.

Evolution of gaseous volume

Four steps are followed to model the evolution of the gaseous volume V_g in the body (see Section d in Supporting Information S4). In Step 1, an assumption is formulated on the ultimate gaseous volume (i.e., the value reached when body bloating can no longer progress) under "standard" conditions, i.e., at atmospheric pressure. We assume that, in such conditions, the maximum gaseous volume equals twice the total lung capacity (TLC), which accounts for both torso and belly bloating, TLC is calculated here with the same empirical equations as those used by Delhez et al. (2023), considering the victim height, sex and BMI as inputs.

In Step 2, an ideal gas law is used to account for the influence of the body temperature T_b and pressure. It is utilized to compute an initial gas quantity n_0 by considering V_g = FRC, the atmospheric pressure and a temperature of 37°C. Similarly, an ultimate quantity n_1 of gas is evaluated by considering $V_g = 2$ TLC, the atmospheric pressure and the water temperature T_w. Step 3 consists in updating the body temperature T_b as a function of its initial value and the value of water temperature T_w. We assume a simple exponential decay of body temperature:

$$T_b = T_w + \left(T_{b,ini} - T_w\right) e^{-\frac{t}{\tau}} \tag{10}$$

with t the elapsed time in seconds and τ a characteristic time assumed equal to 3000 s.

In Step 4, the evolution of the number of gaseous particles n is calculated based on the formulation proposed by Delhez et al. (2023):

$$n = n_0 + \eta(n_1 - n_0) \tag{11}$$

$$\eta\left(\frac{\alpha}{\alpha_1}\right) = \min\left[6\left(\frac{\alpha}{\alpha_1}\right)^5 - 15\left(\frac{\alpha}{\alpha_1}\right)^4 + 10\left(\frac{\alpha}{\alpha_1}\right)^3 ; 1\right] \tag{12}$$

with α the current value of ADD and α_1 the ADD value reached when the body can no longer expand. Formally, ADD is calculated as follows:

$$\alpha = \int_0^t T_w \, dt \tag{13}$$

The value of α_1 is estimated as a function of water temperature T_w, consistently with observations suggesting that the value of ADD reached when the body resurfaces are lower when water temperature is higher (see Section d in Supporting Information S4).

The gaseous volume V_g can then be calculated as follows:

$$V_g = \frac{nRT_b}{p_{atm} + \rho_w g h_w} \tag{14}$$

with n given by Eqs. (11)-(12), T_b by Eq. (10), g is the gravity acceleration and h_w the vertical distance between the body and the water surface. This equation allows the gaseous volume to be smaller than FRC when the hydrostatic pressure is high enough, i.e. in deep areas, leading to cases where the victim body never resurfaces.

4.3 Numerical discretization

The mathematical model presented in Section 4.2 was discretized in time using a second-order two-step Runge-Kutta algorithm. The time integration scheme is written out in full in Supporting Information S3b. An adaptive time step was used to ensure stability of the computations. Its value was set as follows:

$$\Delta t = \max\left[\min\left(\frac{\xi \Delta x}{\|\boldsymbol{u}_f\|}, \Delta t_{\max}\right), \Delta t_{\min}\right] \tag{15}$$

with ξ a parameter similar to a CFL number, set here at 0.01, $\Delta t_{\min}$ = 0.01 s and $\Delta t_{\max}$ = 1 s.

4.4 Collisions

The fluid velocity $\boldsymbol{u_f}$ is defined over a domain denoted Ω. When the computed position of the centre of mass of a body at the end of a time step is positioned outside the domain Ω (e.g., body positioned on a riverbank), a correction is applied on the values of body position and velocity. The location of the body centre of mass is set on the domain boundary (i.e., the edge of a computation cell of the Eulerian model), and the body velocity is adjusted by assuming an elastic collision with the domain boundary. A sketch representing a collision can be found in Supporting Information S5. The sign of the velocity component normal to the wall is reversed and the magnitude of this velocity component is reduced to a fraction e of its approach value, where e is a restitution coefficient (equal here to 0.1, as mentioned in Table S5 in Supporting Information):

$$\boldsymbol{u_b} = \tilde{\boldsymbol{u}}_b - (1+e)\left(\tilde{\boldsymbol{u}}_b \cdot \boldsymbol{n}\right)\boldsymbol{n} \tag{16}$$

with $\tilde{\boldsymbol{u}}_b$ the body velocity before correction and $\boldsymbol{n}$ the unit vector normal to the wall.

5 Coupling between Eulerian and Lagrangian models

The Eulerian flow model depicted in Section 3 provides values of water depth, as well as depth-averaged, mean (i.e., Reynolds-averaged) flow velocities at the cell centres of a Cartesian grid, at an hourly time step. This contrasts with the continuous and instantaneous flow field necessary as an input for running the 3D Lagrangian model introduced in Section 4. Therefore, the following four operations were conducted for transforming the outputs of the Eulerian flow model into suitable inputs for the 3D Lagrangian model.

- First, a bilinear interpolation was used to evaluate the flow depth H and the depth-averaged mean flow velocity components $[\,U, V\,]^{\mathrm{T}}$ at any location (x, y), from the outcomes of the Eulerian flow model available at discrete positions (x_i, y_j) corresponding to cell centres. This operation is detailed in Supporting Information S6.
- Second, a linear interpolation in time was performed to estimate the flow depth H and the depth-averaged mean flow velocity $[\,U, V\,]^{\mathrm{T}}$ at any time t from the simulation results of the Eulerian model which were stored at an hourly time step.
- The depth-averaged mean flow velocity components computed by the 2D Eulerian model were used to approximate the components $\overline{u}_{f,x}$ and $\overline{u}_{f,y}$ of the mean fluid velocity at any depth in the fluid layer by assuming a logarithmic profile over the flow depth:

$$\overline{u}_{f,x}(x,y,z) = \frac{u_*}{\kappa}\ln\left(\frac{z}{z_0}\right)\frac{U(x,y)}{\sqrt{U^2+V^2}} = \frac{U(x,y)}{\kappa}\frac{n\sqrt{g}}{H^{1/6}}\ln\left(\frac{z}{z_0}\right) \tag{17}$$

$$\overline{u}_{f,y}(x,y,z) = \frac{u_*}{\kappa}\ln\left(\frac{z}{z_0}\right)\frac{V(x,y)}{\sqrt{U^2+V^2}} = \frac{V(x,y)}{\kappa}\frac{n\sqrt{g}}{H^{1/6}}\ln\left(\frac{z}{z_0}\right) \tag{18}$$

  with n the Manning coefficient, u_* the shear velocity, κ the von Kármán constant ($\kappa \approx 0.41$) and z_0 the zero-velocity level above the bed, set here to 0.0027 m.
- Instantaneous flow velocity values ($u_{f,x}$, $u_{f,y}$) were estimated from the mean flow velocity components $\overline{u}_{f,x}$ and $\overline{u}_{f,y}$ by adding a random fluctuation, the magnitude of which is controlled by a turbulence rate $\grave{o}_f$ and a random variable λ following a standard normal distribution (Garcia et al., 2013; McDonald and Nelson, 2021; Li et al., 2023; Nelson et al., 2023):

$$u_{f,x}(z) = \overline{u}_{f,x}(z)\left(1+\grave{o}_f\lambda_x\right). \tag{19}$$

$$u_{f,y}(z) = \overline{u}_{f,y}(z)\left(1+\grave{o}_f\lambda_y\right) \tag{20}$$

6 Stochastic framework

To account for the considerable uncertainties affecting input data (such as body volume, body mass, and decomposition kinetics) as well as some model parameters, the model described in Section 4.2 was implemented within a stochastic framework using a Monte Carlo method

(Metropolis and Ulam, 1949). The uncertainties affecting input data and model parameters were represented through statistical distributions, adjusted to available field information.

All assumed distributions for input data and their parameters are detailed in Table S3 in Supporting Information S7. The considered types of distributions include a Bernoulli distribution (for the victim sex if it were unknown), a discrete uniform distribution (for the victim age if it were unknown), beta distributions (for continuous quantities varying in a predefined range, such as body height, mass and BMI), and a generalized Bernoulli distribution (for a categorical variable such as the type of clothing)

For body height, mass and BMI, when a field value is available (e.g., from forensic medicine reports or media reports), the quantity is still handled stochastically to account for assumed uncertainties in reported values (e.g., ± 2.5 cm for body height, ± 1 for BMI ± 2.5 kg for body mass). When no field information is available for these quantities, distributions characterizing the whole Belgian population were used (Van Der Heyden et al., 2018).

Similarly, several model parameters (V_c, dm, m, δ, λ_x and λ_y) were handled stochastically, based on the assumed statistical distributions detailed in Table S4 in Supporting Information S7. For others, fixed values were considered in the current model (Table S5 in Supporting Information S7).

Finally, an uncertainty was considered on the initial body position. The initial position used in the model runs was determined by adding stochastic disturbances to the coordinates of the reported drowning point (Table 1). These disturbances were applied independently along the x and y directions, and their magnitude was assumed to be uniformly distributed between – 15 m and + 15 m.

7 Results and discussion

7.1 Types of body trajectories

In the computational results, three types of body trajectories can be distinguished, depending on whether the body remains at the surface, reaches the bottom and resurfaces, or sinks to the bottom and remains there. The type of body trajectory has a substantial effect on the horizontal travelled distance due to the potentially large difference in horizontal drift velocity between a body situated at the surface and a body in contact with the bottom. The latter is subject to lower flow velocities and to the solid-solid friction on the riverbed.

For each drowning case, the partition of the Monte Carlo runs between the three types of body trajectories is shown in Figure 4. The displayed partitions are based on the computational results at the time corresponding to the reported submersion interval (Table 1), i.e., at the time when the real body was recovered at the surface. There is a considerable difference in these partitions between the seven considered drowning cases.

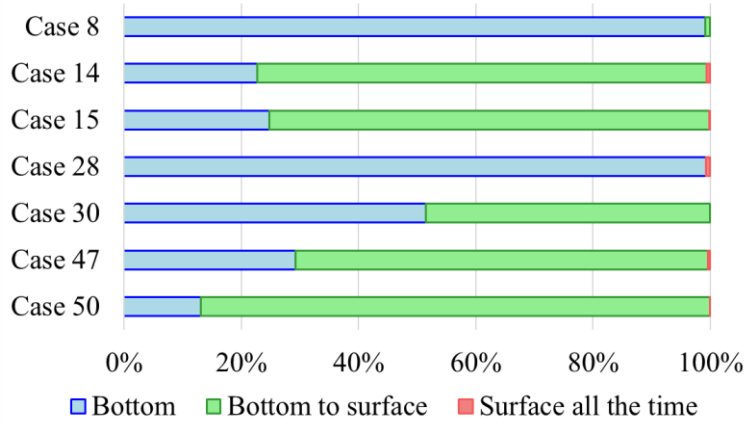

Figure 4: Partition between model runs in which the body remains at the surface (■), in which the body reaches the bottom and then resurfaces after a time less than or equal to the reported submersion interval (■), and in which the body is predicted to be on the river bottom at the time corresponding to the reported submersion interval (■).

In all cases, the share of model runs predicting that the body remains at the surface (■) is less than 1%, because the computed initial body density is typically 5% greater than the density of water.

For most drowning cases (i.e., Cases 14, 15, 47 and 50), the portion of Monte Carlo runs where the body sank and resurfaced at the reported submersion interval is between about 67% and almost 90%. This type of trajectory is consistent with the field observations since the body was recovered at the surface in all considered cases.

In Case 30, the portion of model runs predicting that the body is on the bottom at the end of the reported submersion interval slightly exceeds 50%. This higher value compared to the other cases can be explained by the combination of a relatively low water temperature (9.2°C) and a limited submersion interval (Table 1), leading to a comparatively low ratio α / α_1 in Eq. (12), so that in the computations the body decomposition at the end of the reported submersion interval is less advanced in this case than in the Cases 14, 15, 47 and 50.

Cases 8 and 28 lead to more than 99% of the model runs predicting that the body is still at the bottom at the end of the reported submersion interval, which contradicts the field reports. For Case 8, this computational result is explained by the presence of 10 kg of weights in a backpack tight to the body (Section 2.2), leading to a higher effective density. The real body was recovered at the surface almost five days after the drowning, indicating that in reality the decomposition of the body was sufficiently advanced to compensate for the extra weight attached to the body. Here, the model seems to underestimate the extent to which decomposition influences buoyancy. To test the sensitivity of the results, simulations were also carried out in which the 10 kg weights were neglected. These resulted in about half of the model runs predicting that the body is at the surface at the end of the reported submersion interval, highlighting the large influence of considering accessories or objects attached to the victim's body. For Case 28, the short submersion interval (6 hours) explains why, in the computations, the decomposition of the body has hardly started (ratio $\alpha / \alpha_1 << 1$) and therefore most model runs predict that the body has not resurfaced. Again, the model appears to underestimate the rate of body decomposition and/or the magnitude of the effect of body decomposition on buoyancy as well as the initial buoyancy.

7.2 Horizontal travelled distance and submersion interval

For each drowning case, Figure 5 compares the simulated horizontal travelled distance to the reported travelled distance at the end of the reported submersion interval. The reference travelled distance is taken equal to the streamwise distance between the reported drowning and recovery points (Figure 1). The results of the simulations are presented in the form of boxplots reflecting the variability of the results across the Monte Carlo runs. In Figure 5a, a single boxplot is used to communicate the model results for a given drowning case, while in Figure 5b, three boxplots are used to highlight the distributions corresponding to each of the three types of body trajectories (Section 7.1).

A distinctive pattern appears in the results depending on the range of river discharge, which controls whether a body moves considerably faster when it is at the surface (lower range of discharge) or regardless of whether it is at the bottom or at the surface (higher range of discharge).

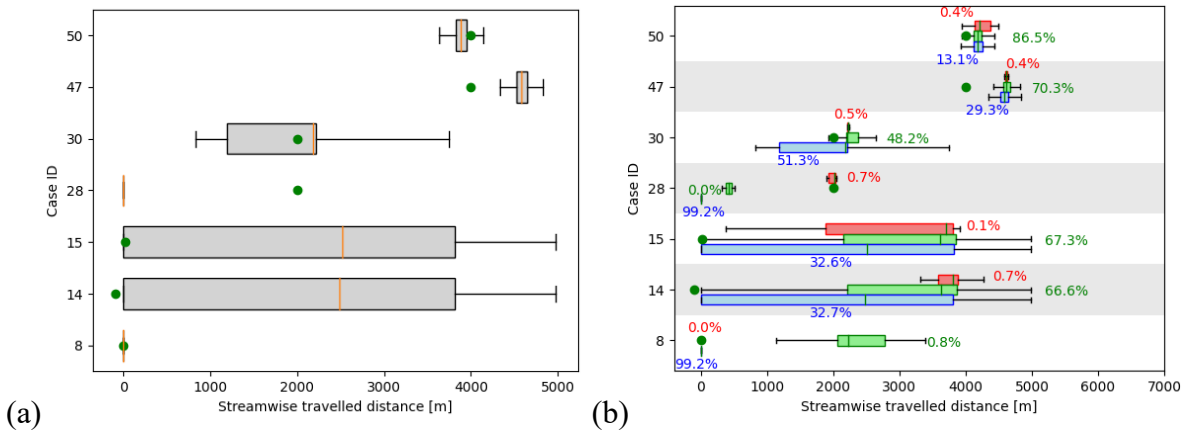

Figure 5: Reported (●) and computed distance travelled by the body at the reported moment of body recovery. The model results are displayed in the form of boxplots, reflecting the variability of the results across the Monte Carlo runs. (a) A single boxplot is used for each drowning case and each boxplot extending from the first quartile to the third one, with whiskers going from the box to the furthest data lying within 1.5 times the width of the box.

(b) A different boxplot is used to display the runs in which the body is found to remain at the surface (■), those which predict that at some point the body reaches the river bottom but resurface (■) and those who reached the river bottom but not resurfaced yet (■).

7.2.1 Low river discharge (Cases 8 and 28)

For Cases 8 and 28, the river discharge is particularly low (~ 10% of the annual mean, see Table 1 and Section 2.3.3). In both cases, the computations predict a very low probability of a significant horizontal motion, with more than 99% of the model runs indicating that the body sinks and remains on the riverbed (Figure 4), mostly immobile due to the relatively low river discharge encountered in these cases (Table 1). A close examination of the forces acting on the body in these computations reveals that the Coulomb friction force can exceed the hydrodynamic forces by more than one order of magnitude (Figure S13a in Supporting Information S10). The added mass force due to flow non-uniformity and unsteadiness is about two orders of magnitude lower than the hydrodynamic forces, and could thus be neglected.

For Case 8, the predicted travelled distance appears to be in perfect agreement with the field observations (Figure 1 and Table 1). Nonetheless, the model does not predict the correct type of trajectory. Hence, the reason why the body did not drift is different between the reality and in most of the model runs (body remaining on the riverbed). In reality, the body did not drift when it resurfaced because it had become entangled between a ship and a quay, while in the model the body remains immobile due to low flow velocity (Figure S11a in Supporting Information S8), particularly at the river bottom (in line with Eqs. (17) and (18)).

For Case 28, the field observations indicate a travelled distance of about 2 km. The model incorrectly predicts that the body has a very high probability of sinking and remaining on the riverbed; but the small portion (< 1%) of model runs leading to the body drifting at the surface predict a travelled distance in good agreement with the reported one (Figure 8a and Figure 8b). This hints at a strong dependence of the model outcomes on the estimation of the body density (based on empirical closures), which controls the vertical motion of the body and hence the type of body trajectory. Indeed, only the few model runs that predict a body trajectory at the surface also predict the distance travelled by the body well.

7.2.2 Intermediate river discharge (Cases 14 and 15)

Case 14 and Case 15 correspond to a river discharge close to the annual mean (Table 1 and Section 2.3.3), and they both lead to similar computational results, as can be seen in Figure 5b. In both cases, most of the model runs (~ 67%) predict that the body is at the surface at the end of the reported submersion time, with a median travelled distance of almost 4 km (Figure 8a and Figure 8b). This predicted distance does not agree with the information provided by the field reports, which indicate that the bodies moved over a limited distance (~ 0.25 km). As these bodies were found in a busy part of the centre of the city of Liège (Figure 1), it is likely that the actual bodies were quickly recovered after resurfacing and before they could be drifted by the flow. As shown in Figure 7a and Figure 7b, the computed resurfacing time in Cases 14 and 15 is generally underestimated compared to the reported value. This also explains why the model tends to overpredict the travelled distance. Indeed, an error in the computed resurfacing time may translate into a significant error in the travelled distance due to the considerable difference in body dynamics (in this range of river discharge) when the body is close to the bottom or when it has resurfaced (Figure S13 in Supporting Information S10). In the computations, when the body lies at the bottom, it has a lower chance of moving (as the hydrodynamic forces need to exceed the bottom friction) and, when it moves, it does so entrained by a lower flow velocity than when it is at the surface, as expressed by Eqs. (17) and (18). The influence of the body

resurfacing time on the body drift is reflected in the large variability in the predicted travelled distance for the model runs where the body has resurfaced (from no motion up to about 5 km, see Figure 8a and Figure 8b).

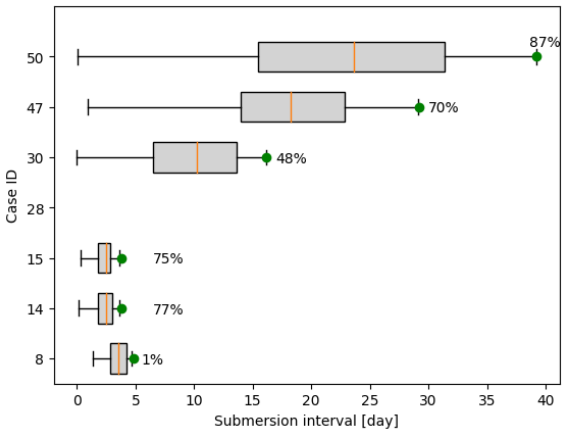

Figure 6: Reported submersion interval (●) and computed resurfacing time in the model runs predicting sinking and resurfacing of the body before the end of the reported submersion interval. The displayed percentages indicate the portion of all model runs corresponding to body sinking and resurfacing before the end of the reported submersion interval.

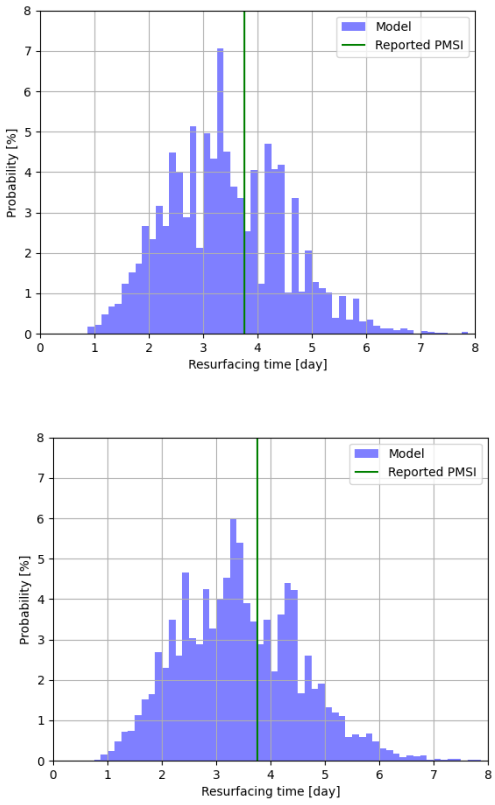

Figure 7: Distribution of computed resurfacing time in the model runs predicting sinking and resurfacing of the body for (a) Case 14 and (b) Case 15, based on simulations extending way beyond the reported submersion interval. The vertical line (|) corresponds to the end of the reported submersion interval.

Again, interactions with boats are also a possible explanation for the behaviour of the real bodies, especially for the upstream movement in Case 14 (Table 1). In the model runs which predict that the body is at the bottom of the river at the reported submersion time (32-33%), the computed distance travelled by the body is very small and appears in agreement with the reported values, but these predictions remain nonetheless unsatisfactory since the actual bodies were recovered at the surface and not on the bottom.

Figure S13b in Supporting Information S10 represents the evolution of the forces acting in one model run corresponding to Case 14 or 15. Up to the computed resurfacing time in this model run (~ 54 h), the magnitude of the friction force at the bottom can be high enough compared to the hydrodynamic forces to prevent the body from moving on the bottom. Due to the low flow velocities in this range of river discharge, the forces induced by the flow are extremely weak and can be considered negligible. Body decomposition induces bloating of the body and hence an increase in its buoyancy, leading in turn to a gradual decrease of the bottom friction force, until the moment when the body leaves the bottom and resurfaces (after approximately 54 hours). Its drift is then controlled by the hydrodynamic forces. Again, the added mass force remains in general two orders of magnitude lower than the hydrodynamic forces.

7.2.3 High river discharge (Cases 30, 47 and 50)

Unlike in the cases discussed above, in Cases 30, 47 and 50, the model runs predict a substantial motion of the body regardless of whether it remains at the surface, sinks and resurfaces, or sinks and remains at the bottom. This is visible in Figure 8a and b as well as in Figure 8c and d. It may be attributed to the higher flow rates in the river at the time when these drowning cases occurred, with discharge values two to almost four times higher than in Cases 14 and 15 (Table 1). These higher values of discharge translate into flow velocities about an order of magnitude larger in Cases 30, 47 and 50 (Figure 9c and d) than in Cases 14 and 15 (Figure 9a). As shown in Table 1, another important feature of drowning Cases 30, 47 and 50 is the water temperature, which ranges between 7 and 9°C, considerably lower than in all the other cases (20-23°C). This leads to a slower decomposition of the body in water and therefore a longer submersion interval (between 16 and 40 days, compared to a maximum of four days in any of the other cases).

In Case 30, almost half of the model runs predict that the body has resurfaced at the end of the reported submersion interval, with a median travelled distance in close agreement with the reported value (2.3 km). The same applies for Cases 47 and 50, with an even greater proportion of model runs predicting that the body is at the surface at the end of the reported submersion interval (63% and 87%, respectively). The median travelled distances in Cases 47 and 50 are equal to, respectively, 4.6 and 4.2 km, to be compared to a reported travelled distance of about 4 km. The model predictions appear significantly more accurate in these cases involving higher flow rates. Nonetheless, this apparent good performance of the model is partly attributable to the Monsin weir (south-east branch) which acts as an obstacle attracting and blocking the body (Figure 8c and d, Figure 9c and d), both in reality and in the computations, hence making it easier to end up with a good match between computed and observed travelled distances. This aspect is also supported by Figure 6, which shows substantial underestimations of the body resurfacing time in Cases 30, 47 and 50, but nonetheless a close match between the computed and reported travelled distances.

Another area where the model runs frequently predict that the body remains is at the bifurcation between the Meuse river and the Albert canal (Figure 8c and d), particularly in Case 30 (in which the drowning point is very close to the left bank of the river). In some of these model runs, the body ends up slowly drifting towards the Albert canal (north-east branch), either at the bottom or after resurfacing. This result is consistent with the flow field, which shows a shear region between high flow velocity in the Meuse and almost still water in the Albert canal (north-

east branch, which is a dead end connected to the left bank of the river) as displayed in Figure 9c and d. Although not reported in the sample of observations available here, it seems plausible that a real body could remain trapped in such a shear region. This result underscores the value of examining the flow fields for guiding search and rescue operations in practice. This approach is similar to the identification of hot spots by Gonzalez et al. (2022) for locating human remains in rivers when the point and time of origin are unknown.

Figure S13d-f (in Supporting Information S10) show that in drowning Cases 30, 47 and 50, the friction force at the bottom is not high enough to prevent body motion when the body is at the bottom, unlike in cases corresponding to a lower river discharge. The motion of the body at the bottom seems to adopt a velocity leading to a balance between the friction force and the hydrodynamic driving forces. Like in other cases, the added mass force is at least two orders of magnitude lower than the other forces. Body horizontal and vertical positions can also be found in Supporting information S11.

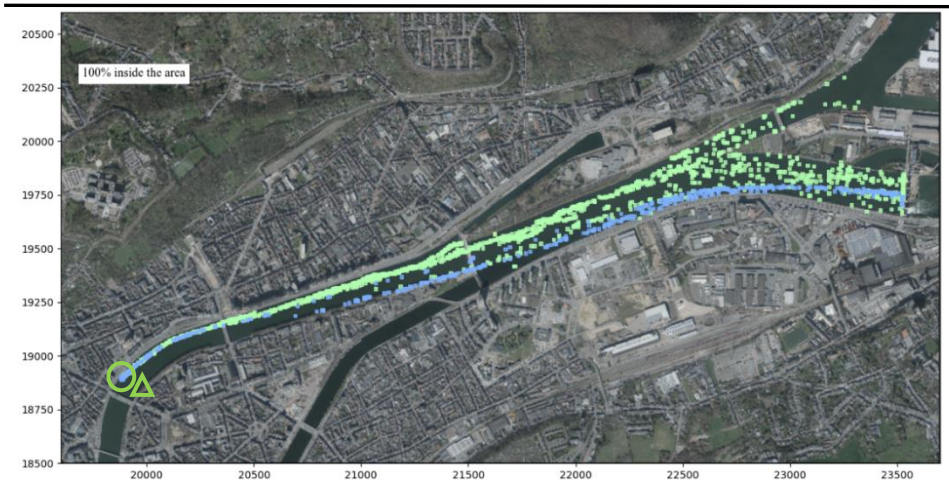

(a) Case 15 (similar pattern as in Case 14)

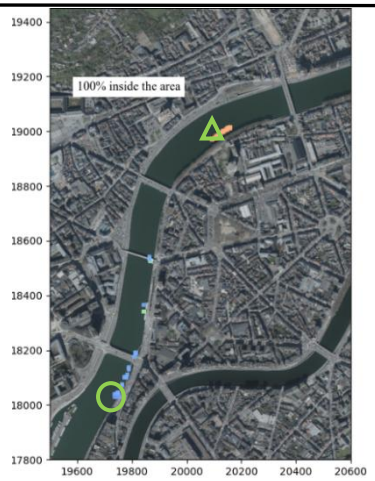

(b) Case 28

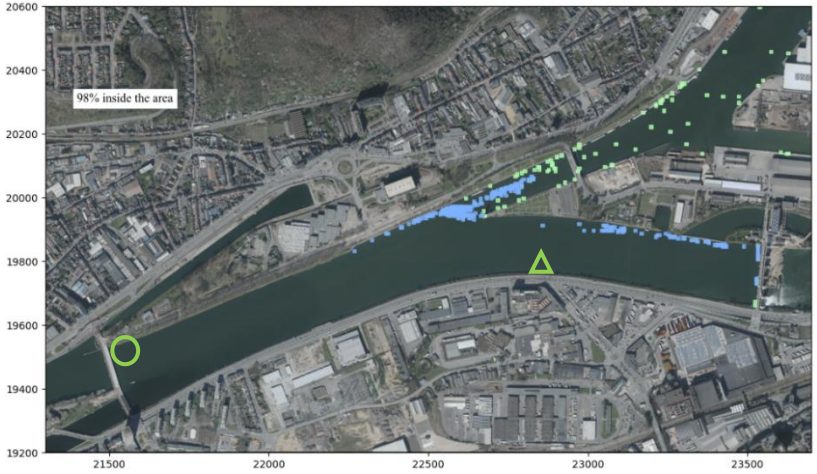

(c) Case 30

(d) Case 47 (similar pattern as in Case 50)

Figure 8: Computed body position in the various model runs (Monte Carlo simulations) at the time corresponding to the end of the reported body submersion interval (Table 1). Blue squares represent the body position in model runs predicting that the body is at the bottom of the river at the considered time, green squares represent the model runs in which the body initially sank but that have resurfaced, while orange dots refer to models runs predicting that the body remains at the surface. Green circles and triangles are the reported drowning and recovery locations, respectively. Corresponding maps for Cases 8, 14 and 50 can be found in Figure S11 in Supporting Information S8.

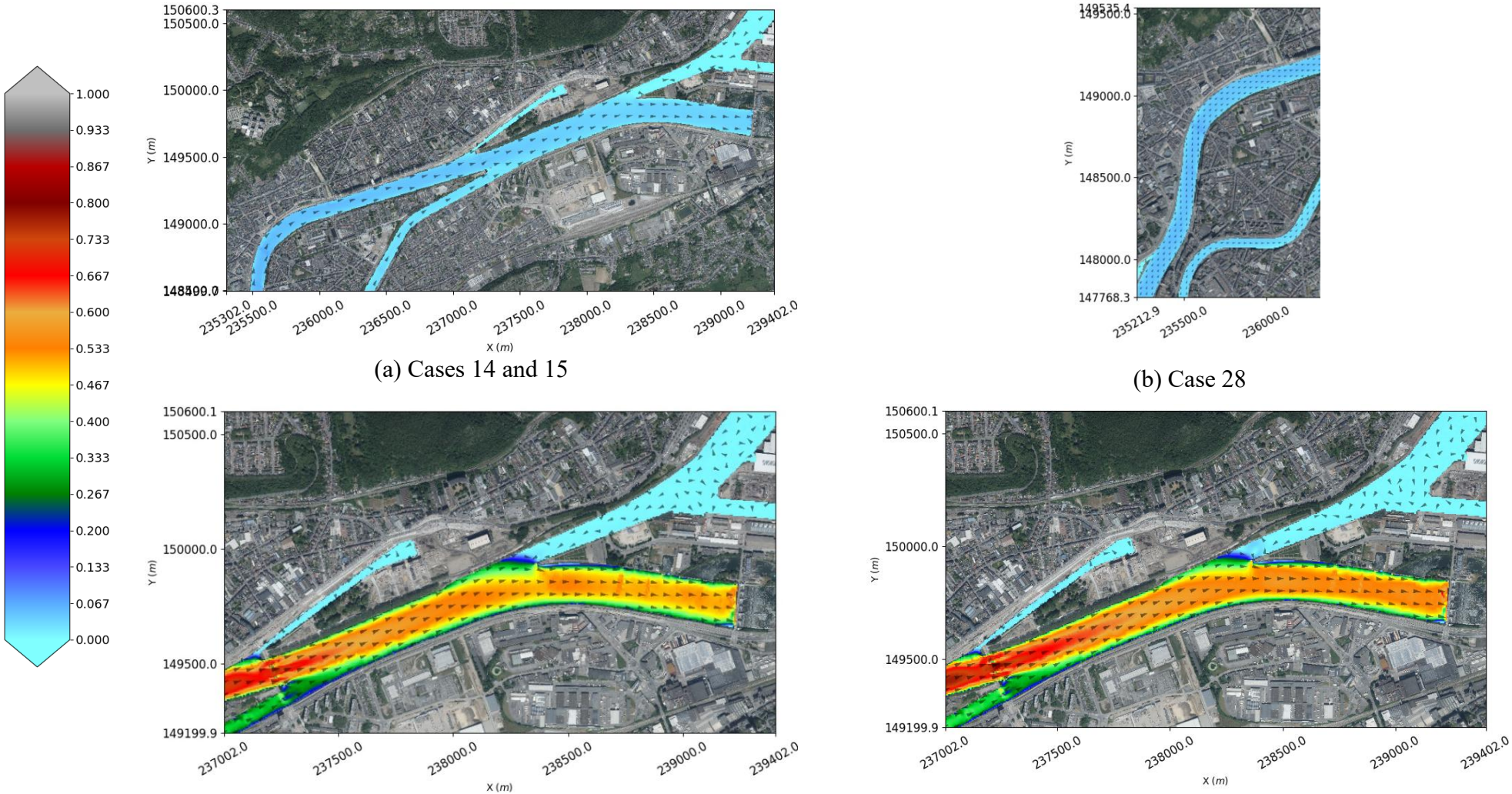

(a) Cases 14 and 15

(b) Case 28

(c) Case 30

(d) Case 47

Figure 9: Flow direction and magnitude (m/s) of the depth-averaged flow velocity for (a) Cases 14 and 15 , (b) Case 28, (c) Case 30 and (d) Case 47 at the time corresponding to the respective reported submersion intervals. Corresponding maps for Cases 8 and 50 can be found in Figure S12 in Supporting Information S9.

7.3 Communication of the results

Communicating the simulation results in the form of computed travelled distance (Figure 5), submersion interval (or PMSI) or body position according to individual model runs (Figure 8) may be complemented by maps of probability of presence of the body more straightforward to interpret in the course of real search and rescue operations. Such maps can be plotted by means of kernel density estimation (KDE), a non-parametric technique applying a smoothing kernel (Gaussian) to discrete data points, therefore producing a continuous representation of the probability density function.

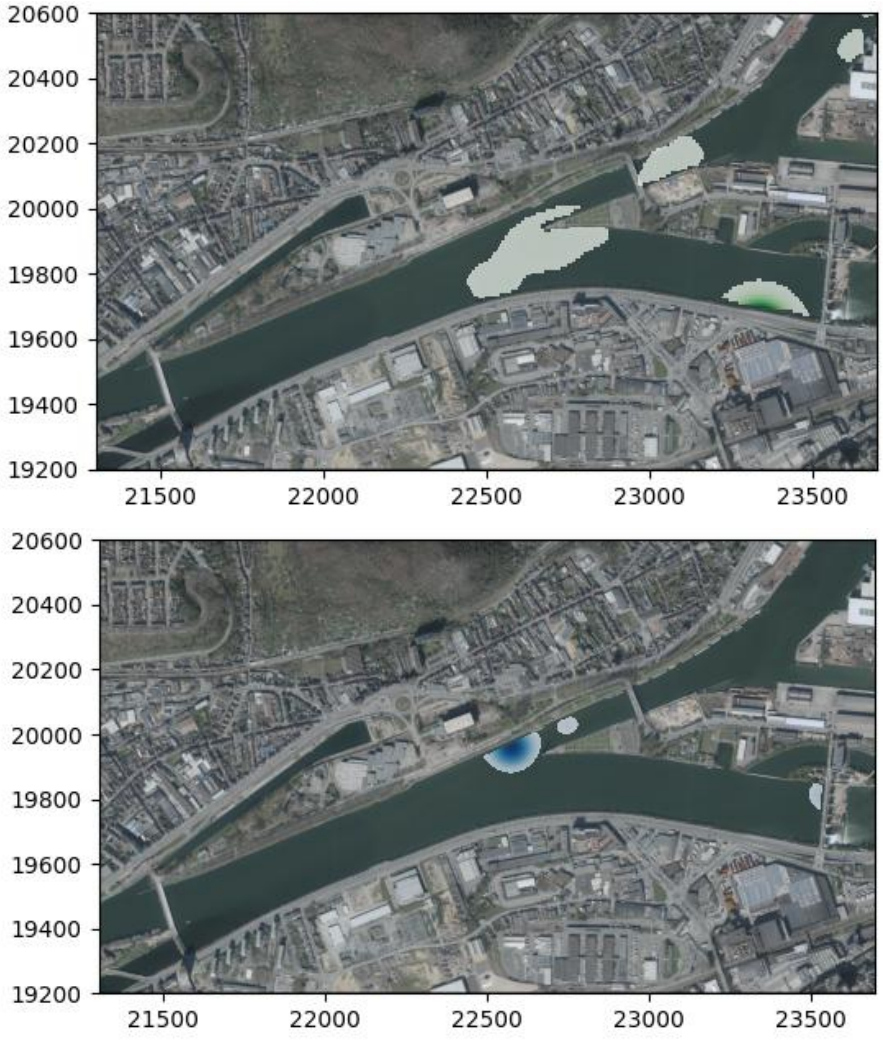

Figure 10: Map of the probability density of presence of the body (based on kernel density estimation) for drowning Case 30 at the time corresponding to the reported body submersion interval. (a) Map based on the model runs predicting that the body is at the surface. (b) Map based on the model runs predicting that the body is on the bottom.

Figure 1010 provides an example of such maps. The maps were clipped based on the extent of the simulation domain. Consistently with previous results (e.g., Figure 5b and Figure 8), the model runs predicting that the body lies at the bottom or is situated at the surface were treated separately. This is motivated by the operational objective of providing first-respondents with a probability density map of locations which should be explored underwater (by divers) and another one highlighting where the surface of the water should primarily be inspected. We believe that the rendering of Figure 1010 facilitates an intuitive understanding of the computational results for practical field use. The probability density maps in Figure 1010 are consistent with the results displayed in Figure 8 and the flow fields shown in Figure 9.

7.4 Comparison with the coastal and marine environments

The Lagrangian drift model presented here differs from those used in coastal and marine environments in two major respects: it is three-dimensional rather than two-dimensional, and body inertia is considered here. As shown in Figure 4, the vast majority of the model runs predict here that the victim body sinks in the first moments following the drowning. To the best of the authors' knowledge this sinking is overlooked in existing drift models used in coastal and marine environments, which are restricted to the two-dimensional body motion at the surface of the sea (Carniel et al., 2002; Mateus et al., 2015; Ličer et al., 2020). Therefore, the complex interactions between the body and the river bottom, involving the Coulomb friction force either slowing down or preventing body motion on the riverbed, is also ignored in existing models used in coastal and marine environments.

The results displayed in Figure S13 in Supporting Information S10 emphasize that the hydrodynamic forces (drag and, to a lesser extent, side and lift forces) are not negligible and, in many instances, their horizontal component is the dominating contribution to the force balance. This results from the rapid changes in the velocity field occurring over relatively short distances in an urban river, leading to a difference in the instantaneous velocity of the body and the surrounding flow velocity. These effects are also neglected in existing models for coastal and marine environments (Carniel et al., 2002; Mateus et al., 2015; Ličer et al., 2020), while our results demonstrate the relevance of considering these forces in the case of urban rivers.

8 Conclusion

For the first time, an Eulerian flow model has been coupled to a three-dimensional Lagrangian drift model to simulate the trajectory of the body of a victim of drowning in a real-world urban river. The model considers the effects of body decomposition on the body buoyancy, as a function of environmental factors such as water temperature and external pressure on the body. Monte Carlo simulations were performed to account for uncertainties in input data and model parameters. The model predictions were assessed against seven real cases of drowning for which the body was recovered at the surface and field information was available regarding the position and timing of drowning and recovery, the flow conditions, water temperature and some characteristics of the victim's body (age, sex, …).

In virtually all runs of the stochastic model, the body is predicted to sink shortly after drowning. The proportion of model runs predicting body resurfacing before the reported submersion interval varies greatly with the water temperature. The computed distances travelled by the body reveal distinct patterns depending on the river discharge. When the discharge is in a lower range, a body lying at the bottom of the river has a much lower chance of moving (as the hydrodynamic forces need to exceed the solid-solid friction between the body and the riverbed) and, when it moves, it is entrained by a low, near-bed flow velocity. This induces a significant difference between the drift velocity of a body situated close to the bottom and near the surface, therefore making the accurate prediction of the body buoyancy and resurfacing time a critical issue for improving the model performance. In the case of a drowning occurring when the river discharge is high, the difference in drift dynamics is reduced as, in this case, the flow velocity is high enough so that body moves regardless of whether it is close to the bottom or at the surface. In these cases, the model predictions appear in better agreement with the field observations, though the results are largely controlled by distinctive features in the flow fields (e.g., influence of hydraulic structures, or shear regions where the body remains trapped).

Results show that hydrodynamic forces are dominating in the force balance, while they were neglected in earlier studies focused on applications in coastal and marine environments. In contrast, the added mass force was negligible in all cases considered here. We finally showcase a synthetic representation of the model results in the form of maps of probability of body presence, either at the bottom or at the water surface. These visuals can be used to provide search and rescue teams with valuable information on locations to be prioritized for underwater search (by divers) and for inspection of the water surface. This simulation-based approach is novel in the field. It paves the way for more tactical planning of search and rescue operations, ultimately contributing to increase the chances of locating victims of a river drowning in a timely manner. Nonetheless, the model exercise here is pioneering in many aspects and, as such, limitations remain.

Overall, the model performance is limited as regard the prediction of the body resurfacing time. This stems from the challenging estimation of the rate of body decomposition and/or the magnitude of the effect of this decomposition on the body buoyancy. Both aspects are modelled mostly based on empirical closures, which need further verification and refinement (e.g., using larger sample sizes). The modelling of the frictional force between the body and the river bottom is another major source of uncertainty as it has a substantial influence on the body dynamics. Its representation should be improved based on tailored laboratory and/or in situ measurements.

The flow model used here assumes a two-dimensional flow and, in line with many operational approaches used in practice such as for inundation mapping, a turbulence closure is not included in the Eulerian model. This is a major limitation, particularly in the near-field of obstacles (e.g., bridge piers) and hydraulic structures (e.g., weirs). Coupling the Lagrangian drift model

presented here with the outcomes of more detailed flow field computations should be a priority for future research.

It would be highly valuable to test the model in real operational conditions to assess the added-value of the proposed modelling and implement improvements based on feedback collected from search and rescue staff. Engaging in such a close cooperation with first-respondents is critical to ensure that the simulation tool meets the practical needs and eventually contributes to improving the success rate of search and rescue operations for the sake of saving lives.

Acknowledgements

This work was supported by the LabEx IMU (ANR- 10-LABX-0088) of Université de Lyon and by l'Agence Nationale de la Recherche (ANR), project ANR-23-CE39-0012.

References

Barwood, M.J., Bates, V., Long, G., Tipton, M.J., 2011. Float First:“ Trapped Air Between Clothing Layers Significantly Improves Buoyancy on Water After Immersion. International Journal of Aquatic Research and Education 5.

Blondel, P., 2014. Searching for Dead Bodies with Sonar, in: Drowning. Springer-Verlag Berlin and Heidelberg GmbH & Co. K, New York, pp. 1161–1165.

Breivik, Ø., Allen, A.A., 2008. An operational search and rescue model for the Norwegian Sea and the North Sea. Journal of Marine Systems 69, 99–113.

Byard, R.W., 2018. Putrefaction: An Additional Complicating Factor in the Assessment of Freshwater Drownings in Rivers. Journal of Forensic Sciences 63, 899–901.

Carniel, S., Umgiesser, G., Sclavo, M., Kantha, L.H., Monti, S., 2002. Tracking the drift of a human body in the coastal ocean using numerical prediction models of the oceanic, atmospheric and wave conditions. Science & Justice: Journal of the Forensic Science Society 42, 143–151.

Conn, A.W., Miyasaka, K., Katayama, M., Fujita, M., Orima, H., Barker, G., Bohn, D., 1995. A canine study of cold water drowning in fresh versus salt water: Critical Care Medicine 23, 2029–2037.

Daalen, M.A. van, Kat, D.S. de, Oude Grotebevelsborg, B.F.L., Leeuwe, R. de, Warnaar, J., Oostra, R.J., M Duijst-Heesters, W.L.J., 2017. An Aquatic Decomposition Scoring Method to Potentially Predict the Postmortem Submersion Interval of Bodies Recovered from the North Sea. Journal of Forensic Sciences 62, 369–373.

Delhez, C., Andrianne, T., Erpicum, S., Riviere, N., Hallot, P., Pirotton, M., Archambeau, P., Dewals, B., 2024. Force coefficients for modelling the drift of a victim of river drowning. Natural Hazards.

Delhez, C., Rivière, N., Erpicum, S., Pirotton, M., Archambeau, P., Arnst, M., Bierens, J., Dewals, B., 2023. Drift of a Drowning Victim in Rivers: Conceptualization and Global Sensitivity Analysis Under Idealized Flow Conditions. Water Resources Research 59, e2022WR034358.

Dewals, B., Kitsikoudis, V., Angel Mejía-Morales, M., Archambeau, P., Mignot, E., Proust, S., Erpicum, S., Pirotton, M., Paquier, A., 2023. Can the 2D shallow water equations model flow intrusion into buildings during urban floods? Journal of Hydrology 619, 129231.

Du Bois, D., Du Bois, E.F., 1989. A formula to estimate the approximate surface area if height and weight be known. 1916. Nutrition (Burbank, Los Angeles County, Calif.) 5, 303–311; discussion 312–313.

Garcia, T., Jackson, P.R., Murphy, E.A., Valocchi, A.J., Garcia, M.H., 2013. Development of a Fluvial Egg Drift Simulator to evaluate the transport and dispersion of Asian carp eggs in rivers. Ecological Modelling 263, 211–222.

Gonzalez, J.R.P., Escobar-Vargas, J., Vargas-Luna, A., Castiblanco, S., Trujillo, D., Guatame, A.C., Corzo, G., Santos, G., Perez, L.A., 2022. Hydroinformatics tools and their potential in the search for missing persons in rivers. Forensic Science International 111478.

Gunduz, M., 2017. Possible recovery site of four non-recovered bodies lost in the Marmara Sea by using an ocean circulation model. Australian Journal of Forensic Sciences 49, 154–160.

Hart-Davis, M.G., Backeberg, B.C., 2023. Towards a particle trajectory modelling approach in support of South African search and rescue operations at sea. Journal of Operational Oceanography 16, 131–139.

Heaton, V., Lagden, A., Moffatt, C., Simmons, T., 2010. Predicting the Postmortem Submersion Interval for Human Remains Recovered from U.K. Waterways*. Journal of Forensic Sciences 55, 302–307.

Horn, K., 2014. Underwater Search and Evidence Response Teams, in: Drowning. Springer-Verlag Berlin and Heidelberg GmbH & Co. K, New York, pp. 1175–1177.

Kitsikoudis, V., Becker, B.P.J., Huismans, Y., Archambeau, P., Erpicum, S., Pirotton, M., Dewals, B., 2020. Discrepancies in Flood Modelling Approaches in Transboundary River Systems: Legacy of the Past or Well-grounded Choices? Water Resources Management 34, 3465–3478.

Li, G., Elliott, C.M., Call, B.C., Chapman, D.C., Jacobson, R.B., Wang, B., 2023. Evaluations of Lagrangian egg drift models: From a laboratory flume to large channelized rivers. Ecological Modelling 475, 110200.

Li, X., Dellinger, G., Erpicum, S., Chen, L., Yu, S., Guiot, L., Archambeau, P., Pirotton, M., Dewals, B., 2024. 2D and 3D Computational Modeling of Surface Flooding in Urbanized Floodplains: Modeling Performance for Various Building Layouts. Water Resources Research 60, e2023WR035149.

Ličer, M., Estival, S., Reyes-Suarez, C., Deponte, D., Fettich, A., 2020. Lagrangian modelling of a person lost at sea during the Adriatic scirocco storm of 29 October 2018. Natural Hazards and Earth System Sciences 20, 2335–2349.

Lunetta, P., Ebbesmeyer, C., Molenaar, J., 2014. Behaviour of Dead Bodies in Water, in: Drowning. Springer-Verlag Berlin and Heidelberg GmbH & Co. K, New York, pp. 1149–1152.

Mateus, M., Pablo, H. de, Vaz, N., 2013. An investigation on body displacement after two drowning accidents. Forensic Science International 229, 6–12.

Mateus, M., Pinto, L., Chambel-Leitão, P., 2015. Evaluating the predictive skills of ocean circulation models in tracking the drift of a human body: a case study. Australian Journal of Forensic Sciences 47, 322–331.

McDonald, R.R., Nelson, J.M., 2021. A Lagrangian particle-tracking approach to modelling larval drift in rivers. Journal of Ecohydraulics 6, 17–35.

Megyesi, M.S., Nawrocki, S.P., Haskell, N.H., 2005. Using accumulated degree-days to estimate the postmortem interval from decomposed human remains. Journal of forensic sciences 50, 618–626.

Metropolis, N., Ulam, S., 1949. The Monte Carlo Method. Journal of the American Statistical Association 44, 335–341.

Milanesi, L., Pilotti, M., Ranzi, R., 2015. A conceptual model of people's vulnerability to floods. Water Resources Research 51, 182–197.

Mosteller, R.D., 1987. Simplified calculation of body-surface area. The New England Journal of Medicine 317, 1098.

Musolino, G., Ahmadian, R., Xia, J., Falconer, R.A., 2020. Mapping the danger to life in flash flood events adopting a mechanics based methodology and planning evacuation routes. Journal of Flood Risk Management 13.

Nelson, J., Shimizu, Y., Kyuka, T., Charlton, S., 2023. A general Lagrangian tracking methodology for riverine flow and transport. Earth Surface Processes and Landforms 48, 87–103.

Nickerson, B.S., Esco, M.R., Bishop, P.A., Fedewa, M.V., Snarr, R.L., Kliszczewicz, B.M., Park, K.-S., 2018. Validity of BMI-Based Body Fat Equations in Men and Women: A 4-Compartment Model Comparison. Journal of Strength and Conditioning Research 32, 121–129.

Nickerson, B.S., McLester, C.N., McLester, J.R., Kliszczewicz, B.M., 2020. Relative accuracy of anthropometric-based body fat equations in males and females with varying BMI classifications. Clinical Nutrition ESPEN 35, 136–140.

Parks, R.M., Bennett, J.E., Tamura-Wicks, H., Kontis, V., Toumi, R., Danaei, G., Ezzati, M., 2020. Anomalously warm temperatures are associated with increased injury deaths. Nature Medicine 26, 65–70.

Ray, S., 2014. Training and Equipping Rescue Personnel for Flood Rescue, in: Bierens, J.J.L.M. (Ed.), DrowningPrevention,Rescue,Treatment. Springer, Berlin, Heidelberg, pp. 491–494.

Renardy, S., Takriet, A., Benitez, J.-P., Dierckx, A., Baeyens, R., Coeck, J., Pauwels, I.S., Mouton, A., Archambeau, P., Dewals, B., Pirotton, M., Erpicum, S., Ovidio, M., 2021. Trying to choose the less bad route: Individual migratory behaviour of Atlantic salmon smolts (Salmo salar L.) approaching a bifurcation between a hydropower station and a navigation canal. Ecological Engineering 169, 106304.

Ruffell, A., Pringle, J.K., Cassella, J.P., Morgan, R.M., Ferguson, M., Heaton, V.G., Hope, C., McKinley, J.M., 2017. The use of geoscience methods for aquatic forensic searches. Earth-Science Reviews 171, 323–337.

Simpkins, G., 2017. Increasing river flood risk. Nature Climate Change 7, 172–172.

Strom, M.A., Pasternack, G.B., Burman, S.G., Dahlke, H.E., Sandoval-Solis, S., 2017. Hydraulic hazard exposure of humans swept away in a whitewater river. Natural Hazards 88, 473–502.

Tanabe, S., Narita, C., Ozeki, Y., Konishi, M., 2000. Effective radiation area of human body calculated by a numerical simulation. Energy and Buildings 32, 205–215.

Tikuisis, P., Meunier, P., Jubenville, C., 2001. Human body surface area: measurement and prediction using three dimensional body scans. European Journal of Applied Physiology 85, 264–271.

Tipton, M.J., Golden, F.S.C., 2011. A proposed decision-making guide for the search, rescue and resuscitation of submersion (head under) victims based on expert opinion. Resuscitation 82, 819–824.

Tu, H., Wang, X., Mu, L., Xia, K., 2021. Predicting drift characteristics of persons-in-the-water in the South China Sea. Ocean Engineering 242, 110134.

Ung, A., 2014. Main results of the NOYADES survey carried out during summer 2018 in France 9.

Van Der Heyden, J., Nguyen, D., Renard, F., Scohy, A., Demarest, S., Drieskens, S., Gisle, L., 2018. Enquête de santé par examen belge.

WHO, 2014. Global report on drowning: preventing a leading killer.

Wu, J., Cheng, L., Chu, S., 2023. Modeling the leeway drift characteristics of persons-in-water at a sea-area scale in the seas of China. Ocean Engineering 270, 113444.

S1 Inflow hydrographs in the hydrodynamic simulation

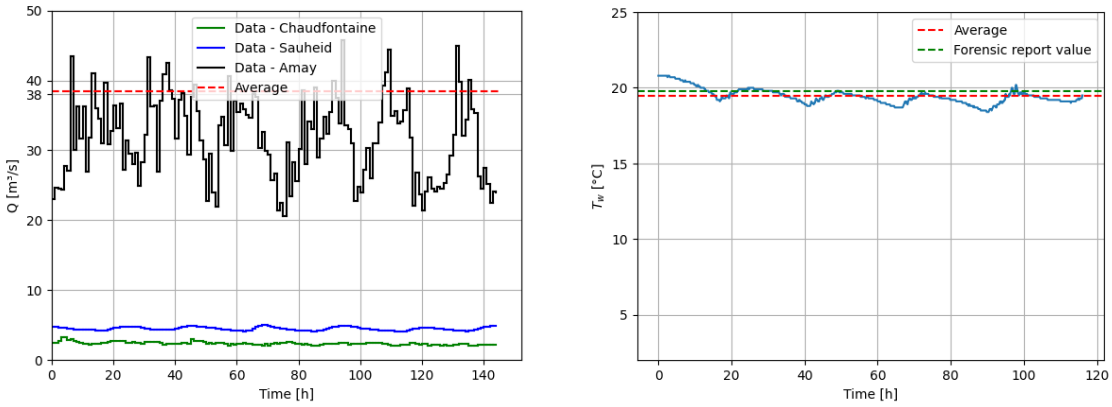

Figure S1: Inflow hydrograph and water temperature corresponding to Case 8.

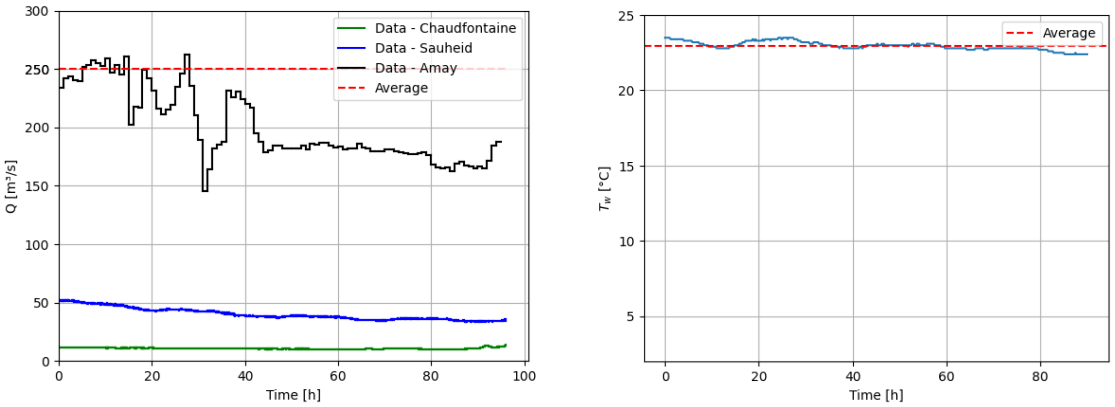

Figure S2: Inflow hydrograph and water temperature corresponding to Cases 14 and 15.

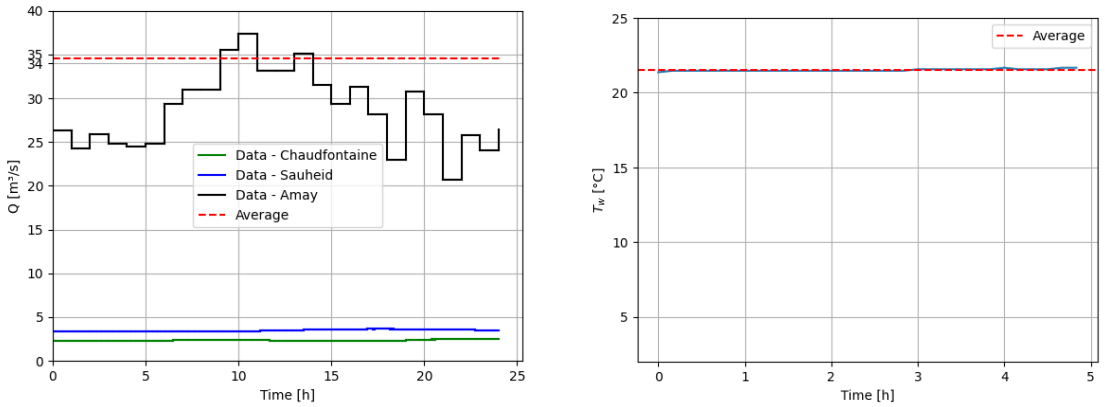

Figure S3: Inflow hydrograph and water temperature corresponding to Case 28.

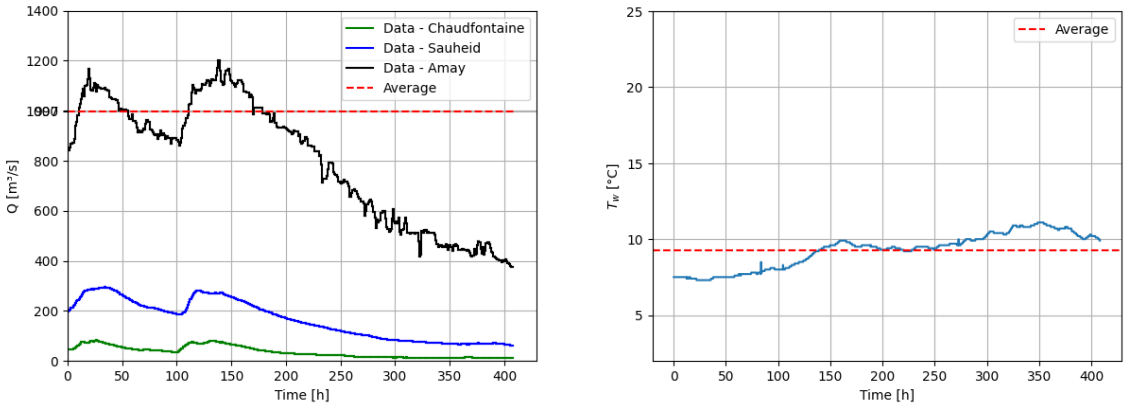

Figure S4: Inflow hydrograph and water temperature corresponding to Case 30.

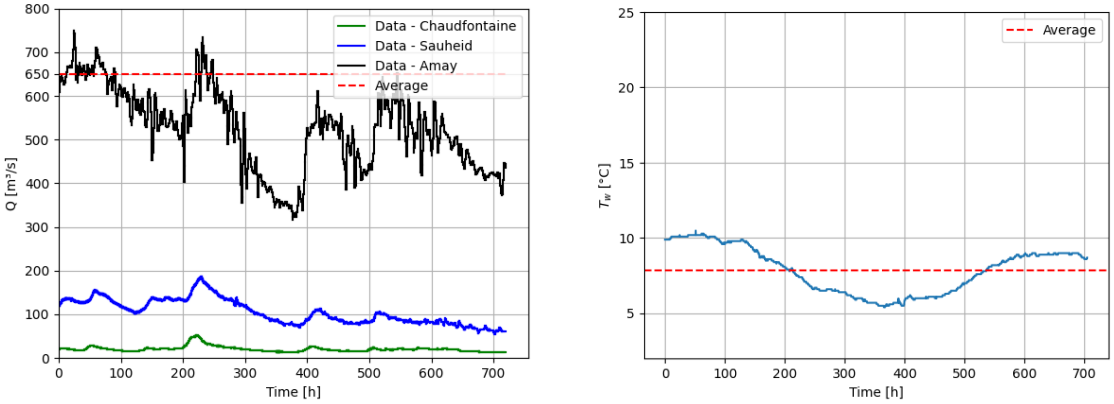

Figure S5: Inflow hydrograph and water temperature corresponding to Case 47.

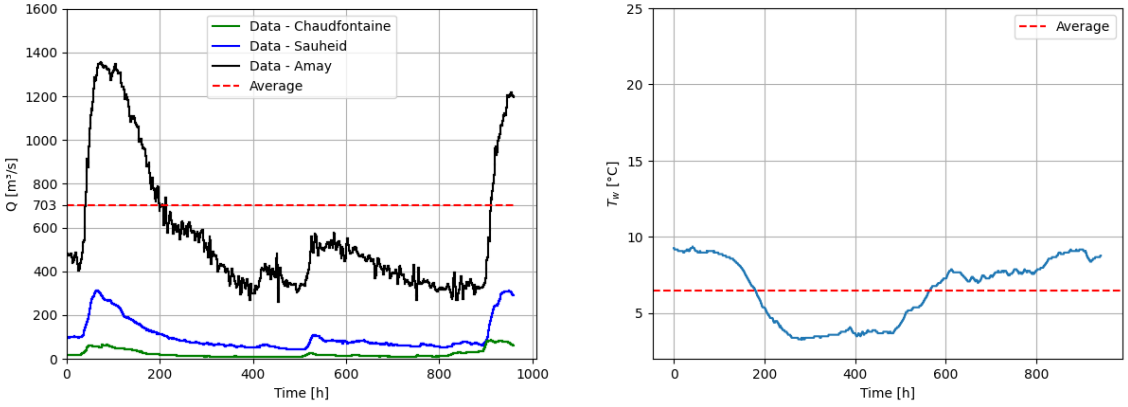

Figure S6: Inflow hydrograph and water temperature corresponding to Case 50.

S2 Formulation of the shape function □(zb – Zb)

Function $\gamma(z_b - Z_b)$ is parametrized as follows:

$$\gamma\left(z_b - Z_b\right) = \begin{cases} \dfrac{1 - \dfrac{z_b - Z_b\left(x_b, y_b\right)}{\varepsilon_{max}}}{1 - \dfrac{\varepsilon_{min}}{\varepsilon_{\max}}} & \text{if } Z_b\left(x_b, y_b\right) + \varepsilon_{min} \le z_b \le Z_b\left(x_b, y_b\right) + \varepsilon_{max} \\ 0 & \text{if } \; z_b \ge Z_b\left(x_b, y_b\right) + \varepsilon_{max} \end{cases} \quad \text{S(1)}$$

It is assumed that when the distance between the bottom and the body centre of mass exceeds a threshold ε_{max}, the bottom friction ceases to influence the body motion. The value of ε_{max} differs from that of ε_{min} typically due to limbs hanging down. The values of ε_{max} and ε_{min} were set here to 0.30 m and 0.15

The formulation of $\gamma(z_b - Z_b)$ was selected so that the effects of bottom friction on the body motion become significant only when the body is located close to the bottom, i.e., when the elevation z_b of the body centroid is close to the bottom elevation $Z_b(x,y)$.

S3 Equations of motion of the Lagrangian drift model

a. Governing equations

The governing equations of the Lagrangian drift model are written out in full as follows, using the notations defined in the main text:

$$\begin{aligned}
\left(m_T + C_A\rho_f V_b\right)\frac{du_{b,x}}{dt} &= -\frac{1}{2}\rho_f\psi\left(C_D A - \sin(2\theta)\, C_S A\right)\left|\boldsymbol{u_b} - \boldsymbol{u_f}\right|\left(u_{b,x} - u_{f,x}\right) \\
&\quad -\frac{1}{2}\rho_f\psi\,\cos(2\theta)\, C_S A\left|\boldsymbol{u_b} - \boldsymbol{u_f}\right|\left(u_{b,y} - u_{f,y}\right) \\
&\quad +\mu\max\left[-g\left(m_t - \rho_f V_b\right) - \frac{1}{2}\rho_f\psi C_L A\left|\boldsymbol{u_b} - \boldsymbol{u_f}\right|^2; 0\right]\gamma(\boldsymbol{x_b}) \\
&\quad +\left(1 + C_A\right)\rho_f V_b\left[\frac{\partial u_{f,x}}{\partial t} + u_{f,x}\frac{\partial u_{f,x}}{\partial x} + u_{f,y}\frac{\partial u_{f,x}}{\partial y}\right] \\
\left(m_T + C_A\rho_f V_b\right)\frac{du_{b,y}}{dt} &= -\frac{1}{2}\rho_f\psi\,\cos(2\theta)\, C_S A\left|\boldsymbol{u_b} - \boldsymbol{u_f}\right|\left(u_{b,x} - u_{f,x}\right) \\
&\quad -\frac{1}{2}\rho_f\psi\left(C_D A + \sin(2\theta)\, C_S A\right)\left|\boldsymbol{u_b} - \boldsymbol{u_f}\right|\left(u_{b,y} - u_{f,y}\right) \\
&\quad +\mu\max\left[-g\left(m_t - \rho_f V_b\right) - \frac{1}{2}\rho_f\psi C_L A\left|\boldsymbol{u_b} - \boldsymbol{u_f}\right|^2; 0\right]\gamma(\boldsymbol{x_b}) \\
&\quad +\left(1 + C_A\right)\rho_f V_b\left[\frac{\partial u_{f,y}}{\partial t} + u_{f,x}\frac{\partial u_{f,y}}{\partial x} + u_{f,y}\frac{\partial u_{f,y}}{\partial y}\right] \\
\left(m_T + C_A\rho_f V_b\right)\frac{du_{b,z}}{dt} &= -g\left(m_t - \rho_f V_b\right) - \frac{1}{2}\rho_f\psi C_L A\left|\boldsymbol{u_b} - \boldsymbol{u_f}\right|^2
\end{aligned} \qquad \text{S(2)}$$

b. Time integration scheme

$$\begin{aligned}
&\mathbf{x}_\mathbf{b}^{*} = \mathbf{x}_\mathbf{b}\left(t - \Delta t\right) + \Delta t\,\mathbf{u}_\mathbf{b}\left(t - \Delta t\right) \\
&\mathbf{x}_\mathbf{b}^{**} = \mathbf{x}_\mathbf{b}\left(t - \Delta t\right) + \Delta t\,\mathbf{u}_\mathbf{b}^{**} \\
&\mathbf{x}_\mathbf{b}\left(t\right) = \left(1 - a\right)\mathbf{x}_\mathbf{b}^{*} + a\,\mathbf{x}_\mathbf{b}^{**} \qquad \text{where} \quad a = 0.5
\end{aligned} \qquad \text{S(3)}$$

$$\begin{aligned}
&\left(m_T + \left(1 + C_A\right)\rho_f V_b\right)\dot{\mathbf{u}}_\mathbf{b} = \mathbf{F_f} + \mathbf{F_g} + \mathbf{F_b} + \mathbf{F_A} = \mathbf{RHS} \\
&\mathbf{u}_\mathbf{b}^{*} = \mathbf{u}_\mathbf{b}\left(t - \Delta t\right) + \Delta t\,\frac{\mathbf{RHS}\left[\mathbf{x}_\mathbf{b}\left(t - \Delta t\right), \mathbf{u}_\mathbf{b}\left(t - \Delta t\right), \alpha\left(t - \Delta t\right), \mathbf{u}_\mathbf{f}\left(t - \Delta t\right), \mathbf{u}_\mathbf{f}\left(t\right)\right]}{m_T + C_A\rho_f V_b\left(t - \Delta t\right)} \\
&\mathbf{u}_\mathbf{b}^{**} = \mathbf{u}_\mathbf{b}\left(t - \Delta t\right) + \Delta t\,\frac{\mathbf{RHS}\left[\mathbf{x}_\mathbf{b}^{*}, \mathbf{u}_\mathbf{b}^{*}, \alpha\left(t\right), \mathbf{u}_\mathbf{f}\left(t - \Delta t\right), \mathbf{u}_\mathbf{f}\left(t\right)\right]}{m_T + C_A\rho_f V_b\left(t\right)} \\
&\mathbf{u}_\mathbf{b}\left(t\right) = \left(1 - a\right)\mathbf{u}_\mathbf{b}^{*} + a\,\mathbf{u}_\mathbf{b}^{**}
\end{aligned} \qquad \text{S(4)}$$

S4 Model of body decomposition

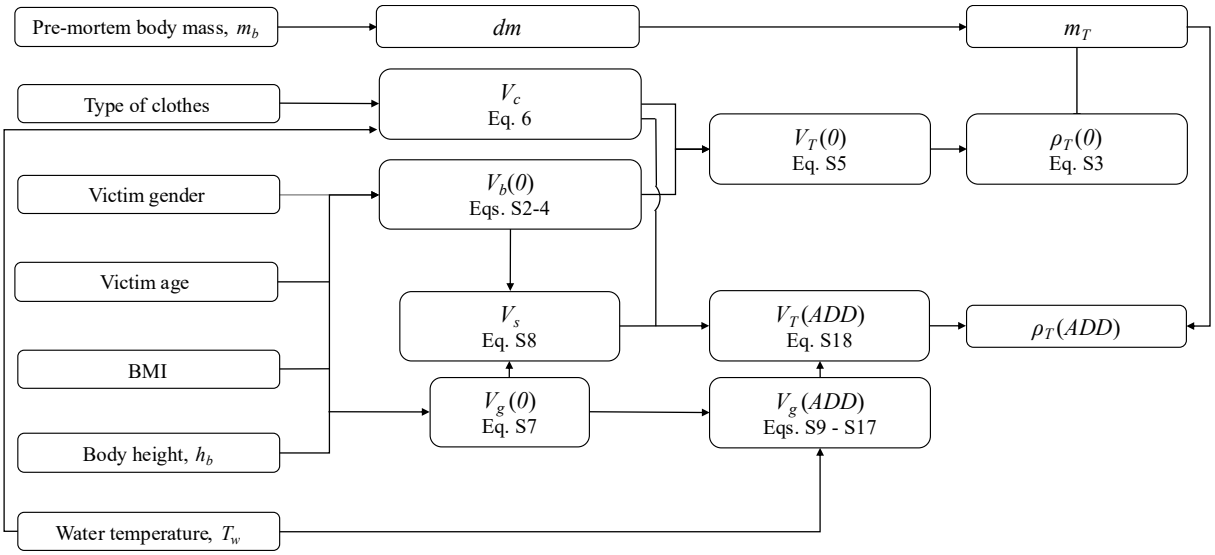

Figure S7: Workflow of the model of body decomposition

a. Initial body volume $V_b(0)$

The initial body volume $V_b(0)$ at functional residual capacity (FRC) of the lungs is a function of the percentage of body fat, $\%fat$, calculated as follows:

$$\begin{aligned}\%\,fat = (&-32.515 + 12.409\,sex + 3.306\,BMI - 0.03\,BMI^2 - 0.006\,age \\ &+0.033\,age \cdot sex - 0.001\,age \cdot BMI) \cdot 10^{-2}\end{aligned} \quad \text{S(5)}$$

with sex = 0 for men and 1 for women, age in years and BMI in kg/m². This equation was proposed by Meeuwsen, Horgan, & Elia (2010) and was adapted from the two-compartment model proposed by Durnin & Womersley (1974).

An uncertainty ε_{fat} is added to this percentage of body fat to reflect the variability in human body composition (Nickerson et al., 2018; Nickerson, McLester, McLester, & Kliszczewicz, 2020). This uncertainty is modelled with beta distributions whose parameters α and β are both equal to 2. These beta distributions are defined over different ranges, depending on the age and sex of the victim. The range of each beta function is set to $[-2\,\sigma; 2\,\sigma]$, with σ the standard deviation of the percentage of body fat observed by Meeuwsen et al. (2010). This value is a function of age and sex, as detailed in Table S1.

Table S1: Statistical properties of variable ε_{fat} from observations by Meeuwsen et al. (2010), and calibrated beta distributions.

	Observations (Meeuwsen et al., 2010)				Calibrated beta distribution					
Age range	Mean		Standard deviation (male)		α	β	Mean		Standard deviation	
	M	F	M	F			M	F	M	F
20-29	19	29.1	7.6	8.1	2	2	19	29.1	6.80	7.24
30-39	21.8	31.7	7	8.5	2	2	21.8	31.7	6.26	7.58
40-49	23.6	34	6.4	8.3	2	2	23.6	34	5.72	7.42
50-59	24.9	36.8	6.2	8.3	2	2	24.9	36.8	5.55	7.42
60-69	26.2	38.4	6.7	8.3	2	2	26.2	38.4	5.99	7.42
70+	26.6	40	6.8	9.4	2	2	26.6	40	6.08	8.41

From the value of %*fat*, the body density is determined with an equation proposed by Siri (1956a, 1956b), adjusted to get the body density in kg/m³:

$$\rho_b(0) = \frac{4.95}{\%fat + \varepsilon_{fat} + 4.5} 1000 \qquad \text{S(6)}$$

The initial body volume, $V_b(0)$, is obtained from this body density and the body mass:

$$V_b(0) = \frac{m_b}{\rho_b(0)} \qquad \text{S(7)}$$

b. Clothing volume V_c and total initial volume $V_T(0)$

The total initial volume $V_T(0)$ does not solely depend on the body volume, but also on the air trapped inside the clothes, V_c:

$$V_T(0) = V_b(0) + V_c \quad \text{S(8)}$$

The clothing volume is computed following the work of Barwood, Bates, Long, & Tipton (2011) who measured buoyancy force of humans immerged during 20 min, either remaining at rest ($V_{c,1}$) or swimming ($V_{c,2}$). In this work, $V_{c,1}$, is associated to a cold shock occurring for cold water (considered here as below 15°C) in which case the victim is assumed not to have moved (Farstad & Dunn, 2019). When the water temperature is over 15°C, it is considered that the victim has moved / swum and the stationary clothing volume is $V_{c,2}$:

$$V_c = \begin{cases} V_{c,1} \; if \; T_w < 15°C \\ V_{c,2} \; if \; T_w \geq 15°C \end{cases} \quad \text{S(9)}$$

This "clothing volume" can be negative, which represents clothing that reduces body buoyancy. The mean value, standard deviation and bounds of $V_{c,1}$ and $V_{c,2}$ are given by Barwood et al. (2011). As detailed in Table S2, we have calibrated beta distribution functions to match these statistical values. Each beta function is defined over the range $[-2\,\sigma; 2\,\sigma]$ with σ the standard deviation given in Barwood et al. (2011).

Table S2: Statistical properties of $V_{c,1}$ and $V_{c,2}$ from observations by Barwood et al. (2011), and calibrated beta distribution.

	Observations								Calibrated beta distribution							
	Mean				Standard deviation				α				β			
	M		F		M		F		M		F		M		F	
	$V_{c,1}$	$V_{c,2}$	$V_{c,1}$	$V_{c,2}$	$V_{c,1}$	$V_{c,2}$	$V_{c,1}$	$V_{c,2}$	$V_{c,1}$	$V_{c,2}$	$V_{c,1}$	$V_{c,2}$	$V_{c,1}$	$V_{c,2}$	$V_{c,1}$	$V_{c,2}$
Naked	0	0	0	0	0	0	0	0	-	-	-	-	-	-	-	-
Summer	0.31	0.51	0.92	0.92	0.91	0.82	0.82	0.82	10^{-6}	10^{-6}	0.54	0.075	10^{-6}	10^{-5}	0.54	0.075
Spring/Fall	0.82	1.23	1.12	1.23	1.12	1.12	1.12	1.02	0.025	0.33	0.33	0.71	0.05	0.67	0.67	1.42
Winter	1.12	0.71	1.94	2.04	0.82	2.45	1.23	0.82	0.85	10^{-6}	3.5	2.33	1.7	10^{-6}	7	4.67

c. Initial gaseous volume $V_g(0)$ and incompressible volume of the body V_s

The initial gaseous volume $V_g(0)$ is assumed equal to FRC. Consistently with Delhez et al. (2023), FRC is calculated with Eqs. S(10), which is based on a combination of equations proposed by Stocks & Quanjer (1995) and an analysis by Abston et al. (2017):

$$FRC = \begin{cases} (2.34h_b + 0.01age - 1.09) \cdot \dfrac{0.102BMI^2 - 7.4504BMI + 229.61}{100} \cdot 10^{-3} & \text{for men} \\ (2.24h_b + 0.001age - 1) \cdot \dfrac{0.102BMI^2 - 7.4504BMI + 229.61}{100} \cdot 10^{-3} & \text{for women} \end{cases} \quad \text{S(10)}$$

with FRC in m³, h_b in m, BMI in kg/m² and age in years.

This initial body volume $V_b(0)$ is then decomposed into a fixed volume and a variable one. The fixed volume V_s corresponds to the incompressible part of the victim body, which is assumed constant in time. The variable volume corresponds to the gaseous part of the victim body. V_s is calculated from $V_b(0)$ and $V_g(0)$:

$$V_s = V_b(0) - V_g(0)\,. \quad \text{S(11)}$$

d. Volume of gas in the body V_g(ADD)

The gaseous part $V_g(ADD)$ varies in time as it depends on the ADD (Heaton, Lagden, Moffatt, & Simmons, 2010). The evolution of the gaseous body volume with ADD is determined in four steps: first, a value is assumed for the ultimate gaseous body volume at atmospheric pressure; second, the influence of actual temperature and pressure is accounted for; third, the evolution of body temperature and ADD are estimated; finally, an assumption is introduced regarding the kinetics of body decomposition and bloating.

Step 1

To determine the ultimate gaseous body volume, which is not clearly defined in literature, an assumption is first introduced regarding this value in "standard conditions", i.e., at atmospheric pressure. We assumed that, in such conditions, the maximum gaseous volume equals twice the total lungs capacity (TLC). This accounts for both torso and belly bloating, under the assumption that they both expand similarly. Consistently with Delhez et al. (2023), the TLC can be calculated as follows:

$$TLC = \begin{cases} (7.99h_b - 7.08) \cdot \dfrac{0.0403BMI^2 - 3.1049BMI + 149.58}{100} \cdot 10^{-3} & \text{for men} \\ (6.6h_b - 5.79) \cdot \dfrac{0.0403BMI^2 - 3.1049BMI + 149.58}{100} \cdot 10^{-3} & \text{for women} \end{cases} \quad \text{S(12)}$$

with TLC in m³, h_b in m, BMI in kg/m².

Step 2

An ideal gas law is used to consider the influence of temperature T and pressure P. It is utilized to compute an amount of gas moles, n:

$$n = \frac{PV_g}{RT} \tag{13}$$

The initial amount of gas moles (noted n_0) is calculated with $P = P_{atm}$ = 101,325 Pa, the atmospheric pressure, $V_g = FRC$, R = 8.314 J/K/mol, and T = 37 + 273.15 K, the temperature of a living body.

At maximum body expansion and atmospheric pressure, the amount of gas molecules (noted n_1) is calculated with $P = P_{atm}$, $V_g = 2TLC$ and $T = T_w$, the water temperature in Kelvin.

Step 3

The evolution of body temperature T_b is estimated from its initial value $T_{b,ini}$ = 37°C and the water temperature T_w, assuming a simple exponential decay:

$$T_b = T_w + \left(T_{b,ini} - T_w\right) e^{-\frac{t}{\tau}} \tag{S14}$$

with t the elapsed time in seconds and τ a characteristic time assumed equal to 3000 s, leading to a rapid adaptation of the body temperature to the temperature of the surrounding water.

Step 4

Between the initial and the final states, the evolution of the number of gaseous particles n is assumed to evolve with ADD following the equations proposed by Delhez et al. (2023), and illustrated in Figure S8:

$$n = n_0 + \eta(n_1 - n_0) \tag{S15}$$

$$\eta\left(\frac{\alpha}{\alpha_1}\right) = \min\left[6\left(\frac{\alpha}{\alpha_1}\right)^5 - 15\left(\frac{\alpha}{\alpha_1}\right)^4 + 10\left(\frac{\alpha}{\alpha_1}\right)^3 ; 1\right] \tag{S16}$$

with α the current value of ADD and α_1 the ADD value reached when the body can no longer expand due to the resistance of tissues or the interruption of putrefaction processes. It can also be associated with the maximum ADD at which the body remains watertight or airtight.

The value of α_1, is calculated as a constant divided by the water temperature T_w, to replicate observations suggesting the value of ADD reached when the body resurfaces are lower when water temperature is higher:

$$\alpha_1 = \frac{C}{T_w}\delta \tag{S17}$$

with C a constant and δ a random parameter following a beta distribution (defined in the interval [0; 1], with parameters $\alpha = 4$ and $\beta = 4$), used to reflect the possibility that the body resurfaces before reaching maximum decomposition. The constant C was set to 5250°C²day, which leads to a value of $\alpha_1 = 189$°Cday (at $T_w = 28$°C) corresponding to a state of advanced decomposition (for a watertight and airtight body) based on Heaton et al. (2010).

The gaseous part V_g of body volume can be calculated as a function of the current values of ADD, temperature and hydrostatic pressure:

$$V_g = \frac{nRT_b}{p_{atm} + \rho_w g h_w} \quad \text{S(18)}$$

with g the gravity acceleration in m/s², T_b the body temperature and h_w the vertical distance (in m) between the body and the surface. This equation allows the gaseous volume to be smaller when the hydrostatic pressure is high enough, i.e. in deep areas, leading to cases where the victim body never resurfaces.

Finally, the submerged total body volume is calculated as the sum of the incompressible, clothing and gaseous volumes:

$$V_b(\alpha) = V_s + V_c + V_g(\alpha) \quad \text{S(19)}$$

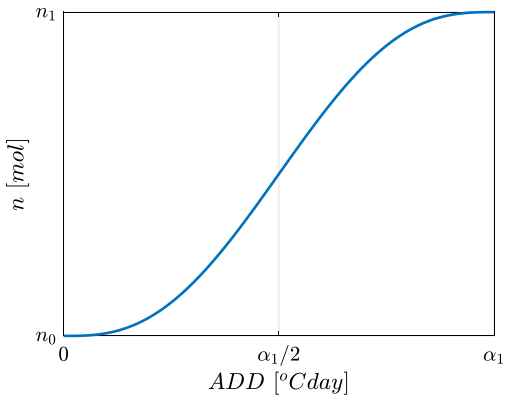

Figure S8: Evolution of gas quantity n as a function of ADD.

S5 Correction of the body position after a collision

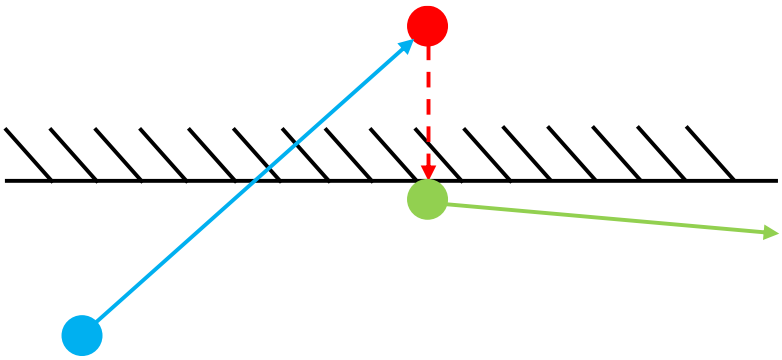

Figure S9: Scheme of the correction after a collision with a wall. The circles represent the body positions, the full arrows the velocity and the dashed arrow the correction of position. Blue represents the initial state before collision detection, red is the calculated position without correction due to collision and green is after the collision.

S6 Interpolation in space

Flow information is available at the geometric centre of each cell in the computational domain at given times. However, this information must be available continuously, both spatially and temporally. To achieve this, we perform a tri-linear interpolation of the X data (horizontal velocities and water height) so that the information is available at all times and positions.

Considering Figure S10, a property X_b at any position $\boldsymbol{x_b}$ can be calculated as follows:

$$X_b = (1-\xi)(1-\psi)X_{i,j} + (1-\xi)\psi X_{i,j+1} + \xi(1-\psi)X_{i+1,j} + \xi\psi X_{i+1,j+1} \qquad \text{S(20)}$$

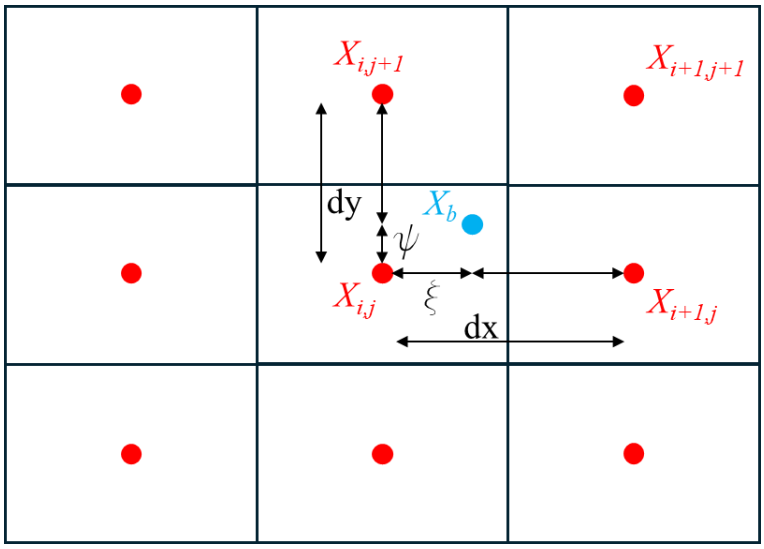

Figure S10: Flow grid with cells and their gravity centres (red dots) and body position (blue dot). dx and dy are the distances between two gravity centres along the x-axis and y-axis, respectively. ξ and ψ are the fraction of dx and dy between the cell centre in which the body is and its position.

S7 Statistical distributions of model parameters and input data

		Field information available			No field information available			
Parameter	Notation	PDF	Interval, or values	Parameters	Assumed distribution	Interval, or values	Parameters	Justification
Sex	*sex*	None. The reported value is used as it.	-	-	Bernoulli distribution	M or F	Equal probabilities	
Age	*age*	None. The reported value is used as it.	-	-	Discrete uniform distribution	[18, 90]	-	
Height	h_b	Beta distribution	M : [1.5, 2.05]	α and β adjusted such that $p_{10} = h_r - 0.025$ and $p_{90} = h_r + 0.025$, with h_r the reported value of body height.	Beta distribution	M : [1.5, 2.05]	$\alpha = 5.87$ $\beta = 6.08$	Delhez et al. (2023) and Van Der Heyden et al. (2018)
			F : [1.4, 1.9]			F : [1.4, 1.9]	$\alpha = 3.98$ $\beta = 5.97$	
Body Mass Index	*BMI*	Beta distribution	[16, 40]	α and β adjusted such that $p_{10} = BMI_r - 1$ and $p_{90} = BMI_r + 1$, with BMI_r the reported value of *BMI*.	Beta distribution	[16, 40]	$\alpha = 3.01$ $\beta = 4.26$	Delhez et al. (2023) and Van Der Heyden et al. (2018)
Mass	m_b	Beta distribution	M : [40, 150]	α and β adjusted such that $p_{10} = m_r - 2.5$ and $p_{90} = m_r + 2.5$, with m_r the reported value of body mass.	Calculated from height and BMI	-	-	Delhez et al. (2023) and Van Der Heyden et al. (2018)
			F : [35, 135]					
Clothing type		None. The reported category is used as it.	-	-	Generalized Bernoulli distribution	Naked, spring/autumn, summer, winter	Equal probabilities	Barwood et al. (2011)

Table S3: Assumed statistical distributions for the input data.

Parameter	Notation	Assumed distribution	Interval, or values	Parameters	Justification
Clothing volume	V_c	Beta distribution	See Section S4b (in Supporting Information)	See Table S2 (in Supporting Information)	Barwood et al. (2011)
Additional body mass	dm	Beta distribution	$[0, 0.1m_b]$	$\alpha = 1.5$ $\beta = 1.5$	Conn et al. (1995)
Coulomb friction coefficient	μ	Uniform distribution	[0.3, 1]	-	Delhez et al. (2023)
Decomposition threshold	δ	Beta distribution	[0, 1]	$\alpha = 4$ $\beta = 4$	
Flow turbulence	λ_x and λ_y	Gaussian distribution	-	$\mu = 0$ $\sigma = 1$	Kleinstreuer & Zhang (2003)

Table S4: Assumed statistical distributions for model parameters.

Parameter	Notation	Fixed value	Justification
Water temperature	T_w	According to measurements	Section 1 of Supporting Information
Drag area	C_DA	Summer clothing: 0.42 m² Spring/Autumn clothing: 0.52 m²	Delhez et al. (2024)
Side area	C_SA	Summer clothing: 0.036 m² Spring/Autumn clothing: 0.041 m²	Delhez et al. (2024)
Lift area	C_LA	Summer clothing: 0.07 m² Spring/Autumn clothing: 0.084 m²	Delhez et al. (2024)
Added mass coefficient	C_A	M: 0.268 F: 0.236	Caspersen et al. (2010)
Restitution coefficient for collisions	e	0.1	As for wooden logs: Persi et al. (2019)

Table S5: Values of input data (T_w) and model parameters not handled stochastically.

S8 Maps of computed body position at the end of the reported submersion interval

(a) Case 8

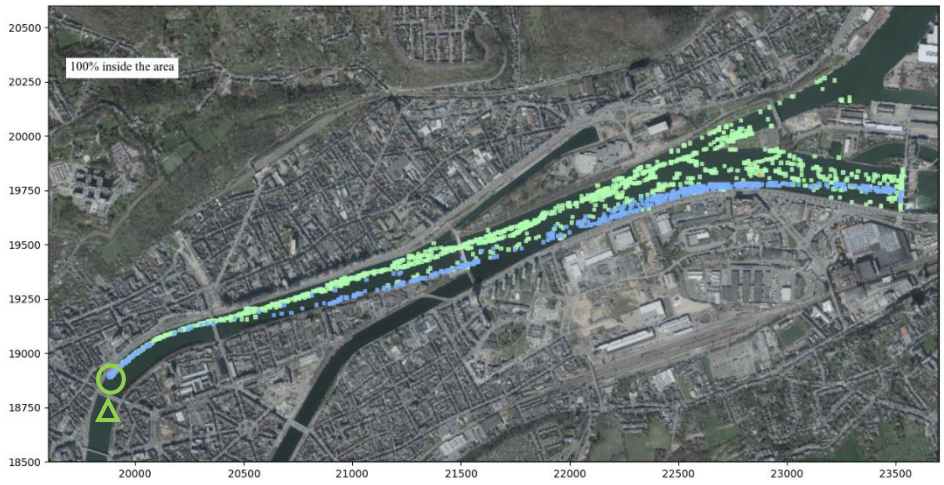

(b) Case 14

(c) Case 50

Figure S11: Maps of computed body position at the end of the reported submersion interval

S9 Flow direction and magnitude

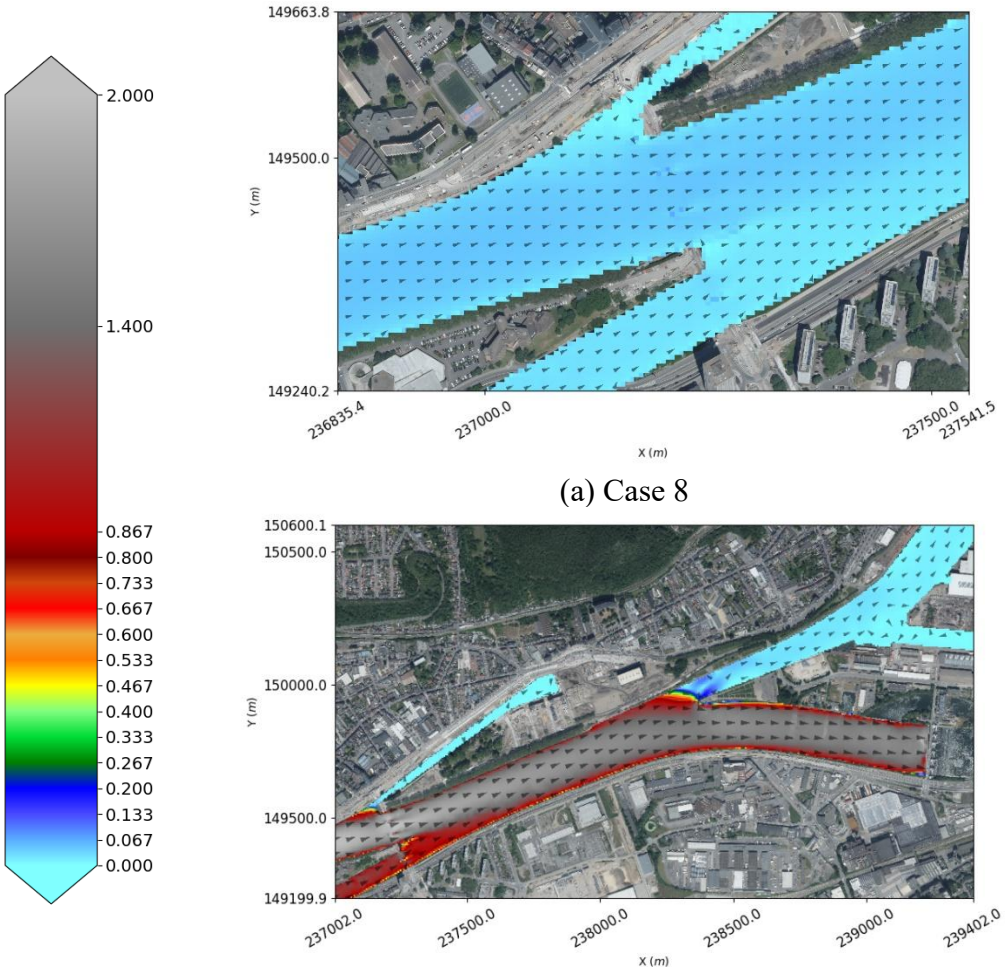

(a) Case 8

(b) Case 50

Figure S12: Flow direction and magnitude (m/s) of the depth-averaged flow velocity for (a) Case 8, (b) Case 50 at the time corresponding to the respective reported submersion intervals.

S10 Forces acting on the body

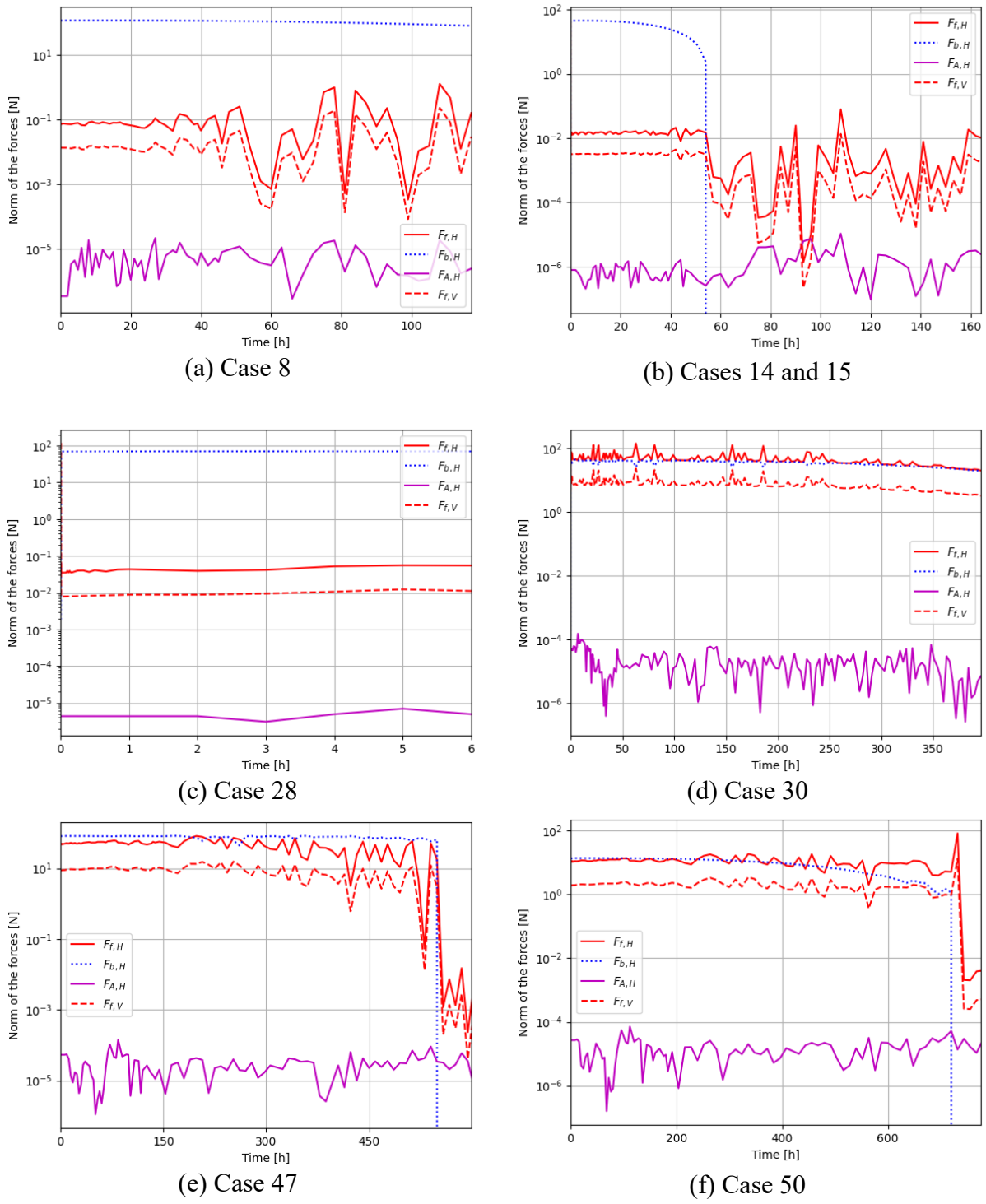

(a) Case 8

(b) Cases 14 and 15

(c) Case 28

(d) Case 30

(e) Case 47

(f) Case 50

Figure S13: Relative importance of the forces in one model run for each drowning case. In the legend, $F_{f,H}$ refers to the magnitude of the component in the x-y plane of force $\mathbf{F_f}$ (hydrodynamic forces), $F_{b,H}$ to the maximum possible magnitude of the component in the x-y plane of force $\mathbf{F_b}$ (friction on the bottom), $F_{A,H}$ to the magnitude of force $\mathbf{F_A}$ (added mass force linked to flow non-uniformity and unsteadiness), $F_{f,V}$ to the magnitude of the component along z of force $\mathbf{F_f}$ (hydrodynamic forces).

S11 Computed body travelled distances and elevations

For each drowning case, the following plots represent (i) the travelled distance as a function of time, (ii) the body elevation as a function of time and (iii) the body elevation as a function of the travelled distance. In each plot, the red area represents the envelope of all model runs. The other lines represent ten randomly selected cases from the whole set of model runs.

Travelled distance | Body elevation | Body elevation vs. travelled distance

Case 8

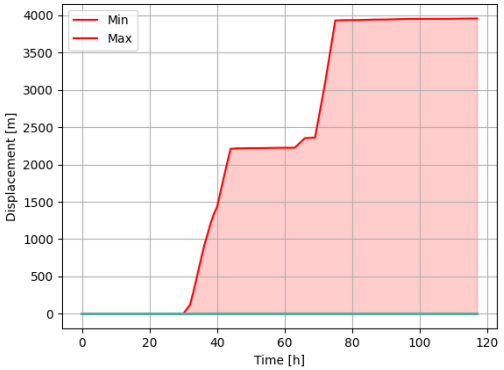

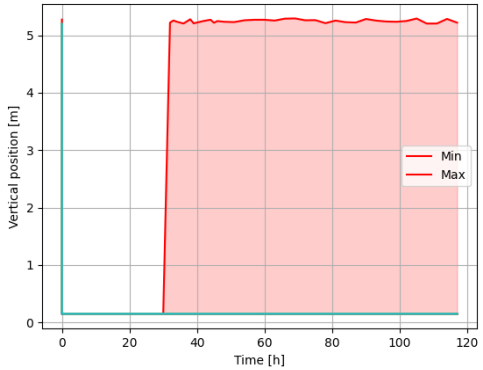

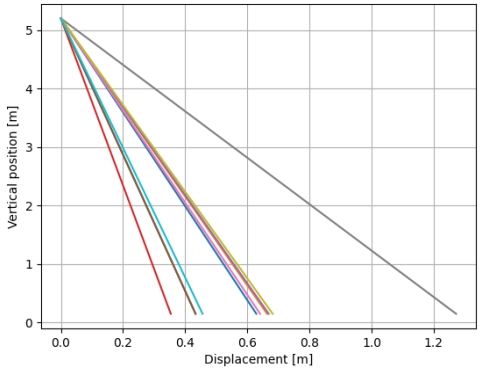

Travelled distance | Body elevation | Body elevation vs. travelled distance

Cases 14 and 15

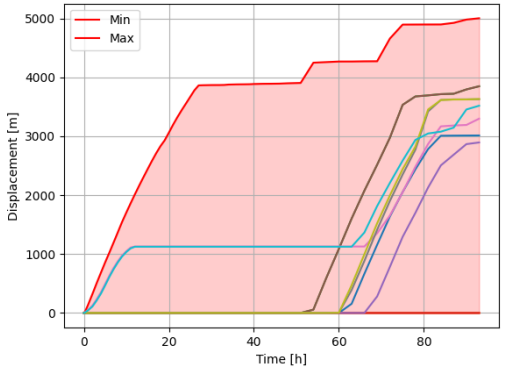

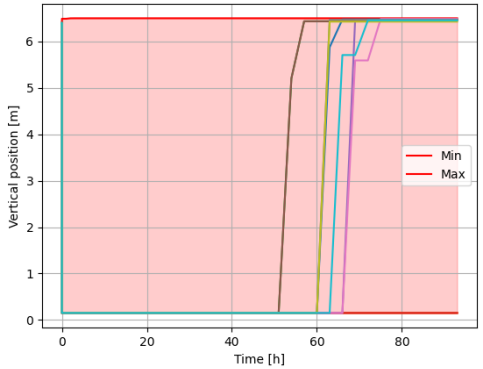

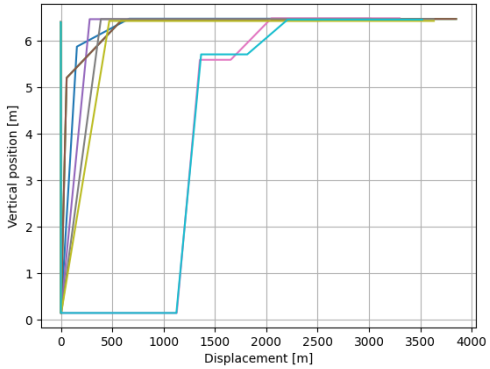

Case 28

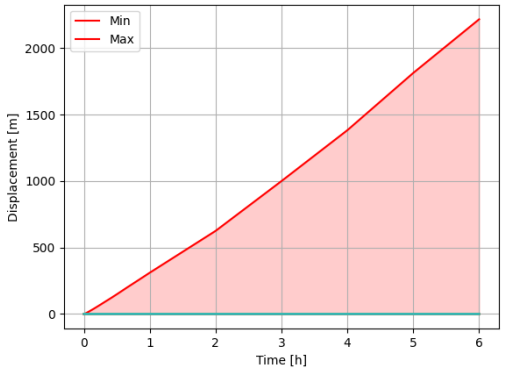

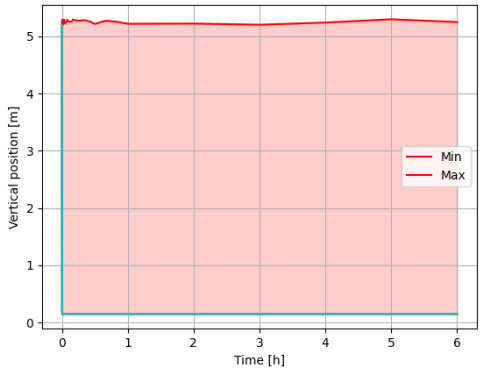

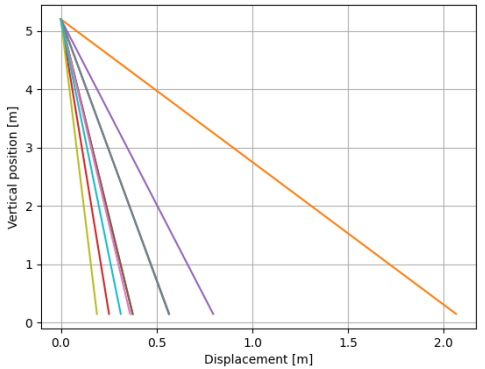

Travelled distance | Body elevation | Body elevation vs. travelled distance

Case 30

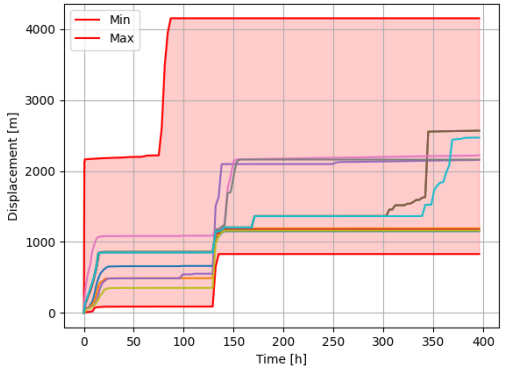

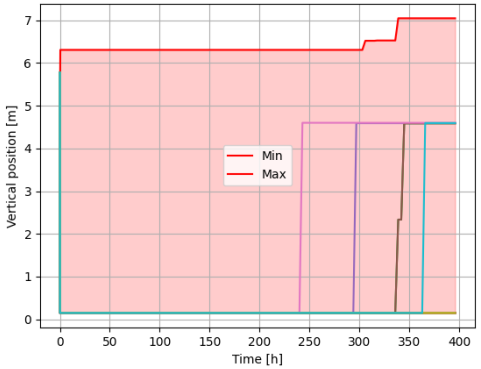

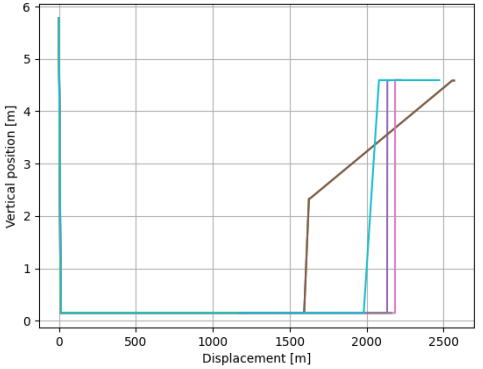

Case 47

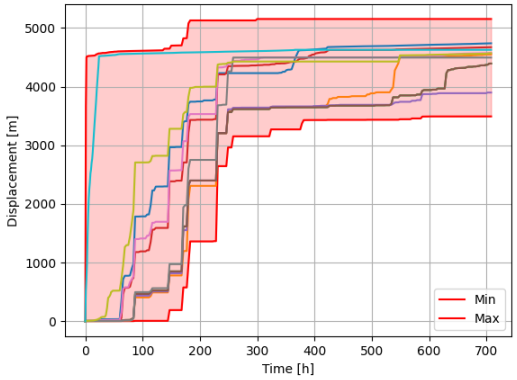

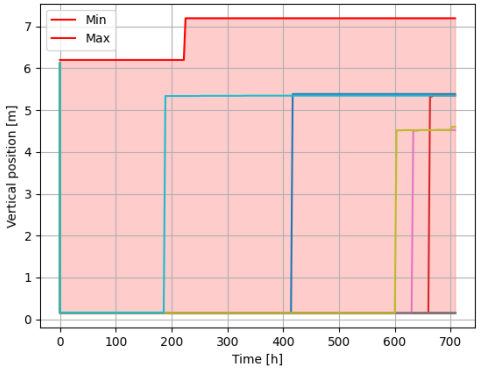

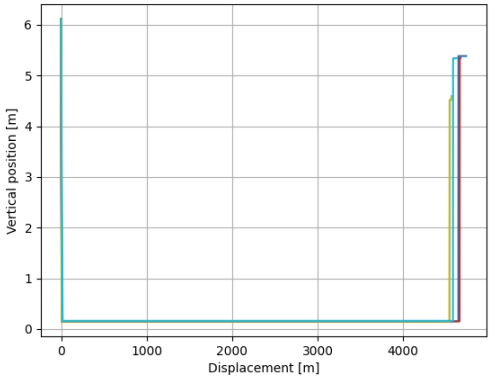

Case 50

Travelled distance

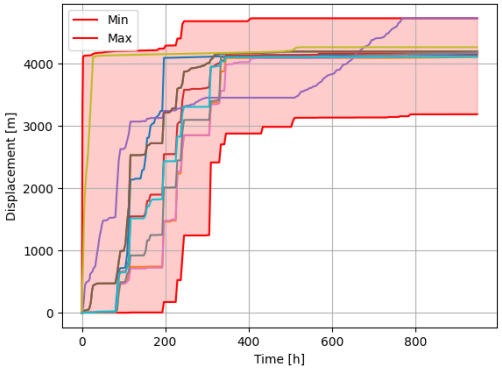

Body elevation

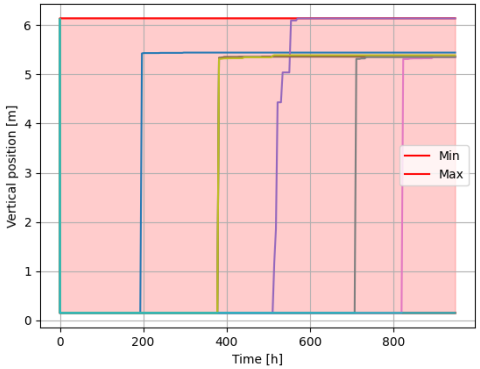

Body elevation vs. travelled distance

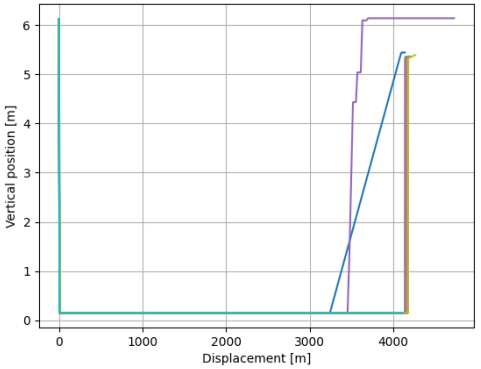

Conclusion

Conclusion

The evaluation of the drift of a drowning victim posed numerous challenges throughout this thesis. To address these, the problem was decomposed into a series of specific objectives, each targeting a different aspect of uncertainty or complexity. A primary model was developed early in the work (Chapter 1), serving as a framework to identify and understand the main factors influencing drowning events. By using this model as a diagnostic tool, we were able to eliminate certain uncertainties and formulate hypotheses about the remaining key variables, ultimately leading to a more refined model tested on real drowning cases (Chapter 4).

When developing a digital model, laying a solid foundation is essential. In this work, we chose to base the model on the fundamental equations of motion. This foundation shaped the direction of our research and informed the choice of variables required to characterize a drowning victim, such as body volume and body area. From there, we turned our attention to real-case data, seeking to convert available information about the victim into usable model inputs. A key task was to identify and assess the uncertainties present in the physical parameters and forces involved in these three equations. A thorough literature review revealed that most of these parameters were poorly constrained, which led us to retain and quantify these uncertainties, while attempting to reduce it for the most influential parameters. The early phase of the thesis thus focused on determining which uncertainties had the greatest impact on the drift of a drowning victim (Chapter 1). After evaluating several approaches, the Monte Carlo method was chosen as the most appropriate, along with the study of drowning in idealized flow conditions as a preliminary step. For sensitivity analysis, Sobol indices were particularly well suited and were used extensively. The study was structured around two victim types (known and unknown characteristics) and two timeframes (short- and long-term drownings), enabling us to explore a wide range of scenarios and uncertainties. Importantly, we observed that identifying the victim can halve the uncertainty in horizontal position. We also distinguished between two distinct drowning patterns—one where the body sinks and resurfaces, and another where the body never sinks. Over short time horizons, hydrodynamic parameters had the greatest impact on drift; over longer durations, the victim's internal parameters became dominant. This analysis established the groundwork for Chapters 2, 3, and 4, where these parameters are investigated in greater depth.

In Chapter 2, we focused on the hydrodynamic interaction between the body and the flow, specifically examining drag, lift, and side forces. These forces had not previously been studied in the context of drowning, largely because earlier models operated at much larger scales, treating the body as a passive tracer in marine environments. Given the force-based approach of our model, we first needed to define the position of a drowning victim in the flow—a position that had been previously described only qualitatively. We formalized this as the drowned position, which then served as a reference configuration for the rest of the study. To characterize the hydrodynamic coefficients, we used a dummy in a wind tunnel, working at Reynolds numbers comparable to those in urban rivers. Across 249 tests, we evaluated two positions (lying and drowned) and two clothing types (tight and loose). The drag coefficient was found to vary between 0.5 and 1.2 depending on Reynolds number and yaw angle, with clothing type inducing a 30% variation. In contrast, lift and side force coefficients showed no clear patterns;

only their measured values were retained. Two qualitative results emerged as particularly important: (1) drag/lift/side areas proved to be less uncertain than the corresponding coefficients due to the complex geometry of the drowned position; and (2) we identified a stable rotational equilibrium for the body, with the head downstream and the back aligned with the flow direction. This justified model simplifications, such as using a single yaw angle and working with areas instead of coefficients, thereby reducing uncertainty.

In parallel to the hydrodynamic study, Chapter 3 focused on real drowning cases through the creation and analysis of a dedicated database. This database aimed to identify statistical patterns in drowning incidents based on basic victim and environmental characteristics. Two key variables were analysed: the initial buoyancy of the victim and their post-mortem submersion interval (PMSI). We found that older individuals, particularly those over 65 years, and those with higher BMI, tend to float more often. Water temperature played a dual role: below 7°C, it tends to induce sinking and was also associated with longer PMSI. We established a reference accumulated degree-day (ADD) value of 95°C·days to help relate temperature and time in typical drowning cases. Additionally, the data revealed that older women were overrepresented in suspected suicide cases, which could inform future prevention strategies.

In Chapter 4, we integrated the findings from the previous chapters into our comprehensive model, which was then tested on real drowning cases in actual flow conditions. Based on our experimental findings, we kept using a simplified model by considering a single yaw angle, and we calculated hydrodynamic forces using the previously determined drag/lift/side areas. We then turned to the problem of decomposition and its influence on body characteristics. Using insights from our database and following the same approach used to reconstruct body characteristics from witness data, we developed a series of simple, adjustable, and modular equations. By applying specific assumptions about decomposition, we employed the ideal gas law to quantify the variation in gas volume within the body. We hypothesized a sigmoid progression for decomposition: starting slowly, increasing to an optimum rate, and then tapering off. Importantly, we introduced the concept of maximum decomposition, which in our context refers to the resurfacing phase, while we deliberately excluded simulation of the second sinking after resurfacing.

All elements were then compiled into a numerically optimized model and tested on seven real drowning cases from Liège and the Meuse River, chosen for their diversity, including accidents and suicides across different seasons and flow regimes, with PMSI going up to 40 days. After generating realistic hydrodynamic simulations using WOLF software, we tested the model's performance. The model proved more reliable at high flow rates than at low flow rates, highlighting the importance of velocity fields and the influence of hydraulic structures on body drift. As anticipated, we observed that accurately estimating resurfacing through the decomposition had a major impact on drift predictions.

Finally, the results were presented in two ways: first as raw spatial distributions of body positions from Monte Carlo simulations, and second using kernel density estimations, which proved particularly effective for visualizing outcomes and of higher operational value for an on-site use.

Perspectives

As mentioned in the Introduction, this thesis addresses only a part of a much broader issue and is designed to be extended in future research.

As shown in Chapter 1, morphological parameters have a significant impact on simulation results. For this reason, the conversion of witness-reported data into model-usable parameters was implemented via a series of simple equations. Each equation is the result of specific research efforts and can be individually refined or replaced as new studies should propose more accurate formulations. Thanks to this modular structure, improving the model's performance may, in many cases, involve simply modifying a single equation within an otherwise complex model, thus facilitating both upgradability and maintainability.

This same philosophy guided the construction of the decomposition model. It too is composed of modular equations, each replaceable as improved data or methods become available. Our current assessment of decomposition is clearly open to refinement, as it is based on a limited dataset primarily representing the Belgian population. This dataset was designed using parameters typically available in most drowning investigations. But, as demonstrated in Chapter 4, it can be enriched using media-reported information. Its potential for geographic and contextual extension is therefore considerable. The database not only serves as a source for study but also as a model for accessible knowledge sharing, with potential applications beyond drowning, such as in assessing the reliability and utility of non-expert testimony.

Furthermore, the hydrodynamic coefficients and areas, while currently quantified through controlled wind tunnel tests (Chapter 2), can be refined via additional experiments. These might explore other Reynolds numbers, clothing types, or attack angles, and importantly, might also account for individual morphological variation. Thanks to detailed documentation, these experiments could also be replicated numerically. If such numerical replications confirm our findings, they could allow for near-instantaneous estimation of hydrodynamic forces in various conditions, significantly enhancing practical applicability.

A critical aspect not yet discussed in detail is the model's computational efficiency. Even a highly accurate model would be impractical for field use if it requires excessive computation time. For example, a model requiring two days to simulate a single day of drift would be of limited operational value in urgent search scenarios. For this reason, the entire model was developed with a strong emphasis on computational optimization, despite this being less relevant in a purely academic context. We employed parallelized Monte Carlo simulations, adaptive time steps, and dynamic variable recording at regular intervals. Together, these optimizations enable a one-day simulation to be completed in approximately one hour on a high-performance computer. This computation time varies depending on flow conditions, morphology, hydraulic structures, number of Monte Carlo runs, and hardware, but provides a useful benchmark for real-world application without even considering the evolution of the used technology.

Another major consideration was compatibility with hydrodynamic simulation models. We deliberately designed our model to require only depth-averaged horizontal flow velocity and water depth matrices as inputs, data typically available from most hydrodynamic solvers.

Obviously, the lack of information on vertical flow velocities and turbulence quantifications provided by the hydrodynamic model are clear limitations. But this simplified flow consideration makes the model broadly compatible and enhances its scalability. In our case, we facilitated the integration with the WOLF hydrodynamic model, developed by our research team. This integration enabled the creation of a user-friendly interface, embedded directly in WOLF, that allows users to recreate a drowning event without prior training. This interface was optimized for use in the field, potentially via tablets or other mobile devices, supporting the goal of making the tool accessible to the stakeholders.

In keeping with this focus on field usability, we implemented kernel density estimation (KDE) for result visualization. Since the ultimate objective of this research is to support targeted search efforts, we actively sought the most effective means of visualizing probable research areas. The use of KDE representation makes the potential and utility of the model immediately apparent to both specialists and non-specialists, enhancing its practical impact.

However, a key area for future work is the interaction between the model and actual field operations, which could not be addressed within the scope of this thesis. Such interaction is essential for refining the model with real-time data and could progressively improve model accuracy. In particular, we envision the use of Bayesian inference, enabling field teams to inform the model of areas where the body has not been found at specific times, thereby generating updated simulations that incorporate this new knowledge.

In conclusion, this research clearly warrants further development, but its multidisciplinary nature, flexible structure, user-friendly first GUI, and accessible result formats represent strong foundations. These features position it well for future adoption and expansion, with the ultimate aim of providing a reliable, real-time decision-support tool for search operations in urban river drowning cases.